Bao-Ji Zhang · Sheng-Long Zhang

Research on Ship Design and Optimization Based on Simulation-Based Design (SBD) Technique

上海交通大學出版社
SHANGHAI JIAO TONG UNIVERSITY PRESS

Springer

Research on Ship Design and Optimization Based on Simulation-Based Design (SBD) Technique

Bao-Ji Zhang · Sheng-Long Zhang

Research on Ship Design and Optimization Based on Simulation-Based Design (SBD) Technique

上海交通大學出版社
SHANGHAI JIAO TONG UNIVERSITY PRESS

Springer

Bao-Ji Zhang
College of Ocean Science and Engineering
Shanghai Maritime University
Shanghai
China

Sheng-Long Zhang
Merchant Marine College
Shanghai Maritime University
Shanghai
China

ISBN 978-981-10-8422-5 ISBN 978-981-10-8423-2 (eBook)
https://doi.org/10.1007/978-981-10-8423-2

Jointly published with Shanghai Jiao Tong University Press, Shanghai, China

The print edition is not for sale in China Mainland. Customers from China Mainland please order the print book from: Shanghai Jiao Tong University Press.

Library of Congress Control Number: 2018940627

© Shanghai Jiao Tong University Press, Shanghai and Springer Nature Singapore Pte Ltd. 2019
This work is subject to copyright. All rights are reserved by the Publishers, whether the whole or part of the material is concerned, specifically the rights of translation, reprinting, reuse of illustrations, recitation, broadcasting, reproduction on microfilms or in any other physical way, and transmission or information storage and retrieval, electronic adaptation, computer software, or by similar or dissimilar methodology now known or hereafter developed.
The use of general descriptive names, registered names, trademarks, service marks, etc. in this publication does not imply, even in the absence of a specific statement, that such names are exempt from the relevant protective laws and regulations and therefore free for general use.
The publishers, the authors and the editors are safe to assume that the advice and information in this book are believed to be true and accurate at the date of publication. Neither the publishers nor the authors or the editors give a warranty, express or implied, with respect to the material contained herein or for any errors or omissions that may have been made. The publishers remains neutral with regard to jurisdictional claims in published maps and institutional affiliations.

Printed on acid-free paper

This Springer imprint is published by the registered company Springer Nature Singapore Pte Ltd.
part of Springer Nature
The registered company address is: 152 Beach Road, #21-01/04 Gateway East, Singapore 189721, Singapore

Contents

1 General Overview . . . 1
1.1 Significance of Ship Form Design and Optimization Based on SBD Technology . . . 2
1.2 The Key Technology of Ship Form Optimization . . . 4
1.2.1 Numerical Simulation Technology . . . 4
1.2.2 Hull Geometry Reconstruction Technology . . . 5
1.2.3 Approximate Technology . . . 6
1.2.4 Optimization Method . . . 6
1.2.5 Integrated Set Technology . . . 7
1.3 Basic Method of Hull Line Optimization . . . 8
1.4 Research Progress of Ship Form Design and Optimization of SBD Technology at Home and Abroad . . . 11
1.4.1 Ship Form Optimization Based on Potential Flow Theory . . . 11
1.4.2 Optimization of Ship Form Based on Viscous Flow Theory . . . 15
1.5 Research Project . . . 20
References . . . 23

2 Basic Theory of Hydrodynamics . . . 27
2.1 Overview . . . 27
2.2 Michell Integral Method . . . 28
2.2.1 Use the Tent Function to Express the Ship Type . . . 29
2.2.2 Derivation of Michell Integral Formula . . . 30
2.3 Rankine Source Method . . . 36
2.3.1 Basic Equation . . . 36
2.3.2 Linearization of Free Surface Conditions . . . 38
2.3.3 Solution of Free Surface Conditions . . . 39

2.3.4 Calculate the Wave Resistance 44
2.3.5 Mesh Classification by Rankine Source Method 45
2.3.6 Calculation Procedure of Rankine Source Method 46
2.3.7 Examples 49
2.4 Basic Theory of CFD 57
2.4.1 Mass Conservation Equation 57
2.4.2 Momentum Conservation Equation (N-S Equation) 58
2.4.3 Reynolds Equation 58
2.4.4 Turbulence Model 59
2.4.5 Wall Function Method 59
2.4.6 Boundary Condition 60
2.4.7 Free Surface Simulation 62
2.4.8 Numerical Solution Method 63
2.4.9 Meshing 63
2.5 The Establishment of Numerical Wave Tank 65
2.5.1 Wave Making at Velocity Boundary 65
2.5.2 Numerical Wave Cancelation 66
2.5.3 The Six Degrees of Freedom (SDOF) Motion Equation of Ship 66
2.5.4 Examples 69
2.6 Study on the Uncertainty of CFD Affecting the Calculation of Ship Resistance 74
2.6.1 Resistance Calculation 74
2.6.2 Analysis of CFD Influencing Factors 75
References 84

3 Geo-Reconstruct Technology of Hull 85
3.1 Overview 85
3.2 Research Progress of Hull Linear Expression 86
3.2.1 Overseas Research Situation 88
3.2.2 Domestic Research 89
3.3 Basic Connotation of Hull Geometric Reconstruction Technology 90
3.4 Fundamental Principles of Hull Geometry Reconstruction Technology 91
3.5 Hull Geometric Reconstruction Method 92
3.5.1 Hull Form Modification Function Method 92
3.5.2 Polynomial Expansion Method 94
3.5.3 Spline Function Method 95
3.5.4 Geometric Modeling Technique 96
References 105

4 Optimization Method and Optimization Platform 109
4.1 Traditional Optimization Methods 110
4.1.1 The Basic Idea of Nonlinear Programming 110
4.1.2 Gradient Method 112
4.1.3 Sequential Unconstrained Optimization Method 112
4.2 Modern Optimization Algorithm 114
4.2.1 Basic Genetic Algorithm 115
4.2.2 Niche Genetic Algorithm 116
4.2.3 Neural Network 119
4.2.4 Particle Swarm Algorithm 123
4.3 Hybrid Optimization Algorithm 130
4.3.1 Hybrid Algorithm I 130
4.3.2 Hybrid Optimization Method II 133
4.4 Optimization Platform 136
4.4.1 ISIGHT Optimization Platform 136
4.4.2 Friendship 139
References 141

5 The Optimization of the Hull Form with the Minimum Wave-Making Resistance Based on Potential Flow Theory 143
5.1 Overview 143
5.2 The Optimization of the Hull Form with Minimum Wave-Making Resistance Based on Michell Integral Method 143
5.2.1 Establishment of the Ship-Type Optimization Model 143
5.2.2 The Data File of the Ship-Type Optimization Based on Michell Integral 145
5.2.3 Examples 146
5.3 The Optimization of the Hull Based Rankine Source Method 152
5.3.1 Establishment of the Hull Form Optimization Model 153
5.3.2 Optimization Process of Hull Form 154
5.3.3 Examples 156
5.3.4 Design of Ship Hull with Minimum Wave Resistance Under Different Constraints 160
5.4 Optimization Design of Ship with Minimum Resistance Based on Genetic Algorithm 169
5.4.1 Ship Form Optimization Model 169
5.4.2 Ship-Type Optimization Based on Basic Genetic Algorithm 169
5.4.3 The Optimization of the Hull Form Based on NGA 171
5.4.4 Examples 172
5.4.5 The Comparisons of the Optimization Result Between GA and LNP 174

5.5 Optimization of Ship Type with Minimum Resistance Considering Viscous Separation . . . 179
5.5.1 Viscous Water Resistance . . . 180
5.5.2 Ship-Type Optimization Model . . . 181
5.5.3 Examples . . . 182
5.5.4 Ship Optimization Process . . . 182
5.5.5 Separation Judgment Method . . . 185
5.6 Ship Model Towing Test Results . . . 191
5.7 Discussion on Practicability of Optimal Ship Form . . . 193
References . . . 195

6 Hull Form Optimization Based on the CFD Technique . . . 197
6.1 Introduction . . . 197
6.2 Optimization Problem . . . 197
6.2.1 Objective Function . . . 197
6.2.2 Design Variables . . . 197
6.2.3 Constraint . . . 198
6.3 Optimization Framework . . . 199
6.4 Hull Form Optimization Based on the RANS-CFD Technique . . . 200
6.4.1 Hull Form Optimization in Calm Water Using the IPSO II Algorithm . . . 200
6.4.2 Hull Form Optimization in Waves Using the Hybrid Algorithm . . . 204
6.5 Hull Form Optimization Based on the Approximate Technique . . . 210
6.5.1 Hull Form Optimization Based on the IPSO I-BP Algorithm . . . 210
6.5.2 Hull Form Optimization Based on the IPSO III-ElmanNN . . . 219
References . . . 225

7 Ship Navigation Optimization . . . 227
7.1 Introduction . . . 227
7.2 Optimization Problem . . . 228
7.2.1 Objective Function . . . 229
7.2.2 Design Variable . . . 229
7.2.3 Optimizer . . . 229
7.3 Optimization . . . 229
References . . . 233

Chapter 1
General Overview

The development of new ships and the optimization of ship design are a highly comprehensive technology which requires integrating many disciplines on the optimization platform (or through self-programming) in order to get navigational performance (such as: rapidity, seakeeping, and maneuverability) optimal ship. It is also the premise and the foundation of overall design and innovative design [1]. The traditional ship design and development is a sequential process, starting from the owner's demands and ending in the operation of the ship, as shown in Fig. 1.1.

Because design factors such as manufacturability and quality assurance in the earlier stage of design cannot be fully considered, designers can repeatedly adapt the design scheme, resulting in a series of problems such as prolonged development cycle, difficult delivery, and cost increase, which makes it difficult to adapt to the intense market competing with the urgent need for new models. In order to solve the above problems, it is necessary to develop a totally new design tool, which is a ship design and optimization method that aims at performance and usage-driven design [2]. With the rapid development of computer science and information technology, it is possible to improve the effect and flexibility in design process by using virtual design technology based on computer numerical simulation and visualization technology, which integrates the preliminary design, detailed design, production design, construction and operation and maintenance of the current ship design. Thus, the technology of SBD (simulation-based design) came into being. The main purpose of SBD technology is to reduce the ship development time and capital investment, lower risk, optimize the design, and improve efficiency. The design and development process of ship form based on SBD technology is shown in Fig. 1.2.

© Shanghai Jiao Tong University Press, Shanghai and Springer Nature Singapore Pte Ltd. 2019

B.-J. Zhang and S.-L. Zhang, *Research on Ship Design and Optimization Based on Simulation-Based Design (SBD) Technique*,
https://doi.org/10.1007/978-981-10-8423-2_1

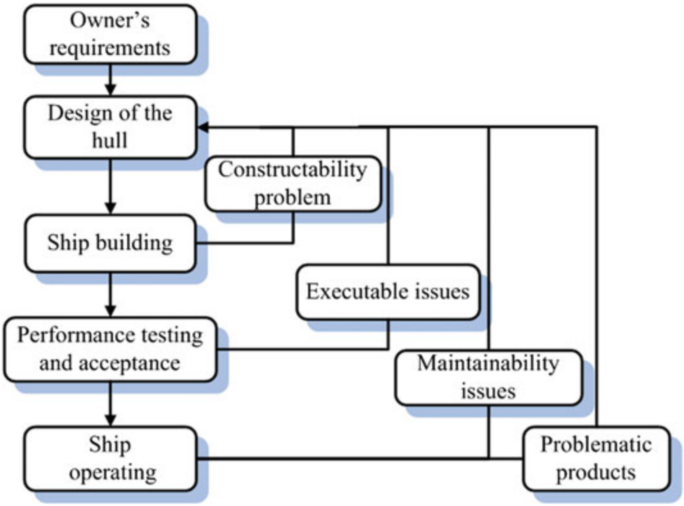

Fig. 1.1 Ship product sequence design process

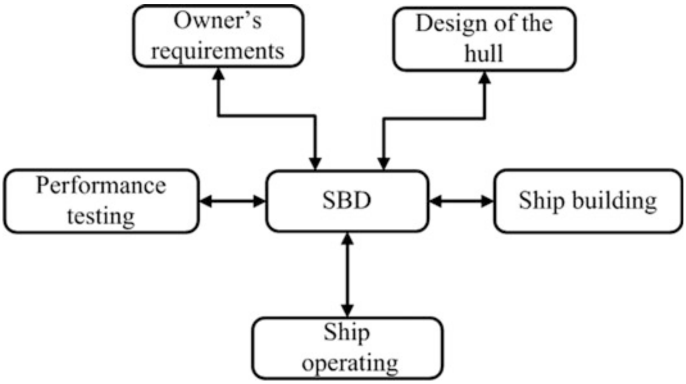

Fig. 1.2 Ship product development process based on SBD technology

1.1 Significance of Ship Form Design and Optimization Based on SBD Technology

Under the condition of low-carbon economy in the post-financial crisis era, great changes have taken place in the concept and thought of ship design. Ship design which seeks the best overall navigation performance has gradually substituted for ship-type optimization with the objective of minimum hydrostatic drag. In the framework of "green ship" design and construction, it is imminent to build a resource-conserving and environment-friendly shipbuilding industry [3]. In 2014, the Energy Efficiency Design Index (EEDI) proposed by the International Maritime Organization required future ship form design safer, greener, more economical and more comfortable. Therefore, energy saving and emission reduction become the theme of the future development of ship design. Under the design conditions, the energy-saving "green" ship hull form design is an effective method to reduce the total resistance and fuel consumption as well as carbon emission, as shown in Fig. 1.3. SBD technology takes the ship's sailing performance as the optimal design objective, and effectively combines the numerical evaluation and optimization theory of CFD (Computational Fluid Dynamics) with the geometry reconstruction technology of ship body to obtain the optimal navigation performance under given constraints. The hull types, namely: the "green" hull with the minimum resistance and the minimum energy consumption, greatly promote the design of ship form from traditional experience mode to intelligent mode and knowledge mode [4]. At present, our country has become the largest shipbuilding country in the world, but there is still a certain distance from world's shipbuilding powers. In particular, the "Green Ship" design and development has seriously affected the strategic transformation of China's shipbuilding industry. In the fierce market competition, it can find an effective green ship design method, which directly determines the survivability of shipbuilding enterprises. Therefore, we must quickly break through the key technologies of shipboard SBD design and develop an optimized design system for the integrated navigation performance of real ship with independent intellectual property rights so as to enhance the capability of independent innovation of our ship by leaps and bounds.

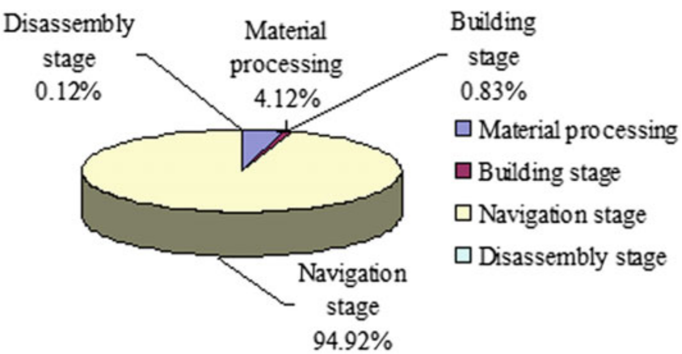

Fig. 1.3 Carbon emissions of the total life cycle of a bulk carrier

1.2 The Key Technology of Ship Form Optimization

Ship form optimization based on hydrodynamic theory is a complex systematic project, which is a concentrated reflection of multi-disciplinary integration and fusion of CFD, CAD, optimization, computer, and grid technologies. It is necessary to integrate various disciplines (software) on the optimization platform or self-programming to achieve the optimization process. The optimization system mainly involves five key technologies: CFD numerical simulation technology, optimization technology, approximation technology, hull grid reconstruction technology, and integrated technology.

1.2.1 Numerical Simulation Technology

Based on the hydrodynamic theory, ship-type optimization requires that the flow field around the hull be carefully described and more effective measures be taken to control the flow around the hull. Therefore, the optimization of ship form is inseparable from the scientific guidance of the ship hydrodynamics theory, including the calculation of hydrodynamic forces methods and analytical techniques. Ship hydrodynamics is the specific application and development of fluid mechanics theory in ship science, so the latest research results of hydrodynamics can promote the development of ship hydrodynamics. The reliability and accuracy of the prediction results are the keys to ensure whether the optimization algorithm can search in the correct direction in the design space. It is also one of the key scientific problems to be solved first in the design and development of new ships. The fluid mechanics theory used to solve ship resistance can be divided into two categories, that is, potential flow theory and viscous flow theory, while potential flow theory can be divided into linear potential flow theory and nonlinear potential flow theory. Ship-type optimization of this book mainly involves linear wave resistance theory of Michell integral method and nonlinear wave resistance theory of Rankine source method. The theory of viscous flow mainly uses the CFD method to forecast the hydrostatic and wave resistance of a ship. When using the CFD method to analyze the ship's resistance, the grid form and the meshing method are the keys. Since the ship has a large variation in the attitude during the six degree of freedom, it is required that the grid near the free surface should have a high resolving power. Therefore, the structure, unstructured, and hybrid meshes in traditional CFD commercial software (Fluent/CFX, etc.) are powerless [5]. The emergence of the overlay grid (Overset Grid) has solved the problems above. In this book, the ship-type optimization based on the CFD method is also based on the RANS method to set up the numerical pool of static water and wave, researching optimization design of ship with minimum resistance based on hydrostatic resistance and wave resistance.

1.2.2 Hull Geometry Reconstruction Technology

Ship geometry reconstruction technology is a bridge between ship resistance performance evaluation and optimization methods, which is the key link to ship form optimization. Ship form optimization based on hydrodynamic theory, especially based on the CFD method, the relations between objective function (minimum total resistance) and design variables are often implicit. How to establish the connection between design variables and objective functions is the precondition to realize the ship form optimization based on CFD method. In the optimization, we first parameterize the hull geometry with few parameters. And then establish the relationship between the hull form parameters and the design variables. Next, change the design variables by using the optimization algorithm. Following this, alter the ship hull geometry using the geometry reconstruction technique. One of the basic problems in the ship hull form optimization is how to build a suitable optimization platform with fewer design variables and more hull configuration space. This book describes in detail the basic theory of hull geometry reconstruction technique based on hull form modification function and ASD free-form surface deformation method.

The hull geometry reconstruction technology can be divided into two categories according to different ship parameters. One is ship parameter method (such as the ship scale ratio, the longitudinal center of buoyancy.). It is through a series of ship characteristic parameters to express the hull geometry, such as: Lackenby transform method, parametric model method. The other is the geometry modeling technology. It realizes the hull geometry reconstruction through a series of control point position changes. Here are some commonly used methods like Bezier Patch method, free deformation method (FFD), and ASD method. Any kind of hull geometry reconstruction methods requires a wider geometric deformation space with fewer design variables; that is, to generate as many different geometry as possible, but to ensure the smoothness of the resulting ship. In recent years, a number of softwares which can realize parametric modeling of ship form has appeared. They have eliminated the need for designers to program and have greatly improved the convenience of ship form optimization. Some commonly used CAD software (UG, Pro-E, CATIA, and so on) can rebuild hull geometry reconstruction through the second development technology and the written interface program. The Friendship is a parameter modeling software specially designed for ship-based optimization, combined with SHIPFLOW can realize ship hull optimization quickly. It is widely used now.

1.2.3 Approximate Technology

Ship form optimization based on hydrodynamic theory involves many disciplines and is a highly complex system science. Therefore, in the process of optimization, it also needs to consider multi-disciplinary coupling, design variables, and nonlinear constraints. Moreover, each optimization needs iterative computation of the objective function multiple times. If it is a high-precision solver like CFD, it will take a lot of computing time. Therefore, if it is difficult to complete rapid optimization in the stipulated time, its practicality will be greatly reduced. How to solve the massive numerical calculation based on hydrodynamic theory in the optimization of ship form is the prerequisite for the application of ship-type optimization engineering. There are two main approaches: one is to use high-performance computers by improving the computer hardware. Due to large amount of capital required by this method, individual studies are very difficult to do and will therefore limit the development of CFD-based ship-based optimization. The other is an approximation technique, which is an effective way to solve the above problems. This method is a comprehensive application of experimental design, mathematical statistics, and optimization techniques. Through multiple analyzes of learning data, it can simulate the design space and obtain the implicit expression of the objective function. The essence of approximation technique is to construct approximate functions, and through the optimization of the sequence, the approximate optimal solution of the optimization problem is obtained by multiple iterations. It can greatly reduce the computational workload in the optimization process and lower the computational cost. At present, the commonly used approximation techniques are response surface method (RSM), variable fidelity model (VFM), kriging model, radical basis function (RBF), and so on. In addition, ISIGHT, a multi-disciplinary optimization platform, also provides a wide range of approximation techniques that researchers can use as needed and is very handy.

1.2.4 Optimization Method

The traditional gradient-based optimization algorithm has obvious shortcomings and deficiencies when applied to ship linear optimization design. Ship-type optimization involves rapid, weather-resistance and maneuverability and many other disciplines. There is no expression between each of the performance indicators (the objective function) and the design variables across disciplines (unable to derive analytic expressions). Gradient information can only be obtained by numerical analysis, and the computation is very costly. For strong nonlinear problem, such as ship-type optimization, gradient-based optimization tend to converge far away from the optimal point. Moreover, it can only guarantee the convergence to the local optimal solution, and the optimization results are very sensitive to the initial point selection. Modern optimization algorithms, such as genetic algorithm, simulated annealing algorithm, particle swarm optimization algorithm, and BP neural network algorithm, have strong global search capability and can quickly approach the global optimal point. However, its local search ability is poor. To find the global optimal point finally, it needs a lot of calculation objective functions and the computational workload increases greatly. Therefore, it is necessary to fuse the two optimization methods and use the advantages of each algorithm to form an efficient hybrid global optimization algorithm, which we called the global optimization algorithm.

These algorithms include the hybrid of genetic algorithm and nonlinear programming method and the combination of genetic algorithm and simulated annealing algorithm. Due to the enormous workload of CFD-based ship optimization calculation, how to adopt scientific optimization strategy to solve the problem of high response time and high computational cost caused by high-precision CFD solver is also a focus of current research in this field, and a key scientific problem that must be solved in ship-type optimization design based on SBD technology. In this book, nonlinear programming, genetic algorithm, and niche genetic algorithm are used to study ship form optimization based on potential flow theory. BP neural network algorithm, Elman neural network, particle swarm optimization algorithm, and improved particle swarm optimization algorithm are used to optimize the ship form design based on the unsteady RANS method. The particle swarm algorithm is applied to optimize the navigation control.

1.2.5 Integrated Set Technology

Ship-based optimization based on hydrodynamic theory is a systematic project involving CAD technology, CFD technology, optimization methods, and computer network technology, etc. How to integrate the above modules to form a unified interface optimization platform is also a key to the realization of optimization process automation. Currently, there are two main methods of integrated technology: one is that all modules are their own programming. This requires a very strong computer language ability, which is difficult for the general individual or unit to achieve, and time is longer. The other is the optimization platform: ISIGHT and OPENFOAM. Taking ISHIGT as the optimization platform is relatively mature; most of the current researchers use this platform for integrated synthesis, such as: Liu Zu-yuan from Wuhan University of Technology [6] integrated SHIPFLOW software based on ISHIGHT platform and, through the self-compiled interface program, optimized the hydrodynamic design of ship. OPENFOAM is a CFD open-source code that can be secondary developed. The main domestic set of ship CFD calculation and optimization developed by Shanghai Jiao Tong University Wan De-cheng team [7] is called naoe-FOAM-SJTU. This book through the FORTRAN language self-compiled algorithm program or interface program, respectively, based on the Michell integral method and Rankine source method for the minimum wave resistance ship line optimization design. It can verify the reliability of the theoretical optimization results through model validation and construct minimum hydrostatic resistance optimization platform based on the potential flow theory. On the ISIGHT optimization platform, the CFD resistance calculation module and the CAD geometric reconstruction module are integrated, and the program interface between the modules is compiled. It also studies on ship optimization based on the ship hydrostatic resistance and wave resistance of unsteady RANS method and the optimization of optimum trim of navigational control during actual navigation, to construct the control and optimization the framework of ship-based SBD design and real ship navigation based on RANS.

1.3 Basic Method of Hull Line Optimization

This book uses the method of theoretical optimization and experimental verification (potential flow theory) to study the minimum hydrostatic and wave resistance of ship-based optimal design. It respectively takes Michell integral method, Rankine source method to calculate the sum of wave resistance and flat frictional resistance and hydrostatic total resistance and wave resistance calculated by unsteady RANS method as the objective function. It takes the control parameters (ship modification function and ASD free-form surface deformation method) which reflect the shape change of the hull as the design variable, the restriction of displacement as the basic constraint and then considers other additional constraints. It combines nonlinear programming method, genetic algorithm, and niche genetic algorithm to study ship optimization based on potential flow theory. The BP neural network algorithm, Elman neural network algorithm, particle swarm optimization algorithm, and improved particle swarm algorithm are combined to study the optimization of ship design based on the unsteady RANS method and the optimal pitch navigation optimization problem. Hull linear optimization design program with independent intellectual property rights is developed. Taking four typical ship types as the research objects, such as Wigley, S60, DTMB5415, and KCS container ships, we optimize the calculation to obtain the theoretical linear optimal ship, and then use them as a basis for real ship navigation optimization. Finally, the validity of the theoretical optimization is proved by the model test (potential flow theory), so as to construct a ship-based SBD design and a real-frame optimization design framework based on hydrodynamic theory. The specific research methods are as follows:

(1) Hull geometry reconstruction technology

Based on Michell integral method of ship form optimization, since the expression of the objective function contains the ship type (type value), its file can be directly inputted for optimization. Ship form optimization based on Rankine source method is, because of the implicit expression relation between objective function and design variable, more difficult to optimize the wave resistance directly. Therefore, it is necessary to associate the objective function with the design variable by using the ship modification function, and then, the hull form is optimized for the design variables by the parameters of the ship modification function. In addition to the implicit relationship between the objective function and the design variables, the ship-type optimization based on the RANS method also requires parameterize the model and automatically divide the mesh after reconstruction. The hull form optimization based on CFD in this book is the hull geometry reconstruction using ASD free-form surface deformation method.

(2) Numerical evaluation of resistance

The accuracy of numerical evaluation of hydrodynamic theory has a direct impact on the reliability of the optimization results. The Michell integral method and the Rankine source method are used to calculate the wave resistance in this book. Because the method is based on linear and nonlinear wave-making resistance theory, the calculation accuracy for slender ships or high-speed ships is high, and it can meet the requirement of engineering accuracy. Because of the large proportion of the wave resistance in this type of ship, it takes the minimum wave resistance ship as the main target, and the optimization design is more practical. Moreover, based on Michell integral method and Rankine source method, the calculation speed is fast, and the optimal ship form can be quickly obtained. This book takes Wigley ship, S60 ship model, and DTBM5415 ship model as the example to evaluate and optimize the resistance. The high accuracy of RANS method based on viscous theory has long been confirmed by engineering practice. In addition, it is very difficult to evaluate the resistance of a ship by using CFD method, and then optimized the algorithm combined with the optimization design. The time of the calculation is too much to accept. However, its calculation accuracy is higher, especially for some mast or unconventional ship type, whose resistance composition is more complicated, so the CFD method is still needed to optimize the ship form. Especially in recent years, with the enhancement of computer storage capacity and calculation speed, the ship-type optimization based on CFD can be realized by adopting workstations and servers.

A numerical tank based on unsteady RANS method is established in this book, using the VOF method to capture the free surface and the turbulence model is k-ε two-equation models. It uses the volumetric center finite difference scheme discrete control equations, the second-order Euler backward difference format is used for the time term, the second-order hybrid finite difference format is used for convection term, the second-order central difference format is adopted for viscoelastic flow. SIMPLE algorithm is used to solve the RANS equation and continuity equation. Based on the RANS method, the numerical calculation method of hydrostatic (wave) resistance and motion response of the ship are finally obtained through the given boundary conditions and initial conditions, combined with six degrees of freedom equations of motion.

For the numerical solution of ship wave resistance and motion response, the key technologies are automatic mesh generation and free surface simulation method. In this book, the overlapping grid technique is used to simulate the six degree of freedom ship movement, using a single VOF method to simulate the free surface. For the hull and watershed area in this book, the structure overlay grid technology is used to perform the grid layout and generate the calculation grid. In the grid strategy, a stationary Cartesian rectangular grid is used to ensure the free surface grid resolution. The hull adopts the dynamic body-fitted grid, and the prototype and all deformed grids adopt a unified topology. In the process of calculation, as the hull moves continuously, the relative position between the hull mesh and the background mesh is constantly changing, resulting in the change of the overlapping area between the grids, and the flow field information exchange between the grids should be carried out at each time step. At the same time, the search of the cave boundary and internal and external boundary contribution units should be carried out at each time step. Therefore, the key to improve the computation efficiency of dynamic structure overlay grid lies in the establishment of cave boundaries and contribution unit search.

(3) Optimization algorithms and approximation techniques

Based on the Michell integral method and the Rankine source method, this book separately studies the minimum wave resistance ship and the minimum total resistance ship based on the nonlinear programming, genetic algorithm, and niche genetic algorithm. The real physical model is directly used as an objective function optimization without the use of approximation techniques. Based on the RANS method, the minimum hydrostatic resistance ship type and the minimum wave resistance ship type are studied based on BP neural network (improved neural network), Elman neural network, and particle swarm optimization (improved particle swarm optimization), respectively.

Because of the complexity of the physical model based on CFD ship model optimization, it is necessary to adopt approximate models instead of real physical models to achieve CFD-based optimal design of minimum resistance ship and the optimization of navigation control.

(4) Integrated technology

Ship optimization for Michell integral method and Rankine source method realizes the entire optimization calculation by self-programming. For the RANS method of ship optimization, the optimization integration platform ISIGHT is needed, the various modules will be integrated to complete the hull form optimization, and the framework of hydrostatic resistance design based on CFD and the framework of optimization of minimum wave resistance based on CFD are constructed respectively. Finally, taking the optimal navigation pitch as the design variable, a ship design framework with the best comprehensive navigation performance is constructed.

1.4 Research Progress of Ship Form Design and Optimization of SBD Technology at Home and Abroad

1.4.1 Ship Form Optimization Based on Potential Flow Theory

Under the load conditions, the determination of the optimum hull shape (lines) is both a complicated and critical design technique in ship design as it directly affects the ship rapidity (resistance and propulsion), maneuverability, and seakeeping performance, etc. The determination of hull shape with the least resistance is the first goal pursued by ship designers [8, 9]. The past ship line design, mainly through the successful mother ship, based on the designer's experience and the comprehensive method of ship model test to complete, which takes a lot of time and cost, and has great limitations. The real ship-based optimization is target-driven design to meet the four major factors: the objective function (e.g., minimum resistance), design variables (the bridge connecting the ship and the objective function), constraints (optimization range and constant region), and optimization methods (traditional optimization method, modern optimization method, and hybrid optimization method) and finally get ship geometry with the best performance. The optimization model is shown in Fig. 1.4. With the continuous progress of fluid mechanics theory and the rapid development of computer technology, it is becoming possible that the hull linear optimization design based on hydromechanics theory. Countries with advanced shipbuilding technologies such as Europe, the USA, Japan, and South Korea have applied their research achievements in actual ship design. However, some ship design departments in our country still adopt the traditional empirical design method to design ship hull lines. This situation is very unfavorable to the rapid development of the shipbuilding industry.

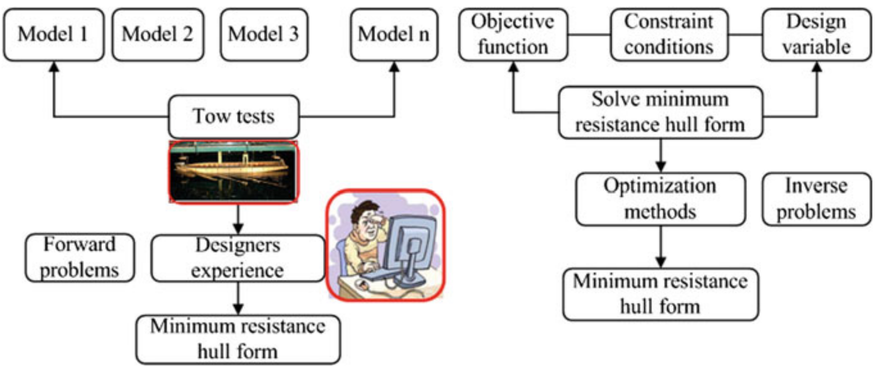

Fig. 1.4 Comparison of the ship design modes

Therefore, in order to enhance the competitiveness of China's shipbuilding industry in the international market and improve the shipbuilding capability of China's shipbuilding enterprises, it is urgent to study how to quickly generate a hull linear optimization design with excellent resistance to drag method to develop the hull line optimization design software with independent intellectual property rights.

Based on the theory of linear wave resistance, the research of ship-type improvement and optimization design has been carried out at home and abroad. Bian Bao-qi, an American Chinese, proposed the theory of "application of wave resistance theory to design hull alignment" in 1967, which caused a world sensation [10]. Japanese scholars Rongchang Farm (1972), Di Xiao Xing (1978), Masao Matsui (1980), and others were put forward to improve the use of waveform analysis of the ship. The method adopted was ship planning in the form of a complement to the thin-walled theory and waveform analysis data. The method of Rongmai and Masahiro Matsui only needs data of one ship model, and the method of Diochangxiao requires optimization of the model and requires a series of model test data for multiple ships, and is only applicable to the improvement of the second half of the hull [11]. CC Hsiung of Canada firstly proposed the method of expressing the hull surface by Tent function, and used the Michell integral method to carry out the calculation of the wave resistance value, and expressed the wave resistance of the ship as a function of its type value to form the quadratic programming problem for ship-type optimization [12, 13].

In China, Ye Heng-kui firstly explored the optimization problem of the minimum wave-making resistance ship based on linear wave theory. The wave resistance is calculated by Michell integral method, referred to C.C.Hsiung's Tent function to express the hull surface. The constrained optimization problem is transformed into an unconstrained one by using the mixed penalty function method. This method is simple, easy to operate, easy to program implementation, less demanding on objective functions and constraints, and applicable to a wide range of applications [14]. The concept of equivalent thin-vessel was put forward by Xia Lun-xi and Liu Ying-zhong and they improved ship form on the basis of this concept [15]. Huang De-bo substitutes the half-width function of the hull represented by the unit tent function into the Michell integral formula to calculate the wave resistance coefficient and has carried on a successful optimization design study on a high-speed ship type [16]. Using the Mathieu function, Pan Zhong-qing and Du Shao-qiu et al. described the wave resistance as the integral of the area curve based on the linear wave theory and the straight-wall assumption and introduced the infinite water depth boundary to improve the ship type under given ship speed and prismatic coefficient and reduce the resistance [17]. Zhang Xuan-gang and Dou Shao-qiu broke through the shortcomings of tent function in characterizing the sparse and large approximation of hull surface meshes in terms of ship type. They have conducted fruitful studies on the application of B quadratic spline function to calculate the wave resistance of high-speed catamaran and improve ship form [18]. Shi Zhong-kun and others modified the theory of amplitude function by combining linear wave theory and waveform analysis and adopted nonlinear programming method to optimize the design of high-speed ships [19]. A lot of researches had been done by Ma Kun and Tanaka Ichiroa [20–23] on the optimization of ship types with the minimum resistance based on the wave resistance theory. They studied the design methods of the ship with the least wave-making resistance and the ship with the lowest total drag and take the control of the tail viscosity separation as the constraint condition, and the minimum total hull resistance is taken as the objective function. This not only simplifies the calculation of the model, improve the speed of operation, but also consider the influence of the tail viscosity. In addition, Ji Zhuo-Shang, Lin Yan, Huang Qing, and others have made a great deal of researches on optimization of hull type based on linear wave resistance [24–28].

The above researches are mainly based on the Michell integral method and the waveform analysis method in the linear wave resistance theory, and the nonlinear programming method is used to optimize the shape of the front part of the ship. However, due to the simplified assumption of surface conditions and free surface conditions by linear theory, the calculated results are quite different from the experimental ones in values. In particular, the theory of linear wave resistance excessively exaggerated the "peak" and "valley" values of wave resistance. However, it is of theoretical value and practical significance to qualitatively determine the merits of the hull profile (especially medium-speed and high-speed vessels) by using linear wave-making resistance theory and to improve the ship form.

After entering the 1990s, people began to use the Rankine source method of the potential flow resistance theory combined with the optimization technology to optimize the ship shape and achieved a good reduction in the resistance [29]. Among them, the most representative is the Japanese scholar Suzuki Kazuo's ship form optimization method. His work mainly goes through two stages of Rankine source method of wave resistance numerical calculation and the optimization design based on the Rankine source method of minimum wave-making resistance ship form. The towing test is carried out to verify the effectiveness of the proposed method [30]. In his method, the wave resistance theory is based on the Rankine source method, and the hull modification function adopts a double trigonometric series. The optimization technique adopts a sequential quadratic programming. Suzuki Kazuo also used this method to optimize the design of HTC-type container ships. After designing Fr = 0.305, after $3 \sim 5$ iterations, the resistance of the improved ship's hull has been reduced by about 16%. From his research work, it can be seen that the optimization of ship form based on Rankine source method has both theoretical value and practical significance. In recent years, a number of research institutes in China have also made considerable progress in forecasting ship hydrodynamic performance and optimizing ship shape based on Rankine source theory. Cheng Ming-dao and Liu Xiao-dong have achieved better results in the optimization of the stern sealing plate by using the linear wave numerical method. Chen et al. [31] Liu et al. [32] Chen Jing-pu improved the Dawson method for the trimaran hull layout optimization, but also applies the developed linear wave numerical method to the linear optimization of the container ships [33].

The biggest problem caused by Rankine source method is the long calculation time. Because the Rankine source method cannot express the hull and wave resistance directly, the calculation of the positive problem must be repeated after the ship type is given in the process of optimization iteration, which leads to the increase of the computational workload. As a result, Akawa Hiroshiki used the characteristics that the modified ship type is similar to the mother one to approximately satisfy the surface conditions in the calculation of wave resistance on the mother ship. Thus, in the optimization process, no matter how the ship type changes, the grid only needs to be constructed once, which saves a lot of computing time. Raven of MARIN, the Netherlands, adopted the method of increasing the surface area and iteratively solving the problem. In the early 90s, RAPID, a numerical calculation and optimization software for ship wave resistance, was successfully developed, which solved the nonlinear potential flow problem. The main purpose of using RAPID software to optimize ship form is to reduce wave formation and wave resistance, which has become a common design tool of MARIN [34–36]. At present, although the theory of nonlinear wave resistance has been developed to a certain extent, it is more realistic, based on the theory of potential flow wave resistance, to base on Rankine source method for the optimization of ship form based on resistance performance.

Most of the mentioned ship shape optimization studies are based on nonlinear programming method. In general, such ship shape optimization processes tend to have relatively weird shapes with no practical significance. However, it is easy to understand deeply from the mechanism that the influence of hull line changes on the resistance performance. This is of great significance to clear the direction of optimization and guide the design modification. In order to obtain a practical model, according to the experience in the refinement process, add the appropriate constraints so that the optimized ship profile is closer to the practical model and re-optimization calculation is carried out again.

In this book, the optimal design method of hull lines with excellent resistance performance is developed in the part of potential flow theory, in order to develop the hull line optimization design software with independent intellectual property rights. The optimal design object is not only limited to the front half, but also the overall linear of the hull under the waterline, including the second half, as the optimal design object. To this end, the theory of wave resistance, viscous theory, optimization technology, and CAD technology are organically combined to study the optimization design method of ship line and to develop the optimization design program of hull line type. In the optimization calculation, the main purpose of reducing the wave resistance is to control the tail sticking separation as the constraint condition. The hull shape value of the designed ship is expressed by the mother ship value and the ship modification function. The optimization calculation method adopts the nonlinear programming method which is more mature in ship form optimization. The Rankine source method with better calculation precision is adopted to calculate wave resistance.

1.4.2 Optimization of Ship Form Based on Viscous Flow Theory

With the rapid development of computational fluid dynamics (CFD) and CFD, it is possible to develop high-performance hulls quickly and efficiently [37, 38]. In the field of ship rapid performance calculation, CFD has become a new method of design and optimization of ship profile and has been widely applied abroad. Compared with the previous equipment of making a ship model and then carrying out a tank test, the time and cost of developing a ship can be greatly reduced. It is also beneficial to improve the performance of the developed ship model, and greatly reduce the dependence on the model test tank. The effect of applying the CFD method to the hydrodynamic performance of a ship depends primarily on the mathematical model level of the CFD program. It should be pointed out that the CFD method does not completely replace the model test, but it can reduce the scope of the model test and provide useful information for the line optimization [39, 40]. However, due to the use of CFD technology to evaluate the resistance of a ship requires several hours, if combined with the optimization technology to explore the minimum resistance ship is difficult to achieve practicality. Therefore, when CFD is applied to ship form optimization from the very beginning, it is mainly to analyze and evaluate several ship-type schemes generated in advance, and select the ship-type scheme with better performance.

The design of ship SBD based on RANS method and the optimization of real ship navigation are a new research direction that emerges with the continuous improvement of CFD theory, the rapid development of CAD technology and optimization theory, as well as the drastic increase of computing speed and storage capacity. It breaks through the scheme optimization of traditional CFD optimization technology and truly achieves the goal of performance-driven design and promotes the ship-based design from traditional experience mode to the knowledge-based and intelligent based on numerical simulation technology. The basic optimization framework is shown in Fig. 1.5.

After more than two decades of development, the importance and superiority of this technology have drawn the great attention of all countries. They have invested a

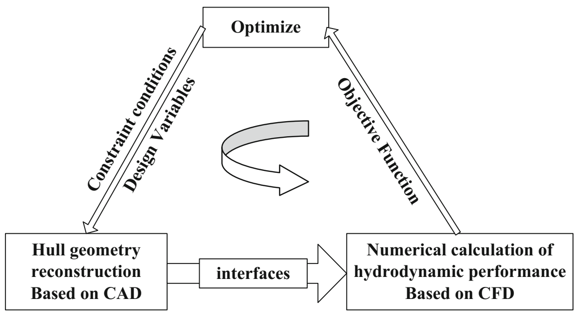

Fig. 1.5 A comprehensive optimization process of hydrodynamic performance based on CFD technology

great deal of manpower, material, and financial resources in research and a series of achievements have been published one after another. Abroad, Professor Campana [41–45] at the INSEAN pool in Italy firstly combined optimization theory with CFD technology to study the optimization of ship hydrodynamic performance based on SBD technology. In recent years, Prof. Campana, Peri, and their group have carried out a lot of research work on the optimization design of hydrodynamic performance (resistance and seakeeping) of ships based on SBD technology. They made a systematic research on the hull geometry reconstruction technology, approximation technology, optimization strategy and integrated technology and developed the disturbance surface method based on Bezier Patch surface to realize hull geometry reconstruction. They apply the approximation technique of variable fidelity model to solve the multi-objective optimization problem, establish a ship-based optimization design framework based on SBD technology, and verify the optimization results by model tests, and the obtain an improved ship model with excellent hydrodynamic performance, confirming the superiority of SBD technology. Professor Tahara [46–50], University of Tokyo, Japan, used the ship design software NAPA for ship parametric expression. CFD software FlowPack was used to calculate the propulsion performance and handling performance. On the self-developed integrated optimization platform, the ball of the container ship was completed and the experiment was carried out. Professor Harries et al. [51], from Berlin University of science and technology in Germany, developed Friendship, full parametric commercial CAD software, to parametrically model the hull. His comprehensive integration on the Mode Frontier optimization platform completes the multi-disciplinary and multi-objective optimization of hydrodynamic performance of the ship, using experimental techniques and approximation techniques in the design process. In addition, Ho-Hwan [52] used the self-compiled RANS method as the solver and the parametric model method to realize the geometric reconstruction of the hull. Sequential Quadratic Programming SQP and Particle Swarm Optimization (PSO) were used to optimize the calculation respectively. Gregory [53] integrated the CAD software Friendship-Modeler with the CFD software SHIPFLOW, and studied ship form optimization problem using Genetic Algorithm GA. Zalek [54] carried out a detailed summary of the research progress on the optimization design of foreign ships and carried out the multi-objective optimization design of ships based on the fastness index and seakeeping index as the objective function. Peri, Tahara, Campana and others [55–57] used two kinds of multi-objective global optimization algorithm (Multi-Objective Genetic Algorithm MOGA and PSO algorithm) respectively for high-speed catamaran under single speed target (resistance) multi-point design, single-objective optimization design (corresponding to three speed-weighted), and multi-objective optimization design (resistance and surge). The reconstruction of the hull was carried out by FFD method and CAD method, respectively. The CFDSHIP software was used for numerical calculation, and the optimization results were verified by the model tests. Kim et al. [58] used SHIPFLOW software to calculate the hydrodynamic performance of single-fin and double-fin LNG vessels, reconstructed the geometry using Friendship software, and optimized the integrated platform through optimization and verified by model tests.

Soonhung et al. [59] proposed fairing B-spline parameter curve to realize geometric parametric expression of ship hull, and realized hull geometry reconstruction of LPG ship through the conversion function. He Jim [60] established a multi-disciplinary optimization design model of ship resistance, seakeeping, and maneuverability. Resistance performance is the main objective function. Seakeeping and maneuverability are related to the objective function as constraints in the optimization process. Vasudev [61] established a multi-objective optimization design framework for ships. He takes the model geometric parameters as the design variables and takes the viscous drag calculated by CFD software SHIPFLOW as the objective function, using the Nondominated Sorting Genetic Algorithm (NSGA-II) as the optimization method and optimizing the design of an intelligent water robot.

At present, there is not any formal publication of the research achievements on the optimization of wave resistance based on the CFD method. However, in numerical simulation, there are a lot of overseas research achievements, which can lay a foundation for the future ship optimization. The more representative ones are as follows. Orihara and Miyata [62] and their group solved the RANS equation by the finite volume method and simulated the wave resistance and motion response of a container ship in a regular wave by using the overlapping grid technique. Carrica et al. [63] calculated the large-scale motion response of DTMB5512 at middle and high speed using overlapping mesh technique. Tezdogan et al. [64] used the unsteady RANS method to evaluate the wave resistance and movement of a container ship during low-speed sailing. It can be seen from the above literature that breakthroughs have been made in the key technologies of SBD ship design optimization such as hull geometry reconstruction technology, high-precision CFD numerical simulation technology, optimization strategy, approximation technology, and integrated technology abroad. A series of commercial software come out one after another and the research results have been applied to the actual ship design. However, the above-mentioned ship-type optimization objective function is basically the hydrostatic resistance, and does not consider the ship’s actual navigation in the wave resistance and the impact of ship movement on the resistance, and does not take the ship’s propulsion and maneuverability and other actual navigation on the optimization effect of the result into consideration as well.

In China, from the late 90s onwards, the design and optimization of ship SBD based on the RANS method has been developed rapidly. The main purpose is to forecast the hydrostatic resistance prediction and optimize the scheme for a given ship type. Chen [65] applied ShipFlow software to select and optimize a catamaran of a small waterline through a series of hull elements such as hull draft, main body shape, body spacing, and pillar length. Xu [66] used CAD–CFD integrated platform Friendship–Framework for automatic deformation, and then selected and optimized by CFD software ShipFlow.

In recent years, with the application of optimization theory in the field of shipbuilding and the development of parametric expression technology of hull, people began to integrate CFD numerical simulation software, and ship geometry reconstruction technology on the commercial optimization platform to carry out the optimization design of the ship with the minimum resistance. Liang [67] used OPTIMUS 5.2 optimization platform to integrate GAMBIT software and fluent software and applied experimental design methods to reduce the number of calculations and established a ship-based optimization strategy based on the response surface model and the optimization of the headline of a submarine was automatically optimized, and the effectiveness and feasibility of the optimization method were verified through model tests. Chang et al. [68], Xie et al. [69], Huang and Feng [70], Su [71] studied the linear multi-disciplinary optimization design of hull based on CFD, integrated the ship geometry reconstruction technology, and CFD software SHIPFLOW with the commercial optimization platform ISIGHT. The application of approximation technology in ship form optimization can improve the optimization efficiency, and the research results have certain engineering practical value. Qian et al. and so on [72, 73] used ISIGHT optimization platform to integrate CFD technology, ship form transformation and automatic generation technology and response surface model, and adopted a hybrid optimization algorithm to carry out ship-type optimization design with minimum resistance as the optimization objective. Shahid [74] studied the ball-head optimization design based on CFD. The total resistance calculated by Fluent was taken as the objective function, and the automatic transformation and meshing of different ball-head shapes were realized by using GAMBIT software. With the optimization of the genetic algorithm in the MATLAB toolbox, an effective CFD-based ship form optimization tool is obtained. Li [75] constructed an optimized design framework of ship hydrodynamic configuration based on SBD technology, focusing on Bezier Patch local geometric reconstruction method and FFD global geometric reconstruction method and PSO optimization algorithm, and solved the problem of automatic generation of complex mesh.

In the aspect of comprehensive navigation performance optimization, people begin to establish the relationship between ship navigation performance and ship-type parameters according to the regression formula of series of ship model test results and carry out ship-type optimization design in the stage of ship design.

Wang et al. [76] proposed a multi-objective ship-type optimization system that minimized the wave resistance and the wave drag increasing, and calculated the sum of the wave resistance calculated by the CFD software and the sum of wave drag based on the potential flow theory as the goal. The full parameterized model is established in Friendship software, and the above modules are integrated through a self-programming interface. The feasibility of this method for the optimization of wave resistance ships is verified by an example of an oil tanker. Zhang [77] studied multi-disciplinary optimization of shipboard vessel in waves of container ships based on Energy Efficiency Design Index EEDI. It takes the navigation performance (wave resistance, EEDI energy efficiency index) as the objective function in the wave and the full parametric model based on the ship's wave resistance standard, and uses the ISIGHT multi-disciplinary optimization platform to carry out integrated integration, which can be used in different optimization strategy to complete the waves in the ship-type optimization. Zhou [78] studied the high-performance ship optimization design method based on the EEDI energy efficiency index. Taking the two important factors influencing the ship energy efficiency index (EEDI) as speed and load capacity, a multi-objective genetic algorithm (Matlab) toolbox was used to optimize the model. The results show that the energy efficiency level of the ship can be effectively improved in the early stage of high-performance ship design. Based on SBD technology, Sheng-Zhong [79] combined with global optimization algorithm, hull geometry reconstruction technology and high-precision RANS method, and established a multi-objective optimization platform for ship navigation performance. Taking a bulk carrier as an example, the total resistance and propeller flow fraction of the propeller disk are taken as the objective function to optimize the calculation. The total resistance of the improved ship is reduced by 5%, and the navigation performance is remarkably improved.

No research results have been published on ship-type optimization based on minimum wave resistance, but significant results in wave resistance calculation can provide technical support for ship form optimization. Shen et al. [80] and his team developed the naoe-FOAM-SJTU solver based on the open-source code OPENFOAM. In the solution process, the VOF (Volume of Fluid) method is used to capture the free surface based on the RANS method, the SST (Shear-Stress Transport) K-W turbulence model is introduced to deal with the viscous flow and the PISO method is used to deal with the velocity–pressure coupling problem. The heave and pitching motion of the DTMB 5512 ship in regular waves and waves with different wave heights are calculated, and the calculation of wave drag is also discussed. Zhao et al. [81] developed a RANS-based CFD hydrodynamic performance calculation system based on overlapping grids, which can well simulate the resistance and response of ships during the movement. Based on the viscous theory, Shi et al. [82] established a three-dimensional numerical wave-making tank and realized the numerical simulation of the wave motion of the ship model in irregular waves.

The domestic tracking of the international front, the commercial CFD numerical simulation software to calculate the total resistance is as the goal, using parametric modeling methods, stacking and reconciliation method for the geometric reconstruction method, the use of optimization algorithm toolbox or commercial optimization platform (such as ISIGHT) for synthesis integrate and construct SBD-based ship-type optimization system and achieved some results. In the aspect of navigation performance optimization, the regression formula is mainly used to establish the navigation performance optimization formula. In recent years, the wave resistance and energy efficiency index EEDI have been used as the objective function, and the optimization design has been carried out on the commercial optimization platform based on the wave resistance transverse standard.

However, the wave resistance calculation is limited to the potential flow theory and does not evaluate the energy-saving effect after the optimization of the actual ship form. According to the research progress at home and abroad, we can see that the foreign scholars have established the theoretical framework of ship navigation performance optimization system based on SBD technology and made breakthroughs in key technologies to achieve the boat-type optimization model driven by performance-driven design. From a single resistance to multiple performance (seakeeping, maneuverability) of the integrated optimization, optimization of ship type can also be obtained from a simple mathematical ship (Wigley ship, Series 60 ship) to more practical ships. The ship resistance optimization based on RANS method has been basically implemented in China and has been applied to the actual ship design. However, it is mainly dominated by single-objective optimization or simple multi-speed target optimization and does not give multi-speed resistance optimization or multi-speed optimization involving navigation (high-speed craft such as container) nor effect evaluation in waves (while in fact the ship is navigating in the waves).In addition, there is no evaluation on the energy-saving effect under different loadings for this optimized speed, namely, real ship navigation optimization. Therefore, in the part of viscous flow from the actual operation of the ship, this book studies the key technologies of the ship SBD design and the real ship navigation optimization system based on the unsteady RANS method, including: an overall performance evaluation system based on unstructured RANS method for structural overlapping grids, ship hull geometric reconstruction based on ASD freedom surface deformation method, the optimization mechanism of BP neural network, Elman neural network and particle swarm optimization algorithm, and approximation technology based on neural network and CFD parallel computing technology, developing a real ship navigation optimization design system with independent evaluation and optimization by numerical valuation.

The unsteady RANS method is used to calculate the hydrostatic resistance and wave resistance as the objective functions, taking the parameters reflecting the shape change of the hull as the design variables and the displacement as the basic constraint, and then consider the propulsion (i.e., propeller nonuniformity.) and maneuverability index and other additional constraints, combined with the optimization algorithm for ship-type optimization design. In addition, the optimization of navigation control with minimum trim value at design speed is studied to obtain the optimal navigational performance of the ship, which lays a theoretical foundation for the real optimization of the real ship navigation system.

1.5 Research Project

The general research plan of this book is shown in Fig. 1.6.

First, according to the input data of the mother ship, including the type table, the main scale, and other parameters of the hull geometry parametric expression and modeling. For the Michell integral method, the hull type value can be used directly

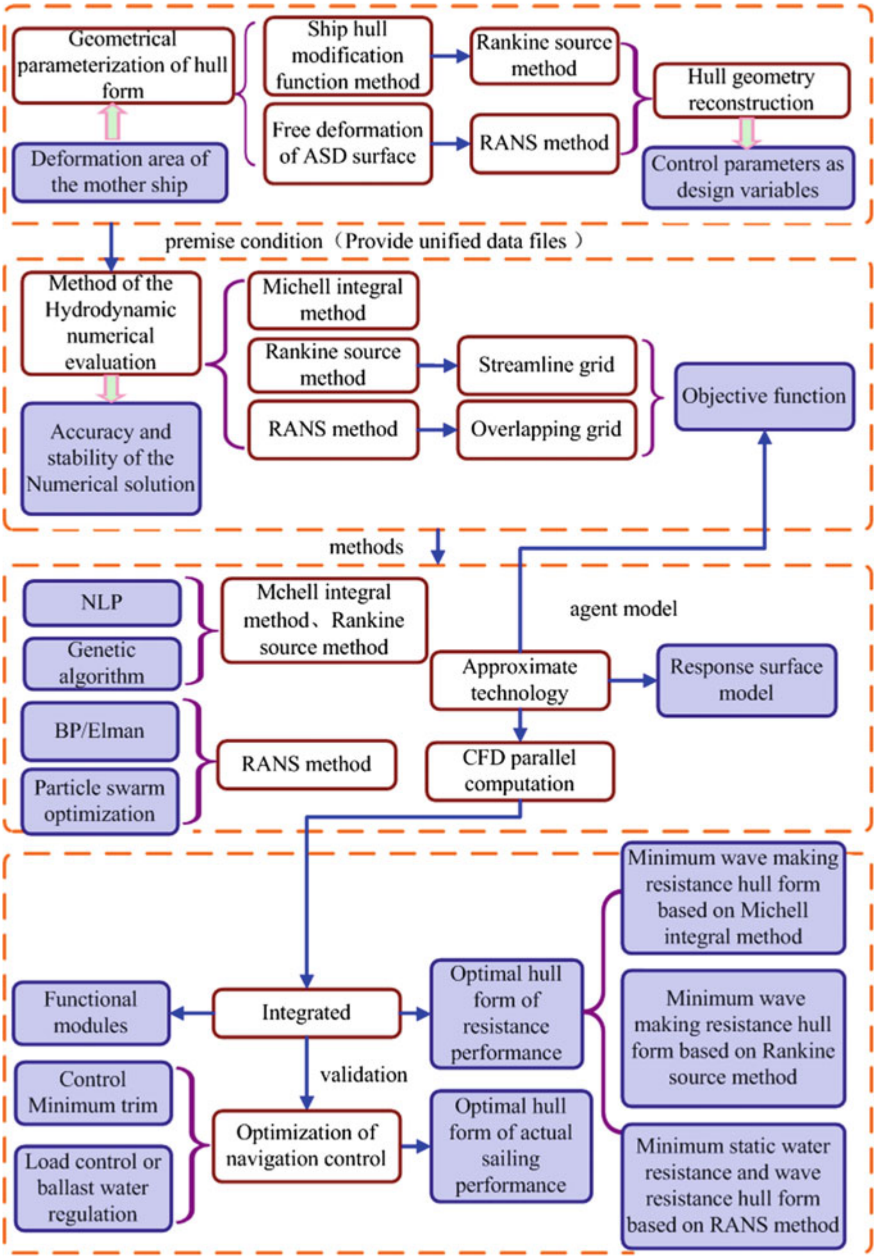

Fig. 1.6 Overall research program

as the design variable because the ship shape value and the wave resistance expression have been linked when expressing the ship type with a tent function, it is unnecessary to reconstruct the ship hull geometry. For the Rankine source method, the boat shape modification function is used to express the shape of the ship hull, and the parameters of ship modification function are taken as the design variables. For the RANS method, the ASD free surface deformation method is used to parametrically express and reconstruct the modified hull and constant part of the hull. In each optimization process, the mesh is performed, and then the deformation of the ASD freedom surface is controlled parameters for design variables, and ultimately achieves the purpose of free deformation.

Second: after reconstruction, the hull values are input into the Rankine source and RANS numerical calculation (for hull value files for Michell integral), computational modeling and grids are performed by determining the boundary conditions and the calculated domain size, the calculation modeling and automatic grid division, generate calculation grid file. The numerical accuracy and numerical stability of the numerical method are verified, and the influence of different degree of mesh density on the calculation results is confirmed. Finally, the final mesh file is determined. Numerical simulation of the design speed of wave resistance is used to calculate the hydrostatic total resistance and the wave resistance as the objective function.

Third: it uses the response surface model instead of the real physical model and studies ship-type optimization of the minimum wave-making resistance and the minimum total resistance using nonlinear programming, genetic algorithm, and niche-based genetic algorithm respectively. BP neural network algorithm, Elman neural network algorithm, particle swarm optimization algorithm, and improved particle swarm optimization algorithm are used to study the ship hydroforming optimization based on the CFD method with the minimum hydrostatic and wave resistance. The convergence and reliability of the algorithm are verified by the test function.

Fourth: integrating the above comprehensive-functional modules, using FORTRAN language to write data interface between the various modules of the program (Michell integral method and Rankine method adopt self-programming to establish optimized mathematical model. Ship model optimization of RANS method integrates CFD resistance solving software, CAD modeling software, and meshing software on the ISIGHT platform to establish optimized mathematical model). Michell integral method and Rankine source method are used to calculate the wave resistance and total resistance calculated by the RANS method hydrostatic resistance and wave resistance as the objective function to reflect the shape change of the hull shape parameters for the design variables. The basic constraint condition is the restriction of displacement. Then the optimal design frame based on hydrodynamic theory is constructed, such as minimum wave resistance, minimum total resistance, and minimum wave resistance. Through the optimization calculation of four typical hulls, such as Wigley ship, S60 ship model, DTMB5415 ship and KCS container ship, the theoretical minimum wave resistance, minimum total drag, minimum wave resistance, and the optimal trim are obtained. The research method can provide theoretical basis and technical support for the design of “green ship” and the development of new ship types based on energy conservation and emission reduction.

References

1. Zhao F, Wu C-S, Zhang Z-R (2015) Preliminary an a lysis of key issues in the development of numerical tank. J Ship Mech 19(10): 1210–1220
2. Gong M, Zhang Y, Wang X (1999) Simulation-based design and its application in auto-flight system design. Journal of Beijing University of Aeronautics and Astronautics 25(3): 288–291
3. Zakerdoost H, Ghassemi H, Ghiasi M (2013) Ship hull form optimization by evolutionary algorithm in order to diminish the drag. J Marine Sci Appl (12): 170–179
4. Li SZ (2012) Research on hull form design optimization based on SBD technique. Wu xi: China Ship Scientific Research Center
5. Wang J-H, Wan D-C (2016) Numerical simulation of pure yaw motion using dynamic overset grid technology. Chinese J Hydrodyn 31(5): 567–574
6. Liu Z, Feng Bai W, Zhan C (2010) Multidisciplinary design optimization of ship hull from. National Defense Industry Press
7. Cao HJ, Wan De-C (2013) Three-dimensional numerical wave tank based on naoe-FOAM-SJTU solver. J Fudan Univ (Natl Sci) 52(5): 627–634
8. Zhang BJ (2009) Research on optimization design of hull lines and minimum Resistance hull form. Dalian: Dalian University of Technology
9. Li ZZ (2005) Optimizaiton research of ship form based on the numerical value calculation of wave resistance. Dalian: Dalian University of Technology
10. Liu YZ (2003) Theory of ship wave making resisitance. BeiJing: National Defense Industry Press
11. Xia LX (1982) Equivalent thin ship method and its application in ship type modification. Shang Hai: Shanghai Jiaotong University
12. Hsiung CC (1981) Optimal ship forms for minimum wave resistance. J Ship Res 25(2):95–116
13. Hsiung CC (1984) Optimal ship forms for minimum total resistance. J Ship Res 28(3):163–172
14. Ye HK (1985) The wave resistance calculation and optimization of ship form with the tent function. Shipbuilding of China, 28–39
15. Xia L, Liu YZ (1984) Equivalent thin ship and ship form improvement. Shipbiulding of China, 1–12
16. Huang D, Mu J (1997) Interpretation, modification and calculation of linearized wave resistance theory. J Harbin Eng Univ 18(5): 18–14
17. Pan ZQ, Cai RQ, Du SQ (1989) A method of hull form improvement by using mathieu function. Shipbiulding of China, 44–53
18. Zhang XG, Du S, Cai R (1990) A method for the calculation of wave resistance of catamaran and hull from improvement by using biquadratic spline functions. Shipbiulding of China, 1–15
19. Shi ZK, Zheng JM, Huang Y (1991) Shipform optimization and a ship form with minimum wave tesistance. J. Huazhong univ Sci Tech 19(5): 121–128
20. Ma K, Ichiro T (1997) A study of optimal hull form for minimum resistance. J Hydrodyn 12 (1): 114–122
21. Ma K, Ichiro, T (1994) A study of minimum resistance hull form with consideration of separation (1nd Report). J Kansai Soc Naval Archit Jpn (221), 9–15

22. Ma K, Ichiro, T (1994) A study of minimum resistance hull form with consideration of separation (2nd Report). J Kansai Soc Naval Archit Jpn (222), 41–47
23. Ichiro T, Ma, K (1995) Low resistance and high efficiency of ship type determination. J Kansai Soc Naval Archit Jpn (223), 49–57
24. Ji ZS, Lishufan, GCJ (1982) An applied mixed integer programming method in ship design. J Dalian Institute of Technology 21(1): 69–76
25. Lin Y, Ji Z, Dai Y S (1996) Mathematical description and computer method for b splnie hull surface. Shipbiulding of China 4: 83–86
26. Lin Y, Zhu ZH, Jizhuo S (1997) Form description with function parameter. Shipbiulding of China 3: 74–78
27. Lin Y, Jizhuo S, Li TL (1999) Optimum approach to bulbous bow design to reduce resistance and improve propulsion. J Dalian Univ Technol 39(6): 785–791
28. Huang Q (1990) Estimation of wave-pattern resistance to ships and optimization of hull forms. J Huazhong Univ Technol 18(5): 69–76
29. Saha GK, Suzuki K, Kai H (2004) Hydrodynamic optimization of ship hull forms in shallow water. J Mar Sci Technol 9:51–62
30. Masut S, Suzuki K (2001) Experimental Verification of optimized hull form based on rankine source method. J Kansai Soc NA Jpn. 236, 27–32
31. Cheng DM, Liu XD, He SL (1999) Wave making resistance calculation of transom ship. J Ship Mech 3(1): 6–12
32. Liu XD, Li BJ, Zhu D (2003) Numerical simulation of the flow of the stern ship. Hydrodyn Res Prog A 18(2): 168–175
33. Chen J-P, Zhu D-X, HE S-L (2006) Resear ch on numer ical pr ediction method for wave makingr esistance of catamar an/tr imar an. J Ship Mech 10 (2): 23–29
34. Chen W-M, Chen X-P (2007) Application of CFD in ship hull lines optimization. J SSSRI 30 (1): 30–32
35. Raven HC (1993) Nonlinear ship wave calculations using the PARPID method. In: Proceeding 6th international conference on numerical ships hydrodynamics, Iowa City
36. Raven HC, Valkhof HH (1995) Application of nonlinear ship wave calculations in design, symp, on practical design of ships and floating structures. Seoul, Korea
37. Heimann J (2005) CFD Based optimization of the wave-making characteristics of ship hulls. Technical University Berlin, 23–42
38. Wang XF, Zhou S, Chen Z (1992) Computational ship fluid mechanics shang hai: Shanghai Jiaotong University Press
39. Deng R, Huang D-B, Zhou G-L (2008) Numerical calculation of resistance of trimarans. J Harbin Eng Univ 29(7): 673–676
40. Tahara Y, Saitoh Y, Himeno Y (1999) CFD-aided optimization of tanker stern form -1st report: minimization of viscous resistance. J Kansai Soc NA, Jpn.231, 29–36
41. Peri D, Campana EF (2003) Multidisciplinary design optimization of a naval surface combatant. J Ship Res 47(1):1–12
42. Peri D, Campana EF (2005) High-fidelity models and multi objective global optimization algorithms in simulation-based design. J Ship Res 49(3):159–175
43. Campana EF, Peri D, Tahara Y, Stern F (2004) Comparison and validation of CFD based local optimization methods for surface combatant bow. In: The 25th symposium on naval hydrodynamics, Canada
44. Campana EF, Peri D, Tahara Y et al (2009) Numerical optimization methods for ship hydrodynamic design. SNAME Annual Meeting
45. Campana EF, Liuzzi D, Lucidi S, Peri D et al (2009) New global optimization methods for ship design problems. Optim Eng 10(4): 533–555
46. Tahara Y, Sugimoto S, Murayama S, et al (2003) Development of CAD/CFD/ optimizerinte grated hull-form design system. Kansai Soc NA, Jpn, (240): 29–36
47. Tahara Y, Tohyama S (2006) CFD-Based multi-objective optimization method for ship design. Int J Num Methods Fluids 52:499–527

48. Tahara Y, Peri D, Campana EF, Stern F (2008) Computational fluid dynamics based multiobjective optimization of a surface combatant. Marine Sci Technol 13(2):95–116
49. Tahara Y, Hino T, Kandasamy M et al (2011) CFD-based multiobjective optimization of waterjet propelled high speed ships. In: 11th international conference on fast sea transportation FAST 2011, Honolulu, Hawaii, USA
50. Tahara Y, Peri D, Campana EF, Stern F (2011) Single- and multiobjective design optimization of a fast multihull ship: numerical and experimental results. J Marine Sci Technol 16(4):412–433
51. Harries S, Valdenazzi F, Abt C et al (2001) Investigation on optimization strategies for the hydrodynamic design of fast ferries. In: 5th International conference on fast sea transportation, Southhampton, UK
52. Ho-Hwan C (2010) Hull form parameterization technique with local and global optimization algorithms. In: Proceedings of MARTEC 2010 the international conference on marine technology, BUET, Dhaka, Bangladesh
53. Gregory J, Grigoropoulos, Dimitris S et al (2010) Hull-form optimization in calm and rough water. Comput Aided Des 42: 977–984
54. Zalek SF (2007) Multi-criterion evolutionary optimization of ship hull forms for propulsion and seakeeping. Michigan University
55. Peri D, Campana EF (2006) Simulation based design of fast multihull ship. In: 26th Symposium on naval hydrodynamics, Rome, Italy
56. Campana EF, Peri D (2006) Shape optimization in ship hydrodynamics using computational fluid dynamics. Comput Methods Appl Mech Eng 196:634–651
57. Tahara Y, Peri D, Campana EF, Stern F (2008) Single and multiobjective design optimization of a fast multihull ship numerical and experimental results. In: 27th Symposium on naval hydrodynamics. Seoul, Korea
58. Kim KT, Bathfield F, Nicolas et al (2014) Hydrodynamic optimization of twin-skeg LNG ships by CFD and model testing. Int J Naval Archit Ocean Eng 6(2): 392–405
59. Soonhung H, Yeon-Seung L, Young BC (2012) Hydrodynamic hull form optimization using parametric models. J Marine Sci Technol 17(1):1–17
60. Jim H, Shari H, Nickolas V (2012) Multidisciplinary design optimization of ship hull forms using metamodels. In: ASME Internationl design engineering technical conferences/ computers and information in engineering conference, Washington, DC, 847–856
61. Vasudev KL, Sharma R, Bhattacharyya SK (2014) A multi-objective optimization design framework integrated with CFD for the design of AUVs. Methods Oceanography 10:138–165
62. Orihara H, Miyata H (2003) Evaluation of added resistance in regular incident waves by computational fluid dynamics motion simulation using an overlapping grid system. J Marine Sci Technol 8(2):47–60
63. Carrica PM, Wulson RV, Noack RW et al (2007) Ship motions using single-phase level set with dynamic overset grids. Comput Fluids 36(9):1415–1433
64. Tezdogan T, Demirel YK, Kellett P et al (2015) Full-scale unsteady RANS CFD simulations of ship behaviour and performance in head seas due to slow steaming. Ocean Eng 97:186–206
65. Chen XN (2007) Research on optimization of ship form for swath. Shanghai: Shanghai Jiao Tong University
66. Xu L (2012) Optimization of ship hull resistance based on CFD method. Shanghai: Shanghai Jiao Tong University
67. Liang J (2008) Ship hull lines optimization based on hydrodynamic performance. Shanghai: Shanghai Jiao Tong University
68. Chang H, Feng B, Liu Z (2012) Research on application of approximate model in hull form optimization. Shipbuilding of China 53(1): 88–98
69. Xie L, Feng BW, Liu ZY (2011) Automatic optimization of high-speed hull forms using CFD. J Huazhong Univ Sci Tech (Ntl Sci Edition), 2011 39(6): 129–132
70. Huang J-F,Feng B-W (2012) Investigation on optimization strategies for the hydrodynamic design of DTMB 5415. In: The 3rd International conference on manufacturing science and engineering Xiamen, Peoples R China (479), 1950–1954

71. Su Z-D (2014) CFD-based hull form resistance and flow field multiobjective optimization research. In: Proceedings of the twenty-fourth (2014) international ocean and polar engineering conference busan, Korea, 15–20
72. Qian J Comprehensive hydrodynamics optimization for hull form Via MDO. Wu han: Wuhan University of Technology
73. Qian J-K, Mao X-F, Wang X-Y (2012) Ship hull automated optimization of minimum resistance via CFD and RSM technique. J Ship Mech 16(1–2): 36–43
74. Shahid M (2012) A research on the ship hull form optimization using viscous CFD and Genetic algorithm. Harbin: Harbin Engineering University2012
75. LI S-Z, Zhao F, Yang L (2010) Multi-objective optimization for airfoil hydrodynamic performance design based on CFD techniques. J Ship Mech 14(11): 1441–1448
76. Wang S, Chen JP, Wei JF (2013) The development and app; ocatopm research of an integrated optimization system based on the resistance in calm water and added resistance due to waves. In: The twenty-fifth national hydrodynamics seminar and the 12th national hydrodynamics academic conference. Zhe jiang, zhou shan, pp 928–933
77. Zhang WX (2012) Comprehensive optimization of hull form for containership in wave based on EEDI. Wu Han: Wuhan University of Technology
78. Zhou Y (2012) Research on optimization method for high performance vessel Research on optimization method for high performance vessel. Dalian:Dalian Maritime University
79. Sheng-Zhong Li, Feng Zhao, Qi-Jun Ni (2014) Bow and stern shape integrated optimization for a full ship by a simulation-based design technique. J Ship Res 58(2):83–96
80. Shen Z-R, Ye H-X, Wan D-C (2014) URANS simulations of ship motion responses in long-crest irregular waves. J Hydrodyn 26(3): 436–446
81. Zhao F-M, Gao C-J, Qiong XIA (2011) Overlap grid research on the application of ship CFD. J Ship Mech 15(5): 332–341
82. Shi B-W, Liu Z-J, Wu M (2014) Numerical simulation of ship motions in irregular head waves. J Ship Mech 18(8): 906–915

Chapter 2
Basic Theory of Hydrodynamics

2.1 Overview

Ship hydrodynamic performance evaluation technique is one of the prerequisites and key conditions for ship-type optimization based on SBD technology, which provides an effective means to establish the mathematical model of ship design optimization problem. The accuracy of the hydrodynamic performance evaluation directly affects the quality of the optimization results [1]. In the optimization process, the optimization algorithm will adjust the next search direction based on the performance prediction results. Therefore, the reliability of the performance prediction results is the key to ensure that the search direction of the optimization algorithm in the design space is correct or not, and is also directly related to the success or failure of the optimization design.

The accuracy of numerical prediction of ship hydrodynamics theory will directly affect the quality of ship model optimization. Therefore, the basic requirements of ship-based optimization based on hydrodynamic theory and numerical simulation technology are:

(1) Rapidity

In the use of hydrodynamic theory for ship-type optimization, the numerical method is required to calculate the ship's resistance performance quickly. In the optimization process, the numerical simulation method needs to constantly calculate the resistance performance according to the hull shape transformed by the hull geometry reconstruction technology, which puts forward higher requirements on the rapidity of the numerical simulation technology. In the theory of ship hydrodynamics, the potential flow theory can generally meet this requirement, so it has been widely used in the 1990s. In recent years, with the rapid development of computer technology and the improvement of mathematical knowledge, CFD-based ship-type optimization is possible, but still much slower than the potential flow theory. In particular, CFD technology strongly depends on computer hardware. In the post-financial crisis era, in the fierce market competition, who can quickly find a

© Shanghai Jiao Tong University Press, Shanghai and Springer Nature Singapore Pte Ltd. 2019

B.-J. Zhang and S.-L. Zhang, *Research on Ship Design and Optimization Based on Simulation-Based Design (SBD) Technique*,
https://doi.org/10.1007/978-981-10-8423-2_2

well-optimized ship design method and who will be able to occupy the market, thus the accuracy of ship hydrodynamics numerical simulation technology is a major issue that must be solved in CFD ship-type optimization.

(2) Accuracy

The accuracy of numerical simulation technology has a direct impact on the quality of the optimized ship. Numerical simulation of ship resistance based on the potential flow theory, such as Michell integral method and Rankine source method, is of great accuracy in evaluating some high-speed and long slender ships to meet the actual engineering requirements. In the evaluation of some special ship form, such as the mast type, the result is far from the experimental value, so the optimization results are often distorted. When using CFD technology to evaluate ship's resistance, the general will get a more accurate resistance value, without restrictions of the ship, but also get more flow field information. Therefore, in recent years, ship resistance evaluation based on the potential flow theory is gradually replaced by the CFD method. However, the calculation of potential flow theory is still unmatched by the CFD method. So, it is more effective to adopt different theories for different types of ship when optimizing the ship form based on the theory of hydrodynamics.

(3) Sensitivity

The numerical evaluation method of ship-type optimization requirements based on the hydrodynamic theory can quickly recognize the influence of small changes of hull geometry on the calculation results. That is to say, the numerical calculation method has high sensitivity to changes of ship type. In the process of ship-type optimization, the optimization method adjusts the design variables according to the numerical simulation results to obtain a new ship model, then the CAD module reconstructs a new ship model, and the numerical simulation is further evaluated. In this way, the variation of the ship type may be very small, which puts higher requirements on the sensitivity of the numerical evaluation method.

At present, there are many methods for forecasting the resistance performance of a ship, and there are generally three kinds of methods: the linear wave resistance theory, the approximate nonlinear wave resistance theory, and CFD method. This book mainly discusses typical representative methods in three kinds of methods: Michell integral method, Rankine source method, and RANS method.

2.2 Michell Integral Method

The application of resistance theory and quadratic programming technology in ship model optimization design is first proposed by Professor Xiong Ji-zhao. He only considers the wave resistance and friction resistance in the ship resistance components. The wave resistance is calculated by the Michell integral of linear wave resistance theory, and the frictional resistance is obtained using the formula recommended by the International Towing Tank Conference (ITTC). This method is characterized by the introduction of a group tent function to approximate the hull function, thus simplifying the formula for calculating the drag and friction resistance to a function that is only related to the (x, z) coordinates, the ship form surface (x, y, z) coordinates are discretized into points on the grid that are fixed x- and z-coordinates unchanged, and the y-coordinate is used as the design variable. And with the additional constraints, the ship with the minimum resistance can be obtained by the optimization method.

2.2.1 Use the Tent Function to Express the Ship Type

The key to the numerical calculation of wave resistance using Michelle's integral method is how to express the hull function [2]. However, the hull surface is usually expressed in the form of discrete point values, whereas the tent function can relate hull shape values to the formula of wave-making resistance. When using the tent function to express the hull value, the hull surface is first divided into rectangular grids with a certain number of waterlines and station numbers, as shown in Fig. 2.1.

When deploying the station number and waterline, place the first station line at the forefront of the hull and the last station line at the rear end of the hull, with the first waterline being the baseline and the last waterline being the design waterline. The rectangular cells at (x_i z_j) grid points are composed of (i − 1), (i + 1) station number lines and the (j − 1), (j + 1)th waterlines. Now, define a unit tent function, as shown in Fig. 2.2, which has a value equal to 1 at the grid point (x_i, z_j) and a value equal to 0 at the cell boundary.

The unit tent function $h^{(i,j)}$ (x, z) related to the grid point (x_i, z_j) can be written as follows:

$$h^{(i,j)}(x,z)=\begin{cases}\left(1-\frac{x_i-x}{x_i-x_{i-1}}\right)\cdot\left(1-\frac{z_j-z}{z_j-z_{j-1}}\right) & x_{i-1}<x<x_i \;\; z_{j-1}<z<z_j\\ \left(1-\frac{x_i-x}{x_i-x_{i-1}}\right)\cdot\left(1-\frac{z_j-z}{z_j-z_{j+1}}\right) & x_{i-1}<x<x_i \;\; z_j<z<z_{j+1}\\ \left(1-\frac{x_i-x}{x_i-x_{i+1}}\right)\cdot\left(1-\frac{z_j-z}{z_j-z_{j-1}}\right) & x_i<x<x_{i+1} \;\; z_{j-1}<z<z_j\\ \left(1-\frac{x_i-x}{x_i-x_{i+1}}\right)\cdot\left(1-\frac{z_j-z}{z_j-z_{j+1}}\right) & x_i<x<x_{i+1} \;\; z_j<z<z_{j+1}\\ 0 & \end{cases} \tag{2.1}$$

Looking closely at the expression, although the unit tent function $h^{(i,j)}$(x, z) is not a linear function, in each quadrant of a cell, $h^{(i,j)}$(x, z) is a linear function of x for a fixed z, or for a fixed x, $h^{(i,j)}$(x, z) is a linear function of z. According to this feature

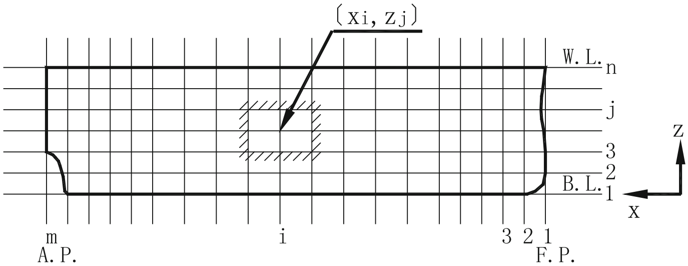

Fig. 2.1 Hull grid arrangement

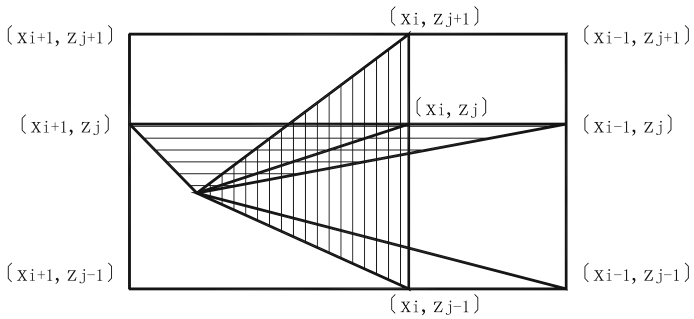

Fig. 2.2 Unit tent function

of the tent function, the tent function family can be used to form a function together with the hull value to approximate the hull surface. If the hull value at (x_i, z_j) is y_{ij}, the approximate hull function can be defined as:

$$\hat{h}(x,z) = \sum_i \sum_j y_{ij} h^{(i,j)}(x,z) \tag{2.2}$$

According to the tent function, we can see that at the grid point (xi, zj), $h^{(i,j)}(x,\, z) = 1$, so

$$\hat{h}(x,z) = y_{ij} \tag{2.3}$$

$$\text{Or } \hat{h}(x,z) = h^{(i,j)}(x,z)$$

Equation (2.3) can be used to approximate the surface function of the hull. The degree of approximation is related to the size of the mesh. Figure 2.3 shows that the family of tent functions approximates the hull surface within a rectangular unit. It can be seen from the figure that the grid points (x_i, z_j) and the nearby grid points (x_{i-1}, z_j), (x_i, z_{j+1}), (x_{i+1}, z_j), (x_i, z_{j-1}) are straight lines to approximate the surface of this part of the hull surface waterline and station line, so the smaller the mesh, the more accurate expression of the hull surface when using Eq. (2.3).

2.2.2 Derivation of Michell Integral Formula

A uniform flow is set as the basic flow, and the wave potential superimposed on this basic flow satisfies the linear free surface condition. Under the conditions of thin hull, infinite water depth, and symmetrical flow, Michell uses the method of separation of variables to get the corresponding velocity potential and the corresponding wave-making resistance formula [3].

Take the right-hand rectangular coordinate system fixed on the hull: The origin o is taken on the undisturbed stationary surface and is at the bow of the load waterline

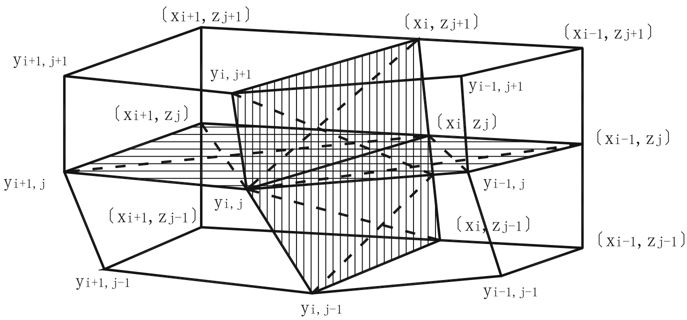

Fig. 2.3 Hull part of tent function family

Fig. 2.4 Coordinate system

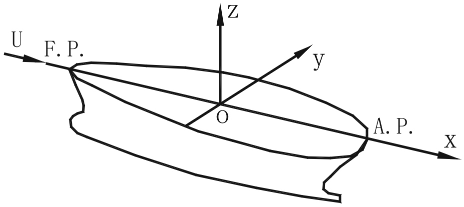

where the ox-axis and the oy-axis coincide with the still water surface. The ship does uniform linear motion along the X-axis in a negative direction at a speed of -U. According to the principle of motion conversion, it can be considered that the ship is in a uniform flow of velocity U, as shown in Fig. 2.4.

$$R_w = \frac{4\rho g K_0}{\pi} \int_0^{\pi/2} (I^2 + J^2) \sec^3 \theta d\theta \tag{2.4}$$

In the formula,

$$I + iJ = \int_{-T}^{0} dz \int_{-L/2}^{L/2} f_x(x,z) e^{K_0 z \sec^2 \theta + iK_0 x \sec \theta} dx$$

$$I = \int_{-T}^{0} e^{K_0 z \sec^2 \theta} dz \int_{-L/2}^{L/2} f_x(x,z) \cos(K_0 x \sec \theta) dx$$

$$J = \int_{-T}^{0} e^{K_0 z \sec^2 \theta} dz \int_{-L/2}^{L/2} f_x(x,z) \sin(K_0 x \sec \theta) dx$$

In the formula, K_0 is wave number, and $K_0 = \frac{g}{c^2}$, unit: 1/m;

c is ship speed, unit: m/s;
g is gravitational acceleration, unit: m/s^2;
ρ is water density, unit: kg/m^3;
$y = \pm f(x, z)$ is surface equation of ship form;
L is length, unit: m;
T is draft, unit: m.

Let

$$\lambda = \sec\theta$$
$$d\lambda = \tan\theta \cdot \sec\theta \cdot d\theta$$
$$d\theta = \frac{\cos^2\theta}{\sin\theta} d\lambda$$
$$\sec^3\theta \cdot d\theta = \frac{\sec\theta}{\sin\theta} d\lambda = \frac{\lambda}{)1 - \frac{1}{\lambda^2}} d\lambda$$

Then, the wave-making resistance formula becomes:

$$R_w = \frac{4\rho g K_0}{\pi} \int_1^{+\infty} (I^2 + J^2) \frac{\lambda^2}{\sqrt{\lambda^2 - 1}} d\lambda \tag{2.5}$$

Among the formula,

$$I = \int_{-T}^{0} e^{K_0 \cdot z \cdot \lambda^2} dz \int_{-L/2}^{L/2} f_x(x, z) \cdot \cos(K_0 \cdot x \cdot \lambda) dx$$
$$J = \int_{-T}^{0} e^{K_0 \cdot z \cdot \lambda^2} dz \int_{-L/2}^{L/2} f_x(x, z) \cdot \sin(K_0 \cdot x \cdot \lambda) dx$$

Define the dimensionless wave number $\gamma_0 = \frac{L}{2} K_0 = \frac{g \cdot L}{2 \cdot v^2} = \frac{1}{2 \cdot Fr^2}$; then $K_0 = \frac{2 \cdot \gamma_0}{L}$; moreover, the X and Z are dimensionless. Let $m = \frac{z}{T} + 1; z = -(1 - m) \cdot T; n = \frac{x}{L};\ \ \lambda = u^2 + 1$ (eliminate the singularity of $\lambda = 1$); then, the wave-making resistance formula becomes:

$$= \frac{8 \cdot \rho \cdot g \cdot \gamma_0}{\pi L} \int_0^{+\infty} (I^2 + J^2) \frac{(u^2 + 1)^2}{\sqrt{(u^2 + 1)^2 - 1}} 2 \cdot u du$$
$$= \frac{16 \cdot \rho \cdot g \cdot \gamma_0}{\pi L} \int_0^{+\infty} (I^2 + J^2) \frac{(u^2 + 1)^2}{\sqrt{u^2 + 2}} du \tag{2.6}$$

Among the formula,

$$I = \frac{1}{2} B \cdot T \int_0^1 e^{-2 \cdot \gamma_0 \cdot (1-z) \frac{T}{L} \cdot (u^2+1)^2} dz \int_{-1/2}^{1/2} f_x(x, y) \cdot \cos(2 \cdot \gamma_0 \cdot (u^2+1) \cdot x) dx$$

$$J = \frac{1}{2} B \cdot T \int_0^1 e^{-2 \cdot \gamma_0 \cdot (1-z) \frac{T}{L} \cdot (u^2+1)^2} dz \int_{-1/2}^{1/2} f_x(x, y) \cdot \sin(2 \cdot \gamma_0 \cdot (u^2+1) \cdot x) dx$$

Introduce tent function below, and then derive Michell points:

$$R_w = \frac{4 \rho g K_0}{\pi} \int_0^{\pi/2} (I^2 + J^2) \sec^3 \theta d\theta; \; K_0 = \frac{g}{V^2}$$

Among which,

$$I = \int_{-T}^{0} e^{K_0 \zeta \sec^2 \theta} d\zeta \int_0^L H_\xi(\xi, \zeta) \cos(K_0 \xi \sec \theta) d\xi$$

$$J = \int_{-T}^{0} e^{K_0 \zeta \sec^2 \theta} d\zeta \int_0^L H_\xi(\xi, \zeta) \sin(K_0 \xi \sec \theta) d\xi$$

Successively transformed $\lambda = \sec \theta; u = \sqrt{\lambda - 1}$, and introduce the following dimensionless variables:

$$x = \xi / L; \; y = \eta / b; \; z = \zeta / T; \; b = B/2$$

The dimensionless hull function $h(x, z) = \frac{1}{b} H(\xi, \zeta)$
The dimensionless hull slope function $h_x(x, z) = \frac{L}{b} H_\xi(\xi, \zeta)$
The nondimensional wave number $\gamma_0 = \frac{g \cdot L}{2 \cdot v^2} = \frac{1}{2 \cdot Fr^2} = \frac{L}{2} K_0$
The formula of wave-making resistance of Michell integral becomes

$$R_w = \frac{8 \cdot \rho \cdot g}{\pi} \cdot \frac{B^2 \cdot T^2}{L} \cdot \frac{\gamma_0}{2} \int_0^{+\infty} (P(u)^2 + Q(u)^2) \frac{(u^2+1)^2}{\sqrt{u^2+2}} du \tag{2.7}$$

Among which,

$$P(\lambda) = \int_0^1 e^{-2\cdot\gamma_0\frac{T}{L}\cdot\lambda^2\cdot(1-z)}dz\int_0^1 h_x(x,z)\cdot\cos(2\cdot\gamma_0\cdot\lambda\cdot x)dx$$

$$Q(\lambda) = \int_0^1 e^{-2\cdot\gamma_0\frac{T}{L}\cdot\lambda^2\cdot(1-z)}dz\int_0^1 h_x(x,z)\cdot\sin(2\cdot\gamma_0\cdot\lambda\cdot x)dx$$

Discrete continuous functions:

$$P(\lambda) = \sum_i\sum_j y_{ij}\iint_{\Delta S_{ij}} h_x^{(i,j)}(x,z)\cdot\cos(2\cdot\gamma_0\cdot\lambda\cdot x)\cdot e^{-2\cdot\gamma_0\frac{T}{L}\cdot\lambda^2\cdot(1-z)}dxdz \quad (2.8)$$

$$Q(\lambda) = \sum_i\sum_j y_{ij}\iint_{\Delta S_{ij}} h_x^{(i,j)}(x,z)\cdot\sin(2\cdot\gamma_0\cdot\lambda\cdot x)\cdot e^{-2\cdot\gamma_0\frac{T}{L}\cdot\lambda^2\cdot(1-z)}dxdz \quad (2.9)$$

Introduce the tent function

$$\mathrm{h_x^{(i,j)}(x,z)} = \begin{cases} \frac{1}{x_i-x_{i-1}}\cdot\left(1-\frac{z_j-z}{z_j-z_{j-1}}\right) & x_{i-1}<x<x_i,\ z_{j-1}<z<z_j \\ \frac{1}{x_i-x_{i-1}}\cdot\left(1-\frac{z_j-z}{z_j-z_{j+1}}\right) & x_{i-1}<x<x_i,\ z_j<z<z_{j+1} \\ \frac{1}{x_i-x_{i+1}}\cdot\left(1-\frac{z_j-z}{z_j-z_{j-1}}\right) & x_i<x<x_{i+1},\ z_{j-1}<z<z_j \\ \frac{1}{x_i-x_{i+1}}\cdot\left(1-\frac{z_j-z}{z_j-z_{j+1}}\right) & x_i<x<x_{i+1},\ z_j<z<z_{j+1} \\ 0 & Others \end{cases} \quad (2.10)$$

Transform $P(\lambda)$ and $Q(\lambda)$, and get the following two formulas:

$$P(\lambda) = \sum_i\sum_j y_{ij}\cdot C_i(\lambda,\gamma_0)\cdot E_j(\lambda,\gamma_0,\frac{T}{L}) \quad (2.11)$$

$$Q(\lambda) = \sum_i\sum_j y_{ij}\cdot S_i(\lambda,\gamma_0)\cdot E_j(\lambda,\gamma_0,\frac{T}{L}) \quad (2.12)$$

Among them:

$$\begin{aligned} C_i(\lambda,\gamma_0) &= \frac{1}{x_i-x_{i+1}}\int_{x_i}^{x_{i+1}}\cos(2\cdot\gamma_0\cdot\lambda\cdot x)dx + \frac{1}{x_i-x_{i-1}}\int_{x_{i-1}}^{x_i}\cos(2\cdot\gamma_0\cdot\lambda\cdot x)dx \\ &= -\frac{1}{2\cdot\gamma_0\cdot\lambda}\left\{\begin{array}{l}\frac{1}{x_{i+1}-x_i}[\sin(2\cdot\gamma_0\cdot\lambda\cdot x_{i+1})-\sin(2\cdot\gamma_0\cdot\lambda\cdot x_i)]- \\ \frac{1}{x_i-x_{i-1}}[\sin(2\cdot\gamma_0\cdot\lambda\cdot x_i)-\sin(2\cdot\gamma_0\cdot\lambda\cdot x_{i-1})]\end{array}\right\} \end{aligned}$$

$$E_j(\lambda,\gamma_0,\frac{T}{L}) = \int_{z_j}^{z_{j+1}} e^{-2\cdot\gamma_0\frac{T}{L}\cdot\lambda^2\cdot(1-z)}\left(1-\frac{z_j-z}{z_j-z_{j+1}}\right)dz + \int_{z_{j-1}}^{z_j} e^{-2\cdot\gamma_0\frac{T}{L}\cdot\lambda^2\cdot(1-z)}\left(1-\frac{z_j-z}{z_j-z_{j-1}}\right)dz$$
$$= \frac{1}{\left(2\cdot\gamma_0\cdot\lambda^2\cdot\frac{T}{L}\right)^2}\left\{\begin{array}{l}\frac{1}{z_{j+1}-z_j}\left[e^{-2\cdot\gamma_0\frac{T}{L}\cdot\lambda^2\cdot(1-z_{j+1})} - e^{-2\cdot\gamma_0\frac{T}{L}\cdot\lambda^2\cdot(1-z_j)}\right] - \\ \frac{1}{z_j-z_{j-1}}\left[e^{-2\cdot\gamma_0\frac{T}{L}\cdot\lambda^2\cdot(1-z_j)} - e^{-2\cdot\gamma_0\frac{T}{L}\cdot\lambda^2\cdot(1-z_{j-1})}\right]\end{array}\right\}$$

$$S_i(\lambda,\gamma_0) = \frac{1}{x_i-x_{i+1}}\int_{x_i}^{x_{i+1}} \sin(2\cdot\gamma_0\cdot\lambda\cdot x)dx + \frac{1}{x_i-x_{i-1}}\int_{x_{i-1}}^{x_i} \sin(2\cdot\gamma_0\cdot\lambda\cdot x)dx$$
$$= \frac{1}{2\cdot\gamma_0\cdot\lambda}\left\{\begin{array}{l}\frac{1}{x_{i+1}-x_i}[\cos(2\cdot\gamma_0\cdot\lambda\cdot x_{i+1}) - \cos(2\cdot\gamma_0\cdot\lambda\cdot x_i)] - \\ \frac{1}{x_i-x_{i-1}}[\cos(2\cdot\gamma_0\cdot\lambda\cdot x_i) - \cos(2\cdot\gamma_0\cdot\lambda\cdot x_{i-1})]\end{array}\right\}$$

$$E_j(\lambda,\gamma_0,\frac{T}{L}) = \int_{z_j}^{z_{j+1}} e^{-2\cdot\gamma_0\frac{T}{L}\cdot\lambda^2\cdot(1-z)}\left(1-\frac{z_j-z}{z_j-z_{j+1}}\right)dz + \int_{z_{j-1}}^{z_j} e^{-2\cdot\gamma_0\frac{T}{L}\cdot\lambda^2\cdot(1-z)}\left(1-\frac{z_j-z}{z_j-z_{j-1}}\right)dz$$
$$= \frac{1}{\left(2\cdot\gamma_0\cdot\lambda^2\cdot\frac{T}{L}\right)^2}\left\{\begin{array}{l}\frac{1}{z_{j+1}-z_j}\left[e^{-2\cdot\gamma_0\frac{T}{L}\cdot\lambda^2\cdot(1-z_{j+1})} - e^{-2\cdot\gamma_0\frac{T}{L}\cdot\lambda^2\cdot(1-z_j)}\right] - \\ \frac{1}{z_j-z_{j-1}}\left[e^{-2\cdot\gamma_0\frac{T}{L}\cdot\lambda^2\cdot(1-z_j)} - e^{-2\cdot\gamma_0\frac{T}{L}\cdot\lambda^2\cdot(1-z_{j-1})}\right]\end{array}\right\}$$

The procedures in the program are as follows:

$$R_w = \frac{8\cdot\rho\cdot g}{\pi}\cdot\frac{B^2\cdot T^2}{L}\cdot\frac{\gamma_0}{2}\cdot \text{integral}[(P(u_k)^2 + Q(u_k)^2)\frac{(u_k^2+1)^2}{\sqrt{u_k^2+2}}],\ u_k\in[0,2] \quad (2.13)$$

$$P(\lambda_k) = \sum_i\sum_j y_{ij}\cdot C_i(\lambda_k,\gamma_0)\cdot E_j(\lambda_k,\gamma_0,\frac{T}{L});$$
$$\lambda_k = u_k^2+1;\ x_i\in[0,1];\ z_j\in[0,1];\ y_{ij}\in[0,1]$$
$$Q(\lambda_k) = \sum_i\sum_j y_{ij}\cdot S_i(\lambda_k,\gamma_0)\cdot E_j(\lambda_k,\gamma_0,\frac{T}{L});$$
$$\lambda_k = u_k^2+1$$

Among them:

$$C_i(\lambda,\gamma_0) = \frac{1}{x_i-x_{i+1}}\int_{x_i}^{x_{i+1}} \cos(2\cdot\gamma_0\cdot\lambda\cdot x)dx + \frac{1}{x_i-x_{i-1}}\int_{x_{i-1}}^{x_i} \cos(2\cdot\gamma_0\cdot\lambda\cdot x)dx$$
$$= -\frac{1}{2\cdot\gamma_0\cdot\lambda}\left\{\begin{array}{l}\frac{1}{x_{i+1}-x_i}[\sin(2\cdot\gamma_0\cdot\lambda\cdot x_{i+1}) - \sin(2\cdot\gamma_0\cdot\lambda\cdot x_i)] - \\ \frac{1}{x_i-x_{i-1}}[\sin(2\cdot\gamma_0\cdot\lambda\cdot x_i) - \sin(2\cdot\gamma_0\cdot\lambda\cdot x_{i-1})]\end{array}\right\}$$

$$S_i(\lambda, \gamma_0) = \frac{1}{x_i - x_{i+1}} \int_{x_i}^{x_{i+1}} \sin(2 \cdot \gamma_0 \cdot \lambda \cdot x)dx + \frac{1}{x_i - x_{i-1}} \int_{x_{i-1}}^{x_i} \sin(2 \cdot \gamma_0 \cdot \lambda \cdot x)dx$$

$$= \frac{1}{2 \cdot \gamma_0 \cdot \lambda} \left\{ \begin{array}{l} \frac{1}{x_{i+1} - x_i}[\cos(2 \cdot \gamma_0 \cdot \lambda \cdot x_{i+1}) - \cos(2 \cdot \gamma_0 \cdot \lambda \cdot x_i)] - \\ \frac{1}{x_i - x_{i-1}}[\cos(2 \cdot \gamma_0 \cdot \lambda \cdot x_i) - \cos(2 \cdot \gamma_0 \cdot \lambda \cdot x_{i-1})] \end{array} \right\}$$

$$= \int_{z_j}^{z_{j+1}} e^{-2 \cdot \gamma_0 \frac{T}{L} \cdot \lambda^2 \cdot (1-z)} \left(1 - \frac{z_j - z}{z_j - z_{j+1}}\right) dz + \int_{z_{j-1}}^{z_j} e^{-2 \cdot \gamma_0 \frac{T}{L} \cdot \lambda^2 \cdot (1-z)} \left(1 - \frac{z_j - z}{z_j - z_{j-1}}\right) dz$$

$$= \frac{1}{\left(2 \cdot \gamma_0 \cdot \lambda^2 \cdot \frac{T}{L}\right)^2} \left\{ \begin{array}{l} \frac{1}{z_{j+1} - z_j}\left[e^{-2 \cdot \gamma_0 \frac{T}{L} \cdot \lambda^2 \cdot (1 - z_{j+1})} - e^{-2 \cdot \gamma_0 \frac{T}{L} \cdot \lambda^2 \cdot (1 - z_j)}\right] - \\ \frac{1}{z_j - z_{j-1}}\left[e^{-2 \cdot \gamma_0 \frac{T}{L} \cdot \lambda^2 \cdot (1 - z_j)} - e^{-2 \cdot \gamma_0 \frac{T}{L} \cdot \lambda^2 \cdot (1 - z_{j-1})}\right] \end{array} \right\}$$

The wave-making resistance coefficient and wave-making resistance formula are as follows:

$$C_w = \frac{\gamma_0}{2} \cdot \text{integral}[(P(u_k))^2 + Q(u_k)^2)\frac{(u_k^2 + 1)^2}{\sqrt{u_k^2 + 2}}], \ u_k \in [0, 2] \tag{2.14}$$

$$R_w = \frac{8 \cdot \rho \cdot g}{\pi} \cdot \frac{B^2 \cdot T^2}{L} \cdot C_w, \ u_k \in [0, 2] \tag{2.15}$$

2.3 Rankine Source Method

2.3.1 Basic Equation

Rankine source method is a method of calculating the wave-making resistance, which replaces the uniform flow in the thin-boat theory with stacked flow around. Take the Cartesian coordinate system fixed on the hull, the X-axis and the Y-axis are taken on the undisturbed hydrostatic surface, the X-axis is directed to the stern of the ship with a uniform flow [4], the Y-axis is directed to the starboard side, and the Z-axis is vertically upward, as shown in Fig. 2.5.

The velocity around the hull is composed of two parts: the velocity potential Φ of the flow around the double model and the wave velocity potential φ which takes into account the influence of free surface, that is

$$\phi = \Phi + \varphi \tag{2.16}$$

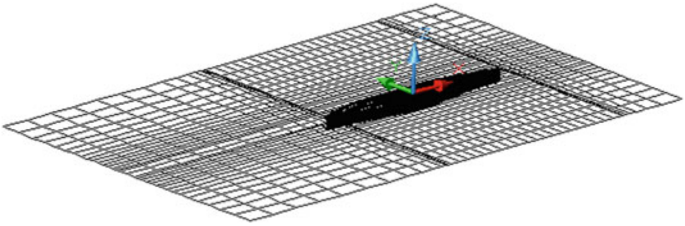

Fig. 2.5 Coordinate system of turbulence flow

Assume that the fluid is a perfect fluid with no spin. The ship's wave problem satisfies the Laplace equation and the following boundary conditions:

$$\nabla^2(\Phi + \varphi) = 0 \tag{2.17}$$

(1) Hull boundary conditions: The normal component of the hull surface velocity component in the direction is zero, which means that streamline cannot penetrate the interior of the ship.

$$\vec{V}_{\hat{n}} = \nabla(\Phi + \phi) \tag{2.18}$$

In the formula, $\hat{n} = n_x \hat{i} + n_y \hat{j} + n_z \hat{k}$ means pointing to the normal direction of the hull.

(2) Free surface condition: The velocity potential of the free surface satisfies the dynamic conditions and kinematic conditions.

$$g\zeta + \frac{1}{2}\nabla\phi \cdot \nabla\phi = \frac{1}{2}U_\infty^2 \text{ on } \mathrm{z} = \zeta(x, y) \tag{2.19}$$

$$\phi_x\zeta_x + \phi_y\zeta_y - \phi_z = 0 \text{ on } \mathrm{z} = \zeta(x, y) \tag{2.20}$$

Eliminate the wave height from Eqs. (2.19) and (2.20) to get the following equation

$$\frac{1}{2}\phi_x(\nabla\phi \cdot \nabla\phi)_x + \frac{1}{2}\phi_y(\nabla\phi \cdot \nabla\phi)_y + g\phi_z = 0 \text{ on } \mathrm{z} = \zeta(x, y) \tag{2.21}$$

The equation must also satisfy the wave-free radiation conditions in the far front of the hull in order to show that the upstream disturbances propagate only downstream, whereas the downstream disturbances do not directly affect the upstream physical facts.

2.3.2 Linearization of Free Surface Conditions

In the free surface condition (2.21), the nonlinear term of $\nabla\phi$ is satisfied in the free surface. The overmold solution Φ can obtain the linearized free surface condition by neglecting the higher order term in φ. The perturbation potential φ is a small quantity relative to the superimposed potential Φ. That is

$$\Phi_z = 0 \,\text{on}\, z = 0 \tag{2.22}$$

It can be obtained from formula (2.21) that

$$\frac{1}{2}\phi_{\mathrm{x}}(\phi_x^2+\phi_y^2+\phi_z^2)_x+\frac{1}{2}\phi_{\mathrm{y}}(\phi_x^2+\phi_y^2+\phi_z^2)_y+g\phi_z=0 \tag{2.23}$$

Substituting formula (2.6) into formula (2.23), we get

$$\begin{aligned}&\frac{1}{2}(\Phi+\varphi)_x\{(\Phi+\varphi)_x^2+(\Phi+\varphi)_y^2+(\Phi+\varphi)_z^2\}_x\\&+\frac{1}{2}(\Phi+\varphi)_y\{(\Phi+\varphi)_y^2+(\Phi+\varphi)_y^2+(\Phi+\varphi)_z^2\}_y+g(\Phi+\varphi)_z=0.\end{aligned} \tag{2.24}$$

Using Eq. (2.22), and neglecting the higher order term of the wave potential φ in free surface condition (2.24), the overmold solution Φ can be linearized into the following form

$$\begin{aligned}&\frac{1}{2}\Phi_x(\Phi_x^2+\Phi_y^2)_{\mathrm{x}}+\frac{1}{2}\Phi_y(\Phi_x^2+\Phi_y^2)_{\mathrm{y}}+\Phi_x(\Phi_x\varphi_x+\Phi_y\varphi_y)_x+\Phi_y(\Phi_x\varphi_x+\Phi_y\varphi_y)_y\\&+\frac{1}{2}\varphi_x(\Phi_x^2+\Phi_y^2)_x+\frac{1}{2}\varphi_y(\Phi_x^2+\Phi_y^2)_y+g\varphi_z=0\,\text{on}\,Z=0\end{aligned} \tag{2.25}$$

For any equation F (x, y) = 0, there is

$$\Phi_{\mathrm{x}}F_X+\Phi_yF_y=\Phi_lF_l \tag{2.26}$$

In the formula, the subscript l denotes the velocity gradient of the double model potential Φ along the streamline direction in the z = 0 planes of symmetry, and then the above equation can be written as

$$\frac{1}{2}\Phi_l(\Phi_l^2)_l+\Phi_l(\Phi_l\varphi_l)_l+\frac{1}{2}\varphi_l(\Phi_l^2)_l+g\varphi_z=0\,\text{on}\,Z=0 \tag{2.27}$$

To further simplify the above equation, we get

$$\Phi_l^2\varphi_{ll} + 2\Phi_l\Phi_{ll}\varphi_l + g\varphi_z = -\Phi_l^2\Phi_{ll} \text{ on } Z = 0 \tag{2.28}$$

2.3.3 Solution of Free Surface Conditions

Rankine sources are used to express the velocity potentials Φ and φ, respectively, on the double model surface and the undisturbed free surface.

$$\Phi(x, y, z) = U_\infty x - \iint_{S_B} \sigma_B \frac{1}{r} dS \tag{2.29}$$

$$\varphi(x, y, z) = -\iint_{S_F} \sigma_F \frac{1}{r'} dS - \iint_{S_B} \Delta\sigma_B \frac{1}{r} dS \tag{2.30}$$

In the formula,

$$r = \sqrt{(x-\xi)^2 + (y-\eta)^2 + (z-\zeta)^2}$$

$$r' = \sqrt{(x-\xi)^2 + (y-\eta)^2 + z^2}$$

The perturbation potential φ of Eq. (2.30) takes into account the interaction between the free surface and the hull. In the current numerical algorithm, the double model equation is modified according to the second combination on the right of formula (2.30). The flow of double model solution is obtained by the numerical solution of the boundary value problem, which belongs to the Neumann-type boundary condition of the double model hull, and the following formula can be obtained from formula (2.18) and formula (2.29).

$$\nabla\left[U_\infty x - \iint_{S_B} \sigma_B \frac{1}{r} dS\right] \cdot \hat{n} = 0 \tag{2.31}$$

In order to obtain the approximate solution of the above equation, the surface S_B of the superposed molded body is divided into N_B facets, the source intensity σ_B in the center of the facet is assumed to be a constant, and the above equation in the ith facet can be expressed in the following form:

$$-2\pi\sigma_B(i) - \sum_{\substack{j=1 \\ j\neq i}}^{N_B} \iint_{S_B} \sigma_B(j) \frac{\partial}{\partial n}\left(\frac{1}{r}\right) dS = \hat{n}(i).U_\infty. \tag{2.32}$$

This equation is the second kind of Fredholm integral equation over the entire hull surface S_B, and after simplification, the above equation can be written as

$$-2\pi\sigma_B(i) + \sum_{\substack{j=1 \\ j\neq i}}^{N_B} \sigma_B(j)\left[n_{xi}\frac{\partial}{\partial x}\iint_{S_B}\left(\frac{1}{r}\right)dS + n_{yi}\frac{\partial}{\partial y}\iint_{S_B}\left(\frac{1}{r}\right)dS + n_{zi}\frac{\partial}{\partial z}\iint_{S_B}\left(\frac{1}{r}\right)dS + \right] = \hat{n}(i).U_\infty. \tag{2.33}$$

$$-2\pi\sigma_B(i) + \sum_{\substack{j=1 \\ j\neq i}}^{N_B} \sigma_B(j)\left[n_{xi}V_{xij} + n_{yi}V_{yij} + n_{zi}V_{zij}\right] = \hat{n}(i).U_\infty, i = 1 - N_B \tag{2.34}$$

The double model solution σ_{B} is obtained from the Hess–Smith (1964) method by calculating the velocity potential components *Vx, Vy,* and *Vz*. When the free surface is rigid and the speed limit is zero Froude, the solution of this double model is close to the free surface solution. After the double model velocity potential Φ is obtained from formula (2.29), the double model streamline is obtained by tracing the water surface. These streamlines cannot penetrate into the hull, and at the same time these streamlines are used to create free surface grids.

Equation (2.28) gives the free surface boundary conditions, while specifying that l is the velocity gradient along the streamline direction and is differentiated from the streamlines of the double model, the velocity potential flow is calculated by the following formula.

$$\varphi_l = \frac{\Phi_x}{\sqrt{\Phi_x^2 + \Phi_y^2}}\varphi_x + \frac{\Phi_y}{\sqrt{\Phi_x^2 + \Phi_y^2}}\varphi_y \tag{2.35}$$

It is noticed that the difference between these methods is that the free flow direction is approximately replaced by the flow direction of the double model. If the free surface is dispersed into N_F surface elements, on the ith element of the free surface, φ_l and φ_{ll} in Eq. (2.28) can be expressed as follows

$$\varphi_l(i) = \sum_{j=1}^{N_F}\sigma_F(j)L_F(ij) + \sum_{j=1}^{N_B}\Delta\sigma_B(j)L_B(ij) \tag{2.36}$$

$$\varphi_{ll}(i) = \sum_{j=1}^{N_F}\sigma_F(j)CL_F(ij) + \sum_{j=1}^{N_B}\Delta\sigma_B(j)CL_B(ij) \tag{2.37}$$

Among them

$$L_B(ij) = -\iint\limits_{S_B} \frac{\Phi_x}{\sqrt{\Phi_x^2+\Phi_y^2}}\frac{\partial}{\partial x}(\frac{1}{r})dS - \iint\limits_{S_B} \frac{\Phi_y}{\sqrt{\Phi_x^2+\Phi_y^2}}\frac{\partial}{\partial y}(\frac{1}{r})dS$$

$$L_F(ij) = -\iint\limits_{S_F} \frac{\Phi_x}{\sqrt{\Phi_x^2+\Phi_y^2}}\frac{\partial}{\partial x}(\frac{1}{r'})dS - \iint\limits_{S_F} \frac{\Phi_y}{\sqrt{\Phi_x^2+\Phi_y^2}}\frac{\partial}{\partial y}(\frac{1}{r'})dS$$

and

$$CL_B(ij) = \sum_{n=1}^{N-1} e_n L_B(i-n,j)$$

$$CL_F(ij) = \sum_{n=1}^{N-1} e_n L_F(i-n,j)$$

In the above equation, e_n is the finite difference operator upstream of point N and is calculated as follows.

In order to satisfy the radiation conditions, the finite difference operator is used to express the two derivative phases along the double-body streamline velocity potential. On the free surface along the streamline direction l, the derivative phase of the function $f\,(x,\ y,\ z)$ can be expressed as:

$$\frac{df(i,j)}{dl} = f_l(i,j) = \frac{\Phi_{xij}}{\sqrt{\Phi_{xij}^2+\Phi_{yij}^2}} f_x(i,j) + \frac{\Phi_{yij}}{\sqrt{\Phi_{xij}^2+\Phi_{yij}^2}} f_y(i,j) \tag{2.38}$$

$$\frac{df(i,j)}{dx} = f_x(i,j) = \frac{df(i,j)}{d\xi}\frac{d\xi}{dx} + \frac{df(i,j)}{d\eta}\frac{d\eta}{dx} \tag{2.39}$$

$$\frac{df(i,j)}{dy} = f_y(i,j) = \frac{df(i,j)}{d\xi}\frac{d\xi}{dy} + \frac{df(i,j)}{d\eta}\frac{d\eta}{dy} \tag{2.40}$$

The introduction of this function is calculated by a single-point finite difference upstream operator

$$\frac{dx}{d\xi} = \begin{cases} x(i+1) - x(i) & (i=1) \\ x(i) - x(i-1) & (i=2) \\ \frac{(3x(i)-4x(i-1)+x(i-2))}{2} & (i=3) \\ \frac{(11x(i)-18x(i-1)+9x(i-2)-2x(i-3))}{6} & (i=4) \end{cases} \tag{2.41}$$

$$\frac{dy}{d\xi} = \begin{cases} y(i+1) - y(i) & (i=1) \\ y(i) - y(i-1) & (i=2) \\ \frac{(3y(i) - 4y(i-1) + y(i-2))}{2} & (i=3) \\ \frac{(11y(i) - 18y(i-1) + 9y(i-2) - 2y(i-3))}{6} & (i=4) \end{cases} \tag{2.42}$$

$$\frac{df}{d\xi} = \begin{cases} f_{i+1,j} - f_{i,j} & (i=1) \\ f_{i,j} - f_{i-1,j} & (i=2) \\ \frac{(3f_{i,j} - 4f_{i-1,j} + f_{i-2,j}}{2} & (i=3) \\ \frac{(11f_{i,j} - 18f_{i-1,j} + 9f_{i-2,j} - 2f_{i-3,j}))}{6} & (i=4) \end{cases} \tag{2.43}$$

Similarly, *dx/dz, dy/dz,* and *df/dz* can also be obtained. The relation between the associated coordinate system *(x, y, z)* and *(ξ, η, ζ)* on the free surface is given below

$$\frac{\partial \xi}{\partial x} = \frac{1}{|J|}\frac{\partial y}{\partial \eta}, \quad \frac{\partial \eta}{\partial x} = \frac{1}{|J|}\frac{\partial y}{\partial \xi}, \quad \frac{\partial \xi}{\partial y} = \frac{1}{|J|}\frac{\partial x}{\partial \eta}, \quad \frac{\partial \eta}{\partial y} = \frac{1}{|J|}\frac{\partial x}{\partial \xi}$$

$$|J| = \frac{\partial x}{\partial \xi}\frac{\partial y}{\partial \eta} - \frac{\partial x}{\partial \eta}\frac{\partial y}{\partial \xi} \tag{2.44}$$

Then, the vertical velocity component on the free surface can be expressed as:

$$\phi_z = \begin{cases} -2\pi\sigma_F(i) \\ 0 \end{cases}, \quad \begin{matrix} (i=j) \\ (i \neq j) \end{matrix} \tag{2.45}$$

By substituting Eqs. (2.36), (2.37), and (2.45) into (2.28), we get a linear system of equations for σ_F and $\Delta\sigma_B$

$$\Phi_l^2(i)\left[\sum_{j=1}^{N_F}\sigma_F(j)CL_F(ij) + \sum_{j=1}^{N_B}\Delta\sigma_B(j)CL_B(ij)\right] + 2\Phi_l(i)\Phi_{ll}(i)\left[\sum_{j=1}^{N_F}\sigma_F(j)L_F(ij) + \sum_{j=1}^{N_B}\Delta\sigma_B(j)L_B(ij)\right] - 2\pi g\sigma_F(i) = -\Phi_l^2(i)\Phi_{ll}(i) \tag{2.46}$$

Rearranging the above equation, we can get

$$\sum_{j=1}^{N_F}\sigma_F(j)A_F(ij) + \sum_{j=1}^{N_B}\Delta\sigma_B(j)A_B(ij) - 2\pi g\sigma_F(i) = B(i), i = 1 - N_F, \tag{2.47}$$

Here,

$$A_B(ij) = \Phi_l^2(i)CL_B(ij) + 2\Phi_l(i)\Phi_{ll}(i)L_B(ij),$$
$$A_F(ij) = \Phi_l^2(i)CL_F(ij) + 2\Phi_l(i)\Phi_{ll}(i)L_F(ij),$$

$$B(i) = -\Phi_l^2(i)\Phi_{ll}(i)$$

Substituting Eq. (2.30) into (2.18) gives us

$$\begin{aligned}&\sum_{j=1}^{N_F}\sigma_F(j)V_F(ij) + \sum_{j=1}^{N_B}\Delta\sigma_B(i)V_B(ij) = 0\\ &i = N_F + 1 \sim N_B + N_F\end{aligned} \tag{2.48}$$

Here,

$$V_B(ij) = -\iint\limits_{S_B}\frac{\partial}{\partial n}\left(\frac{1}{r}\right)dS = -\iint\limits_{S_B}\left\{n_x\frac{\partial}{\partial x}\left(\frac{1}{r}\right) + n_y\frac{\partial}{\partial y}\left(\frac{1}{r}\right) + n_z\frac{\partial}{\partial z}\left(\frac{1}{r}\right)\right\}dS$$
$$V_F(ij) = -\iint\limits_{S_F}\frac{\partial}{\partial n}\left(\frac{1}{r'}\right)dS = -\iint\limits_{S_F}\left\{n_x\frac{\partial}{\partial x}\left(\frac{1}{r'}\right) + n_y\frac{\partial}{\partial y}\left(\frac{1}{r'}\right) + n_z\frac{\partial}{\partial z}\left(\frac{1}{r'}\right)\right\}dS$$

The solution of Eqs. (2.46) and (2.48) is obtained by iterative method, so Eq. (2.46) can be written as

$$\sum_{j=1}^{N_F}\sigma_F(j)A_F(ij) - 2\pi g\sigma_F(i) = B(i) - \sum_{j=1}^{N_B}\Delta\sigma_B(j)A_B(ij) \tag{2.49}$$

For this initial value problem, the source distribution over the entire hull surface can be approximated by the double model solution

$$\Delta\sigma_B = 0 \tag{2.50}$$

In order to find the first-order approximate solution of σ_F, we substitute Eq. (2.50) into (2.49) to get

$$\sum_{j=1}^{N_F}\sigma_F^{(1)}(j)A_F(ij) - 2\pi g\sigma_F^{(1)}(i) = B(i) \tag{2.51}$$

Substituting the solution ${\sigma^{(1)}}_F$ of Eq. (2.51) into Eq. (2.48), we get

$$\sum_{j=1}^{N_F} \sigma_F^{(1)}(j) V_F(ij) + \sum_{j=1}^{N_B} \Delta\sigma_B^{(1)}(i) V_B(ij) = 0 \tag{2.52}$$

After obtaining the first-order approximate solution of $\triangle^{(1)}_{\sigma B}$ from formula (2.52), the second-order approximate solution σ_F can be obtained from Eq. (2.49)

$$\sum_{j=1}^{N_F} \sigma_F^{(2)}(j) A_F(ij) - 2\pi g \sigma_F^{(2)}(i) = B(i) - \sum_{j=1}^{M_1} \Delta\sigma_B^{(1)}(j) A_B(ij) \tag{2.53}$$

By substituting the solution $\sigma^{(2)}_F$ of Eq. (2.53) into Eq. (2.48), we obtain the second-order approximate solution of $\Delta\sigma_\mathrm{B}$

$$\sum_{j=1}^{N_F} \sigma_F^{(2)}(j) V_F(ij) + \sum_{j=1}^{M_B} \Delta\sigma_B^{(2)}(i) V_B(ij) = 0 \tag{2.54}$$

2.3.4 Calculate the Wave Resistance

The hull surface pressure can be expressed by the velocity potential around the hull, which can also be expressed by the Bernoulli equation that satisfies the free surface boundary conditions

$$p + \rho g z + \frac{1}{2}\rho \nabla\phi \nabla\phi = p_\infty + \frac{1}{2}\rho U_\infty^2 \tag{2.55}$$

After arrangement,

$$p - p_\infty = \frac{1}{2}\rho U_\infty^2 - \rho g z - \frac{1}{2}\rho \nabla(\Phi + \varphi) \cdot \nabla(\Phi + \varphi) \tag{2.56}$$

After expansion,

$$p - p_\infty = \frac{1}{2}\rho \left[U_\infty^2 - 2gz - \Phi_x^2 - \Phi_y^2 - \Phi_z^2 - 2\Phi_x\varphi_x - 2\Phi_y\varphi_y - 2\Phi_z\varphi_z \right] \tag{2.57}$$

The pressure coefficient can be expressed as

$$C_p = \frac{p - p_\infty}{(1/2)\rho U_\infty^2} = \frac{1}{U_\infty^2}\left[U^2 - 2gz - \Phi_x^2 - \Phi_y^2 - \Phi_z^2 - 2\Phi_x\varphi_x - 2\Phi_y\varphi_y - 2\Phi_z\varphi_z \right] \tag{2.58}$$

Assuming that the pressure inside the hull is a constant pressure, the wave-making resistance can be calculated by the following formula

$$C_w = \frac{R_w}{1/2\rho U_\infty^2 L^2} = \frac{1}{L^2}\sum_{i=1}^{N_B/2} C_p(i) n_{xi} \Delta S_i \tag{2.59}$$

Here, ΔS_i is the area of the hull surface element; n_{xi} is the component of the normal direction of the surface element unit in the x-direction, and then the waveform can be obtained by (2.19)

$$\zeta(x,y) = \frac{1}{2g}\left[U_\infty^2 - \Phi_x^2 - \Phi_y^2 - 2\Phi_x\varphi_x - 2\Phi_y\varphi_y\right] \tag{2.60}$$

2.3.5 Mesh Classification by Rankine Source Method

Mesh classification is one of the most important aspects in the numerical calculation of the wave resistance using Rankine source method, because the meshes of different shapes will have a certain influence on the calculation results. The Rankine source numerical dispersion is not only carried out on the interface between the hull and the fluid, but also in the entire free surface. However, the free surface is usually considered as infinity, and the numerical dispersion is only carried out in the vicinity of the free surface where the ship interferes. The free surface area further away from the upstream is considered to be unaffected by the ship's interference. The fluctuation of the free surface at the far downstream and side edges is

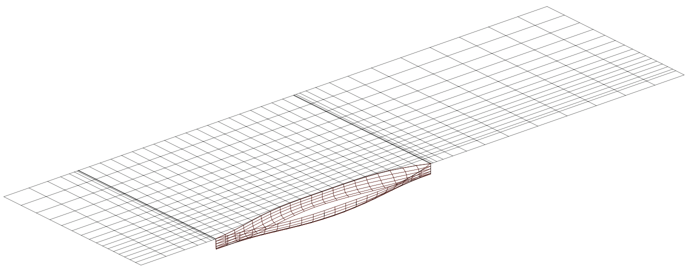

Fig. 2.6 Mesh classification by Rankine source method

attenuated; that is, as the free surface becomes more and more distant from the ship, it becomes less and less disturbed by the ship. Therefore, on the free side of the side and the downstream direction, the influence of the free surface on the flow field around the ship can be considered as long as the sufficiently large area is taken into consideration when the numerical discretization is taken into account [5]. Figure 2.6 shows an example of a grid split on the hull and free surface.

According to Dawson's meshing experience, the free area mesh has a half-width of about $3L/8$, an upstream stretch of $L/4$, a downstream extension of 0.25 wavelength, an entire surface of the grid inclined 45 degrees downstream, and the grid near the bow and stern should be encrypted. Musker (1989) suggested that the free surface grid extend 1.0L forward, 1.5L in the stern, and 1.5L in the breadth of the boat [6]. This section summarizes the experience of predecessors, based on the actual situation of the selected ship to divide the free surface grid and the hull grid.

In the Dawson method, the hull meshing divides the hull surface into many quadrilateral four-node units. Triangular elements are used where necessary at the bow, stern, and the bottom of the ship. The double model solution is calculated by the Hess–Smith method. First, the numbers of streamlines, the number of points on each streamline, the coordinates of each point on the first streamline, the distance between the starting positions of each streamline are given and the coordinates of other unknown points on streamlines are calculated by double model solution. After all the points on the streamlines are calculated, the free surface meshes are formed by the adjacent points in order. The free surface mesh is divided into right-angle area and back-swept area [7]. A four-point streamlined windward difference format is used to satisfy the radiation condition of far front without wave. In order to avoid the excessively high amplitude of the tail, Dawson uses the two-point difference format for the last few rows of the free surface mesh. This section refers to Dawson's experience to generate a mesh.

2.3.6 Calculation Procedure of Rankine Source Method

First enter the ship data, which is required to provide hull value and a small number of input parameters, including the captain, fluid mass density, speed, free surface calculation area (the data sheet below for the data enter format of the S60 ship); then, the hull grid is automatically generated. The Hess-Smith program module uses the Boundary Element Method to calculate the potential flow field and provides the Rankine source module with the streamline distribution over the velocity field and the free surface around the hull without wave or viscous assumptions. The free surface streamline is obtained by Runge–Kutta method, and the free surface mesh is generated by the streamline tracking method. The Rankine program module uses a combination of boundary elements and finite differences to provide a velocity field, a pressure field, a wave-making resistance, and a waveform around the ship in a nontacky and wave-assumed manner. Finally, the results of calculation (the velocity, pressure, wave resistance, waveform, and streamline of the flow field around the hull) are output as data files. The block diagram is shown in Fig. 2.7.

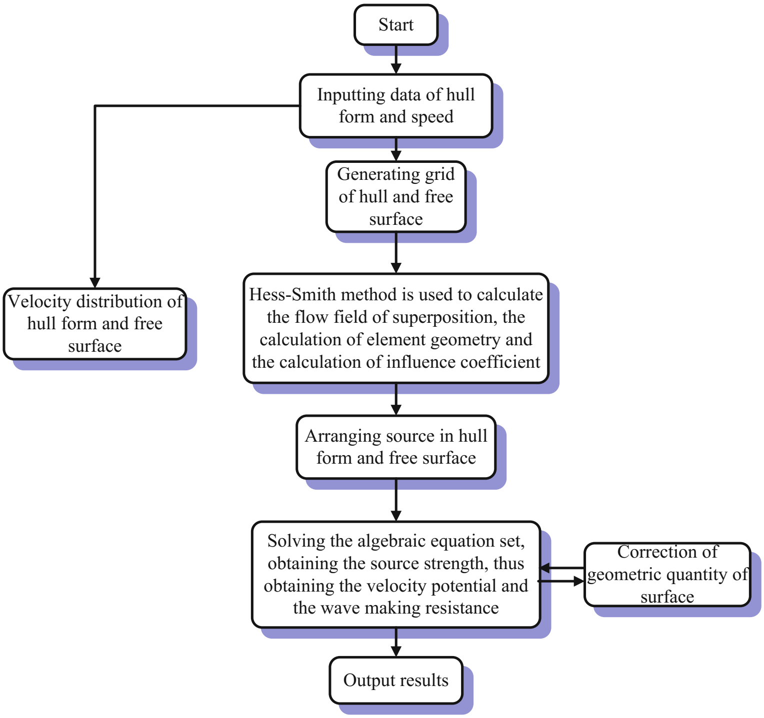

Fig. 2.7 Program flowchart of Rankine source method

```
100   126    1    1    1   101.900     2.000
  0     1    1
  1 000   -1.0000   0.0000   0.1070     Node coordinate value（x,y,z）
  2 000   -1.0000   0.0000   0.0803
  3 000   -1.0000   0.0000   0.0535
  4 000   -1.0000   0.0000   0.0267
  5 000   -1.0000   0.0000   0.0080
  6 000   -1.0000   0.0000   0.0000
  … ……     ……       ……       ……
  … ……     ……       ……       ……
  … ……     ……       ……       ……
121 000    1.0000   0.0000   0.1070
122 000    1.0000   0.0000   0.0803
123 000    1.0000   0.0000   0.0535
124 000    1.0000   0.0000   0.0267
125 000    1.0000   0.0000   0.0080
126 000    1.0000   0.0000   0.0000
```

Hull grid nodes

```
  1   0    1    2    8    7     Node number on the unit
  2   0    2    3    9    8
  3   0    3    4   10    9
  4   0    4    5   11   10
  5   0    5    6   12   11
  6   0    7    8   14   13
  … …    …    … …    …
  … …    …    … …    …
  … …    …    … …    …
 95   0 113 114 120 119
 96   0 115 116 122 121
 97   0 116 117 123 122
 98   0 117 118 124 123
 99   0 118 119 125 124
100   0 119 120 126 125
```

Hull grid units

```
  1.23961    0.00000    0.00000
     16         40         0

 1   -1.63972    0.00000    Coordinate values along the first
                            streamline of the hull（x,y）
 2   -1.38169    0.00000
 3   -1.20850    0.00000
 4   -1.10139    0.00000
 5   -1.04192    0.00000
 6   -1.01357    0.00000
 …    ……           ……
 …    ……           ……
 …    ……           ……
35    1.70203    0.00000
36    2.00000    0.00000
37    2.29797    0.00000
38    2.59594    0.00000
39    2.89390    0.00000

40    3.19187    0.00000
```

Coordinates along the first Streamline of the hull

The coordinates of the starting point of each streamline in the free-surface grid

1	-1.63972	0.06250
2	-1.63972	0.12500
3	-1.63972	0.18750
4	-1.63972	0.25000
…	……	……
…	……	……
…	……	……
13	-1.63972	1.03818
14	-1.63972	1.19111
15	-1.63972	1.36490
16	-1.63972	1.56238

The starting point of the first streamline coordinate value（x,y）

In order to verify the reliability of the program, this section calculates the wave-making resistance of Wigley mathematical model and S60 ship model and plots free surface waveforms. The calculation results are in good agreement with the experimental results (from Osaka University, Japan). At the same time, the calculation results in this section are also compared with the experimental values and the predecessors' calculation results.

2.3.7 *Examples*

(1) Wigley ship

Wigley ship is commonly used in experiments and numerical calculation of the hull and its hull surface can be expressed by mathematical equations. The main parameters are $L = 2.0$, $B/L = 0.1$, and $T/L = 0.0625$. The hull surface is defined as $y = 0.1\ (1\text{-}\xi 2) \times (1\text{-}\zeta 2)$, where $\xi = x/L$ and $\zeta = Z/T$. A total of 160 surface elements are divided into hull surfaces, and 690 surface elements are divided into free surfaces. The cross profile and waterline of the hull are shown in Figs. 2.8 and 2.9; the free surface mesh is shown in Fig. 2.10; the free surface waveform is shown in Fig. 2.11; the wave-making resistance coefficient curves are shown in Fig. 2.12; the curves of the comparison between the calculated value and experimental value of wave-making resistance coefficient are shown in Fig. 2.13.

It can be seen from the wave-making resistance coefficient curve of Fig. 2.12 that for the Wigley ship, Rankine's method has a smooth and stable curve, and its calculation result is closer to the experimental value, but there is still a gap between the measured value and the experimental value, mainly because the calculation does not consider the impact of viscosity and nonlinear factors. However, the curve of Michell integral method shows a great fluctuation, which is far from the experimental value curve. It can be seen from the free surface waveforms that Kelvin wave shapes can be reproduced at high Fourier numbers.

It can be seen from the comparison between the calculated value and the experimental value of the wave-making resistance coefficient in Fig. 2.13 that the wave tendency of the wave resistance coefficient calculated by different authors is consistent with the experimental curve. The wave-making resistance coefficient curve calculated by the method in this section is very close to the experimental curve when Fr = 0.25–0.34, so using the method in this section to evaluate the resistance performance of an elongated ship such as Wigley is still more reliable.

(2) S60 ship

The main design parameters of the S60 ship are shown in Table 2.1. The surface of the hull is divided into 120 bins, and the free surface is divided into 752 bins. The hull cross section and waterlines are shown in Figs. 2.14 and 2.15. The free surface mesh is shown in Fig. 2.16. The free surface waveform is shown in Fig. 2.17. The wave resistance coefficient curve is shown in Fig. 2.18. The calculated value of the wave resistance coefficient curve is compared with the test value in Fig. 2.19.

It can be seen from the wave resistance coefficient curve in Fig. 2.18 that for S60 ship, the trend of the three curves is basically the same. Rankine source method and the test value are relatively close, but there is still a gap with the experimental value, mainly because the nonlinear factors have not been considered. After the Fourier number is greater than 0.24, the Michell integral method shows a large fluctuation in the curve because Michell integral is a thin ship theory, and the actual ship has a certain thickness, so the result will be greatly deviated. From the free surface waveforms of the ship's traveling waves, it can be seen that there are obvious

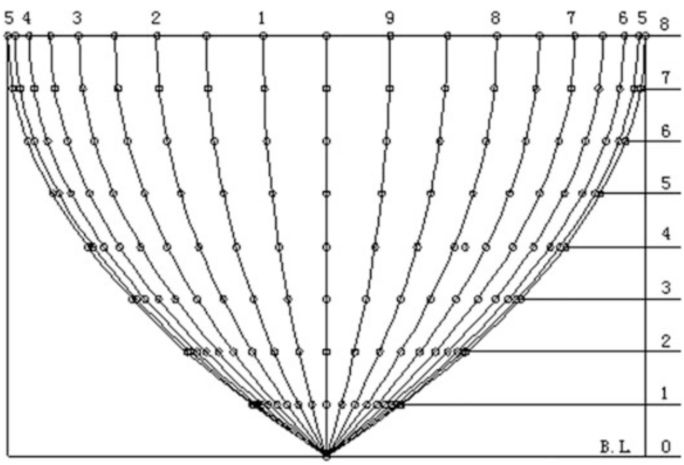

Fig. 2.8 Body lines of Wigley ship hull

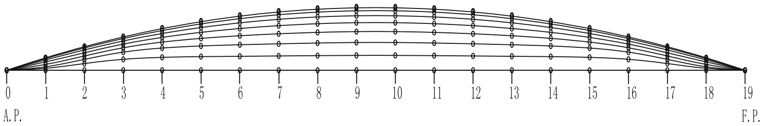

Fig. 2.9 Waterlines of Wigley ship hull

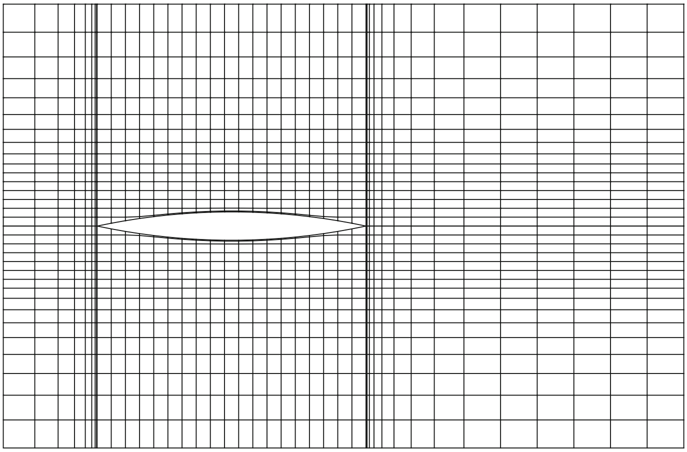

Fig. 2.10 Free surface mesh generation of Wigley ship

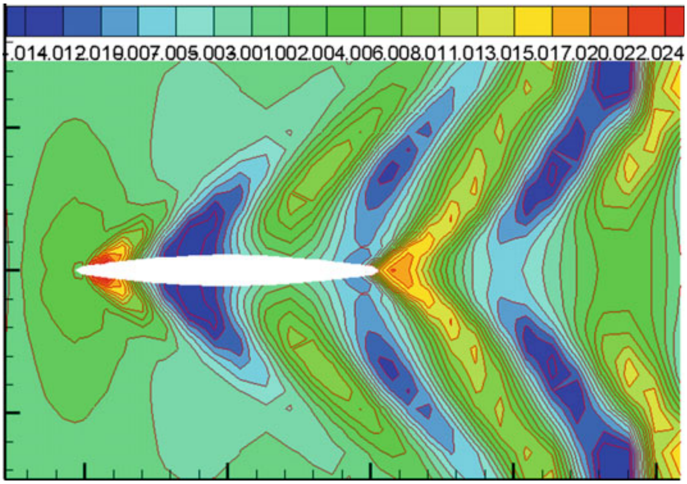

Fig. 2.11 Wave contour map of Wigley ship

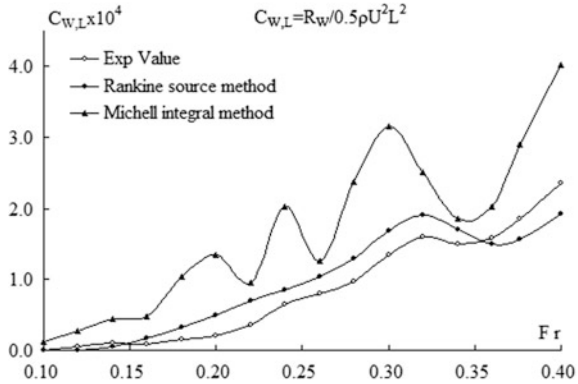

Fig. 2.12 Comparison of wave resistance coefficient curves of Wigley ship

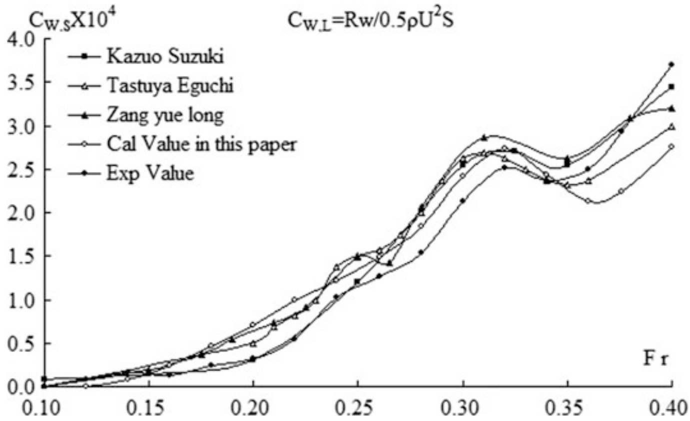

Fig. 2.13 Comparison between the calculated value and the experimental value of wave-making resistance coefficient of Wigley ship

Kelvin wave shapes, transverse waves and scattered waves, and wave regimes limited to ±19º28'.

It can be seen from the comparison between the calculated values and the experimental values of the wave resistance coefficients in Fig. 2.19 that the fluctuation trend of the wave resistance coefficient curve calculated by different authors is basically consistent with the experimental curve. In this section, the calculated

Table 2.1 Main design parameters of S60 ship

Length (L)	Beam (B)	Design draft (T)	Block coefficient (C_b)	Design Fr
2.0	0.267	0.107	0.60	0.285

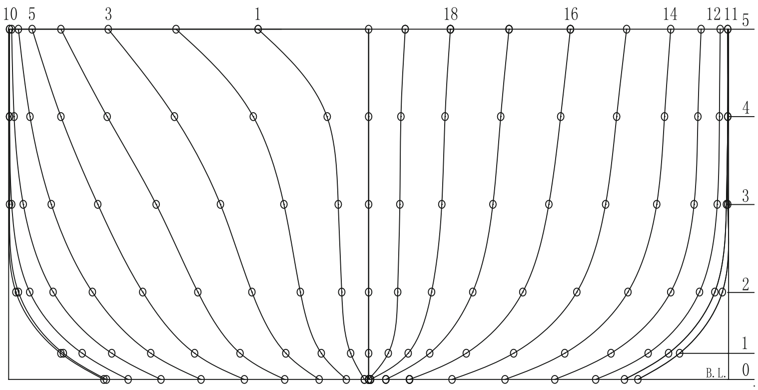

Fig. 2.14 Body lines of S60 ship

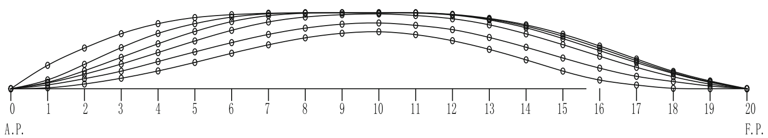

Fig. 2.15 Waterlines of S60 ship

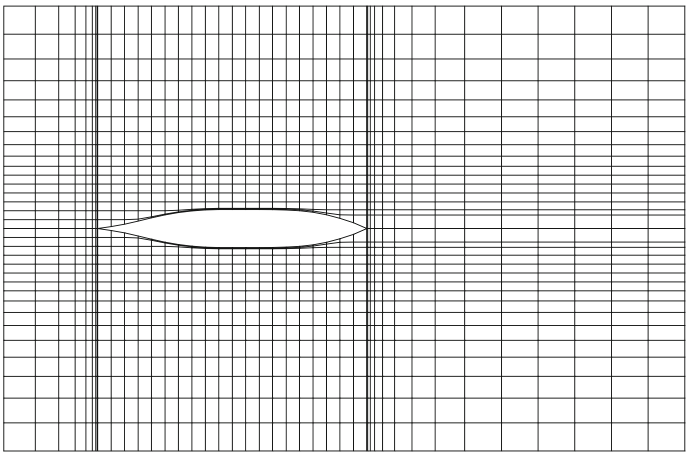

Fig. 2.16 Free surface mesh generation of S60 ship

curves are very close to the curves calculated by Suzuki Kazuo whose results have been confirmed to be accurate by many theories and experiments, and many of them have been published, which shows that it is effective and desirable to use this method to calculate the wave resistance value and optimize the ship type in the future.

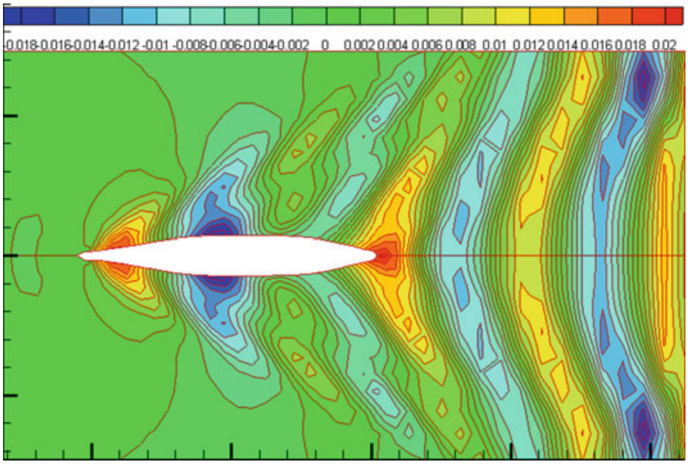

Fig. 2.17 Wave contour map of S60 ship Fr = 0.30

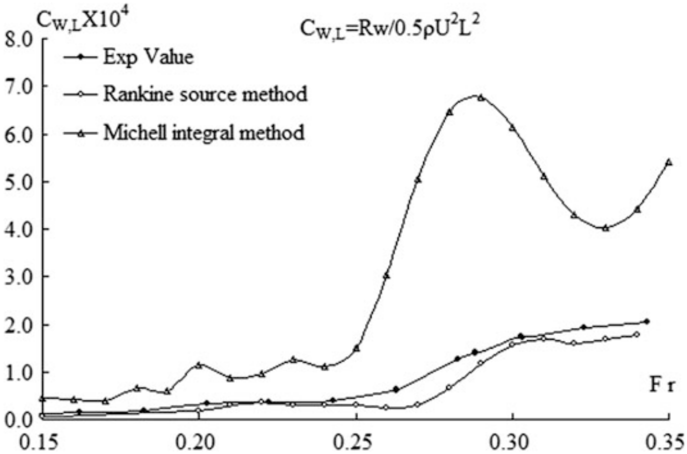

Fig. 2.18 Comparison of wave-making resistance coefficient curves of S60 ship

(3) DTMB5415 ship

DTMB5415 ship is a common international numerical simulation standard model with detailed experimental data. The main dimensions and parameters of the ship are shown in Table 2.2. The hull is divided into 2664 grids, and the free surface is divided into 4,100 grids. The body lines and waterlines are shown in Figs. 2.20 and 2.21, and the meshes of the free surface are shown in Fig. 2.22. The waveform contour is shown in Fig. 2.23, and the comparison between the wave resistance coefficient and the test value is shown in Fig. 2.24.

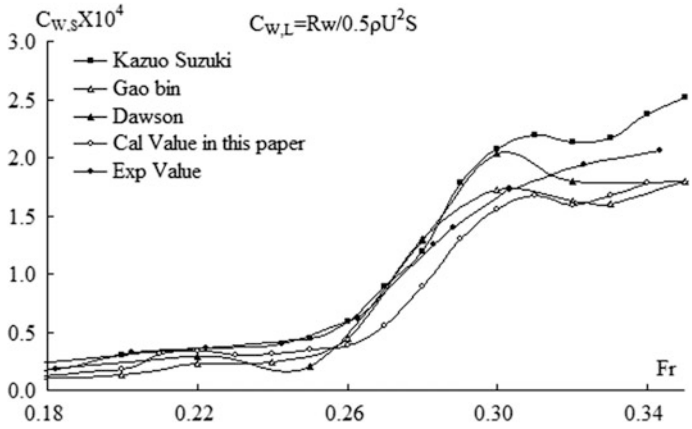

Fig. 2.19 Comparison between calculated value and experimental value of wave-making resistance coefficient of S60 ship

Table 2.2 Principal dimensions of DTMB5415 ship

Length L_{wl}/m	Breadth molded B/m	Draft d/m	Volume of displacement ∇/m^3	Wetted area S/m^2	Design Fr
5.719	0.766	0.248	0.549	4.82	0.28

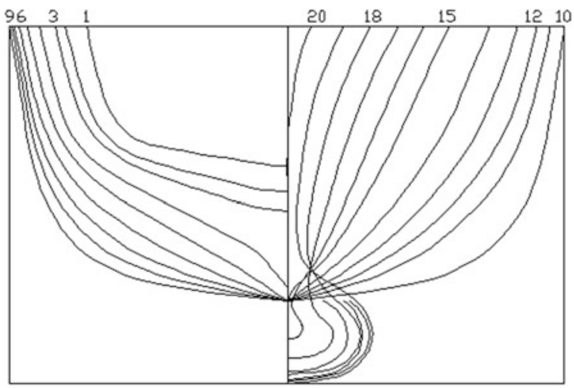

Fig. 2.20 Body lines of DTMB5415 ship

It can be seen from the comparison of the calculated and the experimental values of the wave resistance coefficients in Fig. 2.24 that Rankine source method is in good agreement with the experimental values, especially at the design speed point Fr = 0.28, and they are very close, but the difference between the other speed is very large, especially at low speed. From the free surface waveform, it can be seen that the Kelvin waveform is very obvious, which is basically consistent with the observed waveform.

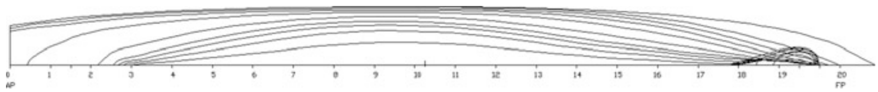

Fig. 2.21 Waterlines of DTMB5415 ship

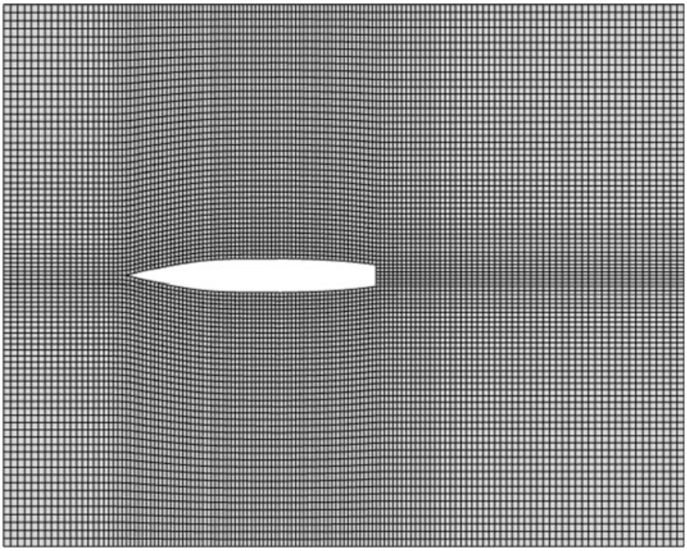

Fig. 2.22 Free surface mesh generation

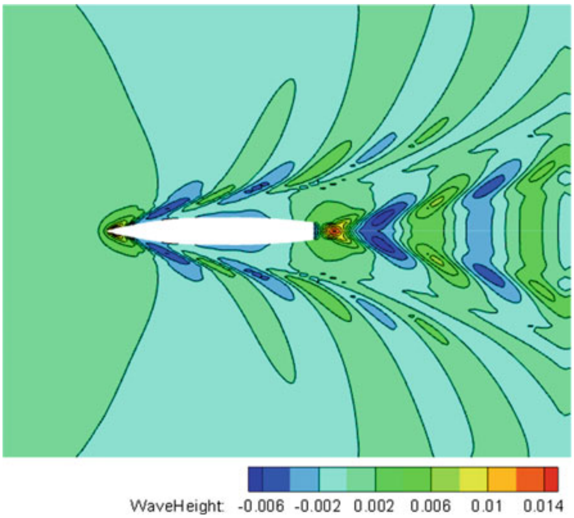

Fig. 2.23 Waveform contour map, Fr = 0.28

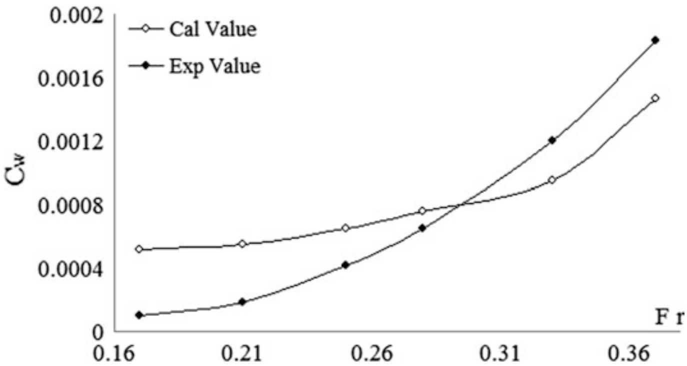

Fig. 2.24 Comparison between wave-making resistance coefficient curve and experimental values

2.4 Basic Theory of CFD

Any phenomenon of fluid flow in nature must follow the law of conservation of mass, the law of conservation of momentum, and the law of conservation of energy. If the fluid flow is in turbulence flow, the system should also obey additional turbulence controlling equations. The basic governing equation involved in this book is as follows [8].

2.4.1 Mass Conservation Equation

This law can be described as: The increase of the mass per unit time in the fluid micro-body is equal to the net increment of the micro-body flowing in the same time interval, and then the Mass Conservation Equation can be obtained as:

$$\frac{\partial \rho}{\partial t} + \frac{\partial(\rho u_x)}{\partial x} + \frac{\partial(\rho u_y)}{\partial y} + \frac{\partial(\rho u_z)}{\partial z} = 0 \tag{2.61}$$

If the fluid is incompressible, the density is constant and the above equation becomes:

$$\frac{\partial u_x}{\partial x} + \frac{\partial u_y}{\partial y} + \frac{\partial u_z}{\partial z} = 0 \tag{2.62}$$

So the Mass Conservation Equation is also called continuity equation.

2.4.2 Momentum Conservation Equation (N-S Equation)

This law can be described as follows: The momentum of the fluid in the micro-body is proportional to the sum of various forces acting on the micro-body by the outside world, which is actually Newton's second law. Its governing equation is expressed as follows:

$$\frac{\partial u_x}{\partial t} + u_x \frac{\partial u_x}{\partial X} + u_y \frac{\partial u_x}{\partial Y} + u_z \frac{\partial u_x}{\partial Z} = X - \frac{1}{\rho} \frac{\partial p}{\partial X} + v \nabla^2 u_x \tag{2.63}$$

$$\frac{\partial u_y}{\partial t} + u_x \frac{\partial u_y}{\partial X} + u_y \frac{\partial u_y}{\partial Y} + u_z \frac{\partial u_y}{\partial Z} = Y - \frac{1}{\rho} \frac{\partial p}{\partial Y} + v \nabla^2 u_y \tag{2.64}$$

$$\frac{\partial u_z}{\partial t} + u_x \frac{\partial u_z}{\partial X} + u_y \frac{\partial u_z}{\partial Y} + u_z \frac{\partial u_z}{\partial Z} = Z - \frac{1}{\rho} \frac{\partial p}{\partial Z} + v \nabla^2 u_z \tag{2.65}$$

In the formula, X, Y, Z, respectively, represent the unit mass force that the micro-body receives in three directions, p represents the fluid pressure, and v is the fluid kinematic viscosity coefficient.

2.4.3 Reynolds Equation

The equations described above are universal equations for Newton continuous media fluids both laminar and turbulent. However, it is unrealistic to use Direct Numerical Simulation (DNS) and Large Eddy Simulation (LES) based on the current calculation conditions, and the actual project focuses more on the mean of turbulence elements. So in our applications, the basic method of calculating turbulence is to solve the RANS equation, which is:

$$\frac{\partial U_j}{\partial x_j} = 0 \tag{2.66}$$

$$\frac{\partial (U_i U_j)}{\partial x_j} = -\frac{1}{\rho} \frac{\partial p}{\partial x_i} + \frac{\partial}{\partial x_j} \left[v \left(\frac{\partial U_i}{\partial x_j} + \frac{\partial U_i}{\partial x_i} \right) \right] - \frac{\partial \left(u_i' u_j' \right)}{\partial x_j} + g_i \tag{2.67}$$

In the formula, we take the Cartesian coordinate system xi (i = 1, 2, 3), g1 = g2 = 0, and g3 = -g (positive in the z-direction); g is the acceleration of gravity; this additional term is called Reynolds stress or turbulent stress.

2.4.4 Turbulence Model

The k-Ɛ turbulence model considers both the turbulence pulsation velocity transport and the turbulence pulsation length transport. Compared with the zero-equation turbulence model and the one-turbulent model, the turbulence model is more widely used and has been subjected to a large number of tests. Turbulence energy transport equations and energy dissipation transport equations are as follows:

$$\frac{\partial(\rho\kappa)}{\partial t}+\frac{\partial(\rho\kappa U_i)}{\partial X_i}=\frac{\partial}{\partial X_j}\left[\left(\mu+\frac{\mu_t}{\sigma_k}\right)\frac{\partial\kappa}{\partial X_j}\right]+G_k-\rho\varepsilon \tag{2.68}$$

$$\frac{\partial(\rho\varepsilon)}{\partial t}+\frac{\partial(\rho\varepsilon U_i)}{\partial X_i}=\frac{\partial}{\partial X_j}\left[\left(\mu+\frac{\mu_t}{\sigma_\varepsilon}\right)\frac{\partial\varepsilon}{\partial X_j}\right]+\rho C_1E\varepsilon-\rho C_2\frac{\varepsilon^2}{k+\sqrt{\nu\varepsilon}} \tag{2.69}$$

where $C_1=\max\left[0.43,\frac{\eta}{\eta+5}\right],\eta=\left(2E_{ij}\cdot E_{ij}\right)^{\frac{1}{2}}\frac{\kappa}{\varepsilon},E_{ij}=\frac{1}{2}\left(\frac{\partial U_i}{\partial X_j}+\frac{\partial U_j}{\partial X_i}\right)$.

2.4.5 Wall Function Method

The basic idea of the wall function method is that the turbulence flow, the core region, is solved by a turbulence model with high Reynolds number instead of solving in the wall region. The semiempirical formula is used directly to relate the physical quantity on the wall to the unknown to be sought in the turbulence core area. In this way, the number of node variables of the control volume adjacent to the wall surface can be directly obtained solving the flow in wall region. When meshing, there is no need to encrypt the wall area, and only the first interior node needs to be developed in a well-developed area of turbulence.

For the wall function method, it is the key to obtain the demarcation point between the logarithmic law and the viscous sublayer. For the current calculation, c^{y+} is selected as the demarcation point, then:

When the control volume node adjacent to the wall satisfies $y^+ < y_c^+$, the flow in the control volume is at the bottom of the adhesive layer, and the velocity is linearly distributed along the normal direction of wall, that is:

$$u^+=y^+ \tag{2.70}$$

When the control volume node adjacent to the wall satisfies $c^{y+} > y^+$, the flow in the control volume is logarithmic and the velocity is logarithmically distributed along the normal direction of wall, that is:

$$u^{+} = \frac{1}{k} \ln E y^{+} \tag{2.71}$$

where k is the Karman constant and E is the constant related to the wall roughness. For smooth walls, k value is 0.4 and E value is 9.8.

Meanwhile, in the CFD software, it is recommended that y^+ is calculated by the following formula:

$$y^{+} = \frac{\Delta y (C_{\mu}^{1/4} k^{1/2})}{\mu} \tag{2.72}$$

where k is the turbulent kinetic energy of the node.

2.4.6 Boundary Condition

The most common boundary conditions are the Dirichlet condition and the Neumann condition on closed boundaries, which can also be called the first type of boundary conditions (Dirichlet boundary conditions)and the second type of boundary conditions (Neumann boundary conditions).

The first type of boundary condition describes the number of variables on the boundary or partial boundary of the calculation region, which is:

$$\phi = \phi', \quad \text{on the boundary} \tag{2.73}$$

where ϕ' indicates the number of a physical quantity ϕ on the boundary.

The second type of boundary condition describes the normal component of the gradient of the variable on the boundary, which is:

$$\vec{n} \cdot \nabla \phi = \phi_n, \quad \text{on the boundary} \tag{2.74}$$

2.4.6.1 Velocity Inlet

The boundary conditions of velocity inlet are used to define the flow velocity at the flow inlet and other associated scalar flow variables. For Dirichlet boundary conditions, the velocity at the entrance is predetermined, generally uniform flow conditions, and if the uniform flow velocity is $\vec{u}_c$, then:

$$\vec{u} = \vec{u}_c \tag{2.75}$$

The turbulent kinetic energy k and turbulent dissipation rate ε are usually derived from the experimental data or given by the following formula:

$$k = \frac{3}{2}(\overline{u}I)^2 \tag{2.76}$$

where $\overline{u}$ is the average velocity and I is the intensity of turbulence, according to the following formula:

$$I = \frac{u'}{\overline{u}} = 0.16(\mathrm{Re}_{D_H})^{-1/8} \tag{2.77}$$

2.4.6.2 Flow Outlet

Outflow boundary conditions are used to simulate the exit boundary where both velocity and pressure are unknown before solving. This boundary condition applies when the flow at the exit is completely developed. Outflow boundary cannot be used for compressible flow. It also cannot be used with pressure inlet boundary in the same flow field. Therefore, the outflow boundary condition can be expressed as:

$$\frac{\partial \phi}{\partial n} = 0, \quad \varphi = \varepsilon \tag{2.78}$$

2.4.6.3 Symmetric Boundary Condition

Symmetric boundary conditions are used when the physical shape and the solution of the desired flow have mirror symmetry. Generally speaking, the ships are symmetrical about the mid-longitudinal section, so the flow field around ship is also symmetrical about the mid-longitudinal section so that the mid-longitudinal section can be set as the symmetrical plane in the simulation. There is no exchange of physical quantities, such as mass and heat on the symmetrical plane so the normal velocity on the plane of symmetry is zero, that is:

$$u_n = \overrightarrow{n} \cdot \overrightarrow{u} = 0 \tag{2.79}$$

where: $\overline{n}$ means the unit normal vector of the symmetrical plane.

2.4.6.4 Wall Condition

In viscous fluids, the wall surface is generally considered to be a nonboundary condition. For example, the velocity of the fluid at the interface is equal to the velocity of the solid boundary.

At the solid boundary, if the velocity of solid boundary is $\overrightarrow{u}_c$, then the flowing solid boundary condition is:

$$\overrightarrow{u} = \overrightarrow{u}_c \tag{2.80}$$

This is called a slip-free condition.

2.4.7 *Free Surface Simulation*

At present, based on the numerical calculation of RANS-based ship's flow field, the free surface simulation can be divided into interface tracking and interface capturing.

Interface tracking method is to track the free surface by moving the grid, the free surface is regarded as a coordinate surface, and the calculation is constantly updated grid to adapt to the free surface. This method only needs to establish control domain for water and can precisely meet the boundary conditions at the free surface, so it is widely used in the field of ships. However, this method is difficult to deal with wave breaking and overlap the free interface, and it needs to update the mesh every time step which is a large amount of calculation.

Interface capture method adopts the Euler viewpoint to describe the moving interface. The calculation mesh covers the entire fluid domain, and it does not need to be moved during the solution process. Instead, the tracking method is to track the free surface through other methods such as setting equivalence functions, labeling particles. This method can handle complicated free interfaces, including wave rolling, stern wave breaking, deck waves, and other issues. Many algorithms can be used on this problem. For example: MAC, level-set, VOF. This book mainly adopts the VOF method to capture the interface between air and water.

2.4.7.1 The Method of VOF

Volume of fluid (VOF) is an interface tracking method under a fixed Euler grid that simulates multiple flow models by solving the momentum equation and volume fractions of one or more fluids. This method regards water and air as the same medium defining a fluid volume function φ throughout the flow field, where φ is the ratio of the volume of one fluid (target fluid) to the mesh volume. If $\varphi = 1$, the cell is filled with the target fluid. If $\varphi = 0$, the cell is filled with another fluid and the area where φ varies rapidly from 0 to 1 is the free surface. The equation is:

$$\frac{\partial a_q}{\partial t} + \frac{\partial(ua_q)}{\partial x} + \frac{\partial(va_q)}{\partial y} + \frac{\partial(wa_q)}{\partial z} = 0 \tag{2.81}$$

$$\frac{\partial \alpha_q}{\partial t} + v_q * \nabla \alpha_q = \frac{S_{\alpha_q}}{\rho_q} + \frac{1}{\rho_q} \sum_{p=1}^{n} (\dot{m}_{pq} - \dot{m}_{qp}) \tag{2.82}$$

where a_1 and a_2 are, respectively, the volume fractions of water and air; $a_q = 0.5$ is the interface between water and air; q = 0–the unit is filled with water; q = 1–the unit is filled with air.

2.4.8 *Numerical Solution Method*

2.4.8.1 Discrete Method

It is complicated and difficult to solve the Reynolds equation directly. The existing CFD algorithms always discretize the differential equations to obtain the approximate value on the computer. Commonly used numerical discretization methods are: finite difference method, finite element method, finite volume method, and so on. Refer to the relevant reference books for details.

2.4.8.2 SIMPLE Algorithm

SIMPLE algorithm is a semi-implicit method used for solving pressure-coupled equations. It is a mathematical method for solving the incompressible flow fields, as well as compressible flow fields. Its core is to use the "guess-correction" process, based on the staggered grid to calculate the pressure field, so as to achieve the purpose of solving the Navier–Stokes equations. The basic idea of the SIMPLE method is to find the velocity field by solving the discrete form of the momentum equation for a given pressure field. Because the pressure field is assumed or imprecise, the resulting velocity field generally does not satisfy the continuous equation and must be corrected for a given pressure field. The correction principle is that the velocity field corresponding to corrected pressure field can satisfy the continuous equation at this iteration level. According to this principle, the relationship between pressure and velocity specified by the discrete form of the momentum equation can be substituted into discrete form of the continuous equation to obtain the pressure correction from the pressure correction equation. Next, a new velocity field is solved based on the corrected pressure field. Then, check whether the velocity field is convergent; if not, use the corrected pressure as a given pressure field and start the next level of calculation. This is repeated until a convergent solution is obtained.

2.4.9 *Meshing*

The proper layout of the grid and proper encryption are crucial to improve the accuracy of the calculation and identify the details of the local flow. The quality of mesh generation will directly influence the quality of simulation and calculation. Therefore, the general grid should follow the following principles:

(1) The mesh distribution should be sparse and reasonable. Free surface needs to capture the wave form, so the mesh close to the free surface should be denser. The impact of fluctuations in the bottom of the basin is small, so the mesh here should be sparser. The gradient of the parameters in the vicinity of the object plane is large, so the mesh should be denser; the parameter variation far from the object is small, so the mesh should be sparser.
(2) Grid lines should be as orthogonal as possible, and curves should be as smooth as possible. The grid line should be consistent with the flow direction.
(3) Discrete meshes should be as close as possible to the body. The boundary conditions of the object surface will use the interpolation method to generate errors as long as mesh nodes are not attached to the surface of the object. The parameters in the flow field depend on the number of boundary parameters, so there is an error correspondingly.
(4) In all the mesh, negative volume cannot appear and the quality of meshes should meet the calculation requirements. In CFD method for numerical simulation of flow field, we must first discretize the computational area, that is, divide the mesh. Mesh can be divided into four categories: structural mesh, unstructured mesh, dynamic mesh, and overlapping mesh. Each mesh has its own advantages and disadvantages, and the following will focus on overlapping mesh.

(1) Overlapping mesh

With the deepening of research in the field of ships, the problem of ship movement has become one of the main contents that must be taken into account in the calculation of ship resistance. Conventional structured mesh and unstructured mesh have great difficulty in simulating object moving. The overlapping mesh is a new type of gridding technology. It not only simulates the various states of the hull more easily, but also has better ability to solve the large-scale movement problems. So far, it has been widely used. Overlapping meshes separate each part of the model into separate meshes, which are then nested into the background mesh. It generates better quality grids and can relatively solve objects with large amplitude motions accurately. First, the hold points and interpolated points need to be marked. Second, overlapping units can be removed by digging the hole. Then, interpolation is carried out to complete data exchange in the interface. Finally, the entire flow field is calculated. As shown in Fig. 2.25: Shaded two receiver grid cells one in the primary domain and one in the secondary domain [9].

The flow between the surface of the acceptor mesh and the surface of the nearest activated mesh unit is approximately the same as the flow between the two activated mesh surfaces. However, regardless of which receiver mesh center is referenced (at the open symbol in the diagram), the weight variable in the data mesh will be replaced:

$$\phi_{acceptor} = \sum \alpha_i \phi_i \tag{2.83}$$

In this equation, αi is the interpolation weight factor, ϕ1 is the dependent variable of the variable supply unit, and i represents the node for all variables (provided by the green triangle in the diagram) for the variable. Thus, an algebraic

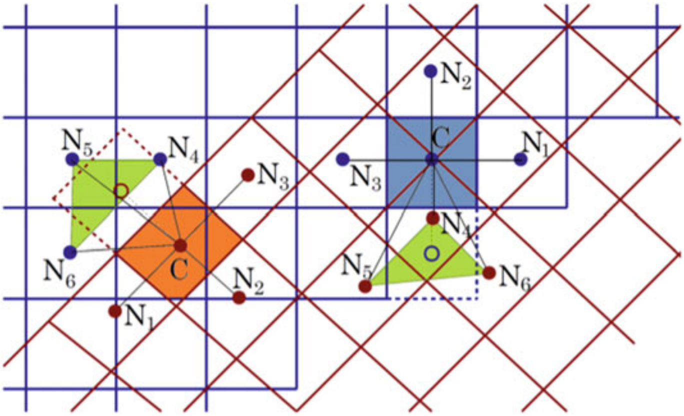

Fig. 2.25 A diagram of overlapping mesh

equation for a C unit is established by three adjacent cells (N1–N3) in the illustration and three cells (N4–N6) in the overlap region. The coefficient matrix of the solution equation (either for the separation solution or coupled solution) should be updated according to ensure that the equation is solved under the condition that the residuals are satisfied.

This section uses overlapping meshes to divide into computational domains. There are various kinds of interpolation methods, in which linear interpolation uses the shape function to connect the centers of variable grids and proceed with passing the receiver mesh center from one interpolation unit to the next. Although this method is inefficient, it is more accurate. The specific meshing is shown in the example in Fig. 2.5.4.

2.5 The Establishment of Numerical Wave Tank

2.5.1 Wave Making at Velocity Boundary

The velocity boundary wave method uses the wave-making method for a given wave velocity at the speed entrance boundary. Compared to physical test tanks, this method is less costly, easier to implement, more accurate, and slower to decay. Compared with the method of imitating the physical method, it is easy to give a fixed velocity of the ship at the entrance boundary as well as to avoid the difficulties caused by the moving boundary [10].

The wave front equation is:

$$\eta = a\cos(kx - \omega_e t) \tag{2.84}$$

The velocity field is as follows:

$$u = a\omega_o e^{kz}\cos(kx - \omega_e t) + U \tag{2.85}$$

$$y(x, y, z) = 0 \tag{2.86}$$

$$w = a\omega_o e^{kz}\sin(kx - \omega_e t) \tag{2.87}$$

where k is wave number, determined by the formula k = 2π/λ, and ω is the natural frequency of wave, determined by the formula $\omega = \sqrt{2\pi g/\lambda}$.

2.5.2 Numerical Wave Cancelation

Damping of waves is possible by introducing resistance to vertical motion. The Choi and Sung's [10] method is used to damping of waves, adding a resistance term to the equation for vertical velocity:

$$S_z^d = \rho(f_1 + f_2|\beta|)\frac{e^{\kappa} - 1}{e^1 - 1}\beta \tag{2.88}$$

where $\kappa = \left(\frac{x - x_{sd}}{x_{ed} - x_{sd}}\right)^{n^d}$, x_{sd} is the starting point of absorbing region, x_{ed} is the outlet boundary of the wave tank, f_1, f_2 and n_d are the parameters of the model, and β is the vertical velocity component.

2.5.3 The Six Degrees of Freedom (SDOF) Motion Equation of Ship

While establishing the equation of motion of the ship, two reference coordinate systems are established, as shown in Fig. 2.26: One is a fixed coordinate system $O_oX_oY_oZ_o$ fixed to the earth; one is a ship-following coordinate system GXYZ [11]. The origin of the moving coordinate system is at the center of gravity (G) of the hull, wherein G_x, G_y, G_z are the middle cross section, the middle longitudinal section, and the water plane passing through the center of gravity G, respectively.

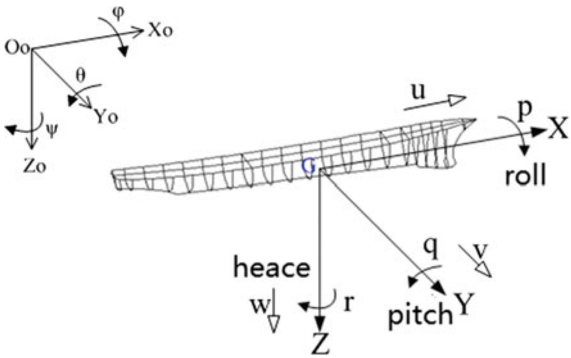

Fig. 2.26 Fixed coordinates and coordinates with the ship

With the ship's coordinate system, the positive direction of X-axis, Y-axis, and Z-axis is, respectively, bow, starboard, and bottom.

The force formula of Newton's second law shows that:

$$\begin{aligned} F &= \hat{i}X + \hat{j}Y + \hat{k}Z = ma = m\frac{d}{dt}(\hat{i}u + \hat{j}v + \hat{k}w) \\ &= m\left(u\frac{d\hat{i}}{dt} + \hat{i}\frac{du}{dt} + v\frac{d\hat{j}}{dt} + \hat{j}\frac{dv}{dt} + w\frac{d\hat{k}}{dt} + \hat{k}\frac{dw}{dt}\right) \end{aligned} \tag{2.89}$$

The moment formula of Newton's second law shows that:

$$\begin{aligned} M_1 &= \hat{i}K + \hat{j}M + \hat{k}N = \frac{d}{dt}(\hat{i}I_x p + \hat{j}I_y q + \hat{k}I_z r) \\ &= I_x p\frac{d\hat{i}}{dt} + \hat{i}\frac{d(I_x p)}{dt} + I_y q\frac{d\hat{j}}{dt} + \hat{j}\frac{d(I_y q)}{dt} + I_z r\frac{d\hat{k}}{dt} + \hat{k}\frac{d(I_z r)}{dt} \end{aligned} \tag{2.90}$$

where

$$\frac{d\hat{i}}{dt} = \hat{j}r - \hat{k}q, \qquad \frac{d\hat{j}}{dt} = \hat{k}p - \hat{i}r, \qquad \frac{d\hat{k}}{dt} = \hat{i}q - \hat{j}p$$

According to the above formulas, combined with the coordinate transformation, the motion equation of the ship with the origin of the moving coordinate system at the center of gravity is:

$$
\begin{aligned}
X &= m(\dot{u} + qw - rv) \\
Y &= m(\dot{v} + ru - pw) \\
Z &= m(\dot{w} + pv - qu) \\
L &= I_x \dot{p} + (I_Z - I_y)qr \\
M &= I_y \dot{q} + (I_x - I_z)rp \\
N &= I_z \dot{w} + (I_y - I_x)pq
\end{aligned}
\tag{2.91}
$$

where m is the hull mass in kg; u, v, w are the hull velocities in m/s; p, q, r are the hull angular velocities in rad/s; X, Y, Z are external forces of the hull, and their units are N; L, M, N are the moments of force on the center of gravity of the hull outside the body, and their units are N-m; $\dot{u}, \dot{v}, \dot{w}, \dot{p}, \dot{q}, \dot{r}$, are, respectively, the derivatives of velocity and angular velocity.

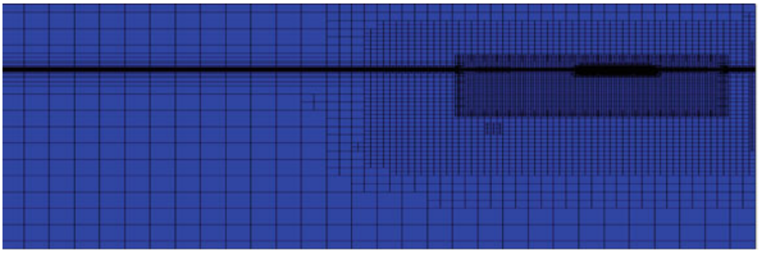

(a) The entire computational domain meshing

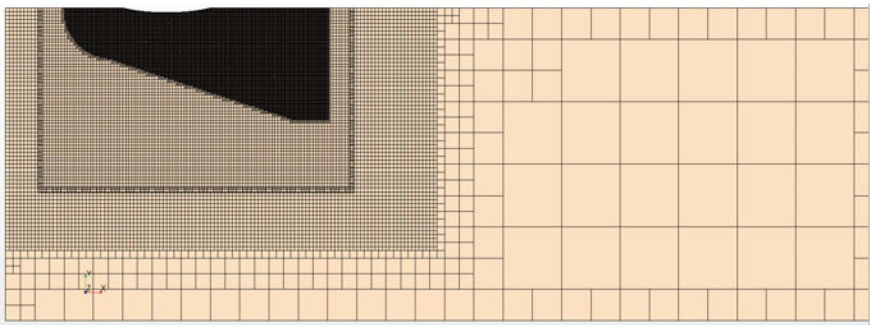

(b) The profile of mesh near the free surface

Fig. 2.27 Meshing of Wigley type

2.5.4 Examples

This section uses the Wigley, S60, and DTMB5415 models as examples, respectively, calculates the total resistance in static water by the method of CFD, compares it with the experimental values to verify the accuracy of the CFD analysis method, and lays the foundation for the next ship-type optimization. For ship parameters and line drawings, see the above sections. Resistance calculation uses STRA-CCM + software.

(1) Wigley type

This study still uses the Wigley ship model in Sect. 2.3.7 as an example for numerical simulation; this model has complete experimental data. The overlapping mesh technique is used to divide the hull and free surface grid, as is shown in Fig. 2.27, a total of 1.18 million meshes are divided, the hull grid is shown in picture Fig. 2.28, and the free surface grid is shown in Fig. 2.29. The performance of the calculation workstation is: DELL workstation of 12 core, 3.4 GHz 64 G

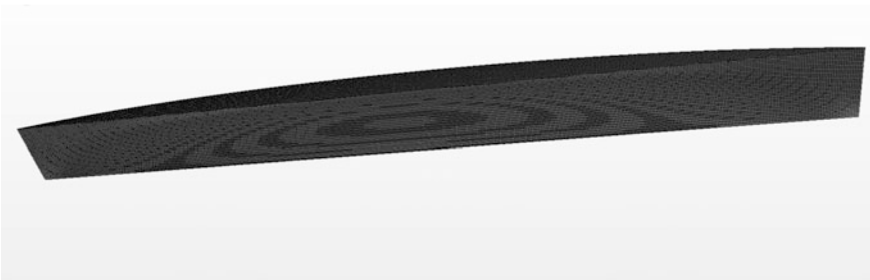

Fig. 2.28 Meshing of the hull of Wigley type

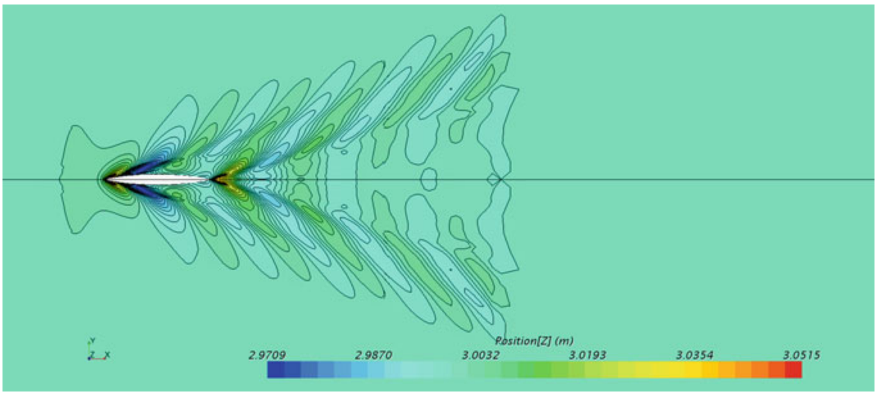

Fig. 2.29 Waveform about free surface of Wigley type, Fr = 0.30

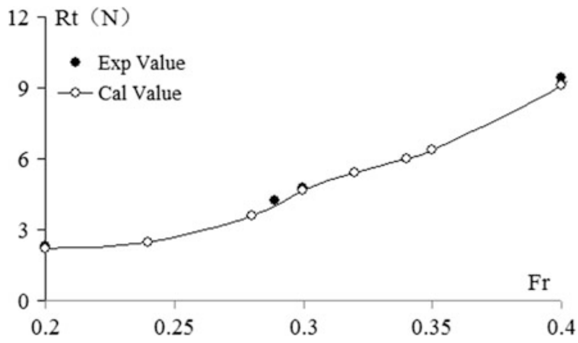

Fig. 2.30 Comparison of total resistance coefficient curve and experimental values of Wigley type

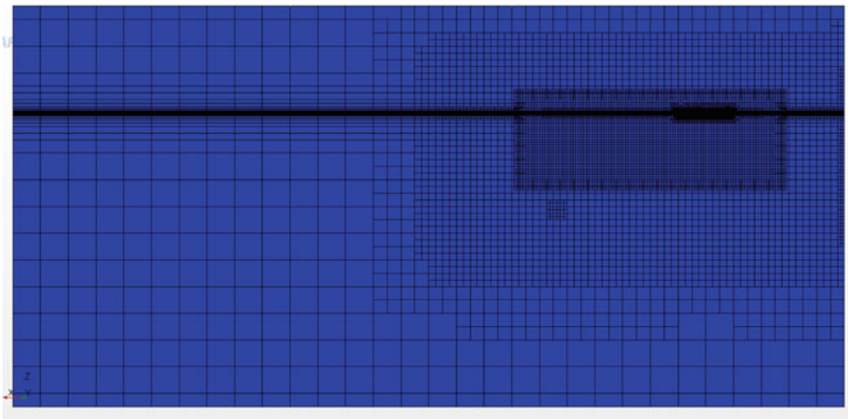

(a) Meshing in whole calculation domain

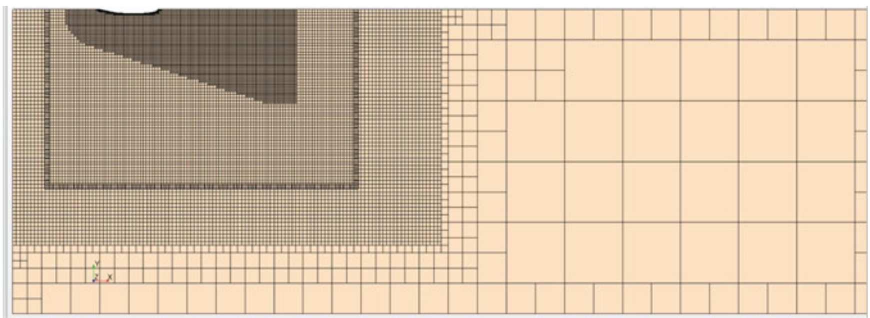

(b) The profile of mesh near the free surface

Fig. 2.31 Meshing of S60 type

Fig. 2.32 Meshing of the hull of S60 type

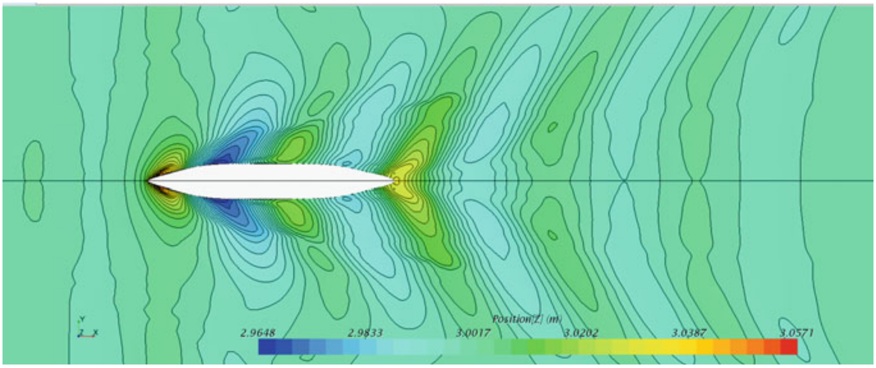

Fig. 2.33 Waveform about free surface of S60 type, Fr = 0.285

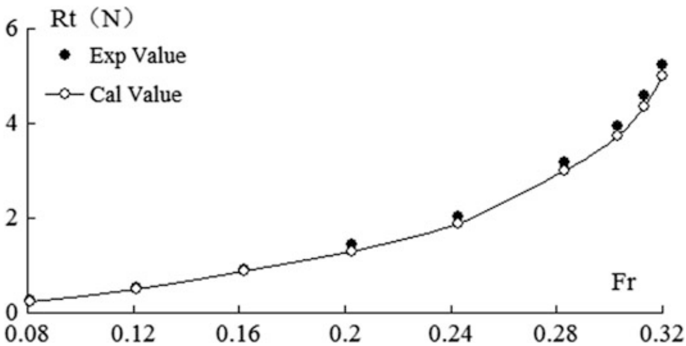

Fig. 2.34 Comparison of total resistance coefficient curve and experimental values of S60 type

memory, hard disk of 256G + 2T, video card of M4000. The comparison of numerical calculation and experimental results is shown in Fig. 2.30. It can be seen from the figure that the calculated results are close to the experimental values.

(2) S60 type

The main dimensions and parameters of the S60 type are shown in Table 2.1. The overlapping grid technique is used to divide the hull and free surface grid, as is shown in Fig. 2.31, and there are a total of 1.32 million meshes divided. The grid of the hull is shown in Fig. 2.32, and the free surface grid is shown in Fig. 2.33. The comparison between numerical calculation and experimental values is shown in Fig. 2.34. It can be seen from the figure that the calculated result is very close to the experimental result.

(3) DTMB5415 type

The main dimensions and parameters of the DTMB5415 type are shown in Table 2.2. The overlapping mesh technique is used to divide the hull and free surface grid, as is shown in Fig. 2.35, and there are a total of 2.23 million meshes divided. The hull grid is shown in Fig. 2.36, and the free surface grid is shown in Fig. 2.37. The comparison between numerical calculation and experimental values is shown in Fig. 2.38. The figure shows that the calculated result is very close to the experimental result.

The CFD method is used to analyze the resistance performance of three typical ship types. Compared with the previous theory of potential flow, the CFD method is closer to the experimental value and has higher calculation accuracy. With an

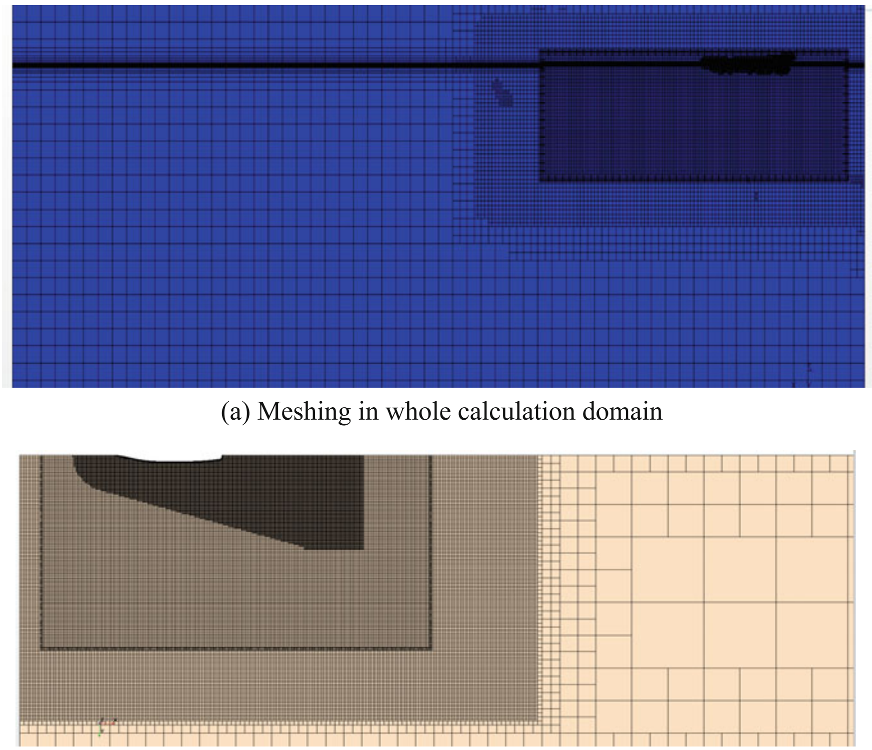

(a) Meshing in whole calculation domain

(b) The profile of mesh near the free surface

Fig. 2.35 Meshing of DTMB5415 type

Fig. 2.36 Meshing of the hull of DTMB5415 type

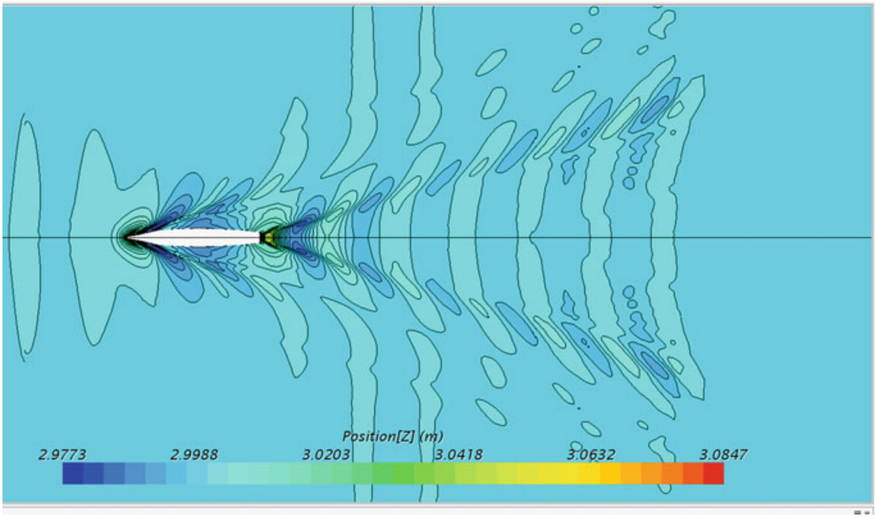

Fig. 2.37 Waveform about free surface of DTMB5415 type, Fr = 0.28

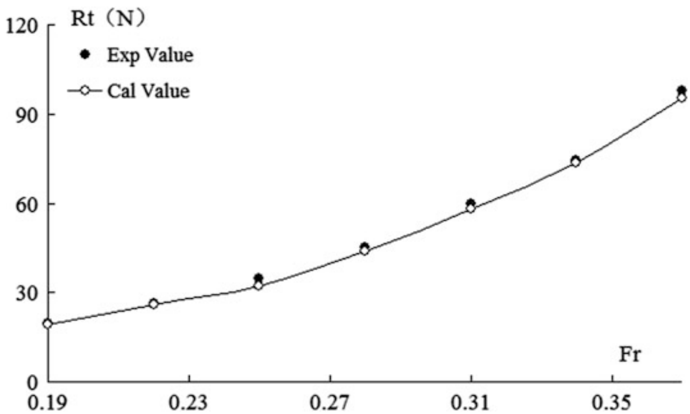

Fig. 2.38 Comparison of total resistance coefficient curve and experimental values of DTMB5415 type

appropriate number of grids and better machine configurations, ship-based optimization with CFD-calculated resistances as targets will yield more reliable results.

2.6 Study on the Uncertainty of CFD Affecting the Calculation of Ship Resistance

In order to study the uncertainties affecting CFD calculation of hull resistance, the DTMB5415 ship model is taken as the research object. First of all, based on the Latin matrix square design in the statistics, a rectangular square matrix with the thickness of the first boundary layer, the turbulence pattern, and the number of grids as the three major uncertainties in CFD ship calculation is established. Take viscosity theory method (CFD) to calculate the hull resistance, and simulate the flow field around the hull. Then, the influence factors of uncertainties on the prediction of hull resistance are discussed by means of regression analysis. Through a series of calculation and analysis, the optimal calculation method for the ship type is proposed and the relevant parameters for calculating the resistance of the ship model DTMB5415 are determined. Secondly, using these two kinds of grids to calculate the resistance at different speeds, respectively, and compared with the experimental values, we obtained satisfactory results. Finally, according to the ITTC regulation, the CFD-based uncertainty analysis and discussion of the resistance of DTMB5415 ship in still water using three grids are carried out. The corrected results are compared with the experimental ones to improve the accuracy of the resistance prediction.

2.6.1 Resistance Calculation

(1) Boundary conditions:

(1) The cutting volume mesh: The front, upper, and lower surface of the numerical simulative tank are set as velocity inlet, and the velocity is defined at the front surface boundary, namely the speed of the ship; the rear surface is set as a pressure outlet; the hull is set as a rigid body surface; the sides are set as symmetry.

(2) Overlapping mesh: According to the requirements of the overlapping meshes, the entire model needs two individuals, namely the background body and the overlapping body, wherein the overlapping body is an entity obtained by performing subtraction on the cuboid and the hull. In the background body, the boundary condition set exactly the same with the cutting volume mesh settings; in the overlapping body, the left side of the cuboid is defined as symmetry, the rest of the outer surface is set as an overset mesh, and the hull surface is set as a rigid body surface.

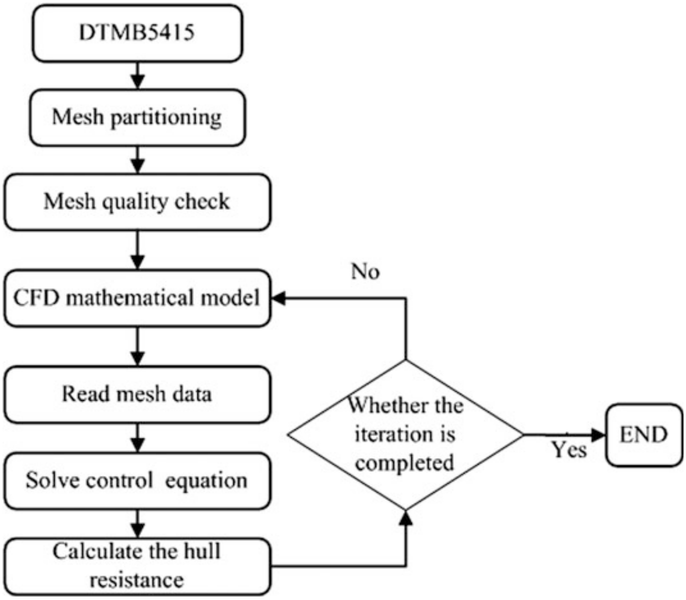

Fig. 2.39 Resistance calculation flow

(2) Calculation process:

Taking DTMB5415 ship as an example, CFD method is used to calculate the total resistance of the hull in the static water.

(1) Calculation pretreatment: Establish geometric model, mesh, grid quality inspection, and set the boundary conditions.
(2) Calculation process: Using three-dimensional nonstationary separation implicit solver and using the continuous equation and motion equation as the control equations of the whole model, the appropriate turbulence model is selected to solve the whole flow field; the free surface is captured by the VOF two-phase flow model; the SIMPLE method is used to couple the pressure and velocity fields. The detailed calculation process is shown in Fig. 2.39.

2.6.2 Analysis of CFD Influencing Factors

There are some errors in the CFD method to calculate the hull resistance in hydrostatic and experimental values, and when the calculation conditions are different, the error is not the same. The results of these errors are mainly caused by a series of uncertainties in the process from the initial stage of modeling to the meshing, the use of calculation methods, and the iterative calculation. These errors mainly include five aspects: mathematical model error, iterative error, rounding error, truncation error, and calculation error. In order to improve the accuracy of resistance prediction, it is necessary to accurately analyze which factors play a leading role in the resistance calculation and which ones play a secondary role. It is very time-consuming if these three factors discussed one by one. Therefore, this section introduces the experimental design to analyze the influencing factors of CFD resistance calculation.

The experimental design can select some of the most representative test points from the system model for analysis to find the close relationship between large numbers of data, with a view to get the maximum calculation results through a minimum number of tests and test cycles. It is a highly efficient, fast, and economical method of calculation. There are many kinds of experimental design methods, of which the Latin square was invented by Euler, a famous mathematician and physicist. It writes n different design elements in n squares with n edges, each row becomes a complete unit group, and each process appears only once per column.

(1) Latin square design

According to previous research experience, the main factors affecting the CFD calculation results include three factors: (1) the first boundary layer thickness, (2) turbulence model, and (3) the number of grids. Therefore, through the Latin square design and analysis of these three factors, the design model of four levels of three factors is constructed in the cutting volume mesh. On the overlapping meshes, due to the error of the RST model in the calculation of overlapping mesh, the resistance cannot be obtained, and thus the design model of three levels of three factors is constructed, as shown in Table 2.3. The Latin square design list, shown in Table 2.4, was designed with 16/9 test design. The total drag coefficient at the speed of $Fr = 0.281$ calculated by the CFD method is listed in this table. Figure 2.40 shows the error between the total resistance calculation and experimental value [12].

Taking the cutting body meshes and overlapping meshes as examples, the hydrodynamic performance of DTMB5415 vessel in hydrostatic water is numerically simulated by 16 kinds and 9 different calculation methods, respectively. It can be seen from Fig. 2.40 that on the mesh of cutting body, the error $|\varepsilon|$ between the total resistance and the experimental value calculated by the CFD method is between 2.5% and 18.5%. The total resistance calculated in case 9 is closer to the experimental value, and the error calculated in case 15 is the largest; on the overlapping meshes, the error between the total resistance value and the experimental value is $|\varepsilon|$ between 1.25% and 14.5%, the total resistance calculated by the working condition 2 is closer to the experimental value, and the calculation error of the working condition 1 is the largest. It can be seen that different calculation methods have a great influence on the calculation results of resistance. Therefore, it is necessary to systematically analyze these three factors to get the factors that greatly affect the calculation results.

Table 2.3 Four levels of three factors

Analysis factor	Factor number	Level	
		Cutting volume mesh	Overlapping mesh
The thickness of the first boundary layer A	A_1	0.0004	0.0003
	A_2	0.0003	0.0002
	A_3	0.0002	0.0001
	A_4	0.0001	Null
Turbulent model B	B_1	$k\!-\varepsilon$	$k\!-\varepsilon$
	B_2	SST $k\!-\omega$	SST $k\!-\omega$
	B_3	SA	SA
	B_4	RST	Null
The mesh number (relative ratio) C	C_1	49.984	35.35
	C_2	35.35	25
	C_3	25	17.68
	C_4	17.68	Null

Table 2.4 Design list and drag calculation results of Latin square array

No.	A	B	C	Cutting volume mesh	A	B	C	Overlapping mesh
				C_{QT}				C_{CT}
1	A_1	B_1	C_1	0.004782	A_1	B_1	C_1	0.003942
2	A_1	B_2	C_2	0.00434	A_1	B_2	C_2	0.004668
3	A_1	B_3	C_3	0.004405	A_1	B_3	C_3	0.00435
4	A_1	B_4	C_4	0.004742	A_2	B_1	C_2	0.004367
5	A_2	B_1	C_2	0.004782	A_2	B_2	C_3	0.004349
6	A_2	B_2	C_1	0.00435	A_2	B_3	C_1	0.003961
7	A_2	B_3	C_4	0.004854	A_3	B_1	C_3	0.004193
8	A_2	B_4	C_3	0.00447	A_3	B_2	C_1	0.004168
9	A_3	B_1	C_3	0.004728	A_3	B_3	C_2	0.004132
10	A_3	B_2	C_4	0.004448	Null			
11	A_3	B_3	C_1	0.005085				
12	A_3	B_4	C_2	0.004456				
13	A_4	B_1	C_4	0.004472				
14	A_4	B_2	C_3	0.004423				
15	A_4	B_3	C_2	0.005447				
16	A_4	B_4	C_1	0.004353				

According to the results of Table 2.4, the data were analyzed by regression. The analysis results are shown in Table 2.5. It can be seen from the table, in the cutting volume mesh, the influence degree from large to small is: turbulence mode B, mesh number C, and the thickness of the boundary layer of the first floor A; in the overlapping mesh, the influence degree is: mesh quantity C, turbulence mode B, and

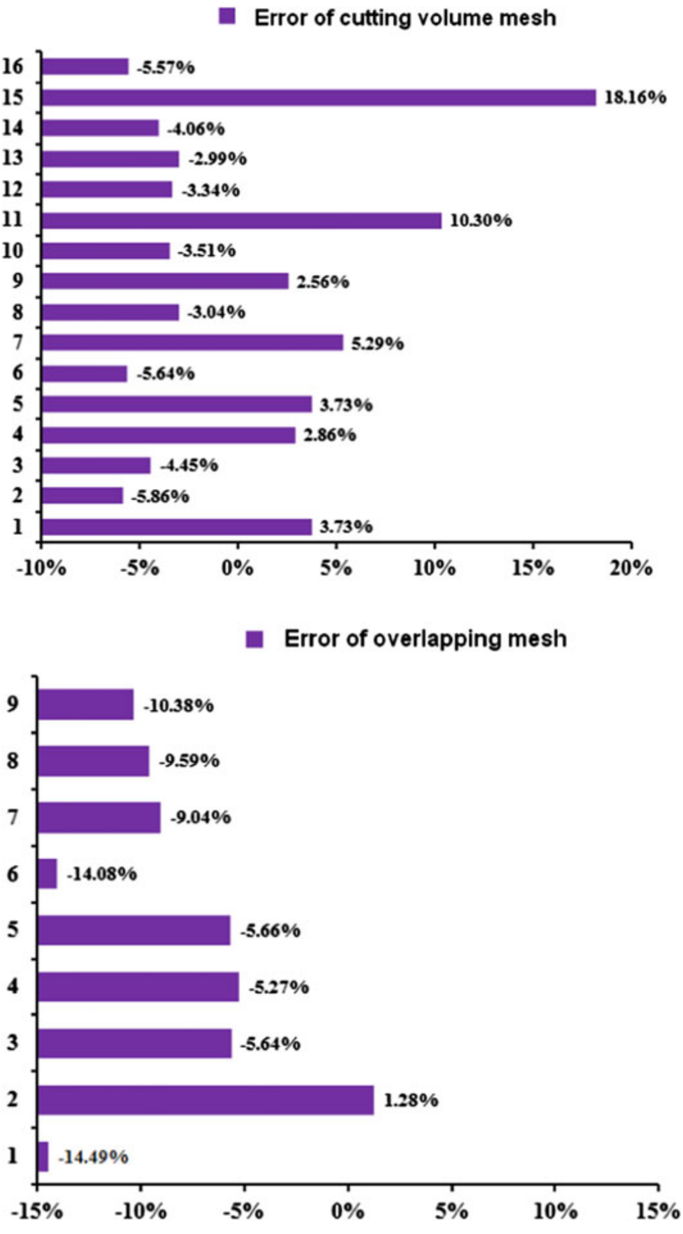

Fig. 2.40 Error ε between the calculation value of CFD and EFD

the thickness of the boundary layer of the first floor A. And the sum of squared deviations, the order of variance from largest to smallest, is exactly the same as the order of influence. Apparently, turbulence model selection has the most significant effect on the calculation results of the cutting body mesh. The number of grids has the most significant effect on the calculation results of the overlapping grids, while the thickness of the boundary layer on the first floor has the least effect on the calculation results of the two.

The data in Table 2.4 are classified according to the turbulence model, as shown in Fig. 2.41. It can be seen from the figure that the mean resistance error calculated by $k\text{–}\ \varepsilon$ turbulence model is the smallest on the cutting volume mesh with the error of 3.25%. However, the average error of SA calculation is the largest, reaching 9.55%. On the overlapping meshes, the average resistance error calculated by SST $k\text{–}\ \omega$ turbulence model is the smallest with an error of 5.51%. The mean error of SA calculation is the largest, reaching 10.03%. It can be seen that the $k\text{–}\ \varepsilon$ model is more suitable for the simulation of cutting volume mesh calculation and the SST k-1 is more suitable for the overlapping grid calculation as long as the appropriate number of meshes and the thickness of the layer boundary of the first floor are selected.

(2) Multi-speed resistance calculation

In this section, multi-speed numerical simulation of DTMB5415 is carried out by cutting volume mesh and overlapping mesh, respectively. It can be seen from the above section that the calculation methods of working condition 9 and working condition 2 can well predict the hull resistance. In order to improve the accuracy of calculation, the same method of meshing and calculation as the working condition is used to predict the hull resistance. The CFD calculation results are compared with the experimental values, and the results are shown in Fig. 2.42.

The calculation results show that the trend of the total resistance of the two meshes coincides with the experimental values, and the calculation errors of the two meshes are very close. Among them, the mean error of the cutting mesh calculated resistance is 2.5%; the average error of overlapping mesh calculated resistance is 2.78%. At the design speed Fr = 0.281, the calculated errors are 2.56% and 1.28%, respectively. Therefore, the calculation method in this section can predict the hull resistance accurately, especially with the overlapping mesh with high accuracy in predicting the drag of the designed speed and its nearby speed.

Table 2.5 Variance analysis

Computational mesh	Factor	Deviation square sum ss	Degree of freedom *df*	Variance *MS*	Influence degree
Cutting volume mesh	The thickness of the first boundary layer *A*	3.39E-08	3	6.23E-08	1.12E-04
	Turbulence mode *B*	7.10E-07	3	3.02E-07	5.57E-04
	Mesh quantity *C*	1.25E-07	3	8.01E-08	2.50E-04
Overlapping mesh	The thickness of the first boundary layer *A*	3.71E-08	2	1.85E-08	1.56E-04
	Turbulence mode *B*	1.14E-07	2	5.69E-08	2.48E-04
	Mesh quantity *C*	2.17E-07	2	1.08E-07	3.66E-04

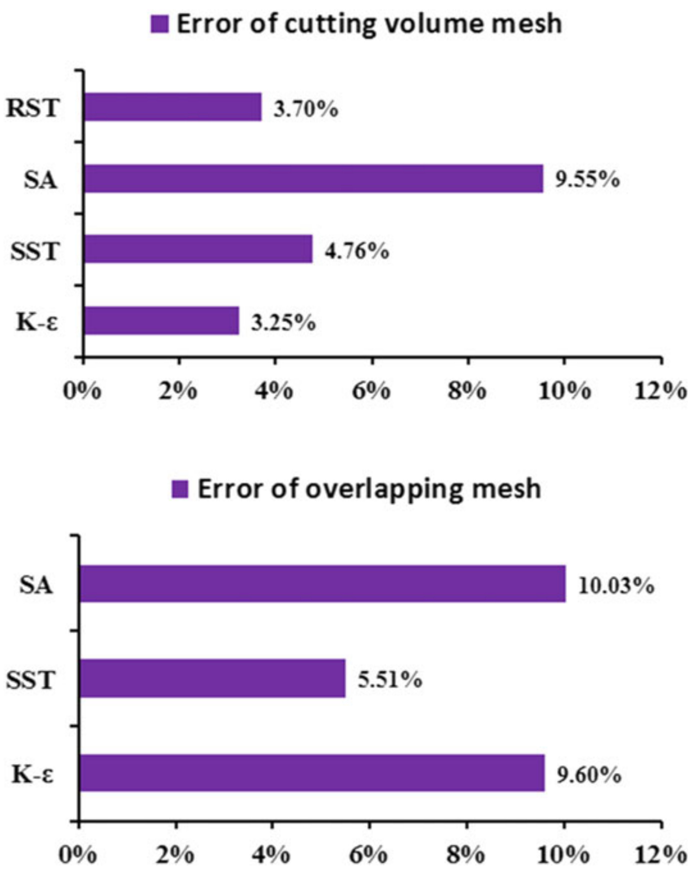

Fig. 2.41 The contrast between the resistance error absolute value of different turbulence modes

Although the error of overlapped grid calculation in design speed is small, the average error is slightly higher, the number of overlapping meshes is more than the total number of cutting volume mesh, and the calculation time is longer. It can be seen that the cutting volume mesh has relative advantages in predicting the resistance of multi-speed hull. As long as the number of meshes increases appropriately, the accuracy of resistance calculation can be improved. Table 2.6 shows the distribution of the flow field around DTMB5415 and the pressure distribution of the stern pressure in two kinds of mesh calculation with the speed Fr = 0.281. Among them, the red region in the overlapping grid flow field is the background area and the blue region is the overlap region.

(3) CFD uncertainty analysis

The uncertainty of the CFD simulation results determines the usefulness of the data. It is difficult to compare the results obtained by different researchers using

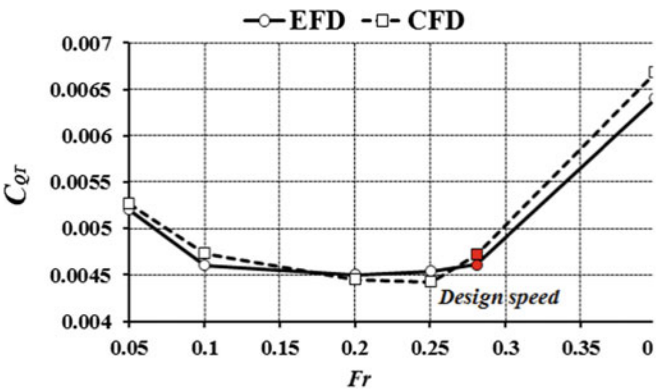

Cutting volume mesh

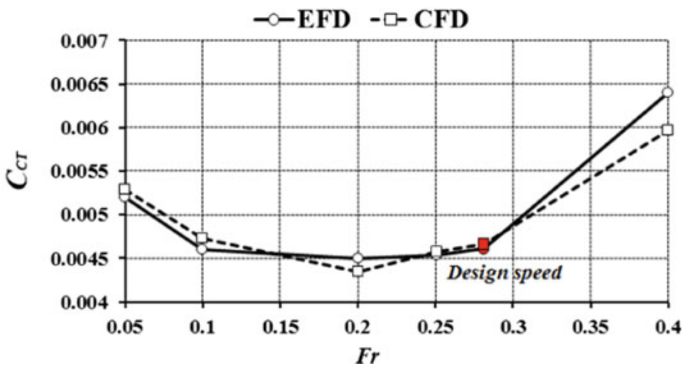

Overlapping mesh

Fig. 2.42 Contrast between total resistance calculation and the experiment value

different evaluation methods. Therefore, the CFD uncertainty analysis has become an important work of CFD research and application [13]. This section analyzes the uncertainty of the CFD in accordance with the ITTC recommendations, namely: verification and validation.

This section takes the cutting volume mesh as an example to analyze and discuss the uncertainty of the total resistance of DTMB5415 in static water. The calculation model takes three sets of meshes for analysis, and the mesh ratio r_G = 1.414 and the free surface mesh and waveform diagram are shown in Table 2.7.

It can be seen from Table 2.7 that the contour of the free surface can be clearly captured by all three meshes. The error of wave height of the coarse grid at the bow and the stern is larger, more accurate, and clear through the calculation of the fine grid after the free surface grid is encrypted. The total resistance coefficient calculation results of the three meshes are shown in Table 2.8. As can be seen from the table as the mesh is encrypted, the results of the resistance calculation are more

Table 2.6 Distribution of flow field

Mesh partitioning	The distribution of the flow field	The distribution of the bow pressure
Cutting volume mesh		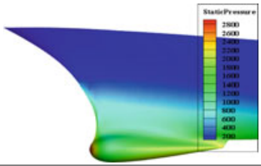
Overlapping meshes (Draw the same as above, remove the red around you)	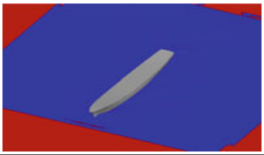	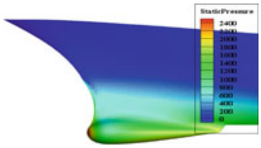

Table 2.7 Meshing and free surface

Mesh configuration	Horizontal mesh distribution	Free surface waveform
Sparse mesh	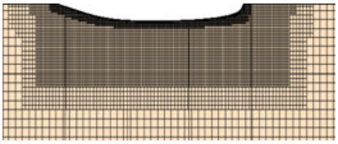	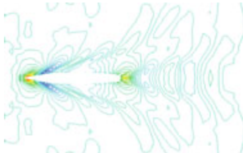
Middle mesh	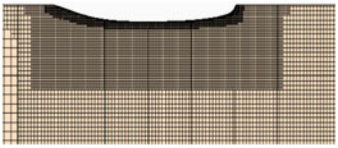	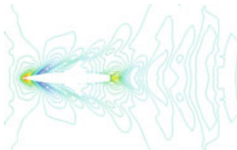
Dense mesh	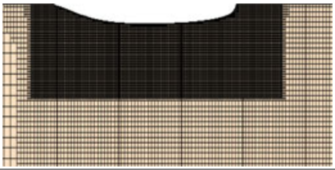	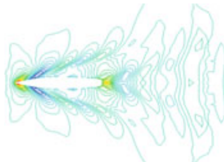

accurate. Table 2.9 shows the validation of the total resistance coefficient C_{QT}, including the convergent rate R_G, the order of accuracy P_G, the correction factor C_G, the mesh uncertainty U_G, the error $\sigma^*{}_{G1}$ with correction factor, the uncertainty of the correction value degree U_{GC}, and modified numerical simulation results S_C. It can be seen from the table that the convergence rate $R_G < 1$ indicating that the grid monotonically converges. As can be seen from Table 2.9, the revised total resistance coefficient S_C value is equal to 4.67E-3, which is closer to the experimental

Table 2.8 Total resistance coefficient of three sets of mesh C_{QT}

Scalar	Sparse mesh	Middle mesh	Dense mesh	Experimental value
C_{QT}	0.004871	0.004789	0.004728	0.00461

Table 2.9 Verification of the calculation total resistance coefficient

Mesh configuration	R_G	P_G	C_G	U_G	σ^*_{G1}	U_{GC}	S_C
Cutting volume mesh	0.751	0.826	0.332	1.85E-4	6.15E-05	1.24E-4	4.67E-3

value comparing with the total resistance coefficient calculated using the CFD technique.

(2) Validation

The validation step is to use the experimental data to evaluate the numerical modeling process of the modeling uncertainty U_{SM} and to estimate the model error σ_{SN} if condition permits. It compares the comparison error and confirms the size of the uncertainty to determine whether to achieve confirmation. If the comparison error is less than the confirmation uncertainty, this level of confirmation uncertainty is achieved. The total resistance of three meshes calculations is shown in Table 2.10. It can be seen from the table that $|E|$ is less than the uncertainty UV, so the calculation results can be confirmed.

(4) Conclusion

(1) The Latin square design was used to establish a rectangular square with the thickness of the first boundary layer, turbulence pattern, and the mesh number as the three main uncertainties in CFD calculation. Taking the cutting volume meshes and overlapping meshes as examples, respectively, it discusses the main and secondary influential factors that affect the CFD resistance forecasting, and calculates the grid form and calculation method suitable for the ship resistance forecasting. Results show that the turbulence model has the most significant effect on the calculation results of cutting body. The selection of the mesh number has the most significant effect on the calculation results of the overlap grids, while the thickness of the first boundary layer has the least influence on the calculated results. The k– ε model is more suitable for the prediction of resistance based on the cutting volume mesh, while SST k– ω is more suitable for the resistance calculation based on the overlapping grid.

Table 2.10 Confirm the result

Error	Results	Confirm the uncertainty	Result	The relationship of size
E_1	1.18E-04	U_{V1}	2.07E-04	$\lvert E_1\rvert < U_{V1}$
E_{C1}	−5.68E-05	U_{V1C}	1.55E-04	$\lvert E_{C1}\rvert < U_{V1C}$

(2) The total resistance of the hull at different speeds is calculated by using the cutting volume mesh and the overlapping mesh, respectively, and compared with experimental data. The results show that the calculation method in this section can predict the hull resistance more accurately, and the cutting body grid is more accurate than the overlapping grid at multi-speed drag prediction, but the design speed is not effective.

(3) According to the ITTC recommendation, taking the cutting volume mesh as an example, the CFD-based uncertainty analysis and discussion on the resistance of DTMB5415 in still water are carried out by using three sets of grids. The numerical solution based on the mathematical model of CFD converges monotonously with the encryption of the grid, the uncertainty of total resistance can be confirmed, and the corrected total resistance is closer to the experimental value.

References

1. Campana EF, Peri D, Tahara Y et al (2009) Numerical optimization methods for ship hydrodynamic design. In: SNAME annual meeting
2. Li GL, Luohuai L, Tan ZS (1990) Energy-saving ship design. Beijing: National Defense Industry Press
3. Li ZZ (2005) Research on ship type optimization based on wave resistance value calculation. Dalian University of Technology
4. Tarafdera MS, Suzuki K (2008) Numerical calculation of free-surface potential flow around a ship using the modified Rankine source panel method. Ocean Eng 35(5–6):536–544
5. Ji X, Zang YL, Cheng YM (1997) Boundary element method progress and general procedure. Shanghai: Tongji University Press
6. Liu YZ (2003) Theory of ship wave making resisitance. BeiJing: National Defense Industry Press, 1
7. Gao B (2002) Wave resistance calculation and ship type optimization. Shanghai: Shanghai Jiaotong University2002
8. Li LY (2006) Numerical simulation of resistance and viscous flow around ship hull. Dalian Polytechnic University
9. STAR-CCM users guide
10. Choi J, Sung BY (2009) Numerical simulations using momentum source wave-maker applied to RANS equation model. Coastal Eng 56(10):1043–1060
11. Longo J, Stern F (2005) Uncertainty assessment for towing tank tests with example for surface combatant DTMB model 5415. J Ship Res 49(1):55–68
12. Gui L, Longo J, Stern F (2005) Biases of PIV measurement of turbulent flow and the masked correlation-based interrogation. Exp Fluids 30:27–35
13. Yang C-L, ZHU R-C, Miao G-P (2012) Uncertainty analysis in CFD for flow simulation around ship using RANS and DES. J Shanghai Jiaotong Univ 46(3): 430–435

Chapter 3
Geo-Reconstruct Technology of Hull

3.1 Overview

The hull shape optimization based on the Michell integral method of the theory of linear wave resistance is based on the hull shape value contained in the wave resistance expression. Therefore, the hull shape value can be directly used as the design variable in the optimization process without the need to parameterize and reconstruct the hull geometry; because of the implicit relationship between the objective function and the design variable, and the automatic deformation of the hull and the automatic demarcation of the mesh in the optimization process, the ship-type optimization based on Rankine source method and the CFD method requires the use of hull geometry reconstruction techniques to connect the objective function with the design variables. With the rapid increase of computational speed and rapid development of computational graphics, CFD-based ship optimization design has become possible. A series of CFD numerical simulation software and CAD graphic design software are available one after another, and the optimization process is shown in Fig. 3.1. The optimization algorithm constantly adjusts the variation of design parameters in the geometric design space and constantly generates new hull geometry—that is, the automatic reconstruction of the hull geometry. The CFD numerical simulation tool then performs a numerical evaluation of the newly generated ship and feeds back the results to the optimization platform [1], and loops until a ship of the highest hydrodynamic performance is found. The whole process does not require human intervention; the degree of automation directly determines the application prospect based on CFD ship optimization, which is a hot spot in the current research. The traditional hull line generation technology and ship form change method mostly use manual or computer interaction mode, which cannot realize fast and efficient ship form transformation, resulting in that the CFD numerical simulation technology cannot be used to optimize the ship form (inverse problem) and can only be optimized or selected for a limited number of ship types (positive issue). It is exactly the emergence of ship geometric automatic

© Shanghai Jiao Tong University Press, Shanghai and Springer Nature Singapore Pte Ltd. 2019
B.-J. Zhang and S.-L. Zhang, *Research on Ship Design and Optimization Based on Simulation-Based Design (SBD) Technique*,
https://doi.org/10.1007/978-981-10-8423-2_3

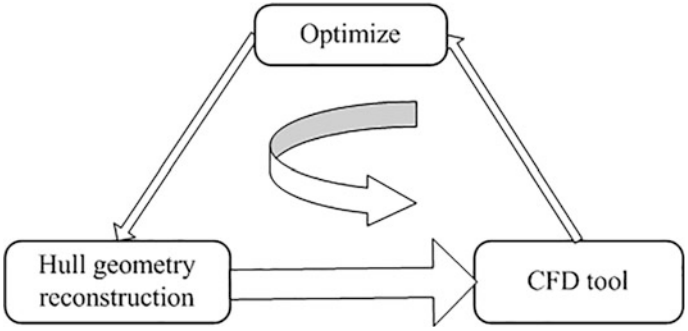

Fig. 3.1 Hull form optimization based on CFD

reconstruction technology that provides a tool for rapid generation of ship types and transformations based on CFD ship optimization, which can realize "ship optimization" in the real sense [2]. It is of great guiding significance for realizing "digital shipbuilding," "green shipbuilding" and promoting the design of ship form from the traditional experience mode to the knowledge-based mode.

3.2 Research Progress of Hull Linear Expression

With the deepening of multi-disciplinary optimization design methods, how to realize automatic generation and geometric reconstruction of ship types has become a hot issue in current research on ship form optimization. The basic methods of ship form generation are self-drawing method, mother ship method, the series of ship-type method, and the mathematical ship method. Self-drawing method is the basic method used when computer technology is not very mature, the method is characterized by simple, intuitive, and the disadvantage is strongly dependent on the experience of the designer; the mother ship method is the most commonly used basic method for the design of ship form at present. The characteristics are simple and practical. The disadvantage is that the performance of the designed ship model strongly depends on the experience of the mother ship and the designer. If the design ship is very similar to the mother ship, the better results can be obtained; on the contrary, the design ship will have poor performance. The series ship method is based on the existing excellent mother ship information or series of ship model data, by constantly changing the main dimensions of the ship and ship parameters to meet the requirements of the new ship [3]. All of the above three methods need to be completed through an interactive method, and the discrete offsets point are obtained. Before the construction, it takes a great deal of time and manpower to accomplish an artificial three-dimensional smoothing, which is inefficient. With the rapid development of computer technology, some breakthroughs have been made in the design and modification of the ship designs using computer-aided techniques.

However, the general idea of design is still based on the traditional design methods. To this end, domestic and foreign scholars attempt to adopt the new ship design concept, to ensure the quality of the design conditions; the design process minimizes human intervention. Firstly, the efficient parametric modeling technology is introduced into the field of ship design, mainly through the analysis of mathematical functions and numerical fitting methods. The expression of ship types in the form of math functions is mainly through mathematical functions to express waterlines, body lines, and longitudinal sections or hull surfaces. Use the computer to complete the entire profile generation process. However, due to the complexity of actual ship types, up to now there is no effective and practical parametric modeling technology. In the twentieth century, several typical mathematical ship types appeared, the most typical such as Wigley ship model, which is the most commonly used ship-type research, but this type of ship is parabolic with no practical value, far away from the actual ship.

In recent years, parametric modeling technology has gained rapid development. Parametric design refers to the change of a relevant part of the ship automatically by changing a certain design parameter without manual intervention. Therefore, it is a goal of ship designers to link the ship type with the ship-type parameter and to generate the complete and smooth ship-type surface with proper size and ship-type parameters. After long-term development, the ship design has made great progress. At present, there are mainly two methods of geometric representation of hull surface: One is the network method, that is, to express the hull surface with a few groups of plane curves with certain rules, which is mainly used for the traditional two-dimensional ship design. Another method is to use surface functions to express hull surfaces satisfying certain boundary conditions. It mainly adopts the Bezier curved surface to express the patches, and the surface is then spliced into a smooth hull surface. Since the 1980s, B-spline surfaces and rational splines had been gradually used in ship line design. After the 1990s, people began to use the nonuniform B-spline (NURBS) method to construct the hull surface. The NURBS surface theory can theoretically guarantee that the transverse line of the hull, waterline, and longitudinal section are three-way smoothness. The resulting hull surface does not require lofting and can be directly used in the production. Some famous foreign ship design software such as FastShip, Maxsurf, and TRIBON almost all use this technique to achieve. China has also carried out research in this area, especially the hull modeling technology has gradually become the focus of research. With this technology, automatic generation and optimization of the ship form can be achieved. Therefore, in the process of ship form optimization, after the accurate hull shape is generated according to the requirements of the designer, the CFD technique is used to numerically solve the set objective function. Finally, the optimal algorithm is used to explore the hull geometry in the design space to obtain the optimal performance of the ship under the constraint conditions. The process needs to be repeated continuously.

3.2.1 Overseas Research Situation

Jochen [4] Harries [5] in Germany put forward a more complete method of parametric design of ships in his doctoral dissertation and developed a set of fully parametric commercial CAD software Friendship. The software can directly generate the desired ship form based on a series of ship form characteristic parameters, which will be directly used as optimization design variables in the optimization process. Germany's Abt and Harries [6–8] based on the fully parametric model system Friendship-Modeler expressed of the hull shape parameters for the design variables, as shown in Fig. 3.2, the ship form optimization design is carried out with SHIPFLOW software to calculate the wave resistance as the objective function. Abt et al. [9] optimized the DTMB5415 model by parametric modeling to realize hull geometry reconstruction. Six parameters were selected to control the ship generation. Tahara et al. [10] Kim et al. [11] used the Lackenby transformation of the ship geometry reconstruction method, the hull local geometry reconstruction method based on the radial basis function and the combination of the two reconstruction methods.

In the optimization of the total resistance, Kim [12] used the Bezier patch method to realize the geometric reconstruction of the bulbous bow. Campana, Para et al. [13] optimized the amplitude of the waves of the surface ships and used the Bezier patch method to rebuild the bulbous bow. During the period 2003–2009, Campana, Ampana et al. [14] Peri and Campana [15, 16] Campana et al. [17] Tahara et al. [18] used the DTMB5415 model as the optimization target and took the wave resistance, seakeeping, and stern flow field as the optimization objectives. The geometrical reconstruction methods of hull (Bezier patch and CAD-based geometric reconstruction method) conducted a more detailed study. Peri, Tahara, Campana et al. [19–21] used two kinds of multi-objective global optimization algorithms to optimize the high-speed catamaran, respectively. The hull geometry reconstruction adopted free-form deformation (FFD) method and CAD-based method, respectively.

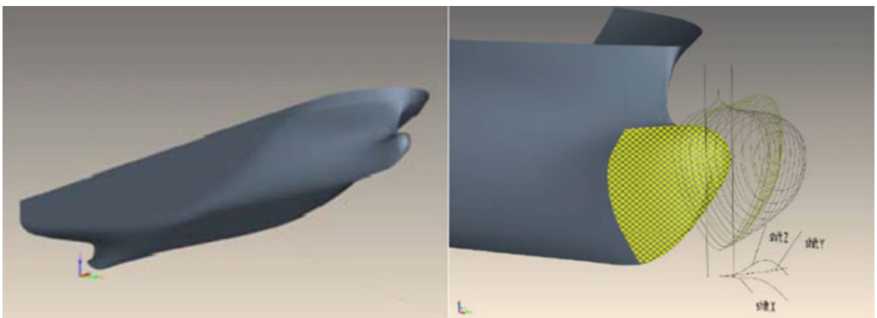

Fig. 3.2 Fully parametric model system Friendship-Modeler expressed of the ship hull

From the above research, it can be seen that foreign scholars have made major breakthroughs in the automatic geometric reconstruction of hull structures. Some general commercial software with independent intellectual property rights have been gradually developed and successfully applied to ship-type optimization. The success of foreign countries lies in the completeness of basic experimental conditions, the relative concentration of researchers, and the result of long-term continuous efforts.

3.2.2 Domestic Research

The optimization of hull line optimization in China starts with the mathematical expression of ship type. With the development of Bezier curve and B-spline curve, interaction design becomes a boom. In the mid-1980s, B-spline surfaces and rational spline curves began to be used in hull surface design. In 1981, Tahara et al. [22] began to describe the hull surface with Bezier surface. In 1985, they applied the B-spline surface to the hull surface for the first time. The above methods are based on the spline ideas to design and expression of the basic idea and are the first to require the original value points and then continue to adjust the surface through human–computer interaction until meet the design requirements.

Since the mid-1990s, the NURBS curve surfaces have become a hot spot in computational geometry and become one of the most popular techniques for describing curves and surfaces. And the use of NURBS method to describe the hull surface has gradually become a research hot spot. It has always been a goal pursued by shipbuilders to generate hull line shapes according to ship shape parameters. Many domestic scholars have made in-depth exploration on the curve and surface expression of ships and the smoothness. However, no one has yet put forward an effective and practical ship-type parametric design technology, nor has it formed design software with independent intellectual property rights. Zhou and Zhang [23, 24] based on Harries's method of applying uniform B-spline curve to Wigley, the NURBS curve is proposed to express the stern and the bulbous bow. In her doctoral dissertation, a detailed study of the method of parametric ship representation was conducted. Ping et al. [25] analyzed the geometrical shapes of circular hulls and established the geometric expression of the characteristic lines and points. Using NAPA BASIC language, he developed a profile parametric design of the macro-program, so as to explore a new and efficient way for the digital design of round-bilge craft. Xie et al. [26] Zhang [27] Bao-Ji et al. [28] studied the method of least resistance ship design method based on Rankine source method. Taking the parameters of the ship modification function proposed by Suzuki and Kazuo as design variables, the nonlinear design was optimized under the condition of ensuring the necessary displacement as the basic constraint. Zhang [29], in his doctoral dissertation, introduced the research methods of the three-dimensional parametric overall design of ships and offshore platforms in detail. Yu [30] adopted the Framework module in Friendship software to modify the 3100TEU prototype.

In order to optimize the hull line, based on the NURBS expression of ship, Fu and Chen [31] Baiwei et al. [32] proposed two different parametric modeling methods based on CAD/CFD ship-type optimization process. One is directly to the NURBS control vertex coordinates as a variable to achieve the transformation of the ship's parameter; the other is based on the mother-based development of ship-based parametric fusion module to achieve the ship's parameters transform. Using ISIGHT software, two kinds of parametric modeling methods were used to optimize the bulbous bow of a container ship. The results show that the method of ship-type modification and fusion is a parameterized modeling method with engineering value.

Our research and application of automatic geometric reconstruction of hull have gradually become mature and perfect, especially in the study of NURBS curve and surface, many scholars have reached the international advanced level. However, compared with the shipbuilding powers such as Japan, South Korea, and Europe, there are still some gaps, mainly in the following problems:

(1) The parametric representation of the hull geometry is mostly the partial design of simple hull types (e.g., math hull types). Therefore, the geometric design space of the hull is limited and it is difficult to obtain the optimal performance hull under a given condition.
(2) Domestic research is relatively fragmented, did not form a unified, shared design platform, but did not form a commercial software with independent intellectual property rights.
(3) There is no effective and open framework for ship-type optimization based on hydrodynamics theory at present, that is, the convergence and integration between the objective function, design variables (parametric representation of hull geometry) and optimization methods have not been solved well.

3.3 Basic Connotation of Hull Geometric Reconstruction Technology

The geometric reconstruction of the hull is a kind of ship formation technology that restores the relationship between the hull geometry and the topological structure during the transformation. It is an important method in ship conceptual design, overall design and hull form optimization. The hull geometrical representation is a very comprehensive technology involving a large number of research fields. It is a prerequisite and core link in the overall hull design and performance calculation and plays a decisive role in the comprehensive navigation performance of ships [33]. The hull geometric reconstruction technology is the premise of CFD-based ship optimization. During the optimization process, the design variables are adjusted according to the optimization algorithm, and the design variables are reflected in the

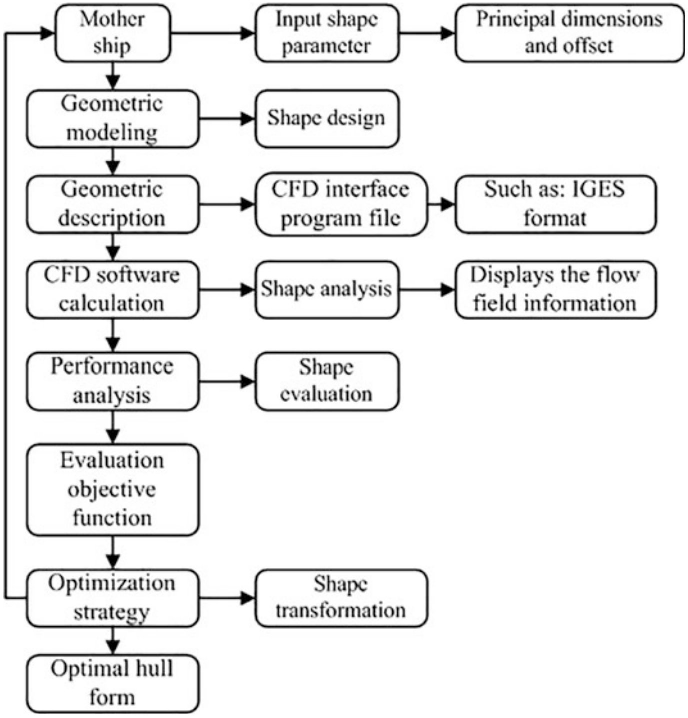

Fig. 3.3 Hull geometric reconstruction to achieve the process of ship optimization

changes of the hull geometry. Figure 3.3 is a hull geometric reconstruction to achieve the process of CFD-based ship optimization.

(1) Enter the model values and major dimensions of the mother ship for geometric modeling (shape design), generate interface files for common CFD software: such as IGES format (geometric description);
(2) Use CFD software for numerical simulation (shape analysis) to show flow field information;
(3) Evaluate the objective function (shape evaluation);
(4) Generate the optimal hull form (shape transform) through optimization strategy.

3.4 Fundamental Principles of Hull Geometry Reconstruction Technology

The hull geometry reconstruction technique bridges the gap between the CFD assessment technique and the optimization algorithm. The design variables are solved according to the optimization algorithm, and the parameters governing the geometry of the hull are output, and the new hull geometry is regenerated. This is the geometry of the hull reconstruction process. CFD software evaluates the performance of the new hull form. The optimization algorithm is analyzed and compared according to the evaluation results and then fed back to the CFD software by controlling the geometry parameters of the hull, which is repeated until the geometry of the hull with the best performance is obtained. Therefore, the hull geometric reconstruction technology is the prerequisite and foundation for ship optimization and it is also one of the key technologies studied. The general study is as follows:

(1) To ensure the smoothness of hull geometry reconstruction

The use of polynomial functions or double trigonometric series to express the hull geometry in part or in whole requires that the changed part and the fixed part be connected broadly and smoothly to ensure the continuity of the second derivative. In this way, the shape of the hull obtained can be made smooth enough that there will be no difference in the optimization results due to the smoothness of the hull, the optimal performance of the hull is entirely due to the difference of the geometric shapes.

(2) To express the hull geometry with a few design parameters as possible

CFD-based hull form optimization is a very complex nonlinear process that requires constant iteration to find the ship that meets the design requirements. In order to reduce the calculation time and ensure the practicality of the optimization method, it is necessary to express the hull geometry by using as few design variables as possible (i.e., ship modification functions or polynomial function parameters) as possible.

(3) To ensure that the design space is as wide as possible

In order to be able to find the best performance of the ship, you need to have a very wide design space, that is, there are numerous different geometry of the ship, which need to determine the parameters of the hull geometry reconstruction technology as much as possible to get more different hull form. This is contradictory to the (2) above, therefore, how to weigh these two aspects, that is, to use as little calculation time as possible, is also a problem that the hull geometry reconstruction technology must solve.

3.5 Hull Geometric Reconstruction Method

3.5.1 Hull Form Modification Function Method

The geometry of the hull is expressed by the parametric method, and the optimization of the ship design is carried out by the mathematical optimization method. In other countries, Japanese researches are more prominent, and parametric techniques were applied to ship generation from the 1960s onward [34]. Since the 1980s, all countries have invested a great deal of manpower and financial resources and many achievements have been published. Suzuki and Iokamori [35] studied the minimum wave resistance ship model based on Rankine source method and designed a modified function of the trigonometric series to express the hull shape, as shown in Figs. 3.4 and 3.5. Since then some scholars [36–40] later modified or deformed this ship modification function to express the local and overall shape of the hull.

The ship modification function method represents the change of the ship type by using a series of numbers, which may be trigonometric or a polynomial. The change of hull shape is completely determined by the parameters of the series. The advantage of this method is that the design parameters can be directly used as the design variables for optimization problems. The whole and part of the ship can be parametrically expressed with fewer design variables. The disadvantage is that it is not flexible enough, and the geometric space is small, and the trend of the shape of the improved ship type is completely limited by ship modification function.

The idea of this method is that the shape y(x, z) of the modified ship is expressed by using a ship-type modification function w (x, z) on the basis of the initial ship type f_0 (x, z), that is:

$$y(x,z) = f_0(x,z)w(x,z) \tag{3.1}$$

where $w(x,z) > 0$ ($x > x_0, z < z_0$) and

$$w(x,z) = 1 - \sum_m \sum_n \alpha_{mn} \sin\left[\pi\left(\frac{x - x_0}{x_{\min} - x_0}\right)^{m+2}\right] \cdot \sin\left[\pi\left(\frac{z_0 - z}{z_0 + T}\right)^{n+2}\right] \; m, n = 1, 2, 3, \ldots$$

$$-L/2 \le x \le 0$$

$$w(x,z) = 1 - \sum_m \sum_n \alpha_{mn} \sin\left[\pi\left(\frac{x - x_0}{x_{\max} - x_0}\right)^{m+2}\right] \cdot \sin\left[\pi\left(\frac{z_0 - z}{z_0 + T}\right)^{n+2}\right]$$

$$m, n = 1, 2, 3, \ldots, \; 0 \le x \le L/2$$

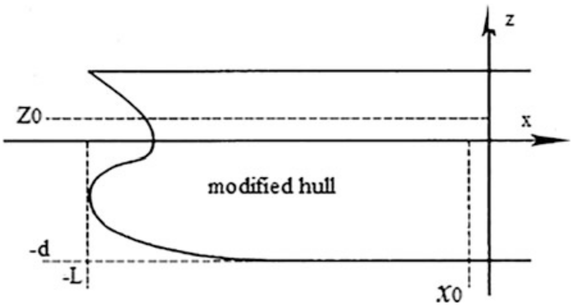

Fig. 3.4 Application of ship-type modification function

Fig. 3.5 Application of ship-type modification function

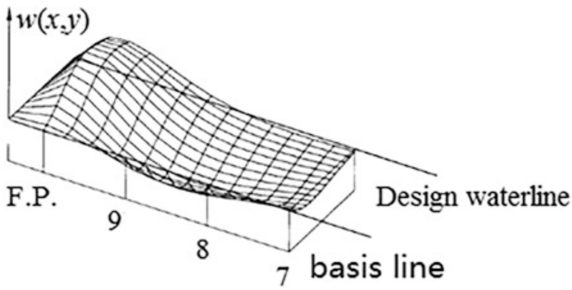

In the equation: L is the foremost longitudinal coordinates of the bow (including the bulbous bow); T is generally the maximum depth of coordinates to be modified, if the baseline remains unchanged, then T is draft. Fixed m, n = 1, 2, 3, 4, 5, a total of 25 α_{mn}, only 25 design variables; therefore, the selection of the ship modification function reduces the number of design variables and improves the speed of optimization.

3.5.2 *Polynomial Expansion Method*

The ship-type function of a design ship can be expressed in the form of the sum of the parent ship-type function and the change amount function with respect to the parent ship, that is

$$y(x,z) = y_0(x,z) + \Delta y(x,z) \tag{3.2}$$

where

$$\Delta y(x,z) = \Delta y(x)_{Z=WL1} + \Delta y(x)_{Z=WL2} + \Delta y(x)_{Z=WL3} + \Delta y(x)_{Z=WL4} + \cdots + \Delta y(x)_{Z=WLN}$$

Fix the z along the depth of the model, so that the unit change function only represents the function of x and then expand the unit change function polynomial along the x-direction, that is

$$\begin{aligned} &\Delta y(x)_{Z=WL1} = a_{01} + a_{11}x + a_{21}x^2 + a_{31}x^3 + \cdots + a_{k1}x^k \Delta y(x)_{Z=WL2} = a_{02} + a_{12}x \\ &a_{22}x^2 + a_{32}x^3 + \cdots + a_{k2}x^k \Delta y(x)_{Z=WL3} = a_{03} + a_{13}x + a_{23}x^2 + a_{33}x^3 + \cdots + a_{k3}x^k \\ &\ldots \Delta y(x)_{Z=WLN} = a_{0N} + a_{1N}x + a_{2N}x^2 + a_{3N}x^3 + \cdots + a_{kN}x^k \end{aligned} \tag{3.3}$$

In the formula, [A] = a_{01}, a_{11}, …,a_{kN} are the parameters of each unit change function to be expanded. If the parameter [A] is given, the value of each unit transformation function can be determined. Therefore, the variation of the ship width in each of the waterline positions (WL1, WL2, WL3, WLN) along the x-direction can be obtained. Second, knowing the value of each unit change function of each water line position (WL1, WL2, WL3, and WLN), the unit change function of any water line position can be obtained by cubic spline interpolation function. This interpolation function is based on $N_{mi}(\zeta)$ and $N_{mj}(\xi)$ as a function of the base, along the depth direction of the interpolation.

$$\Delta y = \sum_{i=1}^{n+m} \sum_{j=1}^{k+m} c_{ij} N_{mi}(\varsigma) N_{mj}(\xi) \tag{3.4}$$

In the formula, $N_{mi}(\zeta)$ and $N_{mj}(\xi)$ are standard B-spline functions; n and k are the number of internal nodes (excluding the endpoints) in the directions of ξ and ζ in the modified range; m is the order of the B-spline function.

Here take m = 4, n = 3, k = 2

$$\xi_{-3} = \xi_{-2} = \xi_{-1} = \xi_0 < \xi_1 < \xi_2 < \cdots < \xi_{n+1} = \xi_{n+2} = \xi_{n+3} = \xi_{n+4}$$

$$\zeta_{-3} = \zeta_{-2} = \zeta_{-1} = \zeta_0 < \zeta_1 < \zeta_2 < \cdots . < \zeta_{n+1} = \zeta_{n+2} = \zeta_{n+3} = \zeta_{n+4}$$

Taking B-spline function parameters as design variables, and the total number of design variables is 12, as shown in Table 3.1.

3.5.3 *Spline Function Method*

There are two main methods to express changes in hull shape by using the spline function method: One is the B-spline curve, the shape of the hull surface can be defined by B-spline function, the parameters of which are used as design variables, but the method is more complex and has more design variables; another method is to use the nonuniform rational B-spline (NURBS) curves or surfaces, and the control vertices can be directly used as design variables for optimization, which has a wide range of applications.

Table 3.1 B-spline function parameters as design variables

Cij	i=1	2	3	4	5	6	7
j=6	0.0	0.0	0.0	0.0	0.0	0.0	0.0
5	0.0	0.0	0.0	0.0	0.0	0.0	0.0
4	0.0	0.0	**1.0**	**1.0**	**1.0**	0.0	0.0
3	0.0	0.0	**1.0**	**1.0**	**1.0**	0.0	0.0
2	0.0	0.0	**1.0**	**1.0**	**1.0**	0.0	0.0
1	0.0	0.0	**1.0**	**1.0**	**1.0**	0.0	0.0

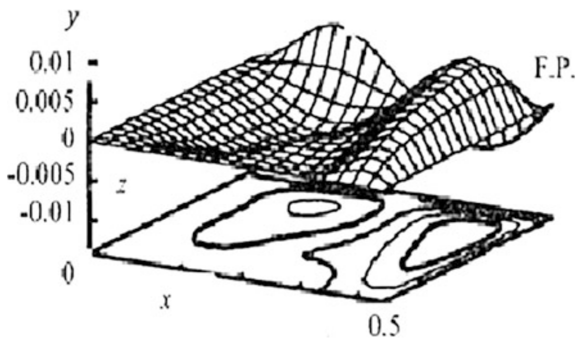

Fig. 3.6 B-spline curve expression in ship-type application

The hull is divided into n sections in the ξ direction, and each section is equally divided into m points in the ζ direction. According to the formula, the B-spline basis functions ($N_{mi}(\zeta)$ and $N_{mj}(\xi)$) of ξ *and* ζ are calculated as shown in Fig. 3.6.

$$\eta = \delta y = \sum_{i=1}^{n+m} \sum_{j=1}^{k+m} c_{ij} N_{mi}(\zeta) N_{mj}(\xi) \tag{3.5}$$

Jun-ichi et al. [41–43] studied the tail optimization problem of ship with minimum viscous resistance based on nonlinear programming method and expressed the shape of hull by B-spline function. Masuda et al. [44] Suzuki et al. [45] used the polynomial function of order N and spline interpolation to express the shape of the hull and studied the minimum thrust deduction fractional hull and the tail optimization problem of the minimum secondary flow energy based on the potential flow theory, respectively, obtaining a larger solution space.

3.5.4 Geometric Modeling Technique

Geometric modeling technology is the perfect combination of computer-aided geometric design and computer graphics. Its core content is to find a mathematical method can not only find shape suitable for computer processing and effectively meets the requirements of shape and geometric design, but also facilitate the shape information transfer and product data exchange. The commonly used geometric modeling techniques for ship design are free-form deformation approach (FFD), Bezier patch method, and NURBS surface method, etc.

3.5.4.1 Free-Form Deformation Method (FFD)

Free-forming technology, an important branch in computer graphics, was first proposed by Sederberg and Parry in 1986 [46] and has achieved rapid growth in the last 20 years. Its main idea is embedding the target to be transformed into the grid formed by several control vertices and then moving the control vertices, and deformation of the grid will be transmitted to the internal target, causing the deformation of the internal target. The method can be applied to the solid modeling system of any surface without being limited by the representation mode and can locally or globally transform the original surface, and the deformed surface can maintain the geometric continuity. Independent of object representations, it is easy to integrate into existing software modeling systems. It has good interactivity and controllability in producing object animation. The disadvantages are that the method is not easy to control deformation; deformation is difficult to accurately achieve the desired results, and there are many design variables when expressing the surface of complex objects.

The FFD method uses the Bernstein basis function to establish the functional relation between the lattice node and the position of any point in the lattice [47], and its expression is:

$$\begin{aligned} & x(s,t,u) + \Delta x(s,t,u) = \\ & \sum_{i=1}^{l}\sum_{j=1}^{m}\sum_{k=1}^{n}\left[B_{l-1}^{i-1}(s)B_{m-1}^{j-1}(t)B_{n-1}^{k-1}(u)\right]\cdot\left[P_{i,j,k}+\Delta P_{i,j,k}\right] \end{aligned} \tag{3.6}$$

$$\Delta x(s,t,u) = \sum_{i=1}^{l}\sum_{j=1}^{m}\sum_{k=1}^{n}\left[B_{l-1}^{i-1}(s)B_{m-1}^{j-1}(t)B_{n-1}^{k-1}(u)\right]\cdot\Delta P_{i,j,k} \tag{3.7}$$

where x(s, t, u)-the global coordinate of any point in the control frame

P_{ijk}-coordinate matrix of control grid points(i, j, k)
ΔP_{ijk}-displacement matrix of control grid points(i, j, k)
$l \times n \times m$-control grid points
(s, t, u)-local coordinates in the control lattice
$B_{l-1}^{i-1}(s)$-an i-1 of l-1-order Bernstein polynomials, the expression of which is:

$$B_{l-1}^{i-1}(s) = \frac{(l-1)!}{(i-1)!(l-1)!}s^{i-1}(1-s)^{l-i} \tag{3.8}$$

The above formula is written in the form of matrix:

$$\Delta x = B(s,t,u)\cdot\Delta P \tag{3.9}$$

Based on the FFD method to generate the geometry of the hull and the deformation of the grid, the deformations of the specific steps are as follows:

(1) Construct a parameter body. Deformation is defined in a closed three-dimensional lattice control vertices and a corresponding set of parameters in the basic function. Thus, each point (x, y, z) is mapped to a set of parameter coordinates (u, v, w).

The three-dimensional grid consists of an ordered grid of control points:

$$V_{i,j,k} = (x_{i,j,k}, y_{i,j,k}, z_{i,j,k}) \tag{3.10}$$

$$\begin{matrix} V_{i,j,k} \\ W_{i,j,k} \end{matrix} \begin{cases} 0 \le i \le a \\ 0 \le j \le b \\ 0 \le k \le c \end{cases} \tag{3.11}$$

where V_{ijk} is the vertex of each control; W_{ijk} is the initial setting unit of each control vertex; a, b, and c are the number of divisions of the direction of u, v, w parameters, respectively.

After the grid points are created, an ordered B-spline basis function (u, v, w) is assigned, and the sequence of each parameter variable may be different as follows:

$$\begin{gathered} 2 \le p \le (a+1) \\ 2 \le m \le (b+1) \\ 2 \le n \le (c+1) \end{gathered} \tag{3.12}$$

where p, m, n are the order of the parameters of the basic functions u, v, w. The corresponding node vector is:

$$\begin{aligned} U &= (u_0, u_1, \ldots, u_q), q = a + 2(p-1) \\ V &= (v_0, v_1, \ldots, v_q), q = b + 2(m-1) \\ W &= (w_0, w_1, \ldots, w_q), q = c + 2(n-1) \end{aligned} \tag{3.13}$$

Build a nonuniform node vector for each endpoint with equal order to ensure the insertion of a new value for the three-dimensional grid volume. The following is the expression of the node vector U (V, W are similar):

$$u_i \begin{cases} 0 & 0 \le i \le p \\ i-(p-1) & p \le i \le (q-p) \\ a & (q-p) \le i \le q \end{cases} \tag{3.14}$$

Assign a random B-spline basis function to each node vector, and the basis function is measured by the W standard recursive formula.

$$B_{i,r}(t) = \frac{t - t_i}{t_{i+r-1} - t_i} B_{i,r-1}(t) + \frac{t_{i+r} - t}{t_{i+r} - t_{i+1}} B_{i,r-1}(t) \tag{3.15}$$

$$B_{i,r} = \begin{cases} 0 & t_i \le t \le t_{i+r1} \\ 1 & others \end{cases}$$

In the formula, $i \in \{0, 1, 2, 3\ldots q\}$, q is the number of nodes, B is a B-spline basis function; except W, it is conventionally interpreted as zero.

The points on the object are calculated based on the simple extension formula of B-spline. The three-variable B-spline formula is:

$$P(u, v, w) = \frac{\sum_{i=0}^{q}\sum_{j=0}^{r}\sum_{k=0}^{s} B_{i,p}(u)B_{j,m}(v)B_{k,n}(w)W_{i,j,k}V_{i,j,k}}{\sum_{i=0}^{q}\sum_{j=0}^{r}\sum_{k=0}^{s} B_{i,p}(u)B_{j,m}(v)B_{k,n}(w)W_{i,j,k}} \tag{3.16}$$

where P is a point on the Cartesian coordinate vector (x ,y, z)model.

(2) "Embed" the object into the parameter body. The inverse point problem has solved the description of the embedded object, that is, the determination of the parameter coordinates (u, v, w) for each point (x, y, z).

As mentioned earlier, objects embedded within a solid include a set of parameter coordinate points that identify the deformed objects. The grid orthogonality and alignment with the data axis need to be divided into H parts; each parameter variable is (u, v, and w). Use Golden Numerical Search to find the coordinates of each parameter and determine the span of which the bounding point belongs to set the search range. Each meaningful vector point interval corresponds to a solid spline span. The boundaries of each span are determined by evaluating the appropriate knot point values, and it is easy to determine the span object for each point. For convenience, the midpoint of the different node segments is used as the initial estimate for numerical evaluation.

(3) Deformation of the parameter body. This process is usually replaced by the vertices of the 3D mesh.

Compared with the previous FFD method, the closed solid can be changed by substituting the lattice control points. Because B-spline basis functions need to be artificially maintained the continuity of the span between solids, deformation is an almost limitless process.

(4) Evaluation of the effects of deformation of embedded objects. Use the parameter coordinate points with the deformation control lattice (step 3) to evaluate the new location of the embedded point set and then use the topology of the original model to reconstruct the deformed object.

Several algorithms are used to evaluate B-spline basis functions effectively. Assessing the effects of distortion on embedded objects is a very simple process. This method provides a real-time assessment of the influence of deformation on an embedded object grid. However, for complex objects with several different transformations, it is usually more practical to perform all grid deformation before the impact of the computation.

Taking the DTMB5415 ship as an example, first establishes the hull surface control point, as shown in Fig. 3.7. Except for the point 1–3 near the bulbous bow, the other control points remain fixed to ensure a smooth connection between the bulbous bow and the main hull. By changing the distance and direction of the control points, the shape of the surface of the bulbous bow changes, generating a smooth new surface.

(1) Bezier patch method

In 1971, Bezier from the France Renault Motor company officially released a method of defining curves by controlling polygons. Designers simply move the control vertices to easily modify the shape of the curve, and the changes in shape were completely predictable and thus being widely used [48]. Since there is no local characteristic for Bezier method, Gordon and Riesenfild modified this method to allow designers to easily modify the surface. This method is more commonly used in the field of ship design. It is through the superposition of one or more Bezier surfaces on the mother ship (local), by changing the node location of the Bezier curve to obtain the shape of different surface, to realize the geometric reconstruction of the hull, and the node position can be directly used as a the design variable of the optimization problem. The advantage of this method is that fewer the design variables are, more easily the smoothness is to satisfy. The disadvantage is that only local geometric reconstruction of the hull is possible.

The Bezier curve shape is only related to the position of the characteristic polygon vertex. As shown in Fig. 3.8. Bezier curve 1 shape is controlled by 4 control points, with the first two points on the original curve and the other two control points, Q1 and Q3, not on the curve. By changing the curve control points Q1 and Q3, the original Bezier curve 1 changes to the new Bezier curve 2, and the

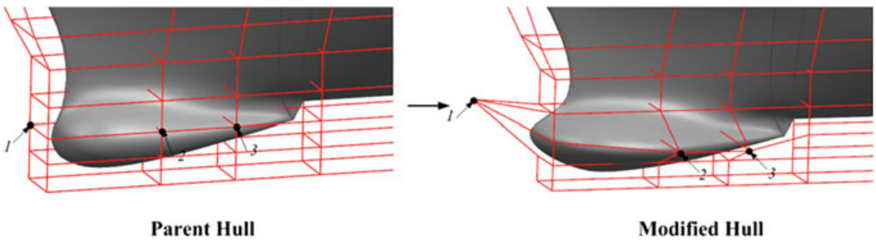

Fig. 3.7 Geometric reconstruction of the bulbous bow

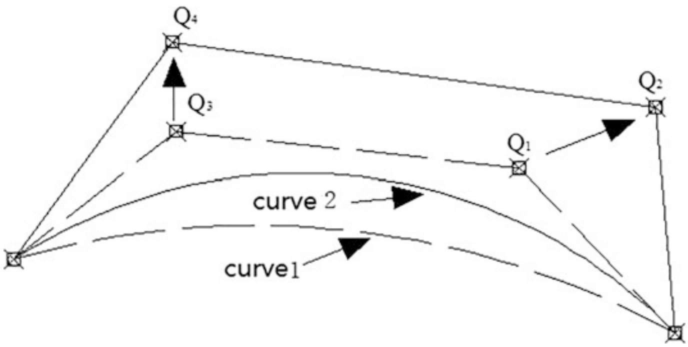

Fig. 3.8 Calculation flowchart

geometry of the bulbous bow is changed to achieve the geometrical reconstruction of the bulbous bow. Given a position vector Qj (j = 0, 1, 2, … k) of space n + 1 points, the interpolation formula of the coordinates of each point on the Bezier curve is:

$$r(u) = \sum_{j=0}^{k} Q_j N_{j,k}(u) \qquad u \in [0, 1] \tag{3.17}$$

where Q_i is the control vertex of Bezier parametric curve.

$$N_{j,k}(u) = C_n^j u^j (1-u)^{n-j} = \frac{k!}{j!(k-j)!} u^j (1-u)^{k-j} (\mathrm{j} = 0, 1, 2 \ldots \mathrm{k})$$

(2) NURBS surface construction method

NURBS is an excellent surface modeling methods that has been widely used in CAD/CAM and computational geometry and computer graphics in recent years [49]. It can use a unified mathematical model in a geometric design system to represent the quadratic curve or surface and modify the surface by modifying the control vertex and the node vector method. This modification has good geometrical characteristics, which can easily express the various shapes the user needs, especially in automobile body design, aircraft shape design, ship design, and other fields. At present, some excellent CAD/CAM software such as UG, CATIA, 3DMAX have adopted the technology.

NURBS surface construction method can accurately express the characteristic surface with good precision and smoothness. NURBS method is also called nonuniform rational B-spline surface reconstruction method. Mathematical expressions can be expressed as:

$$P(u,v) = \frac{\sum_{i=0}^{n}\sum_{j=0}^{m} \omega_{i,j} P_{i,j} N_{i,k}(u) N_{j,i}(v)}{\sum_{i=0}^{n}\sum_{j=0}^{m} \omega_{i,j} N_{i,k}(u) N_{j,i}(v)} \tag{3.18}$$

where P_{ij} is a n*m rectangular array control vertices that has been given to form a control grid. ω_{ij} is the weighting factor sequence of the corresponding control point P_{ij} and specifies that ω_{ij} is greater than zero and ensures that the basis function is greater than or equal to zero. $N_{i,k}(u)$ and $N_{j,i}(v)$ are not regular B-spline basis functions in the u-direction k times and v-direction l, k represents the number of B-splines in the u direction, and 1 represents the number of times of B-spline bases in the v-direction. They have node vectors $u = [u_0, u_1 \ldots u_{m+k+1}]$ and $v = [v_0, v_1 \ldots v_{n+l+1}]$ in u-direction and v-direction, respectively.

NURBS control grid parameterization method is used to modify the hull geometry, and the control vertex coordinate p_{ij} is taken as the design variable. Control vertex coordinates p_{ij} can be moved along the X-, Y-, and Z-axes in three directions. In order to ensure that the changed surface is smoother, the control point is transformed by manually setting the moving distance and the moving direction of the control point. After moving and controlling the vertex coordinates p_{ij}, the changed NURBS surface is calculated according to the surface generation algorithm as shown in Fig. 3.9.

(3) ASD technology

Arbitrary shape deformation (ASD) technology is a B-spline-based geometric transformation method. This method first requires that the ASD control body be built outside the geometry. An ASD control body includes individual control points and connection points between control points. When the control point moves, the shape of the relevant area also changes. The changed geometry can still guarantee the continuity of the third-order surface, and the good deformation quality can be guaranteed even under large deformation [50]. This direct deformation method provides a possibility for the deformation of complex geometry. It can be optimized with fewer design variables based on user-defined motion characteristics and can be defined directly on the grid model, avoiding the need to repartition the grid, saving time compared to traditional methods.

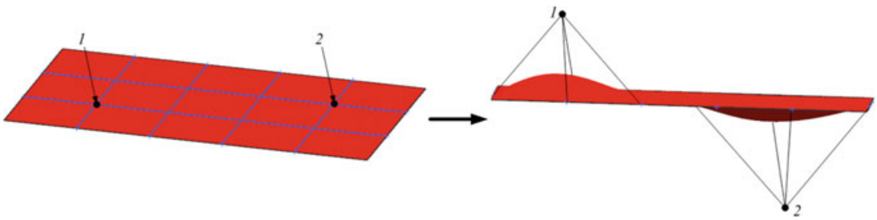

Fig. 3.9 Change of NURBS surface

Sculptor software is based on years of research and experience in computational fluid dynamics research and work, developed by the US Optimal Solutions company to solve the deformation of automated grid applications. It can import the corresponding CFD software grid files, such as Fluent, Star-CD, PlotSd, NASTRAN, according to the requirements of the engineer, the deformation of the mesh operation and be able to observe the effect of deformation in real time. The combined use of Sculptor's mesh morphing and CFD software has been around for many years, and the potential of CFD has been further developed as a result of this technique.

Sculptor simplifies the traditional design process, local deformation based on the original model and smooth transition are carried out and can check whether there is interference between the deformation of the geometry, saving the time engineers need to restructure the CAD geometry and resize the grid when it is necessary to change the appearance of the object. Embedded in a gradient-based optimization algorithm, it optimizes design problems based on the optimization tasks' engineers have developed to help engineers find solutions to meet the design requirements. Using batch mode, it can also be easily integrated with other optimization software (such as ISIGHT) to optimize design issues using optimization algorithms in optimization software. Mesh transformation tools based on NURBS patented technology can rapidly generate high-order smooth and high-quality grids after geometric changes, which greatly saves the time for geometric reconstruction and grid reconstruction. It is especially suitable for the design optimization problems related to fluid, fluid-structure coupling, and structural shape. The deformed shape of the grid can directly lead to the CAD design scheme and improve the design efficiency. After the deformation is still available to be CFD software to read the file, the designer can import it into the corresponding analysis software for analysis. In the traditional process of simulation and design optimization, the process of "updating geometric modeling—re-demarcating grid—the simulating solution—optimization iteration" is followed. That is: when the geometry parameters of the program changes, the engineer needs to update the geometric shape and reuse the CAE preprocessor for meshing and model setting. As shown in Fig. 3.10. There are obvious limitations in this approach:

(1) The requirement of the geometry of the parameterization is quite high and cannot guarantee whether the geometrical parameter changes can generate a reasonable shape, or even geometric shape update failed.
(2) It takes a lot of time to repartition the grid, and the quality of the grid is hard to guarantee (especially in grids at complex geometries or boundary layer grids in CFDs that still require human intervention and inspection), and there is also the risk of the failure of the M grid division.
(3) The traditional design cycle of "updating geometric shapes—re-meshing—simulation solution—optimization iteration" has a long design cycle and development costs have not been effectively reduced, which greatly hinders the popularization and application of simulation and optimization techniques in engineering.

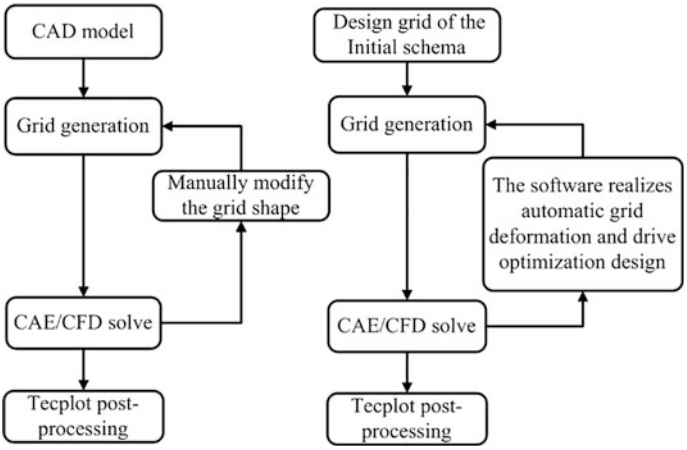

Fig. 3.10 Traditional grid design process and automatic grid deformation design flow

In order to achieve grid deformation, optimal solutions developed arbitrary shape deformation (ASD) technology to add a control field as a Sculptor variable outside of the original CFD grid node. By changing the position of the control points on the control domain, it is easy and convenient to achieve the purpose of grid deformation. As shown in Fig. 3.11:

Sculptor is a mesh deformation and shape optimization tool based on uniform B-spline technology, which can help the simulation engineers save the time of repeated meshing and help designers quickly and automatically optimize geometric shapes and improve product development. Sculptor has the following characteristics:

(1) Customize geometric parameters directly on the CFD/FEM grid model: No need for CAD model parameterization for complex parameterless surface optimization.

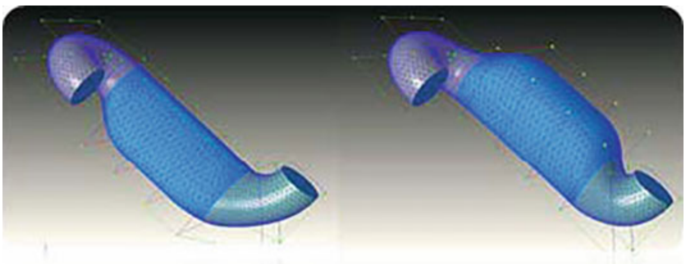

Fig. 3.11 Automatic deformation of multi-bodies

(2) Only change the local area of the grid, without the need to re-divide: greatly reduce the grid time, ensure the quality of the grid, suitable for large-scale simulation problems.
(3) Precisely control the geometry of the local area: Geometric changes do not affect other locations and better capture the intention of the designer.
(4) The curvature derivative of the grid boundary after deformation is continuous: Better control of grid quality, especially the geometric shape of the boundary layer and flowing-sensitive areas.
(5) Structure and fluid grids share the same set of deformation parameters: suitable for fluid-structure coupling-related design optimization problems.
(6) From the grid can be directly returned to CAD geometric model: to help designers quickly obtain the geometric solutions and realize efficient collaboration of simulation—optimization—design.

References

1. Zhao F, LI S-Z, Yang L (2010) An overview on the design optimization of ship hull based on CFD techniques. J Ship Mech 14(7): 406–412
2. Yusuke T, Sugimoto S, Shinya M (2003) Development of CAD/CFD/ optimizer-integrated hull-form design system. J Kansai Soc Naval Archit Jpn (240): 29–36
3. Liu P, Zhang H, Cheng H (2014) An overview on hull form generations and geometric representation methods of surface naval ship. Ship Sci Technol 36(6): 1–6
4. Jochen M (2003) Use of CFD methods for hull form optimization in a model basin. In: MARNET—CFD workshop pp 1–8
5. Harries S (1998) Parametric design and hydrodynamic optimization of ship hull forms. Institut für Schiffs-und Meerestechnik, Technische Universit Berlin, Germany
6. Harries S (2005) Systematic optimization-a key for improving ship hydrodynamics. Hansa 142(12): 36–43
7. Abt C, Harries S (2007) FRIENDSHIP-Framework-integrating ship-design modeling simula-tion and optimization. Naval Archit RINA (1): 1–8
8. Abt, CT, Harries, S, Heimann J (1999) Formal hydrodynamic optimization of a fast monohull on the basis of parametric hull design. In: FAST'99-5th International conference on fast sea transportation, Seattle
9. Abt C, Harries S, Heimann J, Winter H (2003) From redesign to optimal hull lines by means of parametric modeling. In: 2nd International conference on computer application and information technology in the maritime industries, Hamburg
10. Tahara Y, Patterson E, Stern F, Himeno Y (2000) Flow-and wave-field optimization of surface combatants using CFD-based optimization methods. Val de Reuil, France. In: Proceedings, 23rd ONR symposium on naval hydrodynamics
11. Kim H, Yang C, Chun HH (2010) A combined local and global hull form Modification approach for hydrodynamic optimization. In: 28th symposium on naval hydrodynamics
12. Kim H (2009) Multi-objective optimization for ship hull form design. America: George Mason University
13. Peri D, Rossetti M, Campana EF (2001) Design optimization of ship hulls via CFD techniques. J Ship Res 45(2): 140–149

14. Ampana EF, Peri D, Bulgarelli UP (2002) Optimal shape design of a surface combatant with reduced wave pattern. In: Symposium on "Reduction of military vehicle acquisition time and cost through advanced modelling and virtual simulation", Paris, France
15. Peri D, Campana EF (2003) Multidisciplinary design optimization of a naval surface combatant. J Ship Res 47(1):1–12
16. Peri D, Campana EF (2005) High-fidelity models and multi objective global optimization algorithms in simulation-based design. J Ship Res 49(3):159–175
17. Campana EF, Peri D, Tahara Y, Stern F (2001) Comparison and validation of CFD based local optimization methods for surface combatant bow. In: Canada: The 25th symposium on naval hydrodynamics
18. Tahara Y, Peri D, Campana EF, Stern F (2008) Computational fluid dynamics-based multi objective optimization of a surface combatant. Mar Sci Technol 13(2):95–116
19. Campana EF, Peri D, Tahara Y, Kandasamy M, Stern F (2009) Numerical optimization methods for ship hydrodynamic design. In: SNAME annual meeting
20. Peri D, Campana EF (2006) Simulation based design of fast multihull ship. In: 26th symposium on naval hydrodynamics. Rome, Italy
21. Campana EF, Peri D (2006) Shape optimization in ship hydrodynamics using computational fluid dynamics. Comput Methods Appl Mech Eng 196: 634–651
22. Tahara Y, Peri D, Campana EF, Stern F (2008) Single and multi objective design optimization of a fast multihull ship: Numerical and experimental results. In: 27th symposium on naval hydrodynamics
23. Zhou CJ (1992) Computer aided hull form design. Shang Hai: Shanghai Jiaotong University Press
24. Zhang P (2009) The parametric design to hull form. Wu Xi: Jiangnan University
25. Ping Z, De-xiang Z, Wen-hao L (2008) Parametric approach to design of hull forms. J Hydrodyn Ser B 20(6):804–810
26. Xie Y-P, Liu Z, Zhang H (2009) Method of mould lines parameterized design of the round craft base on NAPA. Ship Eng 31(6): 8–11
27. Zhang BJ (2009) Research on optimization design of hull lines and minimum Resistance hull form. Dalian: Dalian University of Technology
28. Bao-ji Z, Kun Ma, Zhuo-shang J (2009) The optimization study for hull form of minimum wave making resistance based on Rankine source method. J Hydrodyn Ser B 21(2):277–284
29. Zhang B-J, M K (2011) Study on hull form optimization for minimum resistance based on niche genetic algorithms. J Ship Prod Des 27(4): 162–168
30. Yu YY (2009) Study on the method of ship and platform 3D parametric general design. Dalian: Dalian University of Technology
31. Fu H-P, Chen Z-G (2010) Stern form optimization aimed at wake uniformity. J Shanghai jiaotong Univ 44(10): 1430–1433
32. Baiwei F, Zuyuan L, Chengsheng Z (2010) Parametrization modeling based on hull form morphing method. Comput Aided Eng 19(4):3–7
33. Li SZ (2012) Research on hull form design optimization based on SBD technique. Wuxi: China Ship Scientific Research Center
34. Mitsuhiro A, Tan O (1966) Application of wave resistance theory in ship type planning. Kansai Soc Nav Archit Jpn 119:60–72
35. Suzuki K., Iokamori N (1999) Studies on minimization of wave making resistance based on Rankine source method. Kansai Soc Nav Archit Jpn (185): 9–19. (in Japanese)
36. Yasukawa H, Heavy M (2000) Ship form improvement using genetic algorithm. Ship Technology Research 47, 35–44
37. Takumi Y, Kazuo S (2001) Hydrodynamic shape optimization of bow bulbs based on rankine source method. Kansai Soc Nav Archit Jpn 325:39–47
38. Saha GK, Suzuki K, Kai H (2004) Hydrodynamic optimization of ship hull forms in shallow water. J Marine Sci Technol 9(2):51–62

39. Saha GK, Suzuki K, Kai H (2005) Hydrodynamic optimization of a catamaran hull with large bow and stern bulbs installed on the center plane of the catamaran. J Marine Sci Technol 10:32–40
40. Hirayama A, Ando J (2008) Study on mul-tiobjective hull optimization for resistance in still water and added resistance in waves-mul-tiobjective optimization using real-coded genetic algorithm. Jpn Soc Naval Archit Ocean Eng (7): 213–222
41. Jun-ichi H, Himeno Y, Tahara Y (1996) Hull form optimization by nonlinear programming (Part 4): Improvement of stern form for wake and viscous resistance. J Kansai Soc Naval Archit Jpn 225:15–21
42. Jun-ichi H, Himeno Y, Tahara Y (1996) Hull form optimization by nonlinear programming (Part 3): Improvement of stern form for wake and viscous resistance. J Kansai Soc Naval Archit Jpn (225): 1–6
43. Jun-ichi H, Himeno Y, Masatoshi B (1995) Hull form optimization by nonlinear programming: Part 2: improvement of hull form for minimizing wave resistance. J Kansai Soc Naval Archit Jpn 224:13–19
44. Masuda S, Suzuki K, Kasahara Y (2002) An optimization method for full form ships using a simple prediction of the thrust deduction factor. J Kansai Soc Naval Archit Jpn 237:33–38
45. Suzuki K, Kai H, Kashiwabara S (2005) Studies on the optimization of stern hull form based on a potential flow solver. J Marine Sci Technol 10(2):61–69
46. Xu G, Wang GZ, Chen X (2010) Free form deformation and its application. J Comput Res Dev 47(2): 344–352
47. Deng ZJ, Cao J (2013) Research and application of FFD algorithm. Comput Technol Dev 23 (12): 116–119
48. Demengel P. Gilberd, DH et al (2000) Mathematics of curves and surfaces. Beijing: Commercial Press
49. Wu G-L, Zhang Q-J (2011) Study on computer aided NURBS surface modeling technology and its implementatio. J Jiangnan Univ (Natl Sci Edition 10(2): 158–161
50. Sun ZX, Song JJ, An YR (2010) Optimization of the head shape of the CRH3 high speed train. Sci China Technol Sci 53(12):3356–3364

Chapter 4
Optimization Method and Optimization Platform

Ship hull form optimization is a typical engineering optimization problem, involving a large number of design variables and constraints. In this optimization, the objective function and design variables are of hidden relationship due to its strong nonlinear phenomenon. Therefore, how to obtain global optimal solution has become a key technique for solving the problem of ship-type optimization. The current optimization techniques can be broadly divided into three categories: The first category, the traditional optimization algorithm, based on the given initial value, searches based on the gradient information, and the local optimal solution can be obtained in the optimization process. When the initial values of multiple peaks are different, different local minima will be searched, which is also called the instant search algorithm. The second category: modern optimization algorithms: also known as the global optimization algorithm, which combines the advantages of directional search and random search, you can get a better regional exploration and spatial expansion of the balance, but the search speed is slow. The third category: hybrid optimization algorithm: the method combines the two advantages of fast search speed of traditional optimization algorithm and wide search space of modern optimization algorithm and can quickly get the global optimal solution. It is one of the methods developing rapidly recently. In recent years, there has been a class of optimization platform and open-source code, more commonly used, such as ISIGHT and OPENFOAM, which integrates the software or program for the problem under study on this platform or performs secondary development to obtain a mathematical model for optimizing the problem, which can save the program trouble and greatly facilitate the ship-type optimization.

© Shanghai Jiao Tong University Press, Shanghai and Springer Nature Singapore Pte Ltd. 2019

B.-J. Zhang and S.-L. Zhang, *Research on Ship Design and Optimization Based on Simulation-Based Design (SBD) Technique*,
https://doi.org/10.1007/978-981-10-8423-2_4

4.1 Traditional Optimization Methods

The use of optimal theory and method to solve practical problems in production and the specific problems in the natural sciences is generally divided into two steps [1]

(1) Establish a mathematical model, that is to analyze the specific problems to be solved, and simplify the formation of optimization problem.
(2) Perform mathematical processing and solving. The resulting optimization problem is organized and transformed, making it an easy-to-solve form; choose or suggest a suitable calculation to solve the problem; compiling calculation program and calculating on computer; analyzing the calculation results to see if they fit the model.

In engineering, for example, the problems encountered in the field of ship mainly include the nonlinear programming problems of constrained optimization. Constrained optimization methods can be roughly divided into the following four categories:

(1) Using linear programming or quadratic programming to gradually approximate the nonlinear programming method, such as SLP method, SQP method.
(2) Transform constraint optimization problems into unconstrained optimization problems, such as SUMT external point method, SUMT interior point method.
(3) Analytical methods such as feasible direction method, gradient projection method, and approximate gradient method are used to deal with the constraint optimization problem without prior conversion.
(4) Direct search methods that do not pre-convert the constrained optimization problem, such as the method of complex line, random test method.

In this book, the mixed penalty function method (SUMT internal and external point methods) is used to transform the constraint optimization problems into unconstrained optimization problems and select the appropriate direct search method for unconstrained optimization.

4.1.1 The Basic Idea of Nonlinear Programming

The general model of nonlinear programming is [2]:

$$(\mathrm{P}) \quad \min_{x \in S} f(x) \tag{4.1}$$

In the formula, S is a subset of R^n, and $f(x)$ is defined on S or R^n.

When $S = R^n$, the corresponding plan (P) is called the unconstrained problem; when S is a subset of R^n, the corresponding (P) is called the constraint problem. The problem $\max_{x \in S} f(x)$ can be turned into an equivalent $\min_{x \in S} -f(x)$, so we only need to consider the minimization problem, which is called the feasible set of S is

(P). The point $\bar{x}$ of feasible set is called the feasible point, which is called the objective function of (P) is $f(x)$. Let f take x^* minimal point in S as the optimal solution of (P), or the solution of (P), and the corresponding objective function value is called the optimal value of the problem.

Definition 1 Let S be a nonempty set in $R^n, f: S \rightarrow R$. For $x^* \in S$, if exist $\varepsilon > 0$, such that

$$f(x) \geq f(x^*), \forall x \in S \cap O(x^*, \varepsilon) \tag{4.2}$$

Among them, $O(x^*, \varepsilon)$ is the open ball R^n with x^* as the center and ε as the radius, which

$$O(x^*, \varepsilon) = \{x \in R^n : \|x - x^*\| < \varepsilon\} \tag{4.3}$$

It is said that x^* is a local minimum point of f in S; if $f(x) \geq f(x^*), \forall x \in S$, then x^* is a global minimum point of f in S; if formula 4.1 or 4.2 is strictly established for $x \neq x^*$, then the x^* is a strictly local (or strictly global) minimum point of f in S.

In particular, we call the problem (NP)

$$\begin{aligned} &\min f(x) \\ &s.t. \quad h_i(x) = 0, i = 1, \ldots, m \quad g_j(x) \leq 0, j = 1, \ldots, p \end{aligned}$$

standard nonlinear programming. There f, h_i, g_j is all real-valued function on R^n,and "$s.t.$" means "restricted." $h_i(x) = 0$ is called the equality constraint, and $g_i(x) \leq 0$ is called the inequality constraint.

The establishment of some theories in nonlinear programming is closely related to convex sets and convex functions. The attempt to extend the theory of linear programming to nonlinear programming leads to an exhaustive study of convex functions. This research, called convex analysis, is a young discipline that began to develop since the 1950s. These contents are not discussed here. "Feasible directions" is an important concept in depicting optimality.

Definition 2 Let $x \in S \subseteq R^n$. To say that $d \in R^n$ is a feasible direction for the x (about S), if exist $\bar{\alpha} > 0$, such that $x + \alpha d \in S, \forall \alpha \in \lfloor 0, \bar{\alpha} \rfloor$, as shown in graph 4.1, d_1, d_2 are possible directions for x, and d_3 is not.

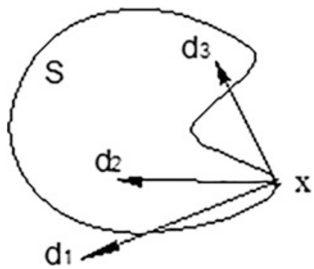

Fig. 4.1 Feasible direction

The system uses nonlinear programming method to solve the problem along the feasible direction from the feasible point.

4.1.2 Gradient Method

Gradient method is one of the simplest analytical methods, and its idea is very intuitive. Since the function $f(X)$ declines most rapidly along the negative gradient $-\nabla f(X^{(k)})$ at $X(k)$, it is natural to think that seeking in this direction will be valid and hence:

$$X^{(k+1)} = X^{(k)} - \alpha_k \nabla f(X^{(k)}) \tag{4.4}$$

In the formula, α_k is the step in the negative gradient direction.

Generally, the optimal step factor α_k^* is determined by one-dimensional minimization in this direction, that

$$f(X^{(k)} - \alpha_k^* \nabla f(X^{(k)})) = \min_{\alpha_k^*} f(X^{(k)} - \alpha_k \nabla f(X^{(k)})) \tag{4.5}$$

When α_k^* is determined, a new design point X (k + 1) can be obtained. Then, find the gradient of the function $f(X)$ at X (k + 1). So iterative, until a point of gradient close to zero, the gradient is zero at the minimum point. Because it is along the direction of negative gradient search, it is called the gradient method, or the steepest descent method.

4.1.3 Sequential Unconstrained Optimization Method

Most of the actual optimization problems are constrained. If a constrained optimization problem can be transformed into an unconstrained optimization problem, the unconstrained optimization method can be used to solve the problem. The sequential unconstrained optimization method is based on this assumption. The idea is in the objective function of the original constrained minimization problem, some additional items that reflect the influence of the constraints are introduced to form a new objective function of the unconstrained optimization problem, and by reasonably selecting these additional terms, the unconstrained optimal point sequence of the new objective function can be converged to the optimal point of the original problem. Therefore, this method is called Sequential Unconstrained Minimization Techniques, referred to as SUMT method [3]. According to the different additional items, it can be divided into: penalty function method, barrier function method, and mixed penalty function method.

(1) Penalty Function Method

Define the penalty function

$$F(x, M_k) = f(x) + M_k p(x) \tag{4.6}$$

Among them, $M_k > 0$ is a constant, known as the penalty factor, and $p(x)$ is a function defined on R^n, called the penalty term. The computational steps to solve the constrained optimization problem with the penalty function method are as follows:

(1) Selecting $M_1 > 0$, the accuracy is $\varepsilon > 0$, $c \geq 2$ and the initial point is $x^{(0)}$, order $k = 1$.
(2) Taking $x^{(k-1)}$ as the initial point to solve the unconstrained optimization problems
$\min F(x, M_k) = f(x) + M_k \sum_{i=1}^{L} g_i^{+}(x)$, let $x^{(k)} = x(M_k)$ be the optimal solution.
(3) Let $\tau_1 = \max\limits_{1 \leq i \leq P}\{|h_i(x^{(k)})|\}, \tau_2 = \max\limits_{1 \leq i \leq m}\{|g_i(x^{(k)})|\}, \tau = \max\{\tau_1, \tau_2\}$
(4) If $\tau < \varepsilon$, the iteration ends and take $x^* = x^{(k)}$; otherwise, let $M_{k+1} = cM_k, k = k+1$, and then back to the second step.

The above algorithm end criterion $\tau < \varepsilon$ can also be changed to: If $M_k p(x^{(k)}) < \varepsilon$, take $x_* = x^{(k)}$ and the iteration end; otherwise, let $M_{k+1} = cM_k, k = k+1$ and continue iterating.

(2) Barrier Function Method

The barrier function method is suitable for the constrained optimization problem of

$$\begin{cases} \min f(x) \\ s.t. x \in S \\ S = \{x | g_i(x) \leq 0, i = 1, 2, \ldots, m\} \end{cases}$$

It starts from a feasible point $x^{(0)}$ and iterates between feasible points. In order to keep the iteration point as a feasible point, a "wall" is built on the boundary of the constraint set S, which blocks the iterative point column from leaving the feasible set S. The calculation steps are as follows:

(1) Let $r_1 > 0, c \geq 2$, and the accuracy is $\varepsilon > 0$.
(2) Finding an interior point of the feasible set S, $x^{(0)} \in \operatorname{int} S$; let $k = 1$.
(3) Take $x^{(k-1)}$ as the initial point, and solve problems using the method of solving unconstrained optimization problems.

$$\begin{cases} \min F(x, r_k) = f(x) + r_k B(x) \\ s.t. x \in \operatorname{int} S \end{cases} \tag{4.7}$$

Let its optimal solution be $x^{(k)} = x(r_k)$.

(4) Checking whether $x^{(k)}$ meets the termination criterion, if $x^{(k)}$ is satisfied, the iteration ends; otherwise, take r_{k+1}, and $r_{k+1} < r_k$, let $k = k + 1$, then back to the third step.

(3) Mixed Penalty Function Method

During the iteration process, the parameter M_k of the external method increases continuously, and the parameter r_k of the interior point method decreases continuously, making it very difficult to solve the unconstrained minimum problem. The selection of r_k and M_k has a great influence on the convergence speed. The approximate solution obtained by the external point method is often not feasible, can only be approximately satisfied, and sometimes cannot be used; it is more difficult to solve problems by interior point method in the feasible area. The interior point method cannot solve the optimization problem involving the equation constraints.

Given the initial point $x^{(0)}$, for those inequalities that are satisfied by $x^{(0)}$ (the initial point is inside the feasible domain), the barrier term B(x) is constructed by the interior point method. For those inequality constraints and equality constraints that are not satisfied by $x^{(0)}$, the penalty term p(x) is constructed by the external point method, that is mixed penalty function method.

Building up the barrier term B(x) with the following conditions: B(x) is continuous; B(x) >= 0; when x approaches the boundary of S, B(x) $\rightarrow \infty$. In this way, x will not move to the boundary point, and it will not jump out feasible field. In this sense, it cannot be allowed to take the boundary point.

Building up the penalty term p(x) with the following conditions: p(x) is continuous; For any $x \in R^n$, p(x) >= 0; if and only if $x \in S$, p(x) = 0. The function of the mixed method is:

$$F(x, r_k) = f(x) + r_k B(x) + \frac{1}{r} p(x),$$

$$B(x) = \sum_{i \in I_1} g_i^+(x), p(x) = \sum_{i \in I_2} g_i^+(x) + \sum_{j=1}^{p} (h_j(x))^2 \tag{4.8}$$

$I_1 = \{i | g_i(x^{(k-1)}) < 0, i \in I\}, I_2 = \{i | g_i(x^{(k-1)}) \geq 0, i \in I\}$, $I = \{1, 2, \ldots, m\} = I_1 \cup I_2 r_0 > r_1 > r_2 > \ldots < r_{k-1} > r_k > \ldots$, and $\lim_{k \to \infty} r_k = 0$. It can be determined by approaches of external point or interior point method.

4.2 Modern Optimization Algorithm

In recent years, modern optimization algorithms have been widely used in engineering, but the most widely used are genetic algorithm, neural network algorithm, and particle swarm algorithm as well as their improved versions, especially in the field of ship design [4]. This book mainly introduces the principles of these algorithms.

4.2.1 Basic Genetic Algorithm

The optimization design is based on the modern probability theory and the optimization method. The optimization model is often characterized by high dimension, nonconvex, and nonlinear and needs to meet a variety of constraints [5]. For such complex nonlinear optimization problems, there are obvious shortcomings and deficiencies when using the traditional optimization methods: The optimization result depends on the selected initial values, and the target function is excessively limited; in the case of the discontinuous or nonderivative functions, many optimization problems that utilize gradient information cannot be performed [6]. Genetic algorithm (GA), a kind of algorithm based on biological evolution, simulates Darwin's natural evolution law of "natural selection and survival of the fittest" and Mendelian theory of genetic variation, which is an intelligent and adaptive probabilistic global optimization search algorithm. The main features of this method are group search strategy and the information exchange among individuals in the community. The search does not depend on the gradient information of the problem, especially for complex and nonlinear problems that are difficult to be solved by traditional search methods. Compared with the traditional optimization methods, it is simple to use and has the advantages of global optimization. It is one of the most effective methods for solving optimization problems today. In recent years, GA has been widely used in the field of engineering design and optimization. In the field of marine engineering, it has been widely used in the conceptual design and preliminary design of ships, the unplanned and unobtrusiveness of lines, the movement of ships, the design of subdivision, the free-floating calculation of ships, and the structural optimization [7].

(1) The basic principle of genetic algorithm

Suppose an optimization problem

$$\max|\{f(x)x \in X\}| \tag{4.9}$$

Here, f is a positive function on X, that means for any $x \in X, f(x) > 0$. X is the solution space of the problem, that is, all possible solutions to the problem. It can be either a finite set or a subset of real space.

Genetic algorithm in solving the problem is from a number of solutions to start and then through a certain law of the gradual iteration to produce new solutions. The geometry of this solution is called a group, or a population, denoted by P(T), where t represents the iterative step, or evolution. In general, the elements in P(t) are invariant throughout the evolutionary process, called the population scale, denoted as N. The elements in P(T) are called individuals. Each individual's degree of adaptation to the environment is called fitness. When we perform genetic operations, we choose the current solution to intersect to generate new solutions. These current solutions are called the parent of the new solutions, and the new solutions are called the descendants.

(2) The implementation steps of basic genetic algorithm

The genetic algorithm solves five major elements of the solution: parameter coding, initial population, evaluation of fitness function, genetic operation (selection, crossover, and mutation), and control parameter settings.

The basic steps of the simple genetic algorithm are as follows:

(1) The solution to the problem under study is coded as a "chromosome", and each code string represents a feasible solution to the problem.
(2) Randomly generate a certain number of initial coding strings $PoP_{0,}$ which is a set of feasible solutions to the problem.
(3) Place the initial code string in the "environment" of the problem, and give the fitness (evaluation) of each individual code string adaptation population in the population.
(4) The initial population PoP_0 (or POP_k) is based on the individual fitness of the code string. Or perform a selection operation to randomly select the paternal population F_k; good individuals are replicated in large numbers, while inferior individuals are less copied and even eliminated.
(5) Population C_k is generated by cross probability P_c for paternal population F_k.
(6) A new population $POP_{(k+1)}$ for mutation operation of population C_k with mutation probability P_m.

This repeated the implementation of the third step to the sixth step, so that the code string population evolved from generation to generation, and finally searches for the most adapted to the environment of the individual, the optimal solution to the problem.

The basic flow and structure of simple genetic algorithm are shown in Fig. 4.2.

4.2.2 Niche Genetic Algorithm

Due to the shortcomings of GA, such as premature convergence and slow convergence in the later stage, GA has not been effective in some optimization problems. Therefore, many scholars have proposed various improvement methods [8]. However, many improved algorithms can only take into account one aspect of the problem. If the core of the algorithm is to improve the accuracy of the solution, the algorithm is bound to spend more time in search scope and search precision. In GA, using proportional selection operator, the selection strategy has obvious flaws. When there are individuals in the population whose fitness is far greater than the average value of the population, these individuals will expand rapidly under the proportional selection operator and fill the entire population, so that the individual

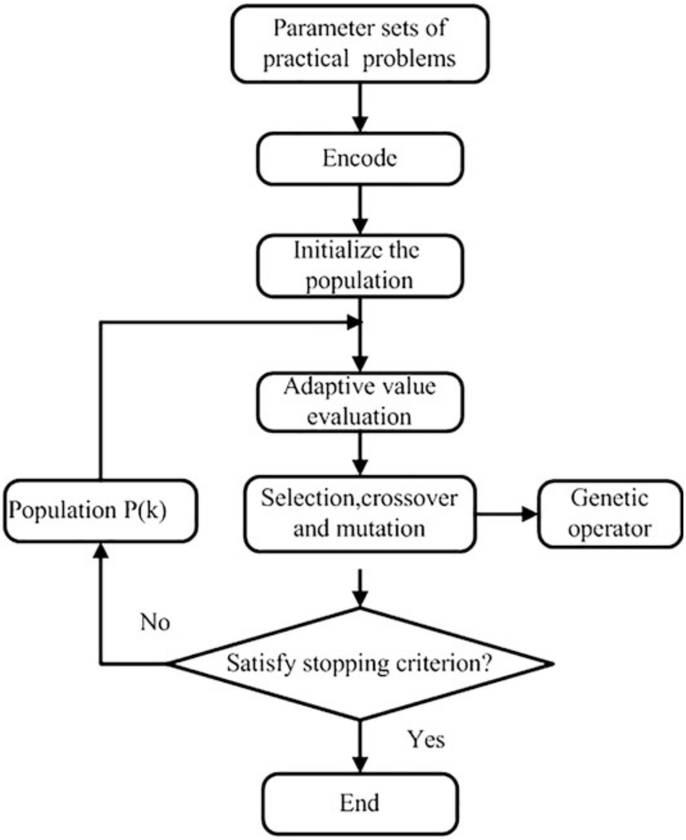

Fig. 4.2 Flowchart of basic genetic algorithm

differences in the population are drastically reduced and the population diversity is severely damaged. The lack of population diversity is the main reason for the poor GA global search ability [9]. The niche genetic algorithm (NGA) can overcome the shortcomings of GA, such as precocious puberty and poor local search ability, so as to keep the diversity of individuals in the population as well as high global search ability and convergence speed [10]. The basic idea of niche comes from the fact that a living organism always lives with its own species in the process of evolution. The basic idea of niche algorithm is derived from a fact that population within its evolutionary process always live with the same species. According to this idea, the population in the niche algorithm is evolved in a specific environment to avoid mass-producing of the high fitness individuals.

(1) The Biological Basis of Niche

Biologically, niche refers to the function or role of a tissue in a particular environment, and species refer to organizations that share common characteristics.

Because creatures tend to live together with similar features, shapes, and other similarities, they are always associated with their descendants of the same species, combined with the restriction of their natural geographical location, so that several species of creatures form a niche. The formation of niche is of biological significance, which offers the possibility of the formation of new species. In the early days of niche formation, the genes of the species in niche are often different. Due to the relative isolation of multiple niches and the lack of essential gene exchange, the genetic differences are preserved. The variation of organisms in each niche occurs randomly and therefore usually has different direction of variation. The difference of these variations causes the genetic diversity among species to expand continuously. Because of the difference of geographical location and natural environment, the direction and pressure of natural selection are also different. This difference leads to greater differences in the genetic composition of species. As a result, each species evolves and develops in its own direction, which is one of the fundamental reasons why creatures in nature remain near-infinite diversity.

(2) Niche Based on Sharing Mechanism

In 1987, Glodberg and Richardson proposed a niche technology based on the sharing mechanism. In this mechanism, Glodberg and Richardson defined a sharing function to determine the degree of sharing of each individual in a group [11–13]. The degree of sharing of an individual is equal to the sum of the shared function values between that individual and each other individual within the group. The shared function is a function of the closeness of two individuals (the similarity of genotypes or the similarity of phenotype); when the relationship between individuals is relatively close, the value of the shared function is relatively large; on the contrary, the value of the shared function is smaller.

Let d_{ij} denote the closeness between individuals i and j (Hamming distance can be used here), S is the shared function, and S_i represents the degree of sharing of individual i in the group, there $S_i = \sum_{j=1}^{M} s_h\left(d_{ij}\right)$, and the shared function can be written as $S_h(d_{ij})$, that:

$$S_h\left(d_{ij}\right) = \begin{cases} 1 - \left(d_{ij}/\sigma\right)^{\alpha} & d_{ij} < \sigma \\ 0 & \text{others} \end{cases} \tag{4.11}$$

$d\ (i, j)$ indicates the Hamming distance (fitness distance) between two individuals which can be defined as:

$$d_{ij} = \left\|X_i - X_j\right\| = \sqrt{\sum_{k=1}^{M} \left(x_{ik} - x_{jk}\right)^2} \tag{4.12}$$

$$(i = 1, 2, \ldots, M - 1; j = i + 1, i + 2, \ldots M)$$

Where X_i and Y_j are, respectively, the ith and the jth individuals; M is the initial population number; σ and α are user-defined constants, and the value of σ is difficult to be determined and appropriately selected according to the needs of the problem. In general, the estimation is based on experiments and errors. In this paper, we take $\sigma = 0.5$; α is a constant that controls the shape of the shared function. Generally, α = 1(linear sharing function); the larger the value of the shared function between two individuals, the closer the two individuals are.

With the shared function, the fitness f'_i can be calculated:

$$f'_i = \frac{f(x_i)}{\sum_{j=1}^{M} S_h(d_{ij})} \tag{4.13}$$

4.2.3 Neural Network

(1) BP neural network model structure

Backpropagation (BP) neural network was proposed by a team of scientists headed by Rumelhart and McCelland in 1986 [14, 15], which is one of the most effective algorithms in artificial networks. The continuous functions of any closed interval can be approximated by a BP network with a hidden layer. Therefore, BP neural network has strong modeling and analysis ability for nonlinear systems. The most commonly used BP neural network model consists of three parts: input layer, hidden layer, and output layer, and the hidden layer can be one layer or multiple layer.

The learning process of BP neural network algorithm can be divided into two stages: The first step is the positive signal propagation. The actual output value of each layer node is calculated from input layer to hidden layer. Each layer node only accepts the input value of the previous layer node, and only affects the state of the next layer node [16]. The second step is the error back-propagation. If the output layer fails to obtain the expected output value, the error between the actual output and the expected output should be calculated recursively layer by layer. Based on the error, the weight of the previous layer is modified to minimize the error accumulation trend. In the direction of decreasing slope of error function, the network weights and threshold changes are continuously adjusted so as to gradually approximate the objective function. Each weight and error change is directly proportional to the influence of network error.

Neural network theory has proved that as long as the number of nodes in the hidden layer is enough, the BP neural network with a single hidden layer can be used to approximate any nonlinear function with finite discontinuity points with arbitrary precision. Moreover, the more the hidden layer is, the more the error transmission link, the lower generalization performance of the neural network, so the BP neural network often adopts three-layer structure as shown in Fig. 4.3.

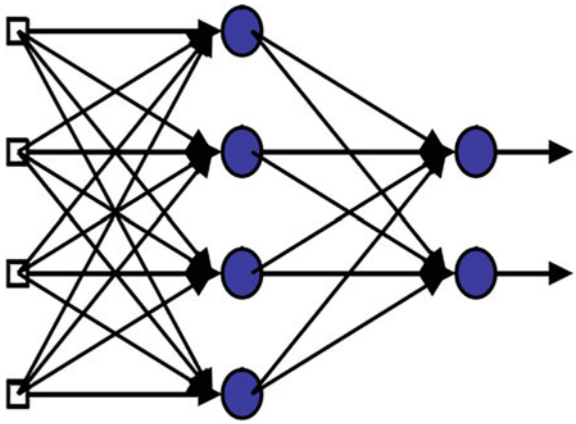

Fig. 4.3 Three-layer BP neural network

Let input and output(X_P, T_P)p = 1, 2, …, p:p as the number of training samples, X_P is the input vector for the pth sample, Xp = (x_{p1}, …, x_{pM}), M is the dimension of input vector; T_P is the output vector of the pth sample (expected output), T_P = (t_{p1}, …, t_{pN}), N is the output vector dimension, and the actual output vector of the grid is O_p = (o_{p1}, …, o_{pN}). The neural network uses a single hidden layer structure, and the number of nodes in the hidden layer is H. The connection weights between the input layer and the hidden layer, the hidden layer and the output layer are represented by w_{ij}, and w_{ij} represents the connection weight between the ith node of the previous layer and the jth node of the latter layer. Sigmoid-type functions are used to transfer the hidden layer and output layer of neural network.

$$f(x) = 1/(1+e^{-x}), \text{ error function } E = \frac{1}{2}\sum_{i=1}^{N}(t_k - o_k)^2 \tag{4.14}$$

The algorithm steps of the three-layer BP neural network are as follows:

Output of hidden layer nodes:

$$y_j = f(net_j) = f\left(\sum_{i=1}^{M} \omega_{ij} x_i\right) \tag{4.15}$$

X_i is the input of the ith input node, and y_j is the output of the jth hidden layer nodes.

The output layer node o_k is:

$$o_k = f(net_k) = f\left(\sum_{j=1}^{H} \omega_{jk} y_j\right) = f\left(\sum_{j=1}^{H} \omega_{jk} f\left(\sum_{i=1}^{M} \omega_{ij} x_i\right)\right) \tag{4.16}$$

$$\frac{\partial E}{\partial \omega_{ij}} = \frac{\partial E}{\partial net_j}\frac{\partial net_j}{\partial \omega_{ij}} \tag{4.17}$$

Define the descending gradient δ_j

$$\delta_j = -\frac{\partial E}{\partial net_j} = \frac{\partial E}{\partial o_j}\frac{\partial o_j}{\partial net_j} = \frac{\frac{1}{2}\sum_k (t_k - o_k)^2}{\partial o_j} f'(net_j) = (t_j - o_j)f'(net_j) \tag{4.18}$$

The weight of output layer and hidden layer nodes is proportional to the decreasing gradient and the updating formula of the weights:

$$w_{ji}(t+1) - w_{ji}(t) = \eta \delta_i o_i \tag{4.19}$$

In the formula, the learning rate is η. α is the momentum factor, and they directly determine the amount of weight update.

But BP neural network also has some problems, mainly in the following aspects:

(1) Slow convergence

BP algorithm is one of the steepest descent methods, and the training step size is difficult to grasp. If the step length is too long, the calculation precision will not reach or even divergence occurs; if the step length is too small, the iteration times will increase, resulting in slow convergence rate. In order to solve the above problems, the improved iterative algorithm can be used to increase the learning rate and speed up the convergence or the use of conjugate gradient method, variable-scale method, and so on.

(2) Easy to fall into local minimum

For a complex neural network, its error surfaces are uneven, with many local minima distributed. When using the BP algorithm to search the optimal solution, it will fall into a local minimum and cannot escape. The most important way to solve this problem is to adopt the global optimization method.

(2) Approximate model of Elman neural network

Elman neural network is a dynamic recurrent artificial neural network based on the Jordan network and proposed by Elman in 1990. It can be viewed as a recursive neural network with local memory units and local feedback connections. The main advantages of this algorithm are [17]:

(1) Elman neural network does not need to know the actual operation of the system and the internal parameters of the direct correlation between the system, just by adjusting the network weights can be achieved on the system modeling.
(2) The acceptance layer of Elman network is equivalent to a delay operator, which can enhance the dynamic information processing capability of the network, and better reflects the dynamic characteristics of the system.
(3) Compared with the feed-forward neural networks like BP and RBF, the Elman network can realize the dynamic modeling of the system and better describe the dynamic mapping relationship between input and output.

Fig. 4.4 Elman neural network model

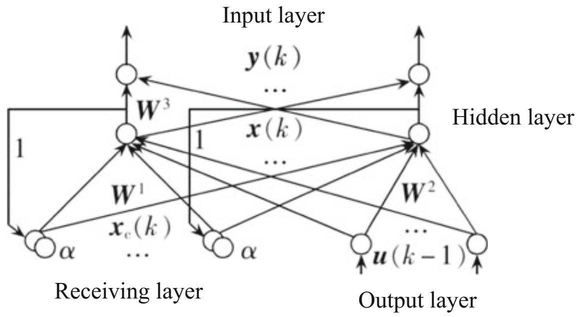

(4) Based on the BP neural network, Elman neural network can store the internal state and make it as the mapping dynamic feature, so that the system has the ability to adapt to the time-varying features.

The main structure of Elman neural network is feed-forward connection, including input layer, intermediate layer (hidden layer), receiving layer, and output layer as shown in Fig. 4.4. Among them, input layer, middle layer, and output layer are similar to feed-forward neural network. The cells of the input layer serve only as signal transmissions; the output layer cells act as linear weights; the receptive layer is used to memorize the output value of the middle layer cell immediately before and back to the input.

The characteristics of Elman neural network is that the output of the intermediate layer is automatically connected to the input of the middle layer through the delay and storage of the receiving layer. This self-linking approach makes it sensitive to historical state data, and the addition of an internal feedback network increases the ability of the network to process dynamic information, so as to achieve the purpose of dynamic modeling. The nonlinear state space expression of Elman neural network is as follows:

$$y(k) = g(w^3 x(k)) \tag{4.20}$$

$$x(k) = f(w^1 x_c(k) + w^2 u(k-1)) \tag{4.21}$$

$$x_c(k) = \beta x_c(k-1) + x(k-1) \tag{4.22}$$

where y represents the m-dimensional output node vector; w^3 represents the connection weight of the intermediate layer to the output layer; x represents the unit vector of n-dimensional intermediate layer nodes; w^1 represents the connection weight of the receiving layer to the middle layer; w^2 represents the connection weight of the input layer to the middle layer; u represents r-dimensional input vector; x_c represents n-dimensional feedback state vector; $g(*)$ represents the transfer function of output neurons; $f(*)$ represents the transfer function of the intermediate layer neurons.

Since Elman neural network is developed on the basis of BP neural network, the learning algorithm is the same as the BP algorithm; that is, the gradient descent algorithm is used to correct the weights, and the learning index function is expressed by the sum of squares of error functions:

$$E = \frac{1}{2}(y_d(k) - y(k))^T(y_d(k) - y(k)) \tag{4.23}$$

where $y_d\ (k)$ is the target output vector.

The dynamic learning algorithm is as follows:

$$\Delta w_{ij}^3 = \vartheta_3 \delta_i^0 x_j(k), \quad i = 1, 2, \ldots, m; j = 1, 2, \ldots, n \tag{4.24}$$

$$\Delta w_{jq}^2 = \vartheta_2 \delta_j^h u_q(k-1), \quad j = 1, 2, \ldots, n; q = 1, 2, \ldots, r \tag{4.25}$$

$$\Delta w_{jl}^1 = \vartheta_1 \sum_{i=1}^{m} (\delta_i^0 w_{ij}^3) \frac{\partial x_j(k)}{\partial w_{jl}^1}, \quad j = 1, 2, \ldots, n; l = 1, 2, \ldots, n \tag{4.26}$$

where ϑ_3, ϑ_2, and ϑ_1 are the learning steps.

$$\delta_i^0 = (y_{d,i}(k) - y(k))g_i'(\cdot) \tag{4.27}$$

$$\delta_j^h = \sum_{i=1}^{m} (\delta_i^0 w_{ij}^3) f_j'(\cdot) \tag{4.28}$$

$$\frac{\partial x_j(k)}{\partial w_{jl}^1} = f_j'(\cdot) x_l(k-1) + \beta \frac{\partial x_j(k-1)}{\partial w_{jl}^1} \tag{4.29}$$

4.2.4 Particle Swarm Algorithm

(1) The origin of particle swarm algorithm

In 1987, biologist Craig Reynolds proposed a very influential flock clustering model [18], in which he argues that each individual follows the principle of avoiding collision with individuals in the neighborhood. Each individual flies toward the flock center, and the flock center is also the target of the entire group. Using only the above three rules in his simulation, the phenomenon of flock flies can be simulated very closely. In 1990, biologist Frank Heppner also put forward a bird model [19], and the difference is that birds are attracted to fly in habitats. In this simulation, each bird did not have a specific target at the outset. Instead, it used simple rules to determine its own flight direction and speed. When a bird flew to the habitat, the birds around it will also fly to the habitat, so that the entire flock of birds will fall in the habitat. In 1995, the American social psychologist James Kennedy and electrical engineer Russell Eberhart, inspired by the construction and simulation results of bird population behavior modeling, proposed a particle swarm optimization algorithm. Their model and simulation algorithms are mainly modified by Frank Heppnerr's model to fly particles to the solution space and land at the best solution. Kennedy described the origins of particle swarm algorithm ideas in his book.

(2) Basic particle swarm optimization

It is assumed that the velocity and position of the *i*th particle on the *d*-dimensional space are $V^i = (v_{i,1}\ v_{i,2}\ v_{i,3} \ldots v_{i,\mathrm{d}})$ and $X^i = (x_{i,1}\ x_{i,2}\ x_{i,3} \ldots x_{i,\mathrm{d}})$. In each iteration, the particle updates itself by tracking two optimal solutions. One is the optimal solution found by the particle itself, that is the individual maximum ***pbest***; the other is the optimal solution currently found by the entire population, namely the global optimal solution ***gbest***. When the two optimal values are found, the particles update their velocity and position according to the following formula:

$$v_{i,j}(t+1) = \omega v_{i,j}(t) + c_1 r_1 [p_{i,j} - x_{i,j}(t)] + c_2 r_2 [p_{g,j} - x_{i,j}(t)] \tag{4.30}$$

$$x_{i,j}(t+1) = x_{i,j}(t) + v_{i,j}(t+1) \quad j = 1, 2, \ldots, d \tag{4.31}$$

where ω is the inertia weight factor; c_1 and c_2 are learning factors; r_1 and r_2 are random numbers evenly distributed between 0 and 1; t is the number of iterations, that is the number of steps a particle flies.

The performance of particle swarm optimization algorithm depends largely on the parameter of the algorithm. The selection principles of several important parameters are as follows [20]:

(1) Number of particles: The number of particles depends on the complexity of the optimization problem. For general optimization problems, 20–40 particles can be selected to get better optimization results; for the simple optimization problems, ten examples are usually selected, and for very complicated problems, the number of particles needs to be over 100.
(2) Learning factors $c_{1,}$ $c_{2:}$ Learning factors help particles to self-summarize and learn from the best of the community, bringing the best of the world in close proximity. Under normal circumstances, $c_1 = c_2 = 2$ can get better results. However, its value is also different according to the complexity and the difficulty of the problem. In general, c_1 is equal to c_2, and between 0 and 4.
(3) The inertia weight coefficient ω: ω determines how much to inherit from the current velocity of the particle, and the proper numerical selection can make the particles have a balanced exploration ability and development capability.

The steps of the basic particle swarm algorithm are as follows:

(1) Randomly initialize the position and velocity of each particle in the population.

(2) Evaluate the fitness of each particle, store the current position and fitness of each particles in the ***pbest***, select all the individuals with the optimal fitness of ***pbest***, and then store those individuals' fitness and location in ***gbest***.
(3) Use formula (4.30) and (4.31) to update the particle velocity and position.
(4) Compare the fitness of each particle with the best position it has experienced. If it is better, it will be the best location at the moment; compare all current ***pbest*** and ***gbest*** and update ***gbest***.
(5) If the stop condition is satisfied, stop the search and output the result, otherwise return to step 3 to continue the search.

(1) Improved particle swarm optimization (IPSO) algorithm I

Although the PSO algorithm has good search ability, in the late optimization, convergence time is long, and the optimization accuracy is not high, easy to fall into local extreme. To improve the global search and local development capabilities of PSO, the adjustment of the inertial factor ω is very critical. In the PSO optimization algorithm, the inertia factor ω represents the successor of the next flight speed of particle i to the current speed. The larger ω can ensure that the algorithm is not easy to fall into the local optimal solution. Later in the algorithm, the smaller ω can speed up the convergence. Inertia weights are generally taken constant method, linear decreasing method, adaptive method, and so on.

In order to improve the convergence of PSO algorithm and prevent it from falling into the local optimum, the inertia factor ω is subject to a randomly distributed random number, so that, to some extent, the instability caused by the linear decrease of ω can be overcome in two aspects. First of all, if the best point is approached in the early stage of evolution, the random ω may produce a relatively small ω and accelerate the convergence speed of the algorithm. In addition, if the optimal point fails to be found in the initial stage of the algorithm, the linear decreasing of ω makes the algorithm not converge to the optimal point ultimately, and random overshoot of ω can overcome this limitation. The updating formula of inertia weight coefficient is as follows:

$$\omega = \mu + \sigma * N(0, 1) \tag{4.32}$$

$$\mu = \mu_{\min} + (\mu_{\max} - \mu_{\min}) * rand(0, 1) \tag{4.33}$$

where N (0, 1) is a random number of standardized normal distribution; $rand$ (0, 1) is a random number between 0 and 1.

In the PSO optimization algorithm, a suitable learning factor can speed up the search speed of particles and reduce the possibility of particles falling into local extremum. The two learning factors vary with time, so in the initial stage of optimization particles have greater self-learning ability and less social learning ability and enhance the global search ability. In the later stage of optimization, the particle has a large social learning ability and a small self-learning ability, which is beneficial to converge to the global optimal solution. Using asynchronous learning factors to update c_1 and c_2, that is to say, the learning factors vary with time in the process of optimization, thus solving the problem of fixed learning factors in the original particle swarm optimization algorithm. The updated formula can be expressed as follows:

$$c_1 = c_{1,ini} + \frac{c_{1,fin} - c_{1,ini}}{t_{\max}} * t \tag{4.34}$$

$$c_2 = c_{2,ini} + \frac{c_{2,fin} - c_{2,ini}}{t_{\max}} * t \tag{4.35}$$

where $c_{1,\,ini}$, $c_{2,\,ini}$ are the initial values of c_1 and c_2, respectively; $c_{1,\,fin}$, $c_{2,\,fin}$ are the final iterative values of c_1 and c_2, respectively.

Specific IPSO algorithm I steps are as follows:

(1) Randomly initialize the positions and velocities of each particle in the population.
(2) Evaluate the fitness of each particle, store the current position and fitness of each particle in the ***pbest*** of each particle, select all the individuals with the optimal fitness of ***pbest***, and then store the fitness of all the individuals in the ***pbest*** into ***gbest***.
(3) Use formula (4.30) and (4.31) to update the velocity and position of the particles.
(4) Use formula (4.32) and (4.33) to update the weights.
(5) Use formula (4.34) and (4.35) to update the learning factor.
(6) Compare the fitness of each particle with the best position it has experienced. If it is better, take it as the current best position; compare all current values of ***pbest*** and ***gbest*** and update ***gbest***.
(7) If the stop condition is satisfied, stop the search and output the result, otherwise return to step 3 to continue the search.

(2) IPSO algorithm II

Obey ω to a random distribution of random numbers, and the formulas are as follows (4.32) and (4.33). Second, drawing on the concept of hybridization in genetic algorithm, in each iteration, according to the probability of hybridization to select a specified number of particles into the hybridization pool, the particles in the pool randomly hybridize each other to produce the same number of progeny particles and replace the progeny particles with progeny particles. Offspring position is calculated by the parent location of the intersection:

$$child(x) = p * parent_1(x) + (1 - p) * parent_2(x) \tag{4.36}$$

where p represents a random number between 0 and 1. The speed of the progeny is calculated by the following formula:

$$child(v) = \frac{parent_1(v) + parent_2(v)}{|parent_1(v) + parent_2(v)|} * |parent_1(v)| \tag{4.37}$$

Specific IPSO algorithm II steps are as follows:

(1) Randomly initialize the positions and velocities of particles in a population.
(2) Evaluate the fitness of each particle, store the current position and fitness of the particles in the ***pbest*** of each particle, select all the individuals with the optimal fitness of ***pbest***, and then store those individuals' fitness and location in ***gbest***.
(3) Use formula (4.30) and (4.31) to update the velocity and position of the particles.
(4) Use formula (4.32) and (4.33) to update the weights.
(5) Compare the fitness of each particle with the best position it has experienced. If it is better, take it as the current best position; compare all current values of ***pbest*** and ***gbest*** and update ***gbest***.
(6) According to the probability of hybridization, a specified number of particles are selected and placed in the hybridization pool. The particles in the pool are randomly crossed every other pair to generate the same number of progeny particles. The progeny position and velocity are calculated according to formula (4.36) and (4.37), and the ***pbest*** and ***gbest*** are kept unchanged.
(7) If the stop condition is satisfied, stop the search and output the result, otherwise return to step 3 to continue the search.

(3) IPSO algorithm III

Obey ω to a random distribution of random numbers, and the formulas are as follows (4.32) and (4.33). Experience has shown that in the traditional PSO algorithm, whether the premature convergence or the global convergence, the particles in the PSO will all appear "aggregation", which is closely related to the convergence of particles and the rapid decline of the population diversity in the PSO. Therefore, it is very necessary to set an index to evaluate the degree of convergence of particle swarm. The degree of convergence of the particle swarm can be expressed as:

$$\Delta = \left| f_g - f'_{avg} \right| \tag{4.38}$$

In the formula, a smaller Δ indicates better convergence. f_g is the fitness of the optimal particle, and the fitness of the particle whose fitness is better than f_{avg} is averaged to get f'_{avg}; the calculation formula is: $f_{avg} = \frac{1}{n}\sum_{i=1}^{n} f_i$, where f_i is the fitness of the ith particle, and n is the size of the particle swarm.

If the calculated value Δ is less than the threshold Δ_d while the optimal theoretical optimal solution or the expected optimal solution f_d is not reached at the same time, the particles tend to premature. Taking into account the minimization problem:

$$\Delta < \Delta_d \tag{4.39}$$

$$f_g > f_d \tag{4.40}$$

In this case, we need to perform Gaussian mutation on some inactive particles and redistribute their positions in the solution space so that the particles can jump out of the local optimum to obtain the global optimal solution. Definition:

$$\frac{f_g - f_i}{f_g - f'_{avg}} \leq \theta \tag{4.41}$$

where θ is the threshold, and for the ith particle satisfying inequality (4.41), the variation is carried out by the following formula:

$$x_{id}^{(k+1)} = x_{id}^{(k)} + \eta\xi \tag{4.42}$$

where η is the coefficient of variation, and ξ is a random variable obeying $N(0,1)$.

Specific IPSO algorithm III steps are as follows:

(1) Randomly initialize the positions and velocities of particles in a population.
(2) Evaluate the fitness of each particle, store the position and fitness of the current particles in the ***pbest*** of each particle, select all the individuals with the optimal fitness of ***pbest***, and then store those individuals' fitness and location in ***gbest***.
(3) Use formula (4.30) and (4.31) to update the velocity and position of the particles.
(4) Use formula (4.32) and (4.33) to update the weights.
(5) Calculate the fitness of the particles f_i. Update individual extreme value ***pbest*** and global extreme value ***gbest***.
(6) Use formulas (4.39) and (4.40) to determine if the algorithm is prematurely converged. If premature convergence occurs, mutate according to formula (4.41) and (4.42); if this does not occur, repeat steps 2–6 until the iteration termination condition is satisfied.
(7) Output global optimal solution.

(4) IPSO-M neural network

The weights and thresholds (self feedback gain factor) of neural networks constitute the necessary parameters of the neural network algorithm and only with the appropriate parameters in order to obtain better prediction performance. Therefore, the IPSO algorithm is used to train the neural network, and then the weights and thresholds (self-feedback gain factor) of the network are modified to obtain the best parameters of the neural network. Then, the optimal parameters are mapped to the weights and thresholds of the neural network (the self-feedback gain factor), the training model is trained, and the prediction results are output, namely IPSO-M algorithm; among them, M algorithm includes BP network and Elman network. Specific design steps are as follows:

(1) According to the given input and output training sample set, the number of nodes in the input layer, middle layer, and output layer of the neural network is designed to determine the topological structure of neural network.
(2) Determine the IPSO algorithm-related parameters, including population scale, number of iterations, inertia factors, and learning factors. Determine speed and population constraints.
(3) Determine the evaluation function of the particle. The mean square error function G is used as a fitness evaluation function of the particle to promote the search of the population. When the algorithm iteration stops, the position corresponding to the particle with the least fitness is the optimal solution of the model. The fitness function of the particle is:

$$fitness = G = \frac{1}{N}\sum_{i=1}^{N}\left(y_{i(M)} - y_{i(CFD)}\right)^2 \tag{4.43}$$

where $y_{i(M)}$ is the network prediction output; $y_{i(CFD)}$ is the network expected output.
(4) Randomly initialize the positions and velocities of particles in a population.
(5) Calculate the fitness of particles in the population under neural network training samples according to formula (4.43).
(6) According to the fitness value of particles, the individual extreme value and the extreme value of population are determined, and the best position of each particle is taken as the best position in history.
(7) Update the velocity, location, and learning factors of particle according to the update formula of the particle swarm.
(8) Update the solution by the speed, position, and learning factor iterated in step (7) so as to adjust the weights and thresholds (self-feedback gain factor) of neural network.
(9) Determine whether the training error of the algorithm achieves the expected error or the maximum number of iterations. If the conditions are satisfied, the global optimal particles are mapped to the weights and thresholds of the neural network, and then the model is trained, and the predicted results are output; if the condition is not satisfied, return to step (6) to continue the iterate.

4.3 Hybrid Optimization Algorithm

4.3.1 Hybrid Algorithm I

The traditional gradient-based optimization algorithm has obvious shortcomings and deficiencies when applied to ship linear optimization design: Ship-based optimization involves many disciplines such as rapidity, seakeeping, and maneuverability. There is no expression between each performance indicator (objective function) and design variables (no analytical expression can be derived). Gradient information can only be obtained by numerical analysis, so the computational cost is great. For the strong nonlinear problems such as hull type optimization, gradient-based optimization will converge more slowly when away from the optimal point. Moreover, it can only guarantee the convergence to the local optimal solution, and the optimization result is very sensitive to the initial point selection. The modern optimization algorithms, such as genetic algorithm, have strong global search capability and can quickly approach the global optimal point, but their local search capabilities are poor. To find the global optimal point finally, a large number of computational objective functions are needed to calculate. The convergence of the two methods is compared as shown in Fig. 4.5. Therefore, the idea of two optimization methods should be integrated and the advantages of each method can be used to form an efficient optimization algorithm.

The hybrid genetic algorithm is a combination of floating-point coding genetic algorithm and constrained scaling method to improve the speed and probability of global solution. In this hybrid algorithm, genetic operators such as selection, crossover, and mutation are solved by a penalty function of nonlinear programming problem. The purpose is to lead the solution to the vicinity of the global solution and provide the initial value for the constrained variable operator; the constrained variable operator solves problem by using the original nonlinear programming

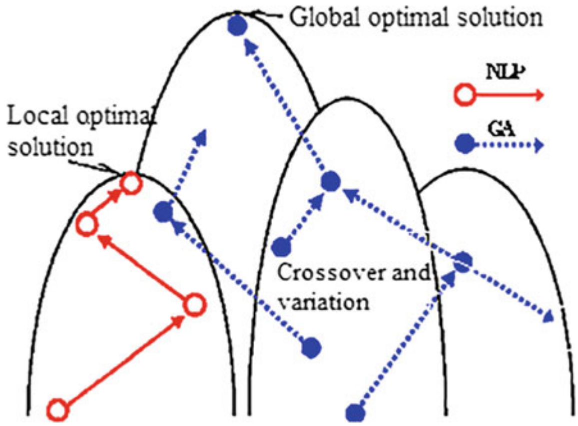

Fig. 4.5 Comparison of convergence between NLP method and GA method

problem directly, in order to exert its advantage of strong local search ability. The calculation principle is as follows [21]:

Suppose the mathematical model of a project nonlinear programming problem is:

$$\min f(x)$$
$$s.t. c_j(x) = 0 j = 1, 2, \ldots, nc' \tag{4.44}$$
$$c_j(x) \geq 0 j = nc' + 1, nc' + 2, \ldots, nc$$

where the objective function f and the constraint condition c are both second-order continuously derivable.

In the hybrid genetic algorithm, the selection, crossover, mutation, and other genetic operators are presented in the form of penalty function in formula (4.44)

$$\min f_p(x) = f(x) + M_1 \sum_{j=1}^{nc'} \max\{0, |c_j(x)|\} + M_2 \sum_{j=nc'+1}^{nc} \max\{0, -c_j(x)\} \tag{4.45}$$

where f_p is the exact penalty function of function f in formula (4.45); M_1 and M_2 are quite large fixed normal numbers. The purpose of this algorithm is to ensure that the algorithm can obtain a larger search range, lead the solution to the vicinity of the optimal solution, and provide an initial value for the subsequent implementation of the constrained scaling method operator. That is to say, genetic operators such as selection, crossover, and mutation can realize large-scale search, and small-scale fast local search can be realized by constrained variable-scale method to take advantage of both genetic algorithm and constrained scaling method.

When constrained variable metric method is used to solve the above nonlinear programming problem, we firstly transform formula (4.45) into (4.46) in order to solve a series of quadratic programming sub-problems:

$$\min QP(d) = f^T(x^k)d + \frac{1}{2} d^T B^k d$$
$$s.t. c_j(x^k) + c_j(x^k)d = 0 j = 1, 2, \ldots, nc' \tag{4.46}$$
$$c_j(x^k) + c_j(x^k)d \leq 0 j = nc' + 1, nc' + 2, \ldots, nc$$

The search direction d_k of each iteration is deconstructed by formula (4.46), and then perform inaccurate one-dimensional search along the direction d_k to obtain the step length T_k, so as to obtain the sequence $x^{k+1} = x^k + T_k d_k$, finally approaching the optimal solution.

In this project, the constrained variable metric method is added to the floating-point genetic algorithm as an operator that is parallel to selection, crossover, and mutation. The available hybrid genetic algorithm can be solved as follows:

(1) The genetic algorithm parameters are assigned. These parameters include the population size m, the number of variables n, the crossover probability P_c, the mutation probability P_m, the probability P_{CVM} for the constrained variable-scale method search, and the maximum evolutionary algebra T allowed by genetic computation.
(2) Initialize the populations: The initial population is generated randomly, the precise penalty value of formula (4.46) is calculated, and further the fitness value is obtained. The fitness value of the ith individual is taken as $f_i^{/} = f_{\max} - f_i$, the objective function value of the ith individual is $f_{i,}$ $f_{\max}$ is the maximum objective function value of current population members and then stretched according to the Goldberg linear scaling transformation model:

$$f_i' = af_i' + b, \ \ f_i' \geq 0, \ \ \mathrm{i} = 1, 2, \ldots\ldots, \ \ \mathrm{m}, \tag{4.47}$$

(3) Perform a selection operation on the proportional selection operator.
(4) Crossover operations are performed by P_c arithmetic crossover operator. For the two selected matrices s_i^t and s_j^t, the two generations generated by the arithmetic crossover are $s_i^{t+i} = rs_j^t + (1-r)s_j^t$ and $s_j^t = rs_i^t + (1-r)s_i^t$, and r is the random number on [0,1].
(5) Perform a nonuniform mutation operator according to P_m. If the element vk of individual $s_i^t = (v1, v2, \ldots, vk, \ldots, vn)$ is selected to mutate, then the variation results are $s_i^{t+1} = (v1, v2, \ldots, v^{k\prime}, \ldots, vn)$

$$vk' \begin{cases} vk + \Delta(t, x_k^u - vk) & rand(0,1) = 0 \\ vk - \Delta(t, xk - vk') & rand(0,1) = 1 \end{cases} \tag{4.48}$$

$$\Delta(t, y) = yr\left\{1 - \frac{t}{T}\right\}^b$$

where T is the maximum algebra; b is the coefficient parameter that determines the nonuniformity; $\Delta(x, y)$ is a value in the interval [0, 1], so that the probability that $\Delta(x, y)$ approaches 0 increases with the increase of the algebra T. This property allows operators to search evenly for space in the initial stage.
(6) For each individual, P_{CVM} is used to optimize the search according to the constrained variable-scale method. If the individual s_i^t is selected to do the constrained variable-scale optimization search, the constrained variable-scale optimization was solved with s_i^t as the initial point of the formula (4.44), and the optimized results are obtained as the subgeneration s_i^{t+1}.
(7) Calculate the individual fitness value, and perform the optimal individual preservation strategy.

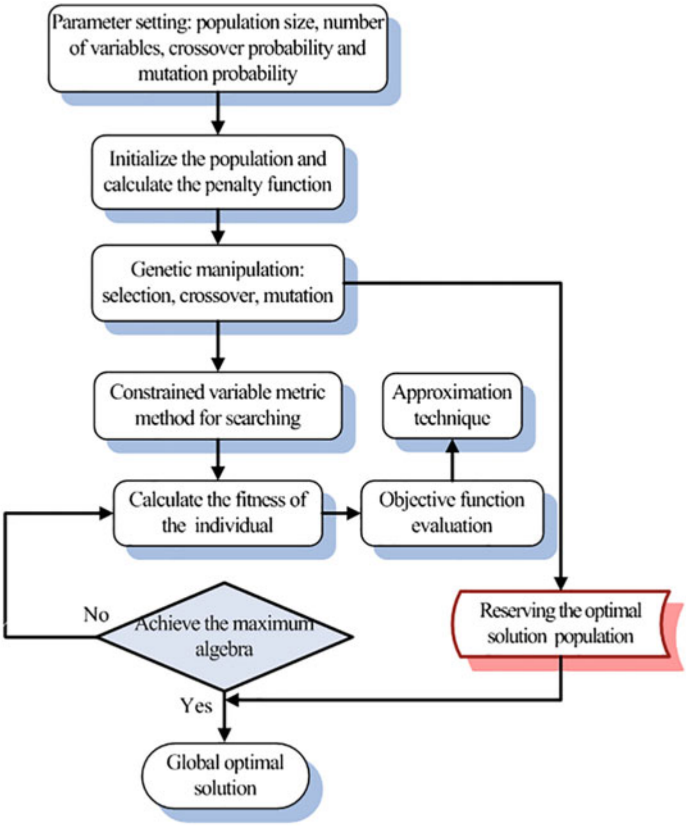

Fig. 4.6 Flowchart of hybrid genetic algorithm

(8) If the genetic calculation reaches the maximum allowed algebra T or the if there is no improvement in the optimal individuals of successive generations, the result is output and the calculation is ended. Otherwise, the procedure goes to step (3) and the above operation is repeated. Program flowchart is shown in Fig. 4.6.

4.3.2 Hybrid Optimization Method II

Optimization system design space is large; the actual optimization process cannot calculate the results of all locations in space. Therefore, a combination of the most representative and optimally accurate results from the optimization system is chosen as the sample points of the optimization space through the experimental design method. The aim is to obtain the best test results with the minimal number of experiments. There are many experimental design methods, for example: full factorial design (FFD), fractional factorial, central composite design (CCD), Latin hypercube design (LHD). Among them, Morris and Mitchell proposed an effective experimental design method [22] in 1995: optimal Latin hypercube design (Opt LHD). It is based on Latin hypercube design and enhances the uniformity of the algorithm in optimizing the design space. The sample selection is more uniform; the fitting of the factor and the response are more accurate and true. Space filling and balance are better. The matrix generation steps of the method are as follows:

Set m test points, and n factors constitute $n * m$ matrix:

$$x = [x_1, x_2, x_3, \ldots\ldots, x_m] \tag{4.49}$$

The ith analysis:

$$x_i^T = [x_{i1}, x_{i2}, x_{i3}, \ldots\ldots, x_{in}] \tag{4.50}$$

According to formula (4.50), a random Latin hypercube algorithm is used to generate an initial design matrix, and then the design matrix is updated by element exchange, and the space filling optimization condition is calculated based on the criterion of selecting minimum and maximum distances.

$$d(x_i, x_j) = d_{ij} = [\sum_{k=1}^{n} |x_{ik} - x_{jk}|^t]^{\frac{1}{t}} \tag{4.51}$$

In the formula: $t = 1$ or 2; $1 \leq i; j \leq m$; $i \neq j$. The sampling point $d(x_i, x_j)$ is the minimum distance between x_i and x_j. Figure 4.7 shows the sample point distribution of the Latin hypercube matrices and optimal Latin hypercube design with three factors and nine experiments. It can be seen from the figure that the distribution of sample points in the optimal Latin hypercube design is more uniform and reasonable, the filling effect is better, and the spatial distribution of sample points can be expressed more accurately.

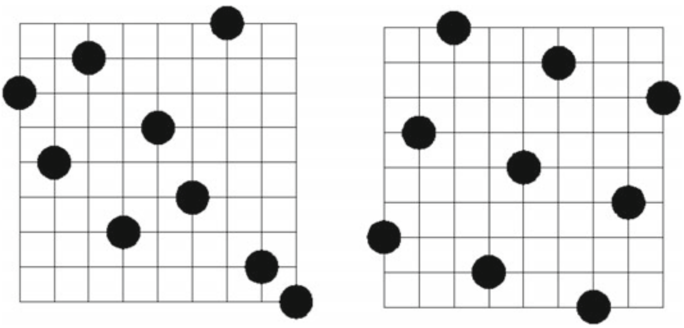

(a) Latin hypercube (b) Optimal Latin hypercube

Fig. 4.7 Comparison of Latin hypercube and optimal Latin hypercube design matrix

Non-Linear Programming by Quadratic Lagrangian (NLPQL) is one of the gradient optimization methods. This method is an improved version of the SQP algorithm, which is more stable than the sequential quadratic programming (SQP) algorithm. It expands the objective function in Taylor series and linearizes the constraints by solving the quadratic programming to get the next design point. Then perform a linear search based on two alternative optimization functions. First, start from an initial guess point x^0, and apply one additional linear search in the calculation to ensure that it can achieve global convergence. $x^{k+1} = x^k + a^k d^k$ will only be executed for new iterations if the x^{k+1} feasible search scheme determines the movement step in that direction.

In the SQP algorithm, the updating of matrix B_k can be performed according to standard techniques in unconstrained optimization. In order to improve the performance of the algorithm, the NLPQL algorithm introduces a variable metric method (BFGS). B_{k+1} is constructed by the scaling matrix B_k to approximate the Hessian matrix to complete the update of B_k. With some security guarantees, all matrix Bk can be guaranteed to be positive definite.

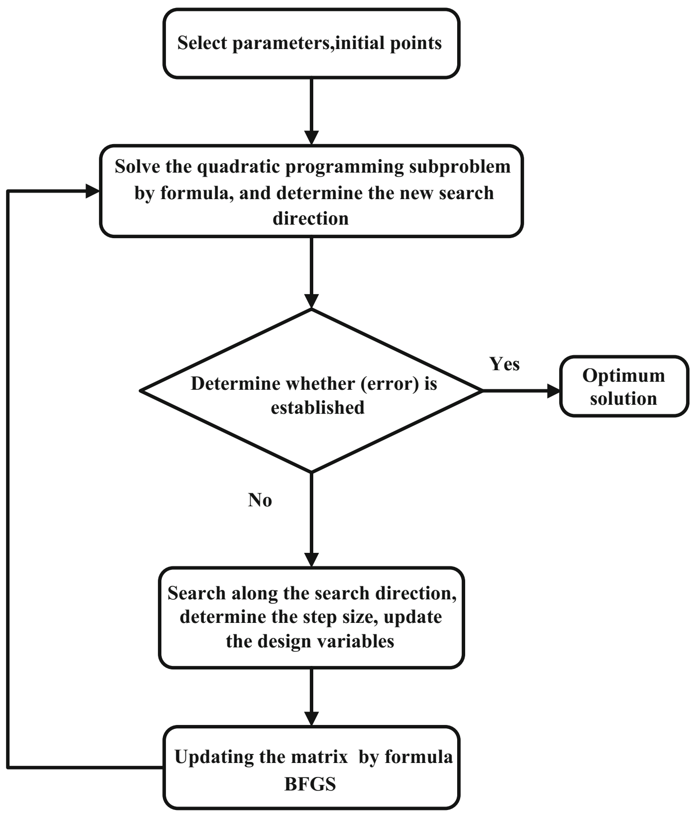

Fig. 4.8 Calculation flowchart of NLPQL

Objective function:

$$q_k(d) = \frac{1}{2} d^T B_k d + \nabla f(x^k)^T d, d \in R^n \tag{4.52}$$

Constraint equation:

$$\nabla g_i(x^k)^T d + g_i(x^k) \ i = 1, 2, 3 \ldots p \tag{4.53}$$

$$\nabla h_j(x^k)^T d + h_j(x^k) = 0 \ i = 1, 2, 3 \ldots m \tag{4.54}$$

The specific iterative steps are shown in Fig. 4.8:

4.4 Optimization Platform

The optimization methods described above require manual programming algorithm or interface program, which requires a lot of labor, but also need to verify the precision and accuracy of the program, far from the actual project. In recent years, there have been some optimization platforms that can integrate some existing commercial software and the platform comes with optimization algorithm. It is very convenient to automatically optimize ship types even if you do not write programs. This chapter mainly introduces the commonly used ISIGHT and Friendship framework in ship design.

4.4.1 ISIGHT Optimization Platform

4.4.1.1 Brief Introduction of ISIGHT

ISIGHT is a software system platform developed by American Engineous software, which can automatically optimize design. It is widely used in aviation, automobile, shipbuilding, machinery, chemical, and other fields. Because ISIGHT is based on multi-disciplinary optimization design and quality engineering-based design methods, it greatly enhances the domestic manufacturing digitalization, information technology, and modern design [23]. ISIGHT focuses on providing multi-disciplinary design optimization and optimization techniques at different levels and optimizing process management. It solves multiple iterations in multi-disciplinary optimization process and automatic operation of data input and output repeatedly. Various optimization methods (numerical iterative algorithm, search algorithm, heuristic algorithm, experimental design (DOE), response surface model (RSM), etc.) effectively organize multi-disciplinary optimization design.

The multi-disciplinary design optimization features provided by ISIGHT are:

(1) Process integration: a complete design of integrated environment

  (1) Multi-disciplinary code integration + Process automation;
  (2) Hierarchical, nested task organization and management;
  (3) Real-time control + Post-processing;
  (4) Scripting language + API customization + MDOL language secondary development.

(2) Optimized design: Advanced exploration Toolkit

  (1) Experimental design + Mathematical programming + Approximate modeling + Quality design;
  (2) Knowledge rule system + Multi-criteria tradeoffs;
  (3) Open architecture: Third-party (optimization/test) algorithm embedding, multi-disciplinary optimization strategy research and implementation.

(3) Network function

  (1) Parallel computing + distributed computing services;
  (2) Remote deployment and invocation;
  (3) CORBA invocation.

4.4.1.2 Task Structure of Multi-disciplinary Design Optimization Platform

The basic elements of MDOF are tasks, each consisting of three modules:

(1) Analysis module: including the implementation of documents, input files, and output files;
(2) Data module: including design parameters, constraint parameters, the objective function parameters, and communication parameters;
(3) Technical parameter modules: including optimization techniques, approximate technical parameters.

The interface of the task execution module is implemented by parameter mapping. Typically, each task execution module consists of input files, executable files (discipline analysis code), and output files. As long as the I/O file is manipulated, the task execution module can be manipulated. Therefore, the designer does not need to care about the encoding and operation of the analysis code and only needs to provide the information in the input and output files to support the repeatability of the discipline analysis code.

4.4.1.3 Application of ISIGHT in Ship-Type Optimization

ISIGHT provides designers with interface software to integrate various softwares such as CAD/CFD into a loop, including the process of changing the design, running the simulation, and analyzing the design results. This cycle continues until you get the optimal design or reach the design bottom line. In this way, the design process is fully automated.

4.4.1.4 Integration Method of ISIGHT and CA/CFD Software

(1) CAD software

Catia:	Method 1:	Simcode command cnext.exe-macro *.vbs
	Method 2:	ISIGHT Catia components
ProE:	Method 1:	Simcode command proe2000i trailfile.txt
	Method 2:	ISIGHT ProE components
UG:	Method 1:	Simcode command ug_update_expressions.exe -p *.prt –e *.exp
	Method 2:	ISIGHT UG components
Solidworks:	Method 1:	Simcode command Cscript *.vbs
	Method 2:	ISIGHT Solidworks components

(2) Mesh pre-processing software

ICEM-CFD: icemcfd -batch -script icem_script
Gambit: "\Fluent.Inc\Gambit2.3.16\ntbin\ntx86\gambit.exe" -inp *.jou

(3) Mesh deformation software

Sculptor: \Sculptor\sculptor.exe -d

(4) CFD numerical simulation software

Fluent:		fluent 3d-wait-i
StarCCM + :	Method 1:	Simcode command starccm + -batch*.java
	Method 2:	ISIGHT StarCCM + components
CFX:		cfx5solve.exe-def cfx5build.exe-b -play

4.4.1.5 The Optimization Integration Process of Ship Form Based on ISIGHT

In the ISIGHT optimization platform, various softwares in the process of ship-type optimization are integrated, such as CAD software for geometry reconstruction and expression of the hull, and objective function calculation software such as ProE and Sculptor. This book mainly integrates resistance calculation software (such as FLUENT, STAR-CCM+) to this platform together, uses the optimization algorithm provided by the platform, or integrates the existing optimization algorithm into the platform to form a ship-type automatic optimization system. The automatic optimization of the ship type can be realized without any manual intervention in the

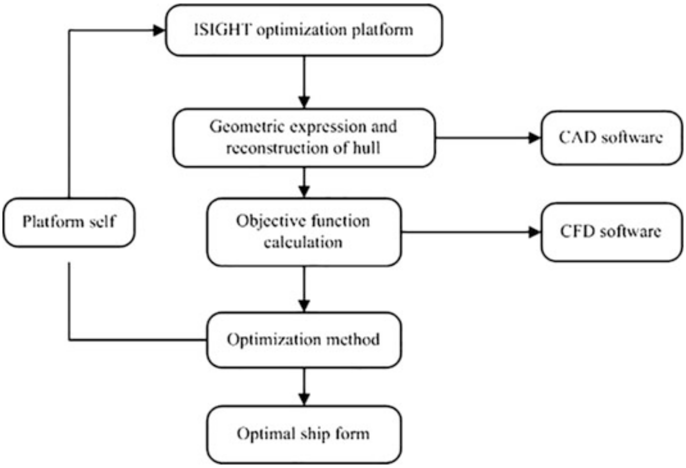

Fig. 4.9 Ship-type optimization based on ISIGHT platform

whole process, and finally the shape of the hull with the best performance is obtained as shown in Fig. 4.9.

4.4.2 Friendship

Friendship framework is full-featured ship parameterization software developed by Lloyds Friendship Systems, which combines parametric modeling, optimization algorithms, and optimized integration framework. It can effectively generate and modify ship models and can be used to optimize the hydrodynamic performance of ships [24]. A large number of application examples at home and abroad have proved the practicability of ship-based optimization based on Friendship software.

Friendship framework is a CAE design platform that combines CAD and CFD with the following functional features:

(1) Full parametric and semi-parametric modeling based on functional surface technique. By setting parameters and constructing corresponding characteristic curves, the establishment of complex parametric model can be realized.
(2) After setting the range of the selected parameters, the software can automatically transform the model, and a collection of a variety of single-target and multi-objective optimization algorithm to optimize for the set objective function.
(3) The ability to integrate external software is strong. It can integrate various external software and CFD simulation program through the standard interface and can perform pre- and post-processing such as grid division and result display.

(4) It has remote or distributed computing capabilities, which can effectively utilize idle or remote settings, thus enabling long-term, heavy task tasks (such as new program generation and optimization) being carried out in a very short period of time.

(1) The principle of Friendship parametric modeling

The parametric model of Friendship based on the characteristic parameters and characteristic curves enables the rapid generation and modification of the ship type. The selection and modeling of the characteristic parameters and the characteristic curves are the most important links in the parametric design of the whole ship and directly affect the design quality of the parametric model.

The Friendship parametric modeling process is as follows:

(1) The selection and determination of characteristic parameters, namely the global parameters (captain, width, draught, etc.) and the local parameters (curve tangent, fullness, etc.), control the longitudinal curve and cross-sectional curve.
(2) Construct the longitudinal curve based on the above characteristic parameters to achieve the correlation between them.
(3) The construction of cross-sectional curve, based on the global characteristic parameters and longitudinal curves, first create a reference cross-sectional curve by using feature in program code, and then use Curve Engine to drive the creation of cross-sectional curves of each station.
(4) Based on the Curve Engine, the hull surface is constructed. First, the first and last positions of the surface are determined. Through the Meta Surface, the cross-sectional curves are fused together to obtain a smooth hull surface.

(2) Interface program

As parametric modeling software, Friendship is usually combined with SHIPFLOW software to create a ship optimization platform that can realize automatic optimization. In order to realize the value data transfer between the Friendship software, the SHIPFLOW, and wave resistance calculation software, to achieve the automatic optimization of the ship type, the IGES model file needs to be firstly transformed into the SHF format model file. The interface program can reconstruct the value data in the SHF file into a hull curve and obtain a new model file by interpolating the hull curve. One of the cubic B-spline curves is used to fit and interpolate the hull curve.

The workflow of the interface program is briefly described as follows: Firstly, the model file in SHF format is read in. Secondly, according to the standard data format of the SHF file, the various hull curves of the model in the document are found; then, the curves are re-fitted, interpolated, and sorted again; finally, generate the model file needed for calculating the wave drag.

(3) Friendship software integration optimization system

Friendship software has a strong external program integration capabilities; it mainly provides three different integration mechanisms: COM integration interface, custom integration through XML files, and generic integration through ASCII templates.

References

1. Lin Y, Zhu Z, Ji Z, Dai Y (1997) Form description with function parameter [J]. Shipbuild China, 3:74–78
2. Jiang JS, He CX, Pan SH (2008). Optimization method [M]. South China University of Technology Press, Guangzhou
3. Xi Shao Lin, Zhao Feng Zhi (1983) Optimization method [M]. Shanghai Science and Technology Press, Shanghai
4. Xing Wen Xun, Xie Jin Xing (1999) Modern optimization method [M]. Tsinghua University Press, Beijing
5. Bei-yue Z, Guang-qi G (2001) Research of improving genetic algorithms based on niche technology [J]. J Yueyang Norm Univ (Natural Sciences), 14(4):18–21
6. Zhou GQ (1999) Practical discrete optimization approach for ship structures based on genetic algorithms [J]. Ship Technol Res, 46(3):179–188
7. Xuan GN, Cheng RW (2000) Genetic algorithm and engineering design [M]. Science Press, Beijing
8. Della Cioppa A, De Stefano C (2004) On the role of population size and niche radius in fitness sharing [J]. IEEE Trans Evol Comput 8(6):580–592
9. Vieira DAG, Adriano RLS (2004) Treating constraints as objectives in mul- tiobjective optimization problems using niche pareto genetic algorithm [J]. IEEE Trans Magn 3 (40):1188–1191
10. Kim JK (2002) Niche genetic algorithm adopting restricted competition selection combined with pattern search method [J]. IEEE Trans Magn 38(2):1001–1004
11. Zhou Y-J, Wang L-Z (2006) An application of elitist model niche genetic algorithms in optimization of functions [J]. J Liuzhou Teachers College, 21(1):107–110
12. Xin X-J1, 2, Pan J3, Xiao G-Z (2005) New proxy signature scheme based on Schnorr signature scheme [J]. J Chongqing Univ Posts Telecommunications (Natural Science), 17(6): 721–724
13. Pereira CM, Sacco WF (2008) A parallel genetic algorithm with niching technique applied to a nuclear reactor core design optimization problem [J]. Prog Nuclear Energy, 1–7
14. Ke F, Li Y (2014) The forecasting method of landslides based on improved BP neural network [J]. Geotechnical Investigation Surveying, (8):55–60
15. Liu Y, Li R, Li C (2014) Application of BP neural network and support vector machine to the accumulated temperature interpolation [J]. J Arid Land Resources Environ 28(5):158–165
16. Gao Peng Yi (2012) Study on the optimization of backpropagation neural network classifier [D]. Huazhong University of Science and Technology, Wuhan
17. Wang HF, Zhao M, Meng G (2002) 3-D shape prediction and global approximate optimization of plastic ball grid array (PBGA) solder joints [J]. J Shanghai Jiaotong University, 36(6):829–833
18. Liu JH (2009) The research of basic theory and improvement on particle swarm optimization [D]. Central South University, Changsha
19. Li YL (2014) The study of particle swarm algorithm based on multi-objective optimization and its application [D]. Chengdu: Southwest Jiaotong University

20. Guang-yu G, Chen G, Li Y-X (2014) Fractional-order control of USV course based on improved PSO algorithm [J]. Syst Eng Electron 36(6):1146–1151
21. Lujia Z, Fang Z, Shan ZP (2001) The parameters of generator are identified by genetic algorithm and constrained variable scale optimization [J]. Hunan Electric Power, 21(3):5–7
22. Yin X (2015) Fundamental research on thermal reliability engineering design for cylinder head [D]. Zhejiang University, Zhejiang
23. Lai YY (2012) ISIGHT parameter optimization theory and examples [M]. Beijing University of Aeronautics and Astronautics Press, Beijing
24. Huang J-F, Wan S-L (2012) The parametric method of FRIENDSHIP hull form based on design feature [J]. Chin J Ship Res, 7(2):79–85

Chapter 5
The Optimization of the Hull Form with the Minimum Wave-Making Resistance Based on Potential Flow Theory

5.1 Overview

Based on the Michell integral method and the Rankine source method, the parameters of the double-triangle ship modification function are used as the design variables. Under the condition of ensuring the drainage volume as the basic constraint, the optimal design model of nonlinear programming method (NLP), traditional genetic algorithm (SGA), and niche genetic algorithm (NGA) are established by considering the influence of tail-viscosity separation. The whole ship linear optimization design program with independent intellectual property rights is developed, and the effectiveness of the program is verified through experiments. The research results have important guiding significance to promote the ship design from the traditional experience mode to the knowledge-based mode.

5.2 The Optimization of the Hull Form with Minimum Wave-Making Resistance Based on Michell Integral Method

5.2.1 *Establishment of the Ship-Type Optimization Model*

(1) Objective function

In the present study, the total resistance R_T is selected as objective function in the optimization design process, R_T is expressed as the sum of wave resistance R_W and frictional resistance of a flat plate R_F, namely

$$R_T = p \cdot R_W + (1 + k) \cdot R_F \rightarrow \min \tag{5.1}$$

© Shanghai Jiao Tong University Press, Shanghai and Springer Nature Singapore Pte Ltd. 2019
B.-J. Zhang and S.-L. Zhang, *Research on Ship Design and Optimization Based on Simulation-Based Design (SBD) Technique*,
https://doi.org/10.1007/978-981-10-8423-2_5

where the R_W is calculated by the Rankine source method, and then multiplied by the correction coefficient p, which is selected by the ratio between theoretical and experimental values of wave resistance corresponding to initial ship design speed point; k is the form factor, selected by model test.

The Michell integral formula is expressed by the following form.

$$R_W = \frac{4\rho g^2}{\pi U_\infty^2} \int_1^\infty \frac{\lambda^2}{\left(\lambda^2 - 1\right)^{\frac{1}{2}}} [P^2(\lambda) + Q^2(\lambda)] d\lambda \tag{5.2}$$

$$P(\lambda) = \int_{-T}^{0} \int_{-L/2}^{L/2} F_X(X, Z) \cos(\frac{g}{U_\infty^2} \lambda X) \cdot \exp(\frac{g}{U_\infty^2} \lambda^2 Z) dX dZ$$

$$Q(\lambda) = \int_{-T}^{0} \int_{-L/2}^{L/2} F_X(X, Z) \sin(\frac{g}{U_\infty^2} \lambda X) \cdot \exp(\frac{g}{U_\infty^2} \lambda^2 Z) dX dZ$$

where U_∞ is the design speed and ρ is the mass density of the fluid. g is the acceleration of gravity, $F_X(X, Z)$ is the longitudinal slope of the hull waterline.

$$F(X, Z) = \frac{B}{2} \cdot f(\xi, \zeta) \tag{5.3}$$

The frictional resistance of a flat plate is calculated by the following formula.

$$R_F = \frac{1}{2} \rho U_\infty^2 S \cdot C_{f0} \tag{5.4}$$

where C_{f0} is the frictional resistance coefficient of a flat plate and it is calculated by Songhai formula. S is the wetted surface area, which is the function of the hull coordinates. It is approximately calculated by tent function.

$$C_{f0} = \frac{0.4631}{(\lg \mathrm{Re})^{2.6}} \tag{5.5}$$

where R_e is the Reynolds number based on the body length.

$$\mathrm{Re} = \frac{UL}{v} \tag{5.6}$$

where U is the speed, L is the characteristic length and here is taken as the design waterline, v is the viscosity coefficient of fluid motion.

(2) Design variables

The offsets of ships are directly selected as design variables.

(3) Constraint Conditions

The constraints are mainly considered to satisfy the geometric constraints and drainage volume requirements, there are two as follows:

(1) All Ship offsets are nonnegative, namely:

$$y(i,j) \geq 0;$$

(2) Ensure the necessary displacement volume, namely:

$$V \geq V_0$$

where V_0 and V are the displacement volumes of the original hull and the improved hull, respectively.

(4) Optimization method

The SUMT interior point method in nonlinear programming is used for optimization calculation. In the objective function, the additional item reflecting the constraint condition is added to make the unconstrained optimization problem in form.

5.2.2 The Data File of the Ship-Type Optimization Based on Michell Integral

The following is the ship-type optimization document based on Michell integral method: The document includes the range of design optimization, the number of design variables, the initial parameters of optimization calculation, the main elements of the initial model, design speed and the hull values, as shown below.

21 0 6 0.414 1.200

0.001 0.010 0.010 0.001 0.001

2.000 0.267 0.107 21 6 0.285

30 0.0 2.000

0.000 0.050 0.100 0.150 0.200 0.250 0.300 0.350 0.400 0.450 0.500 0.550
0.600 0.650 0.700 0.750 0.800 0.850 0.900 0.950 1.000

0.000 0.075 0.250 0.500 0.750 1.000

0.000 0.000 0.005 0.048 0.114 0.232 0.380 0.5180.632 0.712 0.750 0.730
0.670 0.578 0.467 0.346 0.234 0.138

0.062 0.012 0.000

0.000 0.055 0.110 0.170 0.272 0.404 0.546 0.675 0.778 0.835 0.866 0.850
0.798 0.715 0.607 0.485 0.358 0.231

0.132 0.050 0.000

0.000 0.081 0.175 0.290 0.429 0.580 0.722 0.841 0.921 0.964 0.985 0.975
0.944 0.879 0.769 0.629 0.476 0.325

0.190 0.075 0.000

0.000 0.087 0.204 0.346 0.502 0.660 0.802 0.906 0.971 0.996 1.000 1.000
0.994 0.962 0.884 0.754 0.592 0.413

0.236 0.085 0.000

0.000 0.090 0.213 0.368 0.535 0.691 0.824 0.917 0.977 1.000 1.000 1.000
1.000 0.987 0.943 0.857 0.728 0.541

0.321 0.116 0.000

0.000 0.102 0.228 0.391 0.562 0.718 0.841 0.926 0.979 1.000 1.000 1.000
1.000 0.994 0.975 0.937 0.857 0.725

0.536 0.308 0.000

5.2.3 Examples

(1) Wigley hull

Six sections of the front body of the ship are selected as optimize design range, taken from station 14 to the head of the hull. The range from the bow section to station 14, the hull bottom and the surface on the design waterline are fixed, as

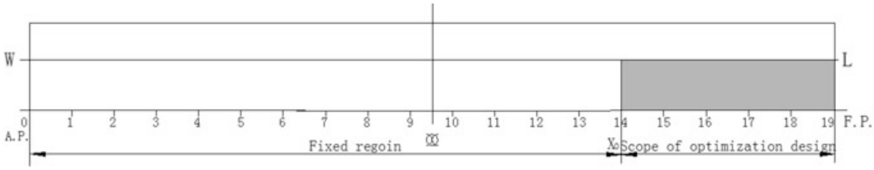

Fig. 5.1 Scope of optimization design of the Wigley hull form

shown in Fig. 5.1. Figures 5.2, 5.3, and 5.4 are comparison between the horizontal section and the waterline of the modified ship and the original ship; Fig. 5.5 is a cross-sectional view of the wave of the modified ship and the original ship; Fig. 5.6 shows the wave resistance coefficient of modified ship and initial ship model; Fig. 5.7 shows the free surface waveforms of the modified ship and the original ship.

(2) S60 hull

Taking S60 ship model as an example, the optimal design range is shown in Fig. 5.1. In order to simplify the optimization, the bow shape of a ship is set as the ship's forward perpendicular (F.P.) and stern shape of a ship is changed to after perpendicular (A.P.). The ship width is set as 0 from A. to A.P. along the ship length direction, and from 0.75W.L. to B.L. along the draft direction, as shown in Fig. 5.8. Figures 5.9, 5.10, and 5.11 are comparison of the horizontal section and waterline of the modified ship and the original ship; Fig. 5.12 is a cross-sectional view of the wave of the modified ship and the original ship; Fig. 5.13 is a graph of

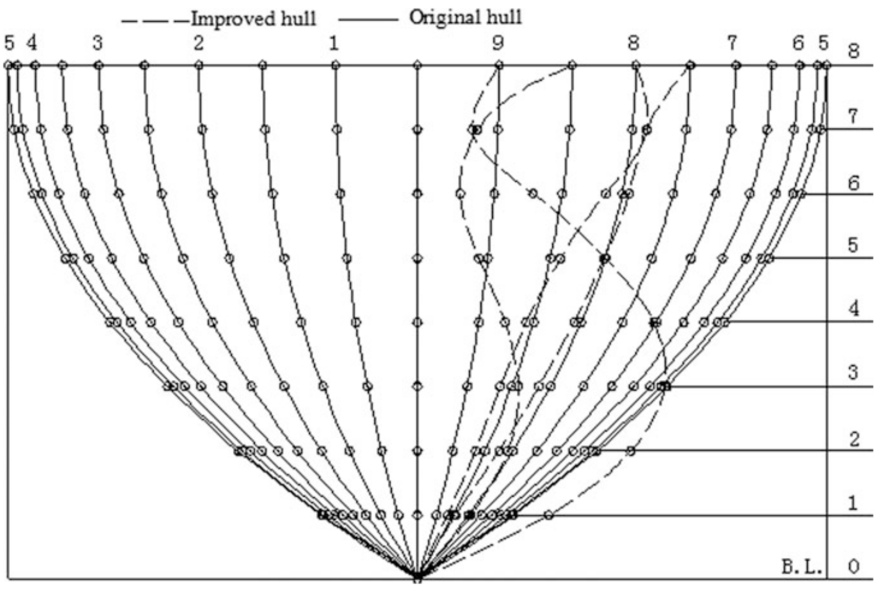

Fig. 5.2 Comparison of body plans of the modified ship and original ship (Wigley)

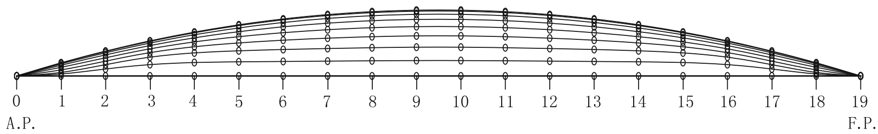

Fig. 5.3 Water plan of the original ship (Wigley)

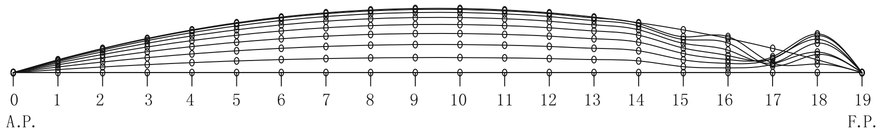

Fig. 5.4 Water plan of the modified ship (Wigley)

the wave-making resistance coefficient of a modified ship and an initial ship; Fig. 5.14 is the free surface waveform of the modified ship and an initial ship. Table 5.1 is the result of optimization calculation based on Michell integral method.

As can be seen from bodyline and waterline diagram of the optimized hull, the improved ship form is characteristic by a cross-sectional shape of two stops near the head, bulging toward the side of the ship with a bow-shaped bow, which is called “non-overhanging ball head” in the book. However, the shape of the bulbous bow is exaggerated and lacks practical significance. While such a bulbous bow is good for

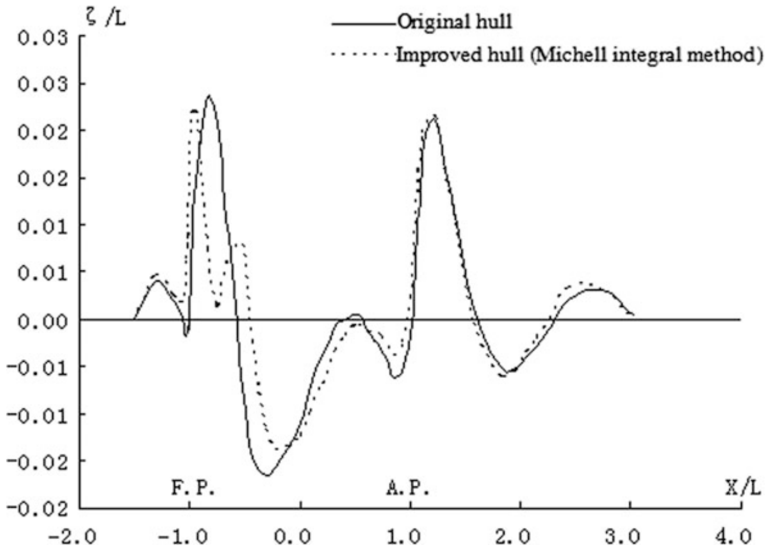

Fig. 5.5 Comparison of the wave profiles along the modified ship and original ship (Wigley)

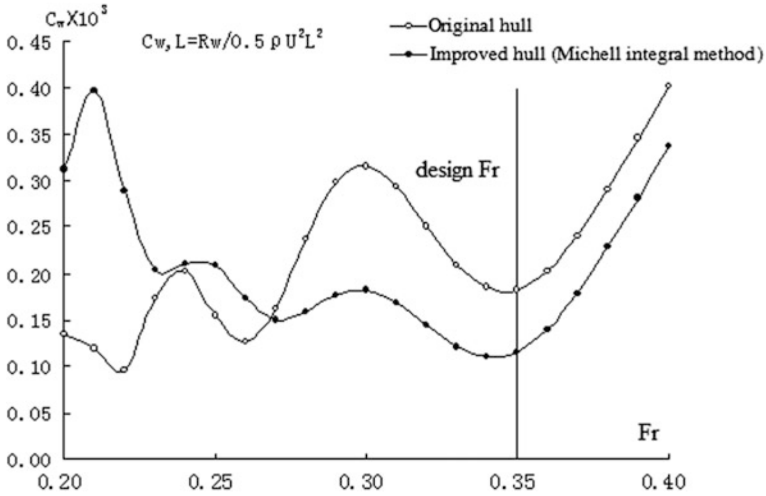

Fig. 5.6 Comparison of wave-making resistance coefficient for modified ship and original ship (Wigley)

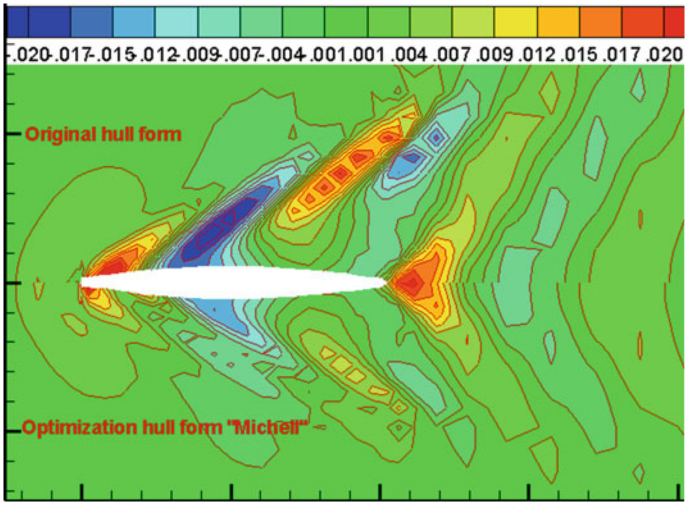

Fig. 5.7 Wave patterns ($2\,g\zeta/U^2$) of modified ship and original ship (Wigley)

drag reduction, it also brings a lot of disadvantages, such as difficult processing and inconveniences for the first equipment installation and operation. The wave resistance coefficient of the modified ship is obviously smaller than that of the original ship within a certain range of designed Fourier number. However, the wave height and waveform of the modified ship have not been significantly improved.

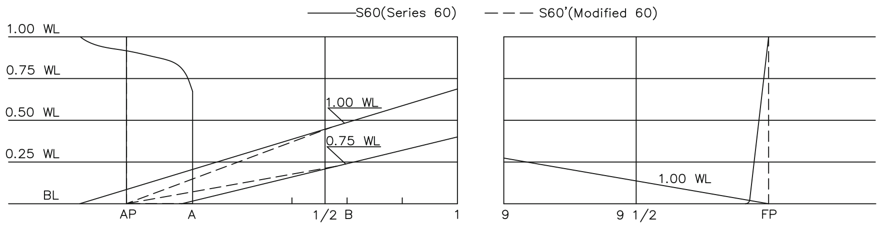

Fig. 5.8 Comparison of hull lines before and after modification of S60 hull form

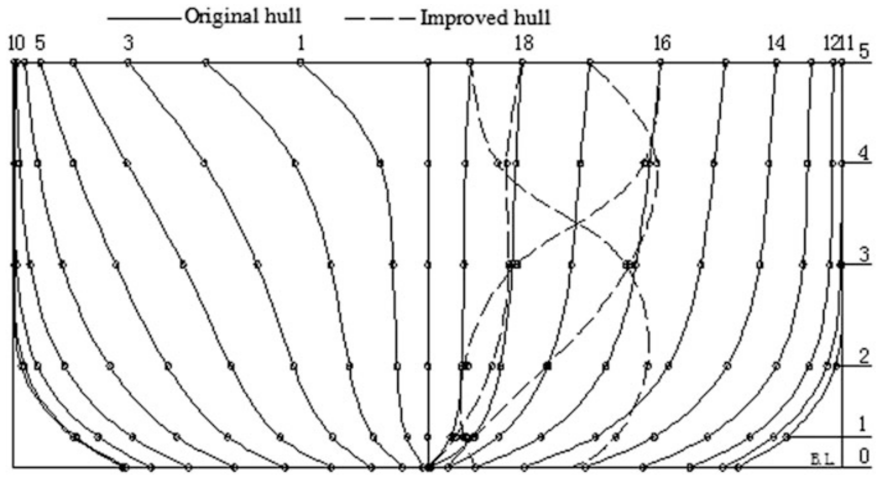

Fig. 5.9 Comparison of body plans of the modified ship and the original ship (S60)

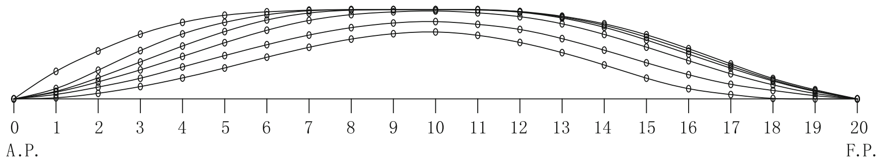

Fig. 5.10 Water plan of the original ship (S60)

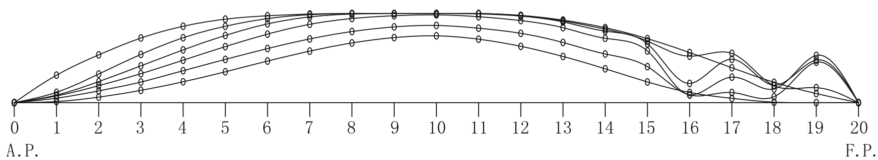

Fig. 5.11 Water plan of the modified ship (S60)

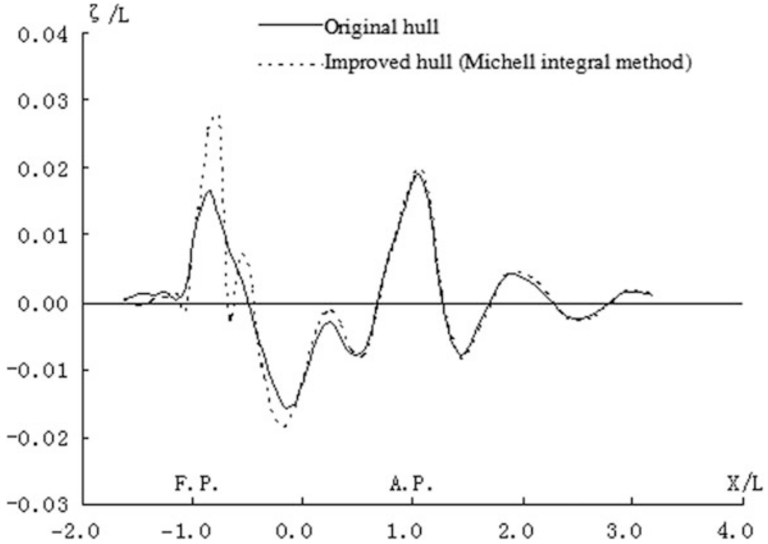

Fig. 5.12 Comparison of the wave profiles along modified ship and the original ship (S60)

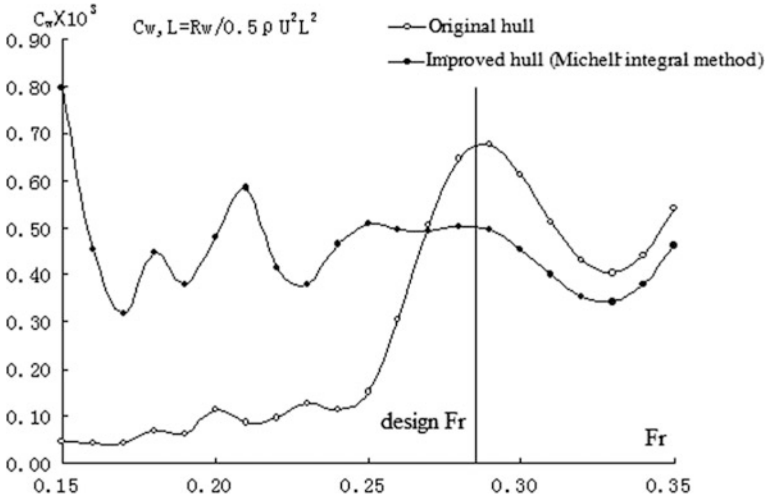

Fig. 5.13 Comparison of wave-making resistance coefficient of modified ship and the original ship (S60)

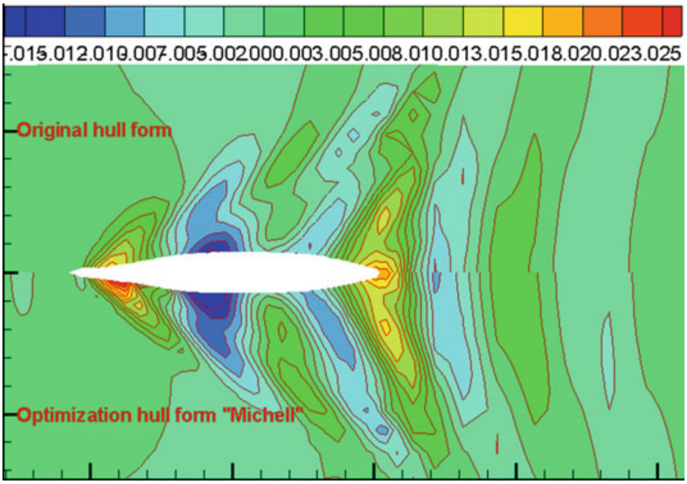

Fig. 5.14 Wave patterns ($2\,g\zeta/U^2$) of modified ship and the original ship (S60)

Table 5.1 The results of optimization calculated based on Michell integral method

Hull form	Constraints	Fr	R_W/R_{W0} (%)	R_F/R_{F0}	R_T/R_{T0} (%)	∇/∇_0	S/S_0
Wigley hull	(1), (2)	0.35	64.5	1.022	90.8	1.014	1.091
S60 hull	(1), (2)	0.285	74.6	1.033	72.6	1.000	1.033

5.3 The Optimization of the Hull Based Rankine Source Method

Based on the Michell integral method, the design of the ship with the lowest resistance is often characterized by a rather weird shape of the boat. This is because the proposed method is based on the linear wave resistance theory and linearizes both the surface conditions and the free surface conditions. Therefore, the calculation results are not as accurate as the slow ship theory, and the thin ship theory is generally used to optimize the curve of transverse section area. Although the Rankine source method does not have the fast Michell integral method in the numerical calculation of the wave resistance, its numerical calculation results are closer to the experimental results. Moreover, with the rapid increase of computing speed and storage capacity, optimization of ship types with optimization techniques can still be realized. Therefore, based on the Rankine source method with good accuracy of numerical calculation of the wave resistance, the optimum design of the ship with the lowest resistance is discussed based on the nonlinear programming method.

5.3.1 Establishment of the Hull Form Optimization Model

(1) Objective function

In the present study, the total resistance R_T is selected as objective function in the optimization design process, the R_T is expressed as the sum of wave resistance R_W and viscous resistance (1 + K)R_F, namely:

$$R_T = p \cdot R_W + (1 + k) \cdot R_F \rightarrow \min \tag{5.7}$$

where the meaning of symbols is the same as above, the form factor K is calculated by following formula [1]

$$\mathrm{k} = 0.11 + 0.128\frac{B}{T} - 0.0157(\frac{B}{T})^2 - 3.10\frac{C_B}{L/B} + 28.8(\frac{C_B}{L/B})^2 \tag{5.8}$$

The R_W is calculated by the Rankine source method and the other parameters are the same as above.

$$R_W = \frac{1}{2} \cdot \rho \cdot U_\infty^2 \cdot L^2 \cdot C_{W,L} \tag{5.9}$$

where $C_{W,L}$ is the wave resistance coefficient based on L^2; L is the ship length between perpendiculars; B is the breadth; T is the draft; C_B is the block coefficient; and U_∞ is the design speed.

(2) Design variables and the scope of optimization design

The optimum design range is taken as the front half body, and the designed waterline, the bottom of the ship, the front end of the hull are fixed, as shown in Fig. 5.15.

In the optimization process, the parameters of ship modification function are chosen as design variables, the shape of the modified ship $y(x, z)$ is expressed as a function on the basis of the initial ship type $f_0(x, z)$ multiplied by a ship modification function $w(x, z)$, namely.

$$y(x, z) = f_0(x, z) \cdot w(x, z) \tag{5.10}$$

$$w(x, z) = 1 - \sum_m \sum_n \alpha_{mn} \sin\left[\pi(\frac{x - x_0}{x_{\min} - x_0})^{m+2}\right] \cdot \sin\left[\pi(\frac{\beta - z}{\beta + T})^{n+2}\right] \tag{5.11}$$

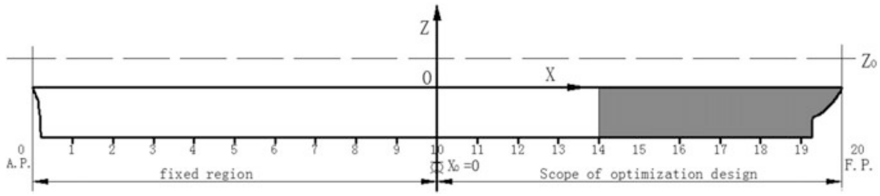

Fig. 5.15 Scope of optimization design of the S60 hull form

$$m, n = 1, 2, 3, \quad -L/2 \leq x$$

$$w(x, z) = 1 - \sum_m \sum_n \alpha_{mn} \sin\left[\pi\left(\frac{x - x_0}{x_{\max} - x_0}\right)^{m+2}\right] \cdot \sin\left[\pi\left(\frac{\beta - z}{\beta + T}\right)^{n+2}\right] \tag{5.12}$$

$$m, n = 1, 2, 3, \quad 0 \leq x \leq L/2$$

$$w(x, z) > 0 \qquad (x > x_0, z < z_0)$$

where x_0 and $x_{\max}$ are the characteristic parameters of the hull form. L is the longitudinal length of the front of the fore-body (including the bulbous bow). d is generally the greatest depth which might be modified. If the baseline is unchanged, then d is the draft, A_{mn} and z_0 are taken as the design variables in the optimization procedure. Fix m, n = 1, 2, 3 we will have altogether 9 variables for A_{mn}, with total number of design variables not surpassing 10. Therefore, the choice of ship modification function reduces the number of design variables and improves the speed of optimization calculation.

(3) The constraint conditions are the same as above
(4) The optimization method is the same as above

5.3.2 *Optimization Process of Hull Form*

The flowchart of ship-type optimization calculation is shown in Fig. 5.16. First, enter the initial ship-type value file, which includes the main elements and types of the initial hull, the design range, the number of design variables, the design speed, the initial parameters for optimization calculation, as follows;

21 0 6 0.414 1.200

0.010 0.010 0.099 0.050 0.050

2.000 0.267 0.107 21 6 0.285

30 0.000 2.000

1 1 1 101.9 2

0 1 1

1.26175 0 0

-1.00 -0.90 -0.80 -0.70 -0.60 -0.50 -0.40 -0.30 -0.20 -0.10 0.000 0.100
0.200 0.300 0.400 0.500 0.600 0.700 0.800 0.900 1.000

0.000 0.050 0.100 0.150 0.200 0.250 0.300 0.350 0.400 0.450 0.500 0.550
0.600 0.650 0.700 0.750 0.800 0.850 0.900 0.950 1.000

0.000 0.075 0.250 0.500 0.750 1.000

0.000 0.000 0.005 0.048 0.114 0.232 0.380 0.518 0.632 0.712 0.750 0.730
0.670 0.578 0.467 0.346 0.234 0.138

0.062 0.012 0.000

0.000 0.055 0.110 0.170 0.272 0.404 0.546 0.675 0.778 0.835 0.866 0.850
0.798 0.715 0.607 0.485 0.358 0.231

0.132 0.050 0.000

0.000 0.081 0.175 0.290 0.429 0.580 0.722 0.841 0.921 0.964 0.985 0.975
0.944 0.879 0.769 0.629 0.476 0.325

0.190 0.075 0.000

0.000 0.087 0.204 0.346 0.502 0.660 0.802 0.9060.971 0.996 1.000 1.000
0.994 0.962 0.884 0.754 0.592 0.413

0.236 0.085 0.000

0.000 0.090 0.213 0.368 0.535 0.691 0.824 0.9170.977 1.000 1.000 1.000
1.000 0.987 0.943 0.857 0.728 0.541

0.321 0.116 0.000

0.000 0.102 0.228 0.391 0.562 0.718 0.841 0.9260.979 1.000 1.000 1.000
1.000 0.994 0.975 0.937 0.857 0.725

0.536 0.308 0.000

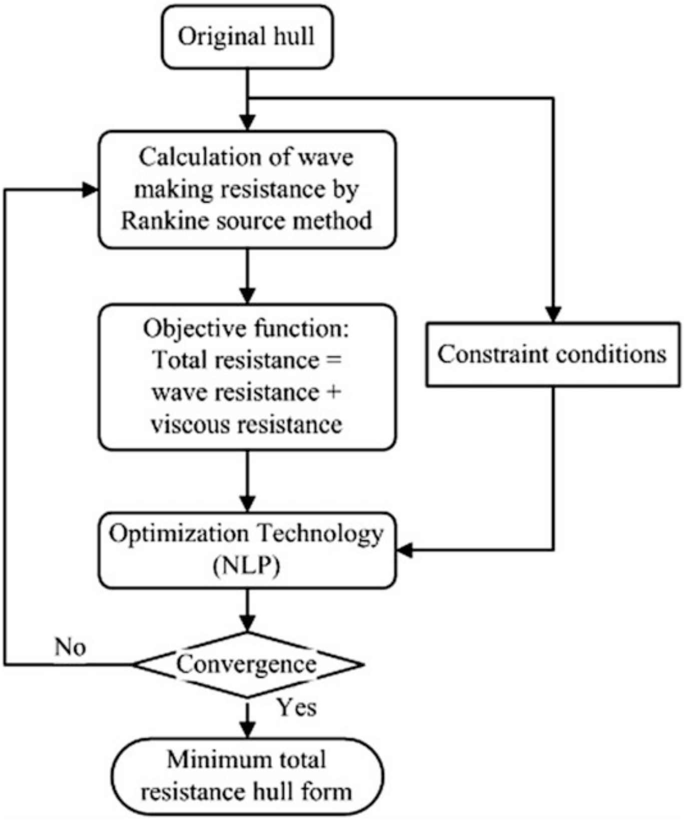

Fig. 5.16 Optimization process

Then, the wave resistance is calculated by Rankine source method and the sum of the wave resistance and equivalent plate frictional resistance is taken as the objective function combined with basic constraints to optimize the nonlinear programming method (NLP) to determine whether the optimization result converges. If not converge, then return to the initial state, repeat the above operation, if convergence, the optimization calculation is finished and the minimum total resistance ship can be obtained.

5.3.3 Examples

(1) Wigley hull

Meshing of Wigley hull and free surface are the same as those in Sect. 2.5.1. The optimization range is shown in Fig. 5.16. Figures 5.17 and 5.18 are comparison

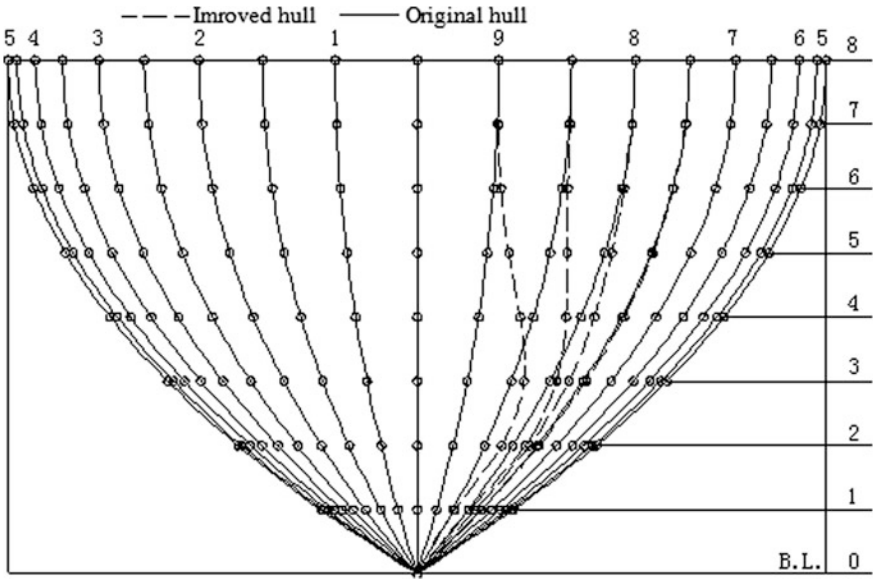

Fig. 5.17 Comparison of body plans of the modified ship and the original ship (Wigley)

between the horizontal section and waterline of the modified ship and the original ship; Fig. 5.19 is a wave profile of an modified ship and the original ship; Fig. 5.20 shows the comparison of the wave resistance coefficient of modified ship and the original ship; Fig. 5.21 shows the free surface waveforms of the modified ship and the original ship.

(2) S60 hull form

Meshing of S60 hull form and free surface are the same as those in Sect. 2.5.2. The optimum design range is shown in Figs. 5.1, 5.22, and 5.23 are comparison of the body lines and waterline of the modified ship and the original ship; Fig. 5.24 is a wave profile of the modified ship and the original ship; Fig. 5.25 shows the wave resistance coefficient of modified ship and the original ship; Fig. 5.26 shows the free surface waveforms of the modified ship and the original ship. Table 5.2 is the result of optimization calculation based on Rankine source method.

Based on Rankine source method, the optimized design of the ship with the lowest resistance is not significant and without big bulbous bow, but the effect of drag reduction is quite considerable. And the hull shape of the improved ship is

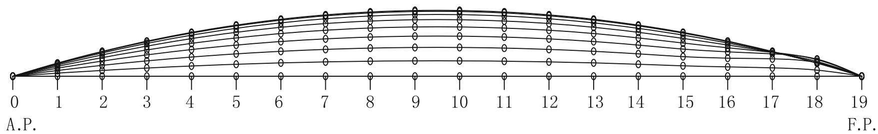

Fig. 5.18 Water plans of the modified ship (Wigley)

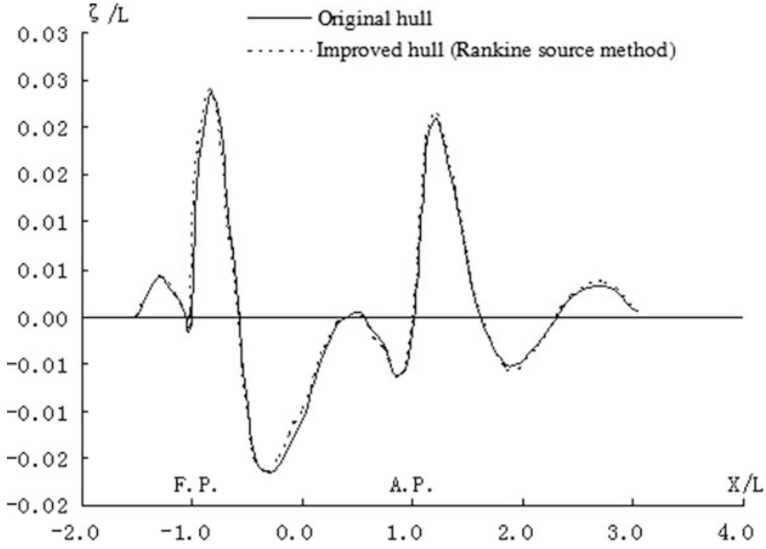

Fig. 5.19 Comparison of the wave profiles along the modified ship and the original ship (Wigley)

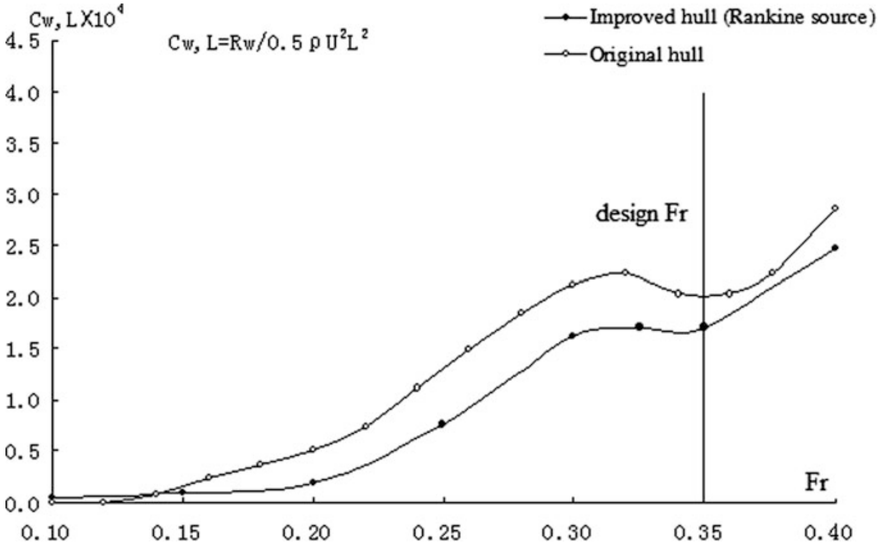

Fig. 5.20 Comparison of wave-making resistance coefficient of modified ship and the original ship (Wigley)

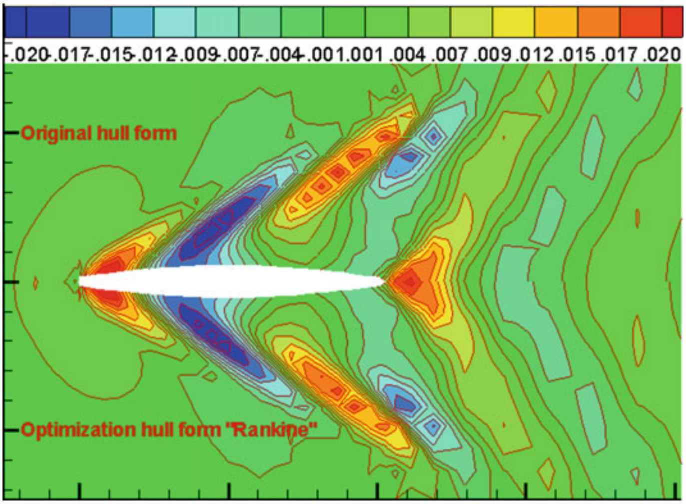

Fig. 5.21 Wave patterns (2 $g\zeta/U^2$) of the modified ship and the original ship (Wigley)

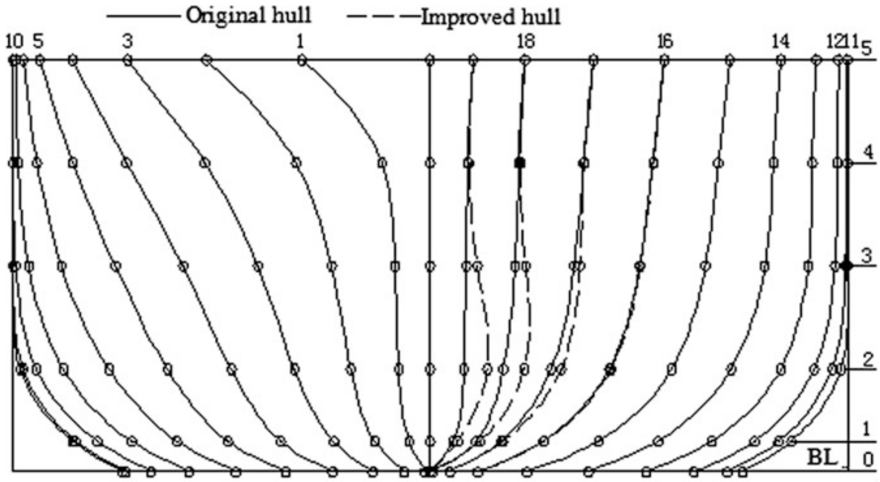

Fig. 5.22 Comparison of body plans of the modified ship and the original ship (S60)

slick and smooth, which is closer to the practical ship type; At the designed speed point, the wave resistance of the two modified ship types was reduced by 13.5% and 23.4%, respectively, and the total resistance was reduced by 4.3% and 9.8%, respectively; the wave height of the modified ship did not change much, and the waveform was clearer, and the clear Kelvin wave system shape appears.

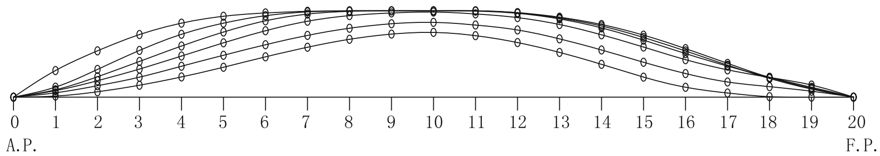

Fig. 5.23 Water plans of the modified ship (S60)

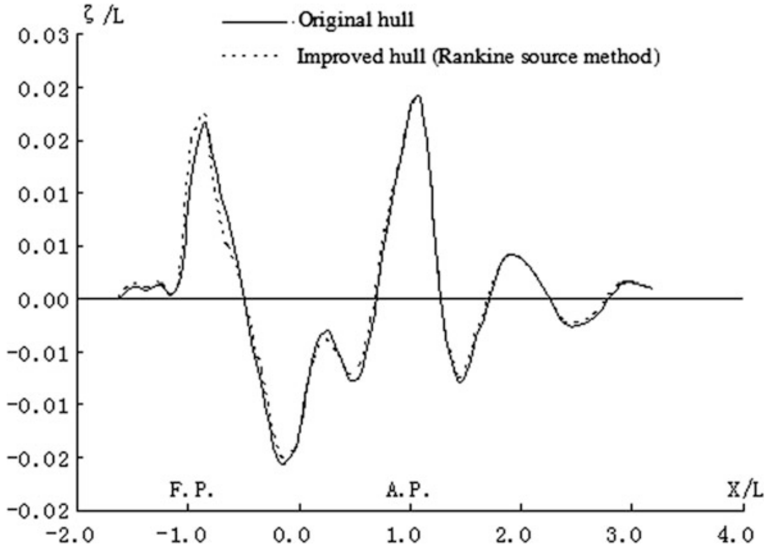

Fig. 5.24 Comparison of the wave profiles along the modified ship and the original ship (S60)

5.3.4 Design of Ship Hull with Minimum Wave Resistance Under Different Constraints

Taking the S60 hull model as an example, the optimization design of the minimum wave-making resistance ship based on the Rankine source method is discussed by changing the constraints and design variables, the specific design schemes are shown in Table 5.3.

The front half of the hull form is selected as the scope of optimization design. From the tenth station to the fore-body, moreover, the hull bottom, stem, and stern profiles cannot be modified in the ship-type modification, as shown in Fig. 5.27. According to the requirement, the water plane can be fixed or not fixed, respectively, as shown in Table 5.3.

For the three design schemes, the optimized optimization calculation is ended with 5, 4, and 4 iterations, respectively, through using the NLP method. The wave resistance of the modified ship is reduced by about 24.8%, 21.5%, 18.6%, respectively. The comparison of body plans between the modified ship and the

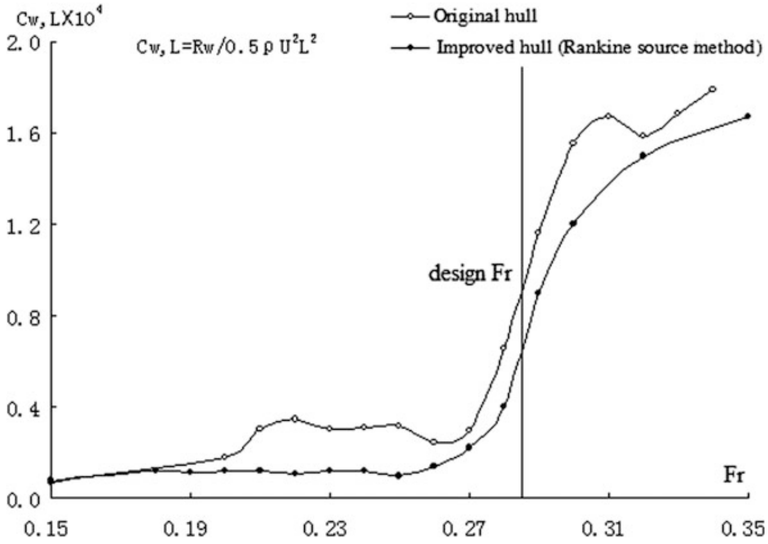

Fig. 5.25 Comparison of wave-making resistance coefficient for the modified ship and the original ship (S60)

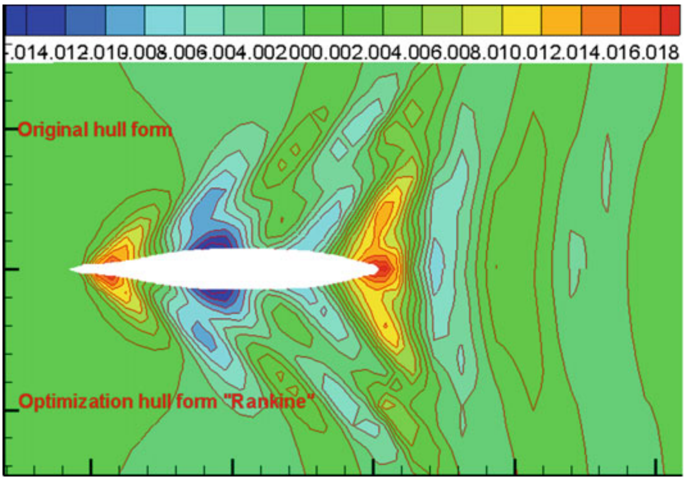

Fig. 5.26 Wave patterns ($2\,g\zeta/U^2$) of the modified ship and the original ship (S60)

original ship is shown in Figs. 5.28, 5.29, 5.30, 5.31, 5.32 and 5.33. In scheme one, from fore-body to S.S.18, between baseline and 4 W.L., the profile lines of the modified ship have a shift to the medial side of the hull. From S.S.18 to S.S.11, between baseline and 7 W.L., the profile lines of modified ship have a shift to the lateral side of the hull, and the offset is decreased gradually. The frame lines of the

Table 5.2 Optimization results using the Rankine source method for Wigley and S60 ships

Hull form	Constraints	Fr	R_W/R_{W0} (%)	R_F/R_{F0}	R_T/R_{T0} (%)	∇/∇_0	S/S_0
Wigley	(1), (2)	0.35	86.5	1.005	95.7	1.091	1.023
S60 hull	(1), (2)	0.285	76.6	1.002	90.2	1.039	1.011

Table 5.3 Design parameters and design conditions

	Design Scheme 1	Design Scheme 2	Design Scheme 3
Object function	R_W	R_W	R_W
Design speed	$Fr = 0.285$	$Fr = 0.285$	$Fr = 0.285$
Design variable	A_{mn} (m, n = 1,2,3)	A_{mn}(m, n = 1,2,3), z_0	A_{mn} (m, n = 1,2,3), z_0
Scope of optimization	Fore-body of hull	Water plane and fore-body of hull	Water plane and fore-body of hull
Constraints	$y(i,j) \geq 0$, $\nabla_0 \leq \nabla$	$y(i,j) \geq 0$, $\nabla_0 \leq \nabla \leq 1.005\nabla$	$y(i,j) \geq 0$, $\nabla_0 \leq \nabla \leq 1.005\nabla$, $A_w \geq A_{w0}$

Note ∇_0, $\nabla$are the displacement volumes of the original ship and the modified ship, respectively, A_{w0}, A_w are the water plane areas of the original ship and the modified ship, respectively.

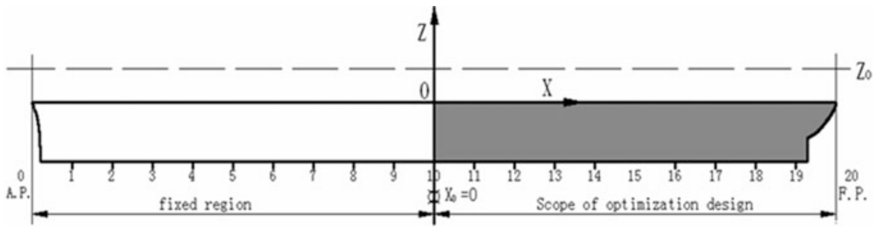

Fig. 5.27 Scope of optimization design

fore part become U-shaped for the modified ship, because the displacement volume moves from the upper to the lower area. Compared with the design scheme one, the water plane area of the modified ship is changed in the design scheme two, which is because the water plane is taken as the object of optimization design and the freedom of the nearby water plane is increased. From fore-body to S.S.11, between 4 W.L. and L.W.L., hull lines, profile lines of the modified ship have a shift to the lateral side of the hull. A great change is found between S.S.18 and S.S.16, but the body lines from the baseline to the 4 W.L. are hardly changed. The changes occurring in the design scheme three is similar to the design scheme two, the change of the hull lines is slightly decreased due to the constrained of the additional

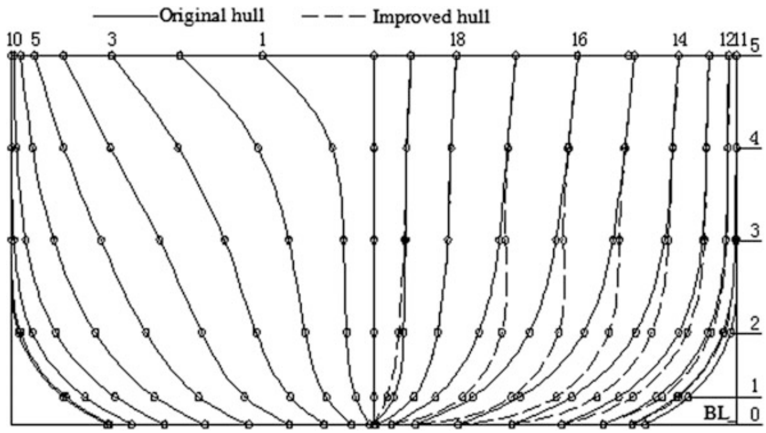

Fig. 5.28 Comparison of body plans of the original ship and the modified ship (design Scheme 1)

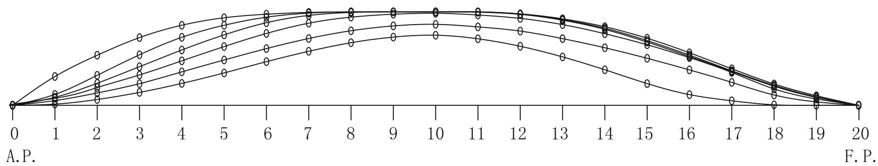

Fig. 5.29 Water plan of the modified ship (design Scheme 1)

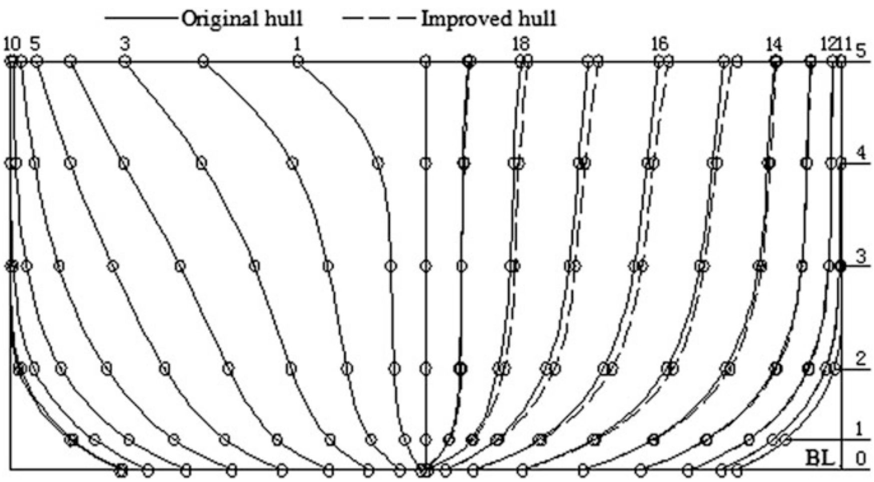

Fig. 5.30 Comparison of body plans of the original ship and the modified ship (design Scheme 2)

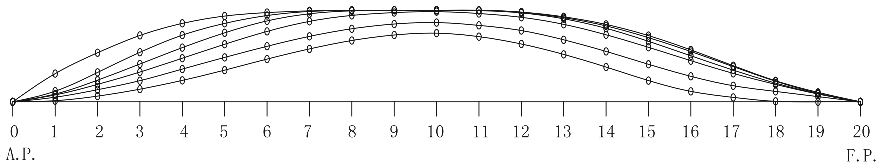

Fig. 5.31 Water plan of the modified ship (design Scheme 2)

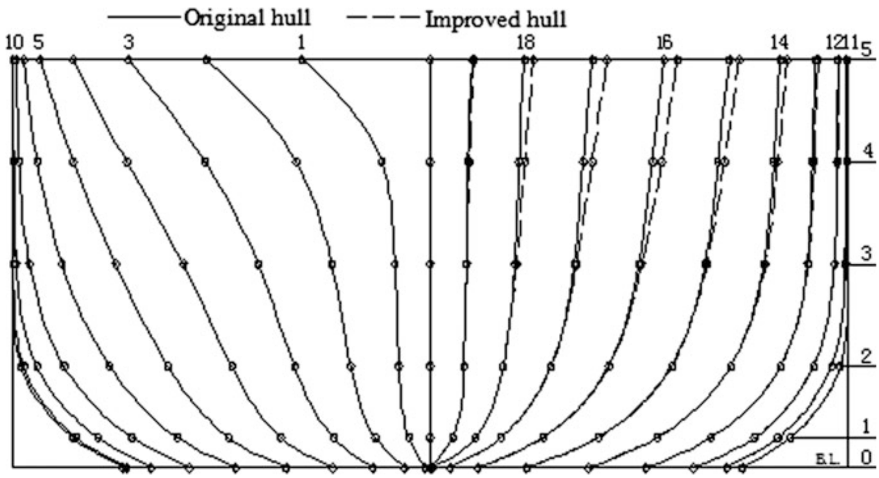

Fig. 5.32 Comparison of body plans of the original ship and the modified ship (design Scheme 3)

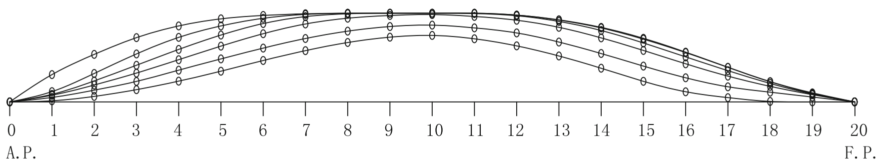

Fig. 5.33 Water plan of the modified ship (design Scheme 3)

Fig. 5.34 Comparison of wave-making resistance coefficient for three hull forms with Fr = 0.285

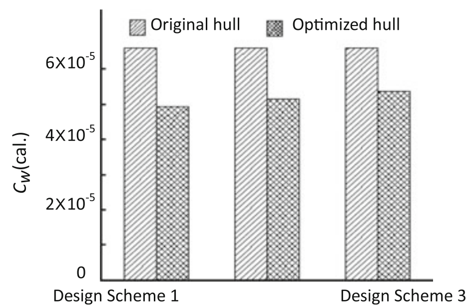

water plane area. Compared with the original hull, the wave resistance coefficients obtained from the three design schemes of the modified ship are significantly reduced with the design speed, as shown in Fig. 5.34.

The comparisons of the calculated wave profiles along the hull are shown in Figs. 5.35, 3.36, and5.37. The wave profiles are taken from the free surface elevation at panels adjacent to the ship's surface. The improved hull generates a slightly greater bow wave than the original ship with the increase of the bow wave steepness (Table 5.4).

Figure 5.38 shows the comparisons of the wave-making resistance coefficient of the original ship and the modified ship. It can be seen that a reduction in the wave-making resistance coefficient is achieved. The optimized forms lead to a less wave-making resistance over a wide range of design speeds.

Figures 5.39, 5.40, and 5.41 give the contours of the nondimensional wave pattern calculated for the modified ship and the original ship, respectively. The differences can be clearly seen in the wave fields generated by the modified ship and the original ship.

The minimum wave resistance based on the Rankine source method is taken as the objective function, and the parameters of the ship-type modification function are taken as the design variables in the optimization. With the displacement taken as the basic constraint, an optimal mathematical model is established according to the requirement of the additional constraint of water plane. The minimum wave resistance hull is obtained by the optimization of the bow body of the hull based on NLP method with S60 ship model as the original. Three modified ships are obtained by three optimal design schemes under the condition that the design speed *Fr* is

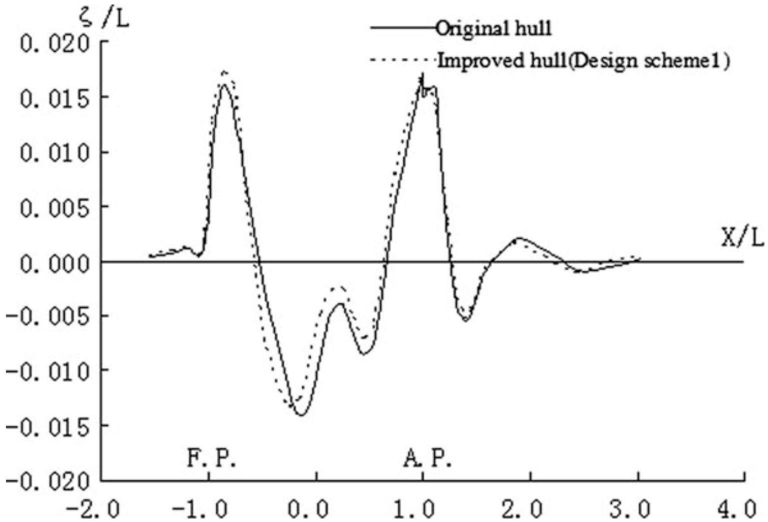

Fig. 5.35 Comparison of the wave profiles along the original ship and the modified ship (design Scheme 1)

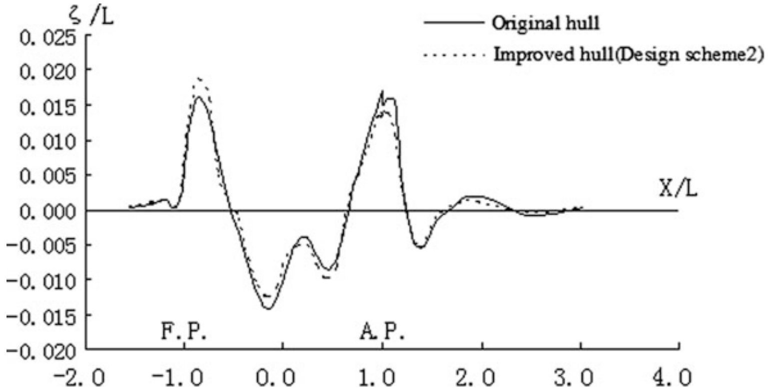

Fig. 5.36 Comparison of the wave profiles along original ship and the modified ship (design Scheme 2)

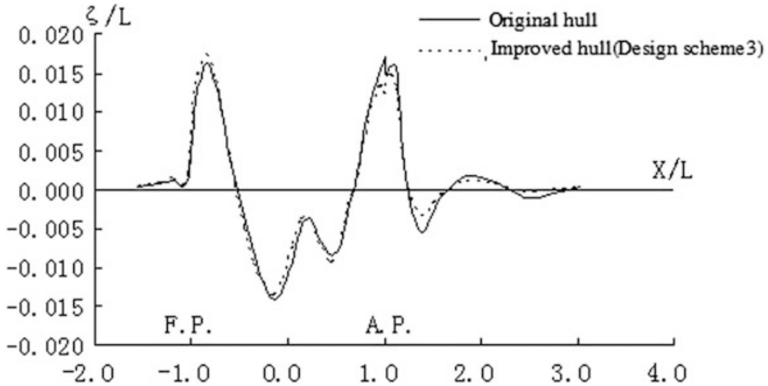

Fig. 5.37 Comparison of the wave profiles along the original ship and the modified ship (design Scheme 3)

Table 5.4 Optimization results using the Rankine source method with three design schemes

Design Scheme	R_W/R_{W0} (%)	∇/∇_0	S/S_0	A_w/A_{w0}	Time (t)
Design Scheme 1	75.2	1.039	1.011	_	1.6
Design Scheme 2	78.5	1.005	1.001	_	1.8
Design Scheme 3	81.4	1.003	1.006	1.002	2.2

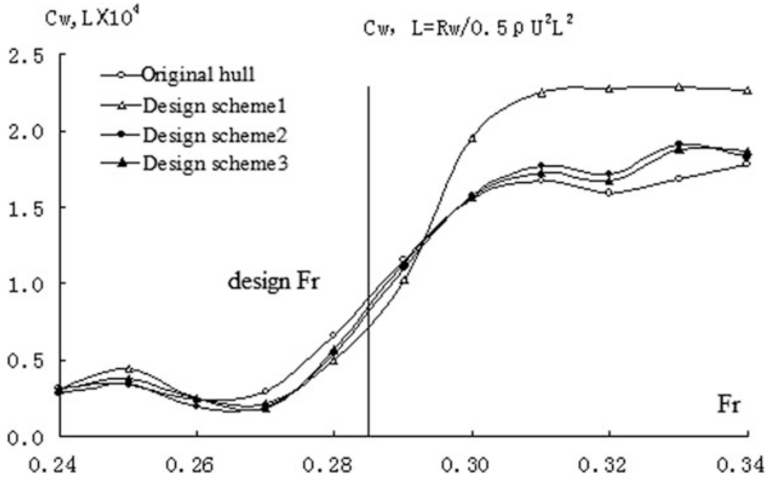

Fig. 5.38 Comparison of wave-making resistance coefficient for original ship and the modified ship

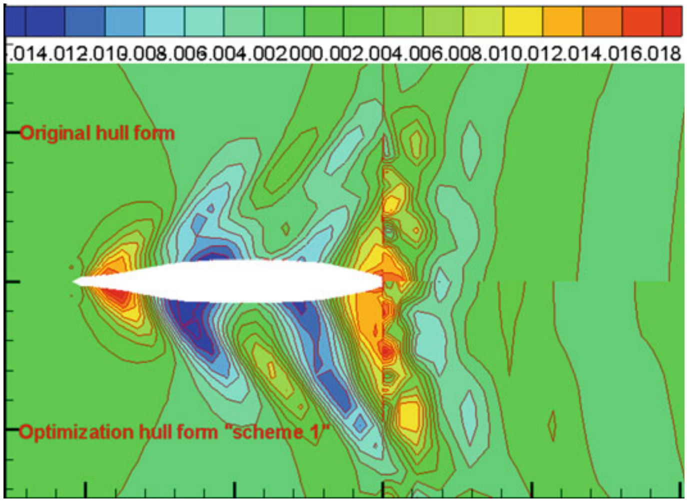

Fig. 5.39 Wave patterns (2 $g\zeta/U^2$) of the original ship and the modified ship (design Scheme 1)

0.285. Compared with the original ship, the wave resistance of the modified ship is reduced by 24.8% in scheme one, 21.5% in scheme two and 18.6% in scheme three. Furthermore, the modified ship is smoother and closer to the actual ship. Therefore, we can conclude that the method based on the Rankine source method is effective.

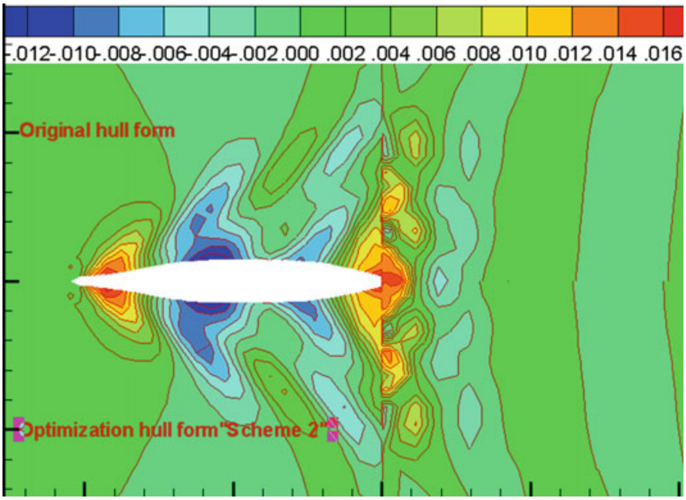

Fig. 5.40 Wave patterns ($2\ g\zeta/U^2$) of the original ship and the modified ship (design Scheme 2)

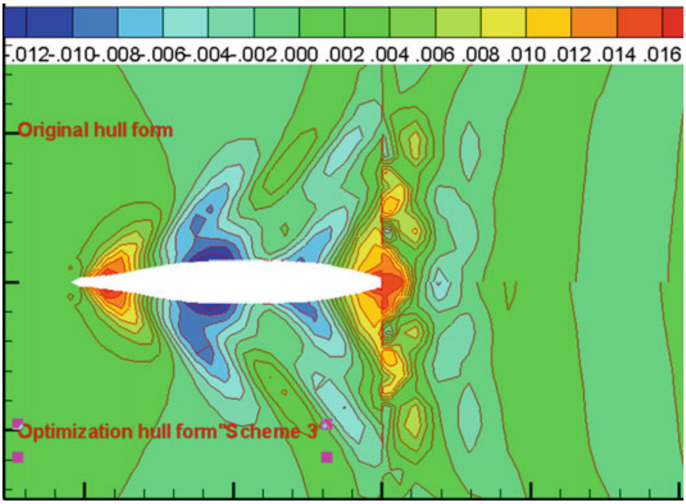

Fig. 5.41 Wave patterns ($2\ g\zeta/U^2$) of the original ship and the modified ship (design Scheme 3)

In order to reduce the resistance further, the viscous resistance should be considered. For the study on the optimization of the hull with the minimum total resistance, the objective function can be expressed as the sum of the viscous resistance and the wave resistance, which will be our next step to study.

5.4 Optimization Design of Ship with Minimum Resistance Based on Genetic Algorithm

5.4.1 *Ship Form Optimization Model*

The objective function, design variables, and constraints are the same as those in Sect. 5.3.1. Reference to the Japanese scholar Yasuhiro Akihiro's thought, using the penalty function method to transform the constrained optimization problem into an unconstrained optimization problem, and then using SGA for the minimum resistance ship-type optimization design.

The total resistance R_T is selected as the objective function to optimize the calculation, and R_T can be expressed as the following form:

$$R_T = p \cdot R_W + (1 + k) \cdot R_F + \alpha \cdot (\nabla_0 - \nabla) + \alpha \cdot \frac{1}{\sum_{i=1}^{M} y_i(x, z)} \rightarrow \min \tag{5.13}$$

where α is the penalty factor, (1) when $y(i, j) \geq 0$, and $\nabla > \nabla_0$, $\alpha = 0$; (2) when $y(i, j) < 0$ and $\nabla < \nabla_0$, $\alpha = \infty$. Other parameters can be obtained using the method in Sect. 5.3.1.

5.4.2 *Ship-Type Optimization Based on Basic Genetic Algorithm*

The validity and feasibility of SGA have been confirmed in practical applications. However, for a specific optimization problem, the user must reasonably determine the genetic operators, algorithm parameters, and constraints processing methods, and they will have a direct impact on the optimization results [2]. Therefore, the following SGA mathematical model is designed for the ship-type optimization problem in this section:

(1) Initialize the population

This section uses real-coded chromosomes, where each chromosome is represented by a real number and has the same dimension as the design variables. Therefore, the ship parameters are represented by binary digits of 0 and 1. The ship-type genes are arranged in a certain order, constituting the ship-type chromosome.

(2) Fitness evaluation

Evaluate the chromosome is to establish the appropriate fitness function. Therefore, each of the chromosomes is decoded to obtain a set of design parameters, and then calculate the corresponding objective function according to this set of design parameters.

(3) Selection

This section uses the competitive selection method, which competes among individuals and the winner becomes the next generation. In each generation, K individuals are randomly selected to form a small population each time, and the most adaptive individuals are then definitely taken from the k individuals to enter the next-generation population. The replicated individuals still return to the parent population, participating in the random selection of the next K individuals. This random selection repeats M times to generate M next-generation individuals.

The specific steps are as follows:

(1) K individuals are randomly selected from the t-th generation population;
(2) Compare the fitness of K individuals, and the individual with the maximal fitness enter into the (t + 1)th generation, and the replicated individuals remain in the t-th generation;
(3) Repeat ①, ② M times until the same number of individuals are produced as in generation t.

(4) Crossover

This section uses the uniform crossover technique in which two genes are exchanged at each locus of two matched individuals with the same crossover probability to form two new individuals.

(5) Variation

The mutation probability $P_m = 0.2 \times 0.9^n$ is determined through the adaptive thought, n is the genetic algebra, with the increase of the excellent characteristics of the population and the value of the mutation probability is reduced, which can better restrain the premature phenomenon.

(6) Constraint handling and judging function

The strategy of dealing with constraints includes rejection strategy, repair strategy, improved genetic operator strategy and penalty strategy. For the optimization problem in this section, the penalty strategy is applied to the strict constraint problem. The judging function after adding the penalty item is:

$$eval(x) = \frac{10^5}{f(x) + 10^7 p(x)} \tag{5.14}$$

In this formula: $f(x)$ is the objective function; $p(x)$ is the sum of the constraint function values which are all normalized and greater than zero.

(7) Termination conditions

Most traditional SGA has chosen to reach a given number of cycles as a termination condition, this approach may result in the failure to be terminated before the calculation accuracy is reached, or the cycle continues after the calculation accuracy has been reached. Therefore, in this section, the target value of the optimal chromosome achieves the given accuracy ε as the termination condition.

Through the local improvement of some genetic operators in SGA, and using the improved SGA in the ship optimization design, the ideal minimum resistance ship type is obtained, and Fig. 5.42 is the flowchart of SGA.

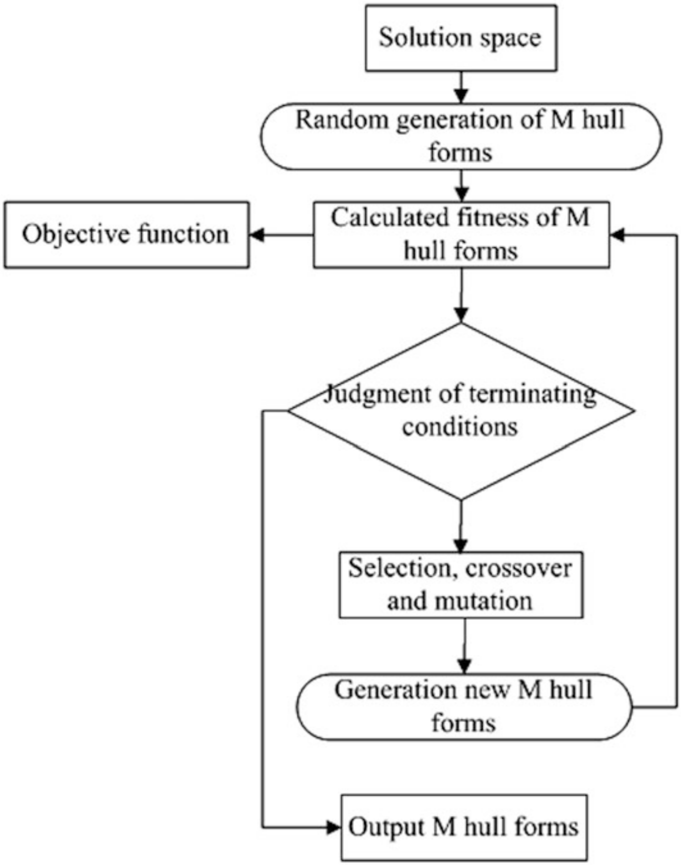

Fig. 5.42 Flowchart of the SGA

5.4.3 The Optimization of the Hull Form Based on NGA

(1) Execution steps of NGA.

Programming with FORTRAN language, as follows:

(1) Initializing population.

First, set the counter t be 1, the hull form parameters are represented by the binary digits of 0 and 1. Then the initial population P (t) with M individuals is generated at random, the maximal number of evolution generations T is also set.

(2) Fitness evaluation.

The fitness evaluation of all individuals is performed, saving the first N individuals after sorting the population by fitness value in descending order ($N < M$). These individuals do not participate in the generation operation of selection, crossover, and variation. They perform niche elimination operations directly with the mutated individuals;

(3) Selection operation.

The competition selection method is used to select individuals from the population P (t), and then generates a new population P $(t)'$.

(4) Crossover operation.

According to the probability of crossover P_c, arithmetic crossover operation is performed in the population. If the two individuals selected for crossover are identical, then one of the individuals is evenly crossed, and then generates a new population P $(t)''$.

(5) Mutation operation.

According to the probability of mutation P_m, uniform mutation operation is performed in the population P $(t))''$, and then new population P $(t)'''$ is generated with M individuals.

(6) Niche elimination operation.

Using Niche generation operation through fitness sharing method, a new population with $M + N$ individuals is generated by putting N saved individuals and P $(t)'''$ together, then carry out the niche elimination operation.

(7) Generate new populations

Sorting new population with $M + N$ individuals by new fitness value in descending order, and memorizing the first N ($N < M$) individuals again, then taking the first M individuals of arrangement as a new generation population.

(8) Termination criterion.

If $t \leq T$, then $t = t + 1$, generating M individuals in (7), and taking them as the next-generation population $P(t)$, then go to step (3); If $t > T$, terminating the algorithm, and outputting the calculation result.

In the present study, the calculations use populations 60, crossover probability 0.50 and mutation probability 0.06.

(2) Flowchart of algorithm is shown in Fig. 5.43.

5.4.4 Examples

This section selects the S60 ship as the initial ship model, respectively, using SGA and NGA for ship-type optimization, the optimum design range of the first half of the ship hull, and the design of the waterline, the bottom of the ship, the front and rear ends of design range are fixed, as shown in Fig. 5.27; Meshing of ship and free surface are the same as those of Sect. 5.3.2.

The optimization calculation results based on NGA and SGA are summarized in Table 5.3. The comparison between the modified ship model and the original ship model is shown in Fig. 5.44, 5.45, 5.46 and 5.47, the modified profile obtained based on the NGA had a larger tendency to swell outward than that of SGA. Figure 5.48 shows the wave resistance coefficient curve of the modified ship and the original ship. The curve of the wave resistance coefficient of the modified ship obtained by NGA is lower than that of the SGA in a certain area of design Fourier number; Fig. 5.49 shows the historical record of the total drag coefficient during the

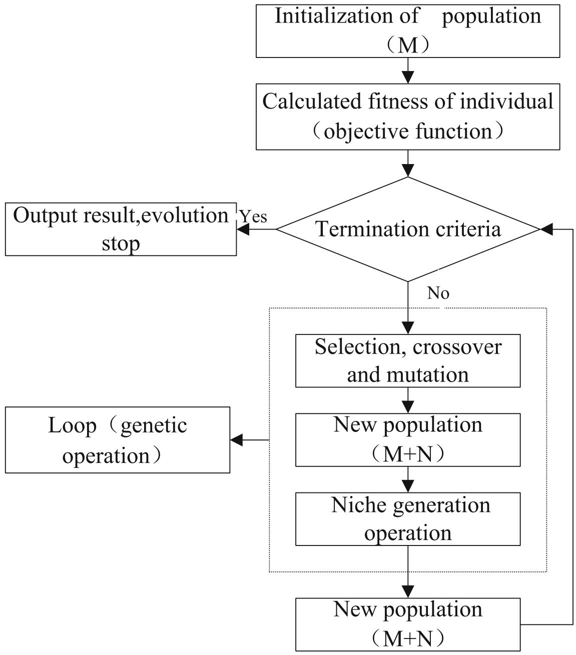

Fig. 5.43 Flowchart of the NGA

optimization of the modified ship at Fr = 0.285. In the early stage of evolution, SGA converges faster, but about 90 generations later, the algorithm entered a certain area of the optimal solution stalled, resulting in local convergence and the population lost its diversity in evolution. Approximately every 35 generations, the NGA ship model can be significantly improved, and its C_T gradually decreases, and results of the 250th generation are considered the best model. NGA shows a stable evolutionary speed during evolution. Even when searching for the global optimal solution, NGA can maintain high population diversity and provide a potential impetus for further evolution (Table 5.5).

Figure 5.50 and 5.51 show the waveforms of the modified and the original ship obtained by NGA and SGA, respectively. In Fig. 5.50, the wave height of the modified ship has little change, and the wave height in other areas has been significantly reduced; in Fig. 5.51, both the bow wave height and the stern wave height of the modified ship are increased, except for a slight decrease in the ship's center.

Figure 5.52 and 5.53 are the free surface waveforms of the modified (upper) and the original (bottom) NGA and SGA models obtained, respectively, at Fr = 0.285. It can be seen from the diagram that the modified ship form has a clear Kelvin wave shape, transverse waves and scattered waves regimes limited within ±9°28′. Among them, the free surface waveforms of the modified ship obtained by NGA are clearer.

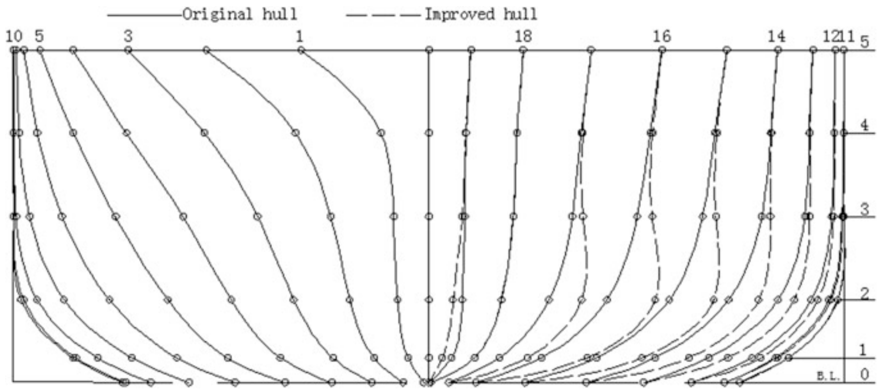

Fig. 5.44 Comparison of body plans of the original ship and the modified ship (NGA)

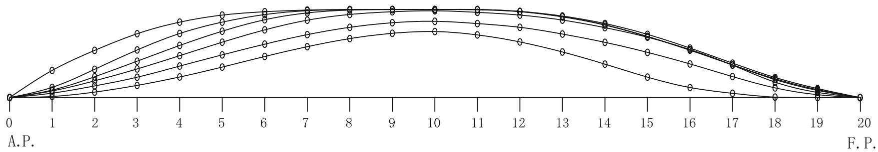

Fig. 5.45 Water plan of the original ship (SGA)

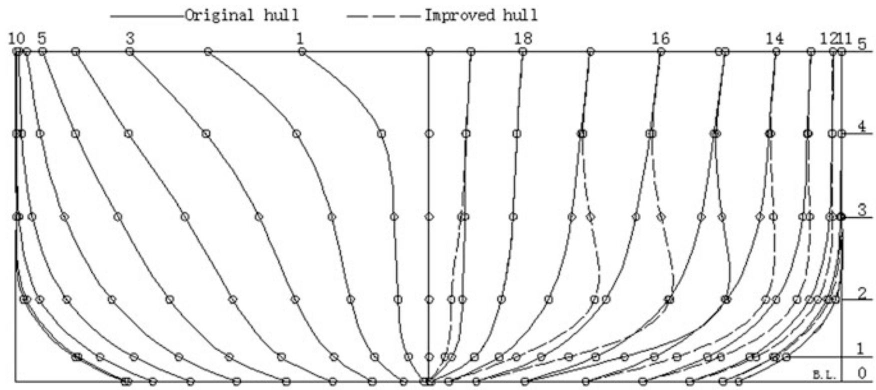

Fig. 5.46 Comparison of body plans of the original ship and the modified ship (NGA)

5.4.5 The Comparisons of the Optimization Result Between GA and LNP

Figure 5.54 and 5.55 represent the reduction effect and time-consuming comparison of NLP, SGA, and NGA, respectively, it can be seen from the figure that the NGA

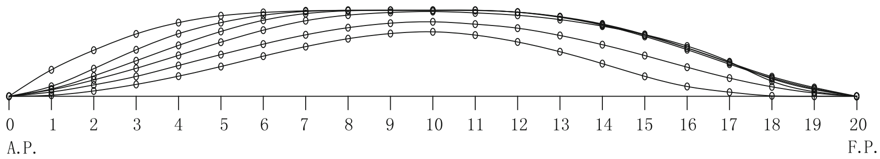

Fig. 5.47 Water plan of the modified ship (NGA)

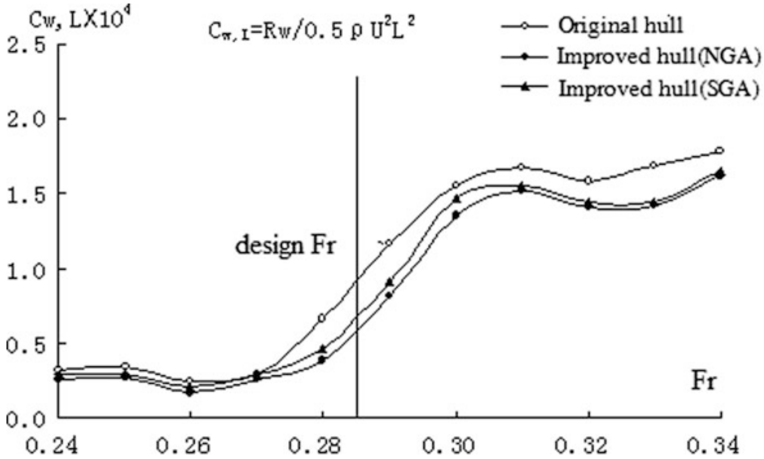

Fig. 5.48 Comparison of wave-making resistance coefficient curves between the original ship and the modified ship

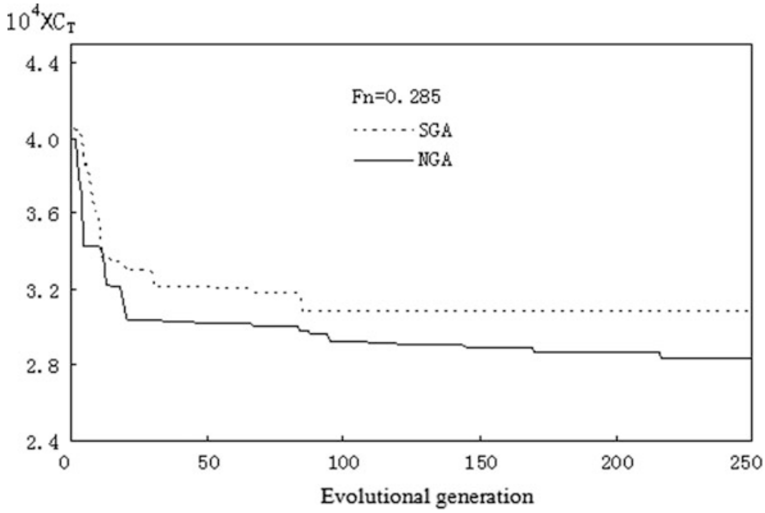

Fig. 5.49 Convergence history of total resistance coefficient in the optimization process

Table 5.5 Optimization results based on the SGA method and NGA method

Optimization method	Constraints	Fr	R_W/R_{WO} (%)	R_F/R_{FO}	R_T/R_{TO} (%)	∇/∇_O	S/S_O
NGA	(1), (2)	0.285	72.5	1.007	91.6	1.017	1.012
SGA	(1), (2)	0.285	81.6	1.001	96.0	1.002	1.001

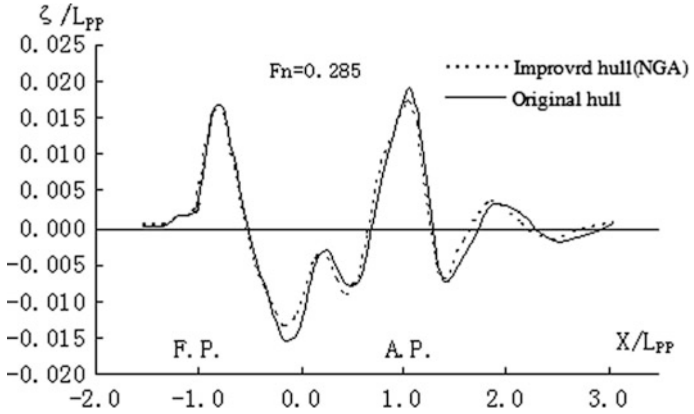

Fig. 5.50 Comparison of the wave profiles along the original ship and the modified ship (NGA)

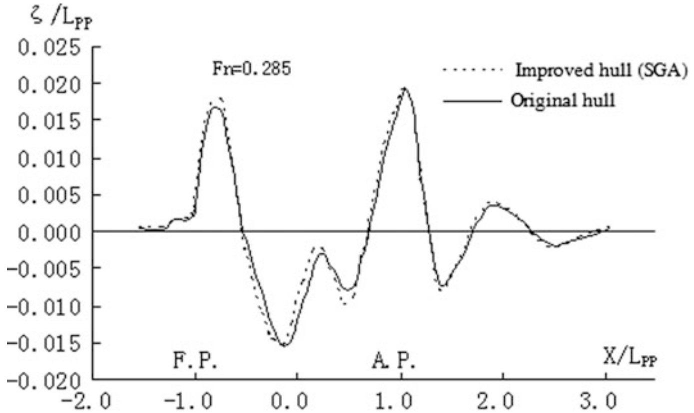

Fig. 5.51 Comparison of the wave profiles along the original ship and the modified ship (SGA)

has the best reduction resistance effect, while the NLP takes the least time, with worst effects of reducing the resistance.

The traditional optimization methods have advantages over genetic algorithms in terms of speed of optimization, but with the increase of design variables, the optimization speed of genetic algorithm is no worse than the traditional algorithm,

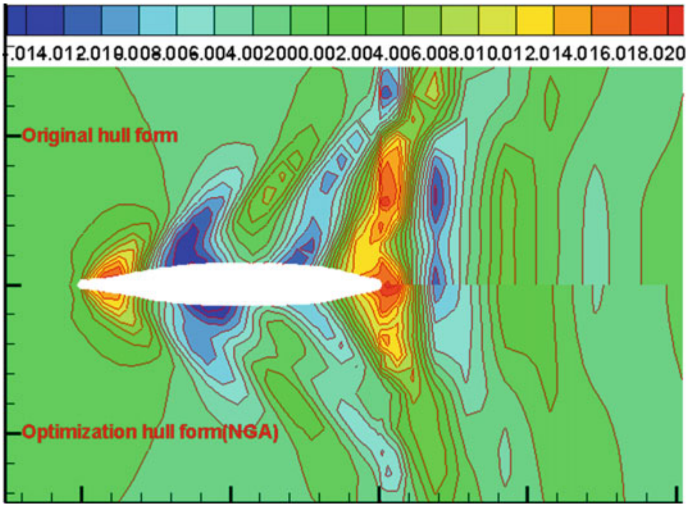

Fig. 5.52 Wave patterns (2 $g\zeta/U^2$) of original ship and the modified ship (NGA)

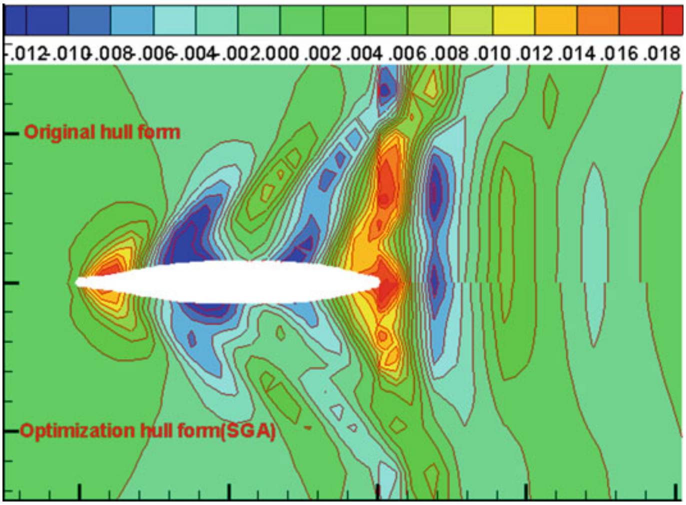

Fig. 5.53 Wave patterns (2 $g\zeta/U^2$) of original ship and the modified ship (SGA)

because the traditional optimization algorithm is directly related to the number of design variables, and the more design variables, the slower the optimization speed. The genetic algorithm is only related to the number of the population, but the number of the population and the number of variables are irrelevant. Therefore, in the calculation of each round, the genetic algorithm takes less time. When optimizing speed dominance, each design variable can be involved in the optimization.

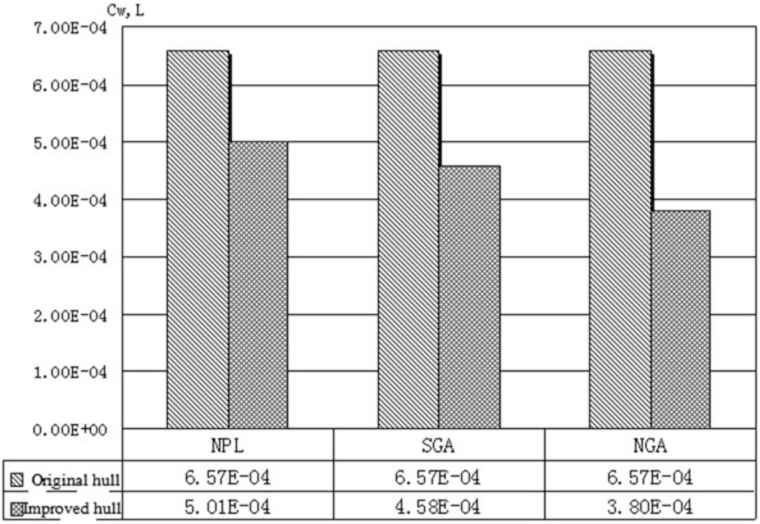

Fig. 5.54 Comparison of the reduced resistance effect of the GA and NLP

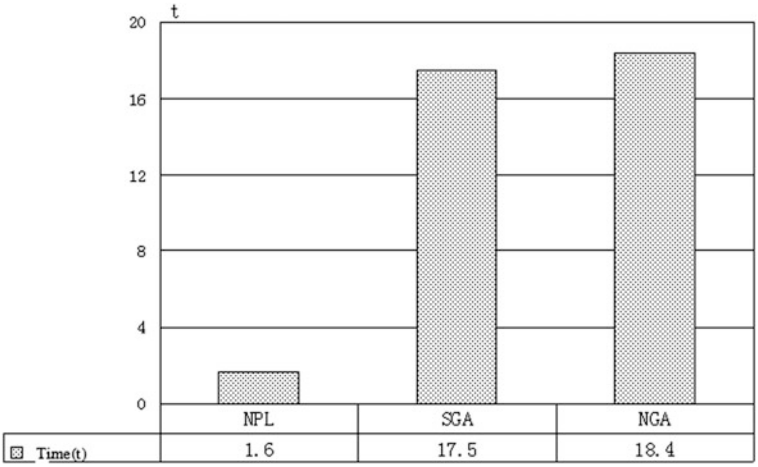

Fig. 5.55 Time-consuming comparison between NLP and GA

When solving the multivariable optimization problem, the genetic algorithm is not slower than the traditional optimization method in the terms of optimization speed, and parallel computation method can be used to increase the speed. Therefore, the genetic algorithm has a great advantage for the optimization problems of multiple design variables. At the same time, when there are multiple extremums in a complex system such as a ship, the genetic algorithm can find the global and local optimum point in the optimization with multiple local optimums. Because of the introduction of probability in genetic algorithms, some completely new ship types will appear in the optimization, which will undoubtedly bring great help to the development of new ship types.

5.5 Optimization of Ship Type with Minimum Resistance Considering Viscous Separation

In order to meet certain loading requirements and design speed conditions, it is often one of the most important problems in ship design to design a ship with the least resistance. Most of the ship designers in the past are based on the wave-induced resistance theory to study the modification of ship types. Suzuki Heffer [3] thesis is one of the most typical representatives. But so far, all the studies have been done to keep the stern line shape unchanged and only y to optimize the shape of the ship as the design object. This is because the ship optimization must consider the design of the after-body shape in many aspects such as wave resistance, viscous, seakeeping, and propulsion performance. Therefore, it is difficult to know how to optimize the tail line type. Therefore, there are few researchers in this field. According to the optimization design concept of ship type, this section minimizes the wave-making resistance under the condition of keeping the tail free of viscous separation. Using two-dimensional turbulence simple separation judgment formula to judge the separation point of airfoils with different shapes and using it for the separation judgment of the streamlines on the hull surface, the minimum resistance ship model considering the viscous separation is designed. The practicability of this method is verified by comparing it with the experimental data. Therefore, based on this design idea, taking S60 ship as the initial ship, taking the minimum total resistance ship type into consideration, considering all aspects of influence factors, the whole ship line type is taken as the optimal design object, Rankine source method based on potential flow wave resistance theory, and SUMT interior point method in nonlinear programming are used to do optimum design of ship with minimum resistance. A simple two-dimensional turbulence separation judgment formula for the ship types is used before and after optimization, obtains the separation points on each streamline on the hull surface, and approximates the separation area and determines whether the separation area of the modified ship type is larger than the initial ship type, so as to ensure that the viscous resistance does not increase when the ship type is optimized with the wave resistance as the main objective function.

5.5.1 Viscous Water Resistance

Viscous water resistance is derived from the frictional resistance of the wet surface of the ship and acts perpendicularly to the hull surface. The viscous effect of the fluid can be described from the boundary layer theory. This means that the viscous effect only acts on the thin layer near the hull surface. The two-dimensional boundary layer on the slab can be used to describe the important characteristics of viscous flow and to approximate the hull surface as a flat plate. If the flow is observed from the Servo coordinate system, the speed of the ship is expressed as the incoming velocity of U_∞^2 at the stationary hull [4], as shown in Fig. 5.1. The flow rate is U_∞^2, the positive direction of the x-axis, and δ is the boundary layer thickness. Water must adhere to the plate, that is to say there is no relative slippage between the water and the plate, which means that the flow rate on the plate is zero. Outside a very short vertical distance δ(x) away from the plate (which is a function of the longitudinal distance x from the leading edge of the plate), the flow rate is equal to U_∞^2. When Reynolds number Rnx = U_∞^2 x/ν is less than about 10^5, the viscous flow is laminar.

The occurrence of flow separation is one of the factors that increase the viscous resistance of the hull. If the flow is separated from the hull, a larger area of viscous action will result after the line is separated. This means more impact on the pressure distribution and increased shape resistance. Flow separates not only from sharp corners but also from the surface without sharply angled surfaces. Figure 5.56 below shows how separations in two-dimensional flow occur. If there is a point S on the surface, there is $\partial u/\partial y = 0$, and there is a backflow at point S, then it is considered that S point is considered; if it is still $\partial u/\partial y = 0$ behind the point S, then it is not considered that the flow is separated from point S. This situation is advantageous because $\partial u/\partial y = 0$ means that the shear stress value τ_w is zero on the object surface. This effect can be achieved by proper design of the hull surface. The

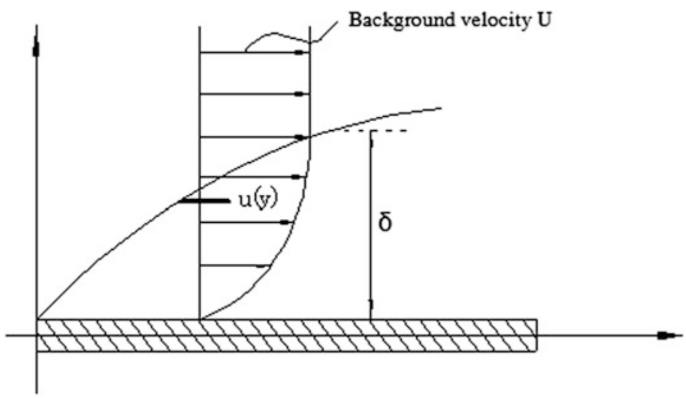

Fig. 5.56 Boundary layer of plate

location of point S depends on the pressure gradient $\partial p/\partial x$ along the hull surface and the flow state (laminar or turbulent flow) in the upstream boundary layer at the point of separation. According to the boundary layer theory, the reverse pressure gradient $\partial p/\partial x$ is positive, which is the necessary condition for the flow separation. As long as $\partial p/\partial x = -\rho U_e dU_e/dx$ is noticed, this can be verified from Eq. (5.15).

$$\frac{\partial p}{\partial x} = \mu \frac{\partial^2 u}{\partial y^2}, y = 0 \tag{5.15}$$

According to calculus, the condition of flow separation $du/dy = 0$ is also the condition that $u(y)$ obtains the local maximum or minimum value. For our problem, $u(y)$ should obviously take the minimum value, so $\partial^2 u/\partial y^2$ is positive at the separation point S. It can be seen from the equation that the necessary condition for the separation point to occur is that $\partial p/\partial x$ is positive at the separation point of the hull surface. Because the flow along the plate is constant at $\partial p/\partial x = 0$, flow separation does not occur in the case of flow along the plate Fig. 5.57.

5.5.2 Ship-Type Optimization Model

(1) Objective function

The objective function in this section is the same as in Sect. 5.3.1 (1).

(2) Design variables

The optimum design range of this section is taken as a whole ship, from station zero to the foremost station 20, and the design waterline, the bottom of the ship, the front and rear ends of the ship are fixed, as shown in Fig. 5.58.

The formula of ship modification function is shown in formulas (5.9) and (5.10)

(3) Constraints condition

The constraints in this section are the same as in Sect. 5.2.1 (3)

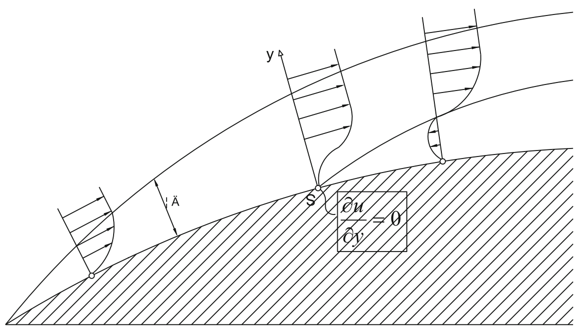

Fig. 5.57 Two-dimensional boundary layer flow

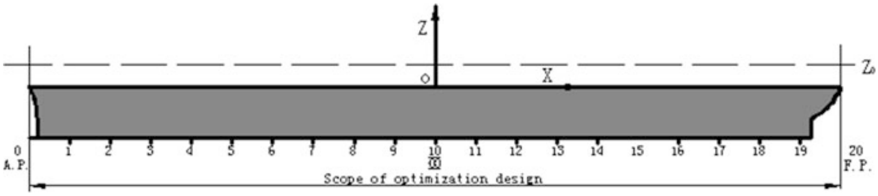

Fig. 5.58 Scope of optimization design of the S60 hull form

5.5.3 Examples

The S60 hull is selected as the initial design optimization of the ship, and mesh of the hull and the free surface of the S60 ship model are the same as those in the Sect. 5.5.2 (Table 5.6).

Based on Rankine source method, the optimization results of the whole ship are summarized in Table 5.1; Figs. 5.59 and 5.60 are the comparison of the bodylines and waterlines between the modified ship and the original ship. The body line of the modified ship varies greatly between the head and tail area. Therefore, it is generally considered that the changes in the stern line shape may cause viscous separation, resulting in other changes in the performance of the ship, to determine the separation is necessary. Next, this section uses a simple two-dimensional turbulence separation criterion to determine the separation. Figure 5.61 shows the comparison of the wave resistance coefficient curves of the original ship model and the modified ship model. The wave profile of the original ship model and the modified ship model is shown in Fig. 5.62; the free surface waveform of the original and modified ship model is shown in Fig. 5.63.

5.5.4 Ship Optimization Process

The flowchart of ship-type optimization calculation is shown in Fig. 5.64. First, enter the original ship-type value file, which includes the main elements and types of the original ship type, the design range, the number of design variables, the design speed, the original parameters of the optimization calculation, etc.; then, according to the Hess–Smith method and the streamline tracing method, the

Table 5.6 Optimize calculation results based on Rankine source method

Hull form	Constraints	Fr	R_W/R_{W0} (%)	R_F/R_{F0}	R_T/R_{T0} (%)	∇/∇_0	S/S_0
Improved hull form	(1), (2)	0.285	86.8	1.000	95.5	1.003	1.000

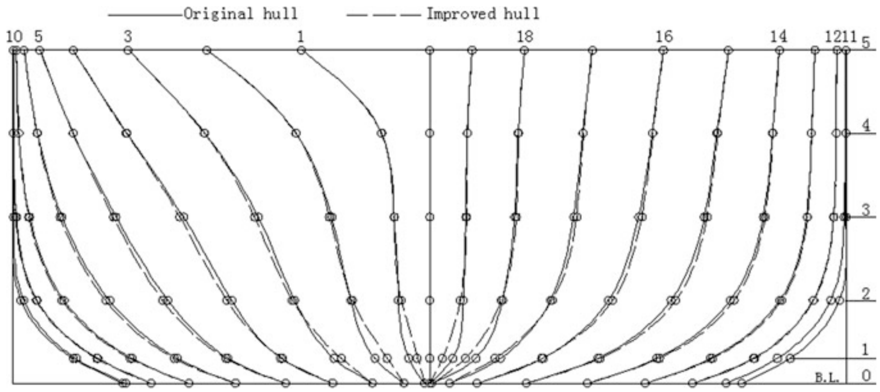

Fig. 5.59 Comparison of body plans of the modified ship and the original ship (S60)

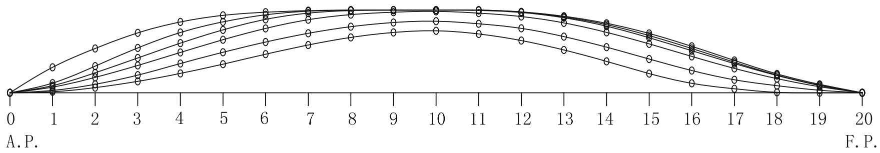

Fig. 5.60 Water plans of the modified ship (S60)

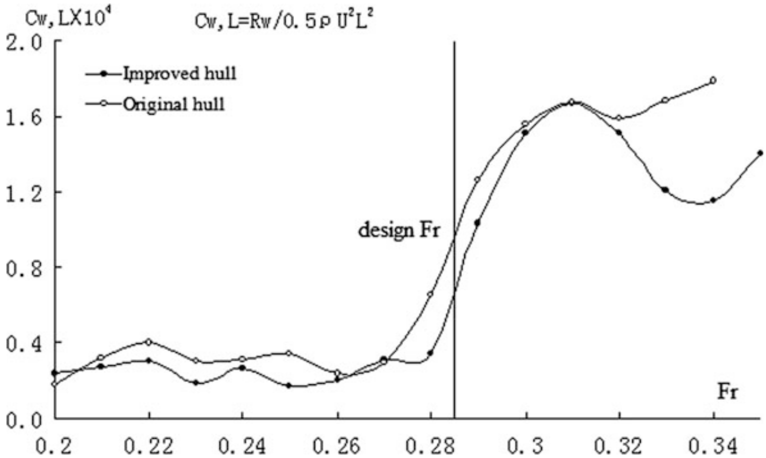

Fig. 5.61 Comparison of wave-making resistance coefficient of modified ship and the original ship (S60)

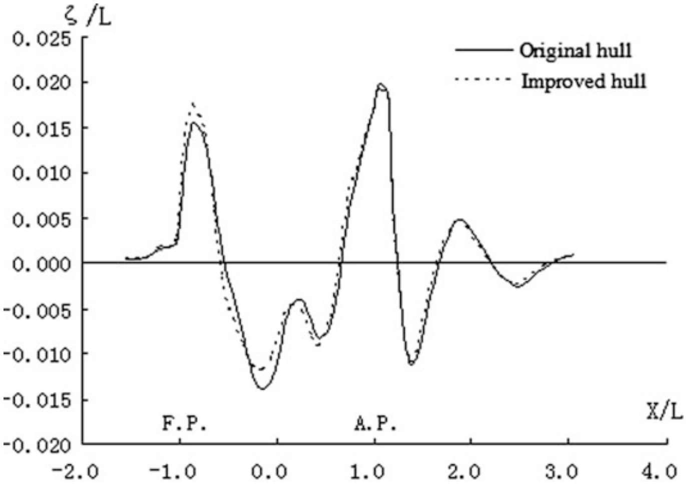

Fig. 5.62 Comparison of the wave profiles along the modified ship and the original ship (S60)

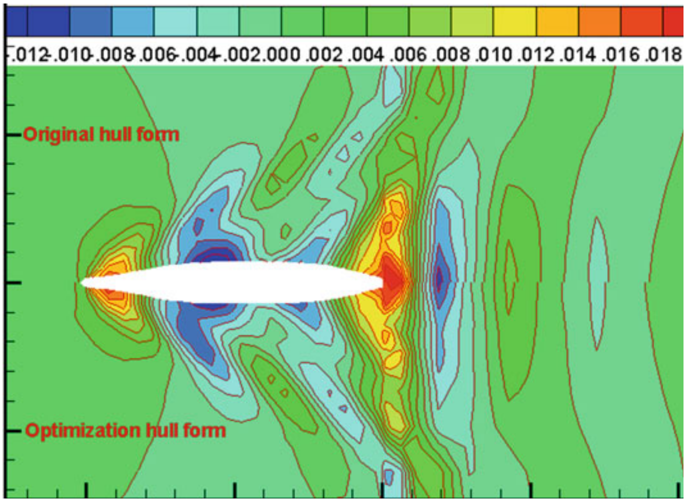

Fig. 5.63 Wave patterns ($2g\zeta/U^2$) of modified ship and the original ship (S60)

velocity distribution on each streamline of the hull surface is obtained, and the separation points on each streamline are calculated to find the separation domain of the original ship. According to the basic constraints (1) and (2), combined with the nonlinear programming method to optimize the calculation, the improved ship form is obtained. Again using simple two-dimensional separation of judgment to determine the separation points on the improved streamlines, find the separation area, and determine whether the improved separation of the ship is greater than the initial

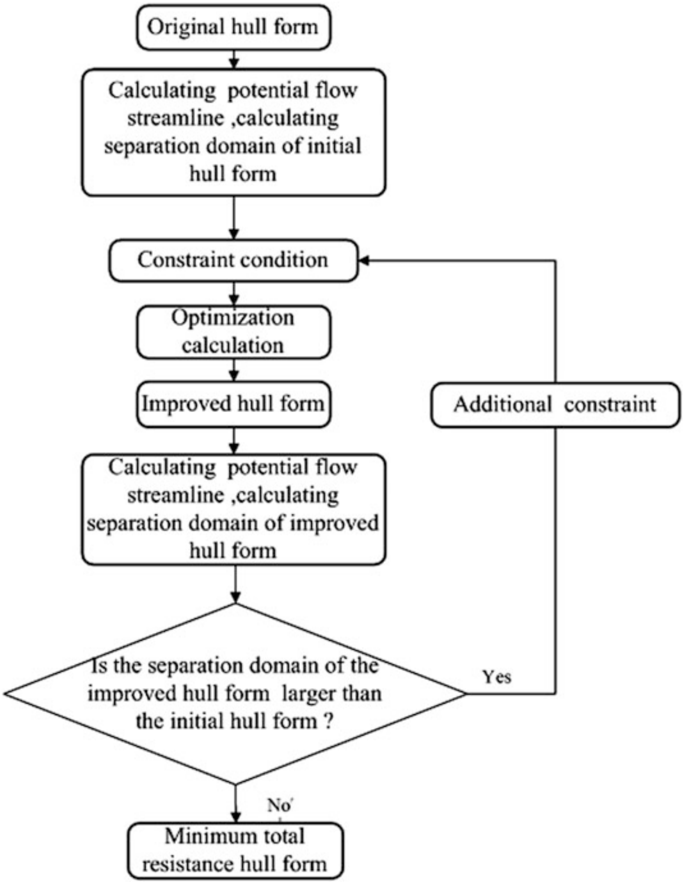

Fig. 5.64 Flowchart of ship-type optimization

ship type, if greater than the initial ship, then change the constraints and return to the initial state, re-optimize the calculation, if not greater than the initial ship, the optimization calculation is finished and the minimum total resistance ship is obtained.

5.5.5 Separation Judgment Method

(1) Two-dimensional simple separation of judgment condition

The idea of ship-type optimization is that the total resistance is minimized without separation of the tail. Due to the complexity of 3D turbulence separation problem [5], this section adopts two-dimensional simple turbulence separation judgment, and it is used to determine the separation of the streamline on the hull surface and finds the separation domain approximately.

The relationship (U = U_∞ in this graph) between the pressure gradient and the local surface friction stress of a two-dimensional turbulent boundary layer with pressure distribution by Tanaka and Tatsuno, as shown in Fig. 5.64, coordinate axis Γ, G is defined as

$$\Gamma = \frac{\theta}{U_\infty}\frac{dU_\infty}{dS}\left(\frac{U_\infty\theta}{v}\right)^{\frac{1}{4}} \tag{5.16}$$

$$G = \frac{\tau_w}{\rho U_\infty^2}\left(\frac{U_\infty\theta}{v}\right)^{\frac{1}{4}} \tag{5.17}$$

where τ_w is the local friction on the surface of the object, U_∞ is the flow velocity at the outer edge of the boundary layer, θ is the loss thickness of the motion, S is the distance along the object surface, and the separation point is defined as $\tau_w = 0$ (that G = 0). It can be seen from the figure that the value of Γ corresponding to G = 0 changes with the Reynolds number $R_\theta(=U_\infty\theta/v)$. Now assume that the Reynolds number of the model $R_L=U_\infty L/v$, the corresponding plate R_θ is about 5.5×10^3. Insert the corresponding curve R_θ into Fig. 5.65, the separation point Γ can be obtained and the value is about −0.03(that $\Gamma \approx -0.03$).

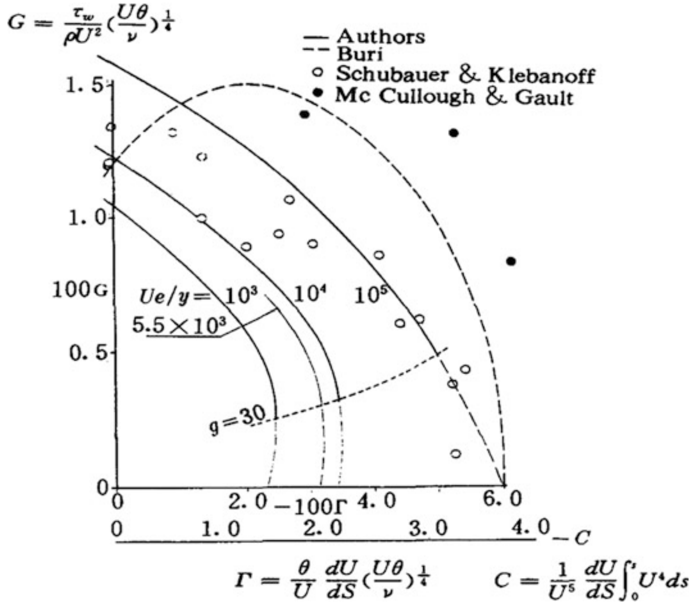

Fig. 5.65 Relationship between pressure gradient and local friction stress on the surface

From the two-dimensional turbulent boundary layer theory, it is shown that θ can be calculated by the following formula:

$$\theta(\frac{U_\infty\theta}{\gamma})^{\frac{1}{4}} = \frac{c}{U_\infty^d}\int_0^s U_\infty^d ds \tag{5.18}$$

where c = 0.016, d = 4.0

Substitute the above formula into Eq. (5.16), it can obtain that:

$$\Gamma = \frac{0.016}{U_\infty^5}\frac{dU_\infty}{dS}\int_0^s U_\infty^4 ds \tag{5.19}$$

Now define a new function C(s):

$$C(s) \equiv \frac{1}{U_\infty^4}\frac{dU_\infty}{dS}\int_0^s U_\infty^4 ds \tag{5.20}$$

The value of C(s) corresponding to the separation point Γs = 0.03 is:

$$C(s) \equiv \frac{1}{U_\infty^5}\frac{dU_\infty}{dS}\int_0^s U_\infty^4 ds \approx -2 \tag{5.21}$$

In this section, formula (5.21) is used as a criterion to judge whether the streamlines on the object surface are separated. The separation point can be obtained simply by calculating the flow velocity $U_\infty(s)$ at the outer edge of the boundary layer, $U_\infty(s)$ can be approximately replaced by the surface potential velocity of the object.

(2) Streamline tracing method

After the stacking mode solution is obtained, the induction velocity of each field point can be calculated as the induction velocity V at point A as shown in Fig. 5.66. β is the sweep angle, α is the angle between the direction of the induced velocity and the axis of X. If directly according to the induction rate of point A to seek the position of the upper and lower streamlines, it will be C, C coordinates:

$$\left(dx\frac{1}{1-tg\alpha ctg\beta}, dx\frac{tg\alpha}{1-tg\alpha ctg\beta}\right) \tag{5.22}$$

where *dx* is determined according to the distance between points on the first streamline. If the ith and (i + 1)th points of the first streamline are separated by the swept angle, the interval in the x-direction is dx; then after the ith and (i + 1)th points on the other streamlines being separated by the swept angle, the interval in the x-direction is also dx. The direct solution may cause a large error when the streamlines are relatively curved, as shown in Fig. 5.66, the difference between point C and the point D on the actual streamline is larger. In this paper, the fourth-order Runge-Kutta method is used to solve the problem, and the effect is better.

The steps to separate the hull surface are as follows:

(1) The velocity distribution on the hull surface is calculated by Hess–Smith method in this section;
(2) The velocity distribution on the streamline of the hull surface is calculated by the streamline tracking method;
(3) Calculate the distribution of C (s) on each streamline, and judge whether the separation occurs by formula (5.21), and determine the position of the separation point;
(4) Connect the separation points on each streamline to find the separation domain.

If we know the velocity distribution outside the boundary layer, we can calculate C according to formula (5.19), which is the two-dimensional simple turbulence separation criterion established in this study. In order to study the accuracy of the formula, the calculated values of two-dimensional objects are compared with the experimental values. As the initial ship type selected by the optimization calculation is S60 model, the model is relatively close to the actual ship type. Therefore, this section uses the experimental results of the second model in the thesis of Bai et al. [2]. Figure 5.67 shows the calculation result of a mast two-dimensional ship. The velocity distribution outside the boundary layer, U_∞/U, can be approximated by the potential velocity on the object surface. It can be seen from this example that the calculated point is slightly offset from the experimental point and the calculated value is not in good agreement with the experimental value. The reason for this may be that the velocity distribution outside the boundary layer is caused by the approximation of the potential velocity on the surface of the object, if the actual viscous flow is considered, the C curve should be slightly backward, then the calculation point should also be slightly backwards. In addition, the separation

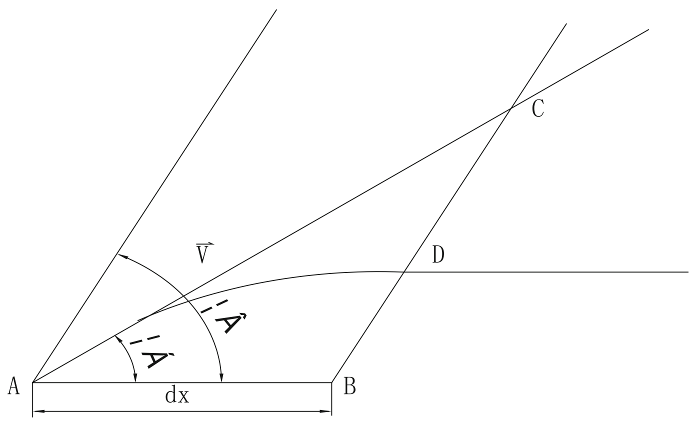

Fig. 5.66 Schematic of streamline tracing

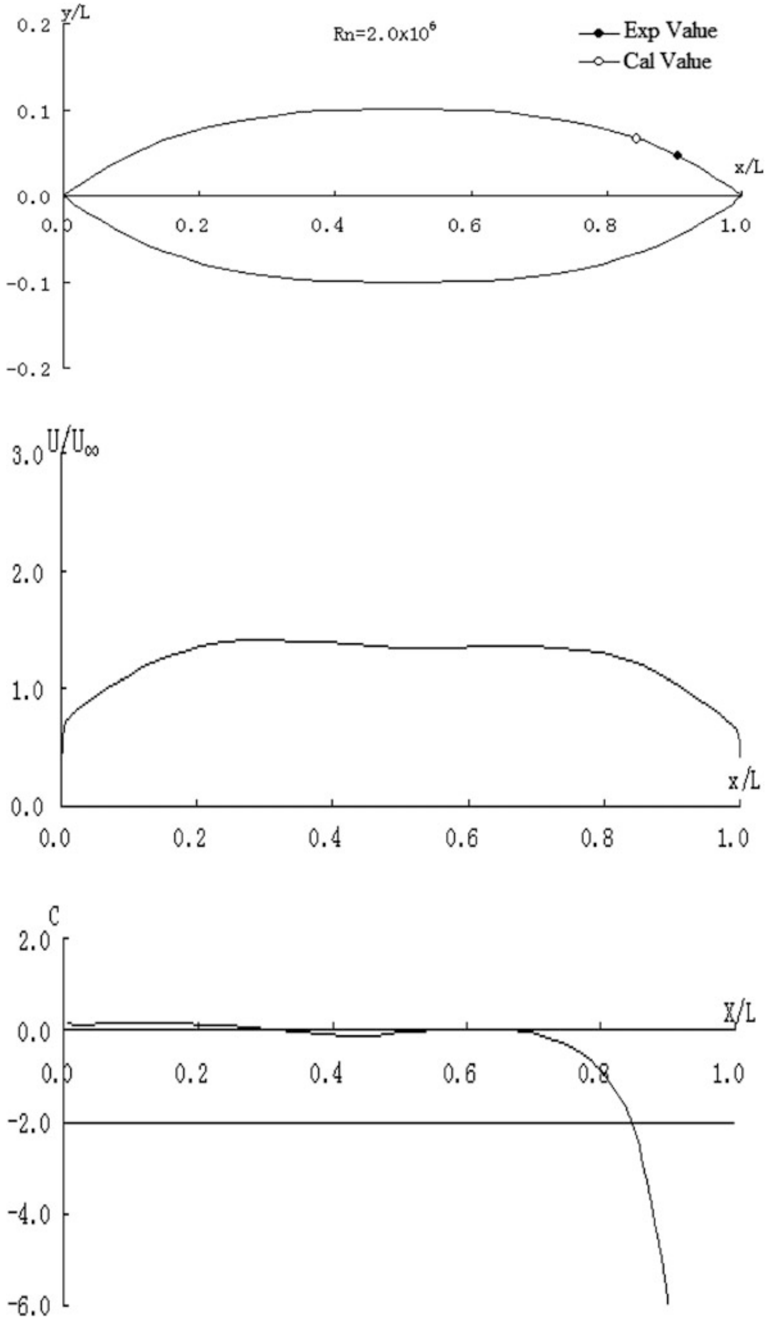

Fig. 5.67 Two-dimensional turbulent separation point

points obtained from various airfoils are compared with the experimental ones by using this discriminant, the difference is great, which may not be able to obtain a stable result. However, it is still of some significance to use the two-dimensional separation discriminant including the influence of *Rn* as a general criterion. In this section, the boundary layer on the streamline of ship surface is approximated, and the velocity distribution of the potential flow is calculated by Hess–Smith method.

(3) Examples

Figure 5.68 is the streamline velocity distribution and curve C of the S60 hull in full load waterline. From the figure, the distribution curve C near the hull bow is not equivalent to -2, so the separation will not occur and there is a phenomenon of separation and attachment near the stern. Accordingly, the turbulent separation domains obtained from the separation and identification of the streamlines are

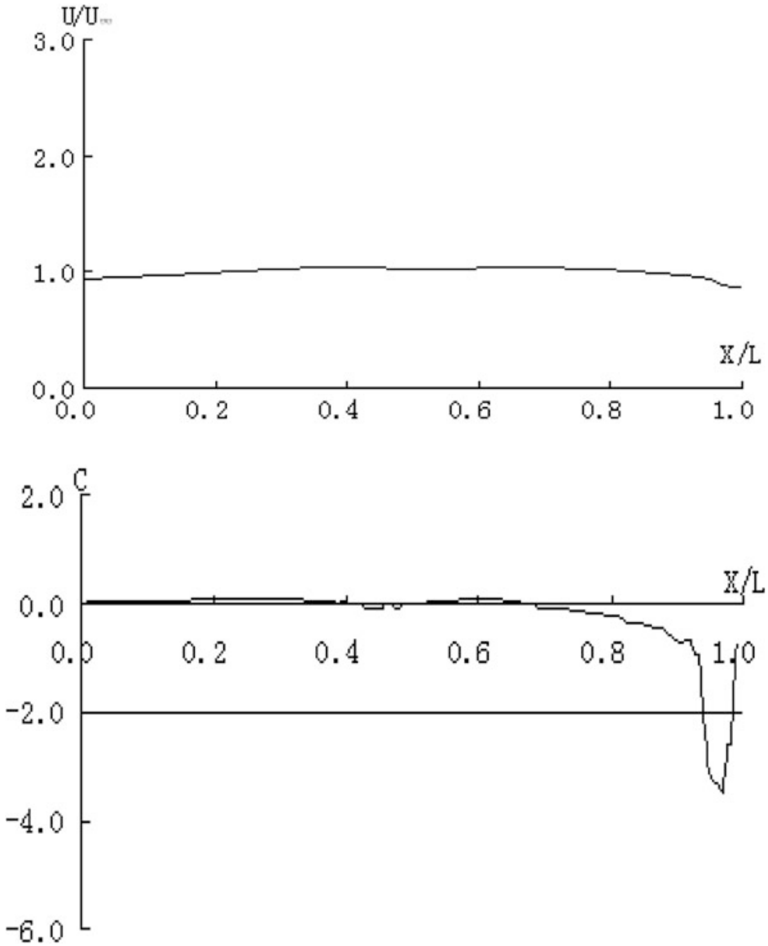

Fig. 5.68 Velocity and separation distribution along the streamlines on the loaded draft

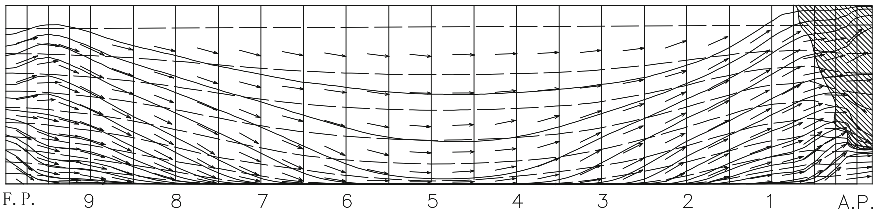

Fig. 5.69 Turbulence separation area of S60 (the original hull)

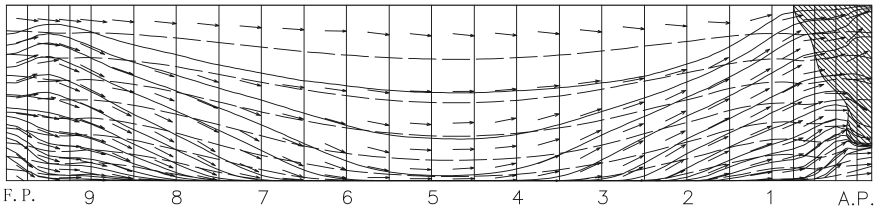

Fig. 5.70 Turbulence separation area of S60-1 (the improved hull)

shown in Figs. 5.69 and 5.70. In the figure, the shadow area is the range of separation, while Fig. 5.69 shows the separation domain of original ship with an area of 3.446, and Fig. 5.70 shows the separation domain of the modified hull with an area of 3.304. Comparing the size of separated domains (Lateral projection area) in the two figures, it can be found that the separation domain of optimized ship is smaller than the initial ship type. It can be concluded that the viscous resistance does not increase significantly during the ship-type optimization with wave resistance as the main objective function.

5.6 Ship Model Towing Test Results

The ship model towing tests were made in the towing tank of Shanghai Ship and Shipping Research Institute. There are two ship models used in the test, the parent ship-series 60 and the modified ship form S60-1 obtained by theoretical optimization. The tests, aiming to verify the reliability of the optimization theory, adopted bounded ship model, and ignored the effort of heave and pitch. Main dimensions of models are 3.0 m in length, 0.4005 m in width, and 0.1605 m in draft. In the test, we set 3 mm in height torrent nail at interval of 10 mm at 9.5 station of the ship model.

The resistance value of the ship model (R_{tm}) is measured by an electricity resist graph (NS-30) imported from Japan. Its maximum range is 10 kg (100 N) and the accuracy of it is 0.1%. The recording system is composed by high-speed data acquisition card, amplifiers, and IPC. Then, the collected data will be input into computers for calculation. Total resistance in test results is calculated by three-dimensional conversion method and the flat friction coefficient is calculated by the 1957 ITTC formula.

The total drag coefficient of ship model,

$$C_{tm} = C_{fm}(1+k) + C_{wm} \tag{5.23}$$

The total drag coefficient of the ship,

$$C_{ts} = C_{fs}(1+k) + C_{wm} \tag{5.24}$$

where the subscripts m and s represent the ship model and the ship, respectively.

$$C_{wm} = C_{ws} \tag{5.25}$$

Therefore, we can get the total drag coefficient of the real ship.

The total resistance of the ship

$$R_{ts} = \frac{1}{2}\rho_s S_s v_s^2 C_{ts} \tag{5.26}$$

The wave resistance of the ship,

$$R_{ws} = R_{ts} - R_{fs} \tag{5.27}$$

The results of total resistance and wave-making resistance of the modified ship (Series 60-1) and the mother ship (Series60) are shown in Figs. 5.71 and 5.72. In the vicinity of the design speed point, the total resistance and wave-making resistance of the modified ship were significantly improved than the mother ship. It is

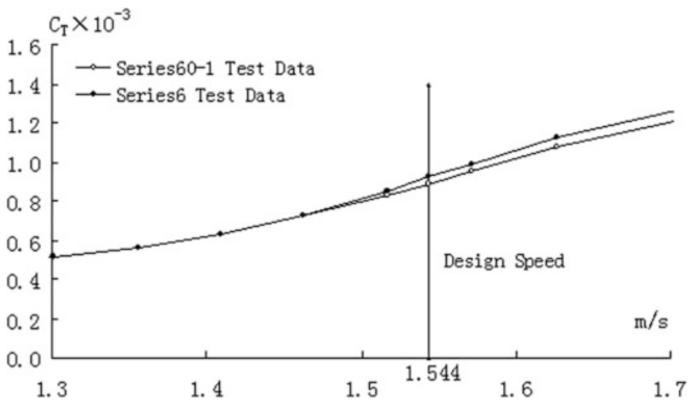

Fig. 5.71 Comparison of total resistance coefficient test results

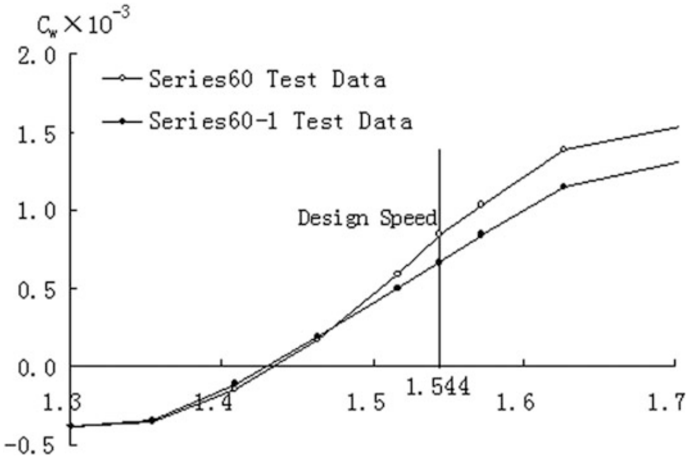

Fig. 5.72 Comparison of wave resistance coefficient test results

consistent with theoretical calculation results by reducing 3.5 and 21%, confirming the applicability of the method.

This section is based on the Rankine source method for wave resistance of potential flow and the total resistance as the objective function. The total resistance is expressed by the sum of the wave resistance and the equivalent plate friction resistance. Taking the parameters of the ship modification function as the design variables, under the condition of ensuring the displacement as the basic constraint, the SUMT interior point method in nonlinear programming method is used to optimize the line shape of the whole ship. Changes in stern profile may cause increased viscous drag. Therefore, in this section, the method of minimizing the wave-making resistance is adopted under the condition of controlling the tail-separating domain, and uses the simple two-dimensional separation criterion for the initial model and the modified model, respectively, to find the separation points on each streamline, seek out the separation domain, and determine whether the modified separation of the ship is larger than the initial shape of the ship. If the separation domain does not change much, it can be considered that the viscous resistance does not increase obviously when ship hull optimization is carried out with wave resistance as the main objective function.

5.7 Discussion on Practicability of Optimal Ship Form

In this section, based on the theory of wave-making resistance (Michell integral method and Rankine source method), this paper studies the optimization of minimum wave-making resistance and minimum total resistance based on nonlinear programming method and genetic algorithms, the modified ship type obtained has obvious resistance reduction effect, but whether the optimal ship type is a practical ship type requires further discussion.

Judging whether an optimal ship is a practical ship depends not only on its resistance reduction effect, but also on whether the line shape of the modified ship meets the actual requirements. For the examples in this section: For the Wigley type (design Fr = 0.35), S60 ship model (design Fr = 0.285), Michell integral method combined with nonlinear programming method is used to optimize and calculate, the wave resistance of the modified ship is reduced by 35.5% and 25.4%, respectively; the total resistance decreased by 9.2% and 27.4%, respectively. The effect of resistance reduction is obvious, but their linear variations are exaggerated. Such a linear pattern may be suitable for some cargo-loaded ships, but may not be suitable for some solid cargoes, bulk cargoes, such as containers and timber. In order to obtain a practical ship type, it is necessary to add additional constraints to control the change of the contour line and re-optimize the calculation. For Wigley type model (design Fr = 0.35), S60 ship model (design Fr = 0.285), Rankine source method combined with nonlinear programming method to optimize, and the wave resistance of the modified ship is reduced by 13.5% and 23.4%, respectively; the total resistance decreased by 4.3% and 9.8%, respectively. Although the speed of optimization calculation of this method is not as fast as that of the Michell integral method, it is much faster than the CFD technique. More importantly, the modified ship model obtained by this method not only has the obvious resistance reduction effect, but also does not change sharply; it is smooth, close to the actual ship type. The original intention of the ship-type optimization is to make a small modification to the given mother ship to achieve the purpose of reducing the resistance. Therefore, this optimization method can provide ship designers with the theoretical basis and technical support for optimizing hull line.

The reason why ship-type optimization based on Michell integral method gets more exaggerated shapes in all kinds of shapes is that, except the reason of theory itself, the selected design variables in the optimization are the direct ship-type value points. The design variables are discrete points, which are more flexible and free and less restrictive. Although the shape of the optimal ship is more exaggerated, lacking in practical significance, it is of great significance to clear the direction of optimization and guide the design modification.

The design variables used for ship-type optimization based on Rankine source method are the parameters of the ship-type modification function. The ship-type modification function has too much limitation on the optimal design range and can still maintain the shape of the original ship type. Therefore, the optimized ship type will not be too bizarre. Based on the Rankine source method for ship-type optimization, in addition to the obvious reduction effect of the modified model obtained at the designed speed point, the effect of reducing resistance at other speed points is also obvious because the actual speed of the ship does not necessarily reach the designed speed Therefore, it is of practical significance to obtain the minimum resistance ship model within a certain range of design speed. So the optimal ship form is relatively close to practical ship type, and the method has more practical significance for researching ship-type optimization.

References

1. Gross A,Watanabe K (1972) Form factor. In: Proceedings of 13th ITTC
2. Guo XD, Jichun Y, Wang ZL (2006) Optimization of mishap section strcture of large crude oil carrier based on genetic algorithm. J Jiangsu Univ Sci Technol (Natl Sci Ed) 20(1):1–6
3. Suzuki K, Iokamori N (1999) Studies on minimization of wave making resistance based on Rankine source method. Kansai Soc Nav Archit Jpn (185): 9–19. (in Japanese)
4. Faltinsen OM (2007) Hydrodynamics of high-speed marine vehicles. National Defense Industry Press, Beijing
5. Ichiro T, Yoji H. (1969) On velocity distribution and local skin friction of two-dimensional turbulent boundary layer with pressure gradient. Kansai Soc Nav Archit Ocean Eng Jpn (132): 43–47. (in Japanese)

Chapter 6
Hull Form Optimization Based on the CFD Technique

6.1 Introduction

Based on the RANS solver, the aim of this section is to present several ship hull form optimization loops in the calm water and in waves. Taking the DTMB5415 and Wigley III ships as examples, the total resistance of a ship in calm water or in waves is regarded as the objective function. Four variables with three points are used to modify the bow section located on the hull by utilizing the arbitrary shape deformation (ASD) technique. Some improved optimizers are employed to optimize these two ships. Finally, the performance of the original and optimal ships is compared in order to illustrate the drag reduction effect. The research approaches in this section can lay a theoretical foundation for the "green ship hull form" design.

6.2 Optimization Problem

6.2.1 Objective Function

The optimization loops presented in this section are employed to find an optimal ship hull form with a minimum total resistance (expressed by using the total resistance coefficient below) at design speed in calm water or in waves. Herein, C_{tc} is the total resistance coefficient in calm water, and C_{tw} is the total resistance coefficient in waves.

6.2.2 Design Variables

The bow section is altered by using four design variables (a_{11}, a_{12}, a_{21}, a_{22}; $b_{11,}$ $b_{12,}$ $b_{21,}$ b_{22}) with three control points (point 1 to point 3; point 4 to point 6, as shown in

© Shanghai Jiao Tong University Press, Shanghai and Springer Nature Singapore Pte Ltd. 2019

B.-J. Zhang and S.-L. Zhang, *Research on Ship Design and Optimization Based on Simulation-Based Design (SBD) Technique*,
https://doi.org/10.1007/978-981-10-8423-2_6

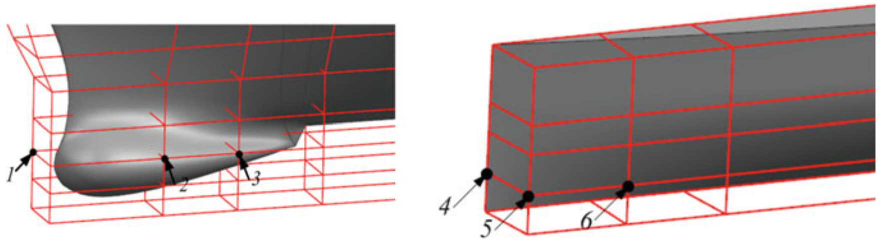

(a) DTMB5415

(b) Wigley

Fig. 6.1 ASD volume built around the hull surface

Table 6.1 Design variables for the two ships

	Design variables							
	DTMB5415 ship				Wigley III ship			
Parameters	a_{11}	a_{12}	a_{21}	a_{22}	b_{11}	b_{12}	b_{21}	b_{22}
No.	1	1	2	3	4	5	6	4
Movement direction	x	z	y	y	x	y	y	z

Fig. 6.1) for each ship. a_{11} and b_{11} are moved along the x-direction; a_{21}, a_{22}, b_{12} and b_{21} are moved along the y-direction; and a_{12} and b_{22} are moved along the z-direction. The range of these design variables is summarized as follows (Table 6.1).

6.2.3 Constraint

For the DTMB5415 ship, the displacement is changed lower than 1%, as shown below:

$$\left|\frac{\Delta_{new} - \Delta_{org}}{\Delta_{org}}\right| \leq 0.01$$

where -$_{org}$ means the original ship, and -$_{new}$ means the modified ship.

For the Wigley III ship, no constraint is considered during the whole optimization.
Optimizer: Hybrid optimization algorithm//IPSO algorithm.
Objective function evaluation method: Numerical simulation based on the RANS solvers//Resistance prediction by using the approximate technique.

6.3 Optimization Framework

Figure 6.2 shows an overview of the optimization design process. The essential steps are summarized as follows:

(1) Change the design variables using the optimization algorithm.
(2) Change the shape of the ship hull form geometry using the ASD technique according to the present design variables.

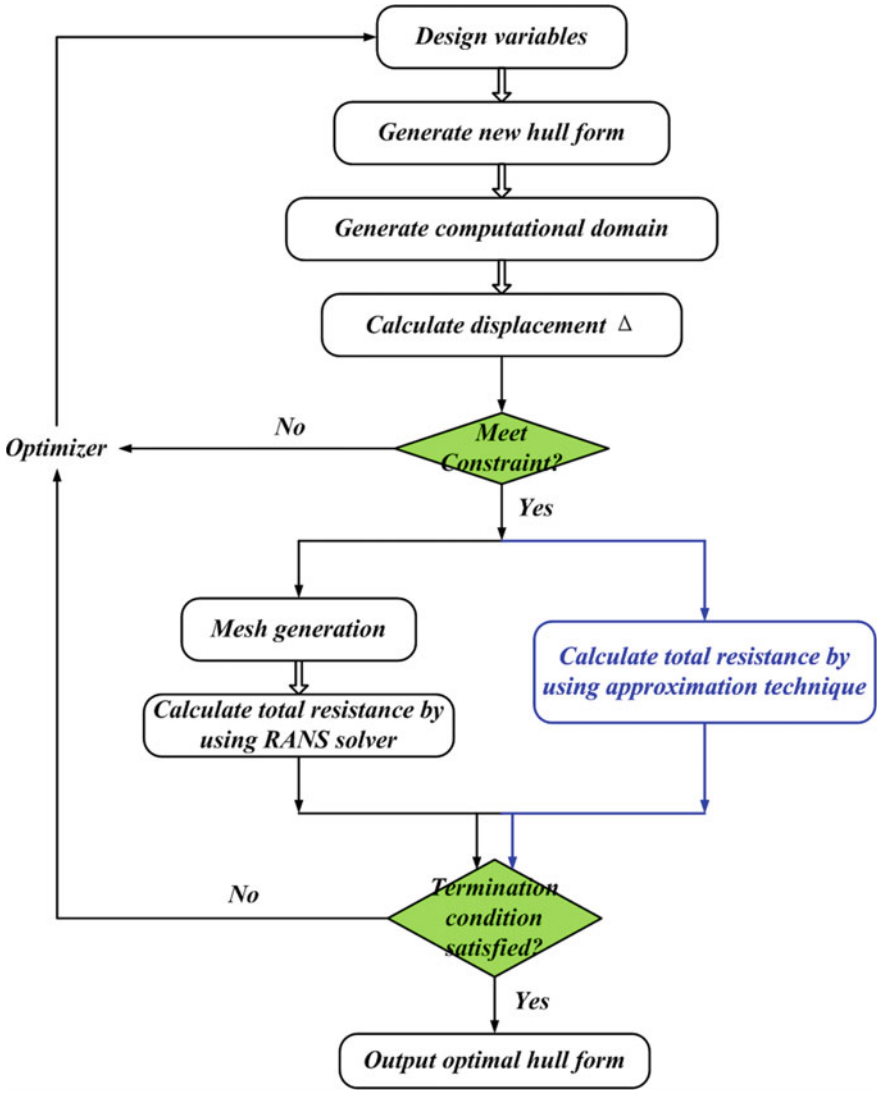

Fig. 6.2 Flowchart of the ship design optimization

(3) Calculate the displacement of the new hull form, and return to Step 1 until the displacement is met.
(4) Calculate the total resistance of the ship in calm water or in waves using the RANS solver or the approximation technique.
(5) Save the total resistance coefficient.
(6) Repeat Steps 1–5 until the convergence is met. Then output the optimal hull form.

6.4 Hull Form Optimization Based on the RANS-CFD Technique

6.4.1 Hull Form Optimization in Calm Water Using the IPSO II Algorithm

In order to reduce total resistance of a ship, an optimization framework for sonar dome optimization was presented in this section. The total resistance in calm water was selected as the objective function, and the RANS-CFD method was used to calculate the total resistance of a DTMB5415 ship. In order to improve the efficiency and smoothness of the geometric reconstruction, the arbitrary shape deformation (ASD) technique was introduced to change the shape of the sonar dome. To improve the global search ability of the particle swarm optimization (PSO) algorithm, an improved particle swarm optimization (IPSO) II algorithm was proposed to set up the optimization model. After a series of optimization analyses, the optimal hull form was found. It can be concluded that the simulation-based design framework built in this section is a promising method for sonar dome optimization.

6.4.1.1 Algorithm Verification

To verify the applicability of the IPSO II algorithm, four functions shown in formulas (6.1)–(6.4) are studied. The PSO and IPSO II algorithms are used to find the minimum value of each of the four functions.

$$f_1(x) = \sum_{i=1}^{D-1} \left(100\left(x_{i+1} - x_i^2\right)^2 + (x_i - 1)^2 \right) \tag{6.1}$$

Table 6.2 Comparison of optimization results

Functions	D	Minimum value	PSO	IPSO II
$f_1(x)$ (Rosenbrock)	10	0	8.6224	0.6657
$f_2(x)$ (Schaffer)	10	0	0.009716	0.009716
$f_3(x)$ (Rastrigrin)	10	0	16.9250	2.9855
$f_4(x)$ (Griewank)	10	0	1.0277	$2.481\mathrm{e}^{-09}$

$$f_2(x) = 0.5 + \frac{\sin^2\left(\sqrt{\sum_{i=1}^{D} x_i^2}\right) - 0.5}{\left[1.0 + 0.001\left(\sum_{i=1}^{D} x_i^2\right)\right]^2} \tag{6.2}$$

$$f_3(x) = \sum_{i=1}^{D} \left(x_i^2 - 10\cos(2\pi x_i) + 10\right) \tag{6.3}$$

$$f_4(x) = \frac{1}{4000}\sum_{i=1}^{D} x_i^2 - \mathop{\Pi}_{i=1}^{D} \cos\left(\frac{x_i}{\sqrt{i}}\right) + 1 \tag{6.4}$$

Table 6.2 provides a comparison of the optimization results with the two algorithms. Figure 6.3 shows the iterative process. The optimization results show that the results obtained from the three functions, $f_1(x)$, $f_3(x)$ and $f_4(x)$, using the IPSO II algorithm are much closer to the theoretical values with a faster convergence rate in the initial optimization, and the results of these functions obtained by using the PSO algorithm have got trapped in a local optimum (Fig. 6.3a, c, and d), especially for multi-modal functions $f_3(x)$ and $f_4(x)$. Although both algorithms produce almost the same results in Fig. 6.3b, the IPSO II algorithm has a faster convergence speed. It can be concluded that the IPSO II algorithm has better performance and faster convergence speed for optimization, especially for multi-optimization problems.

6.4.1.2 Comparison of Results and Discussion for the Hull Form Optimization

Figure 6.4 shows the comparison of total resistance coefficients C_{tc} for the optimal hull and parent hull with the change of Fr in calm water. The figure shows that the total resistance decreases at all speeds and that it decreases more in design speed and high speed.

Figure 6.5 presents body plans of optimal hull and the parent hull, which show that the hull lines are smooth and slightly concave. Figure 6.6 compares the wave profile for optimal hull and the parent hull at y/L = 0.105 (h represents the depth of the water). It is shown that the amplitude of the waves has been reduced, which

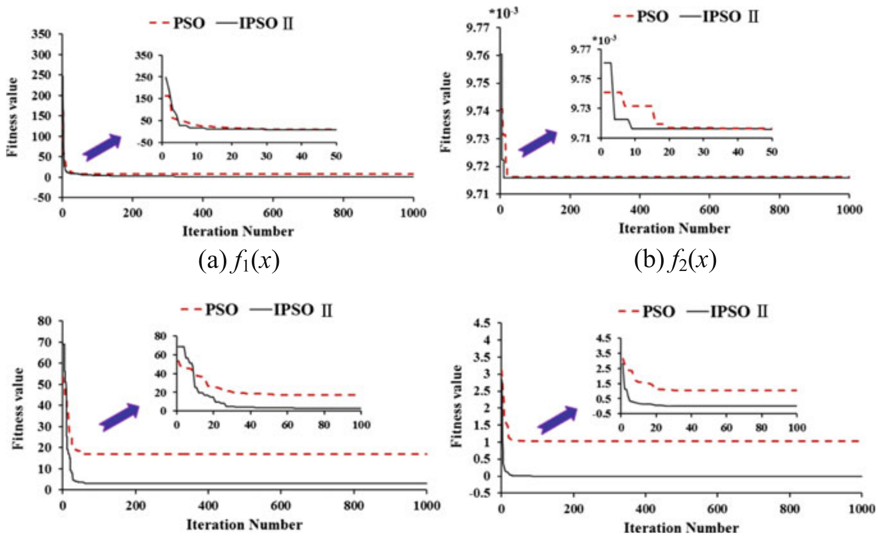

(a) $f_1(x)$ (b) $f_2(x)$

(c) $f_3(x)$ (d) $f_4(x)$

Fig. 6.3 Optimization process

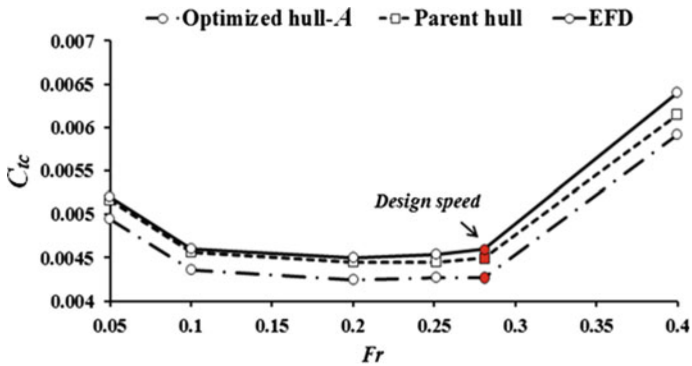

Fig. 6.4 C_{tc} changes with the Fr for optimal hull and parent hull

indicates a reduction in total resistance for optimal hull. Figures 6.7 and 6.8 present a comparison of wave patterns and static pressure for the optimal and parent hulls, respectively. Optimal hull has a smaller splash than the parent hull near the bow, as shown in Fig. 6.7. The pressure distribution of the sonar dome undergoes a significant change, as shown in Fig. 6.8.

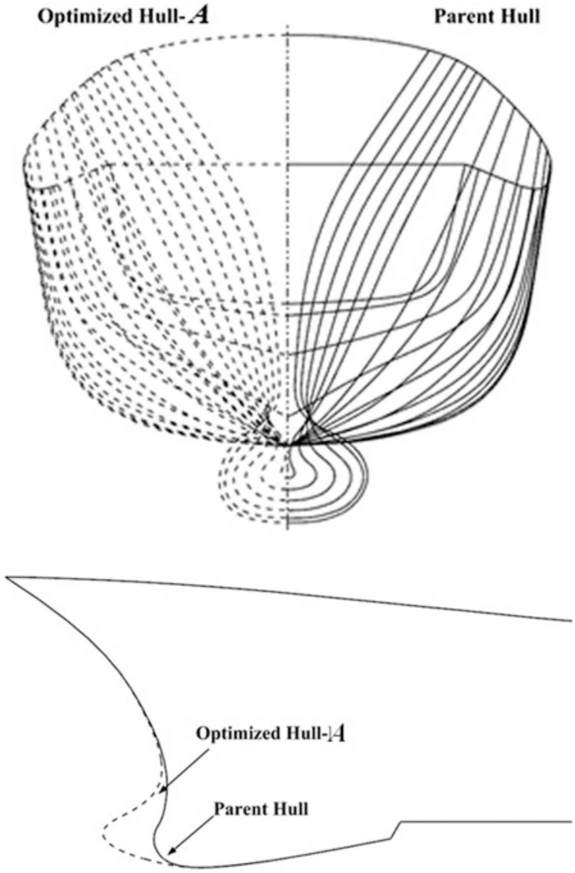

Fig. 6.5 Comparison of body plans

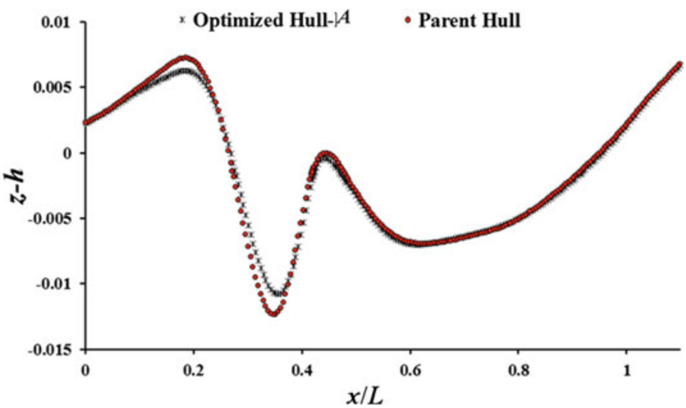

Fig. 6.6 Comparison of wave profile at $y/L = 0.105$

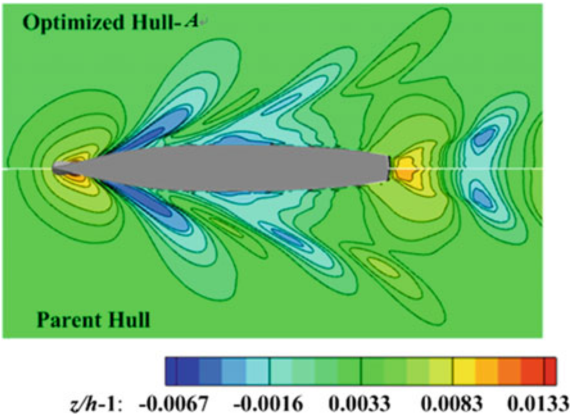

Fig. 6.7 Comparison of wave patterns

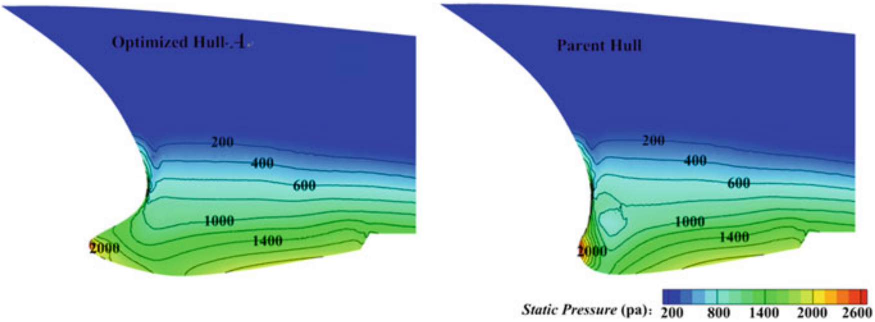

Fig. 6.8 Comparison of static pressure

6.4.2 Hull Form Optimization in Waves Using the Hybrid Algorithm

The seakeeping behavior of a ship in waves is different from its behavior in calm water. The resistance and seakeeping performance of a ship must be considered in the early-stage design. Therefore, this section proposes a hull form optimization framework aiming to achieve the minimum total resistance in waves using a computational fluid dynamics (CFD) technique. A sinusoidal wave was adopted to establish the numerical wave tank, and the overset mesh technique was used to facilitate the motions of the ships in question. The total resistance of the hull in waves was regarded as the objective function which was calculated using the Reynolds-averaged Navier–Stokes (RANS) method. The arbitrary shape deformation (ASD) technique was used to change the geometry. Under displacement and design variables, a hybrid algorithm was developed to evaluate the objective function combining the optimal Latin hypercube design (Opt LHD) and the non-linear programming by quadratic Lagrangian (NLPQL) algorithm. Finally, two examples of hull form optimization were presented and discussed for David Taylor Model Basin (DTMB) model 5415 and Wigley III cases. The results show the effectiveness of the optimization framework developed in the present study can lay the foundation for further optimization of full-scale ships.

6.4.2.1 Data Preparing

The first step of optimization is the design of experiments (DOE) for the hybrid optimization algorithm. DOE can explore the influence of the four parameters effectively. After the DOE, a set of design variables with minimum total resistance coefficients can be selected as the initial point of the NLPQL algorithm. This step can improve the optimization accuracy of the NLPQL algorithm which has been verified below. Table 6.3 indicates the wave conditions used in this paper, and Case 2 and Case 5 are used to optimize the DTMB5415 and Wigley III ships, respectively. Tables 6.4 and 6.5 show the DOE numerical results by using Opt LHD method for the DTMB5415 and Wigley III ships. Figures 6.9 and 6.10 show the space distributions of samples.

6.4.2.2 Optimization and Numerical Results Analysis

Table 6.6 shows the optimization results. It can be seen from the table that the total resistance decreases, respectively, by 3.71% and 4.41% for the DTMB5415 and Wigley III ships, which also signifies the effect of the new bow toward the reduction in resistance. Due to the optimized bow shape, insignificant differences have been seen for TF_3 and TF_5 between the original hull and optimal hulls.

In the table, TF_3 and TF_5 are the heave transfer function and pitch transfer function, respectively.

Since the new bow of the optimized hull-B changes the displacement of the ship, the resistance comparison per unit of displacement has been carried out and details are provided in Table 6.7. From the table, it can be seen that the total resistance

Table 6.3 Wave conditions

	Case no.	Fr	Wave steepness ak	λ/L_{pp}	Encounter freq. f_e (Hz)
DTMB5415	1	0.19	0.025	1	1.0562
	2	**0.28**	**0.025**	**1**	**1.2176**
	3	0.34	0.025	1	1.3251
Wigley III	4	0.2	0.023	1	1.0827
	5	**0.3**	**0.023**	**1**	**1.2636**
	6	0.4	0.023	1	1.4442

Table 6.4 Samples of DTMB5415 ship by Opt LHD

No.	a_{11}	a_{12}	a_{21}	a_{22}	C_{tw1}
1	−0.0201	−0.02442	0.0623	−0.0479	0.004599
2	−0.2533	−0.03809	0.0573	−0.0468	0.004543
3	−0.1065	−0.09362	−0.1148	0.0884	0.004564
4	−0.201	−0.02528	−0.0143	−0.0214	0.004503
5	−0.3075	−0.08337	−0.0721	−0.1115	0.004651
6	−0.2432	−0.01503	−0.145	−0.019	0.004509
7	−0.3176	−0.0808	−0.0759	−0.0329	0.004554
8	−0.0422	−0.00392	−0.1136	0.0769	0.004626
9	−0.0683	−0.10131	−0.0683	−0.0075	0.004643
10	−0.203	−0.13975	0.0824	0.0561	0.004658
…	…	…	…	…	…
…	…	…	…	…	…
197	−0.3437	−0.06286	0.0673	0.0792	0.004563
198	−0.3276	−0.07739	0.0523	0.0098	0.004564
199	−0.2854	−0.10387	−0.0043	0.033	0.00453
200	−0.0121	−0.08764	0.0611	0.0353	0.004685

Table 6.5 Samples of Wigley III ship by Opt LHD

No.	b_{11}	b_{12}	b_{21}	b_{22}	C_{tw2}
1	−0.0369	−0.061	−0.5494	−0.00275	0.005321
2	−0.3791	−0.6747	−0.5237	0.04178	0.005138
3	−0.0932	−0.0161	−0.7357	0.00361	0.005363
4	−0.3068	−0.2924	−0.2731	0.03976	0.005150
5	−0.249	−0.7229	−0.0867	0.04294	0.005174
6	−0.008	−0.1221	−0.3373	0.036	0.005252
7	−0.3936	−0.1896	−0.3502	0.02993	0.005132
8	−0.1044	−0.1542	−0.5783	0.01287	0.005265
9	−0.2506	−0.4305	−0.1382	−0.00969	0.005189
10	−0.0369	−0.061	−0.5494	−0.00275	0.005174
…	…	…	…	…	…
…	…	…	…	…	…
197	−0.2426	−0.7357	−0.0964	0.00477	0.005225
198	−0.2795	−0.6683	−0.0225	0.02414	0.005140
199	−0.3598	−0.1124	−0.5558	0.03022	0.005151
200	−0.2153	−0.71	−0.5398	−0.00448	0.005311

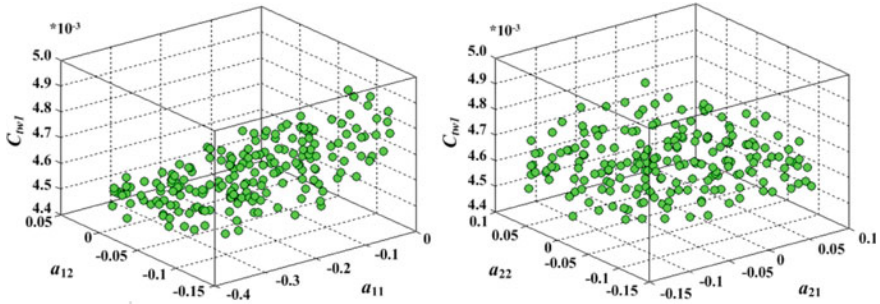

Fig. 6.9 Samples of the DTMB5415 case

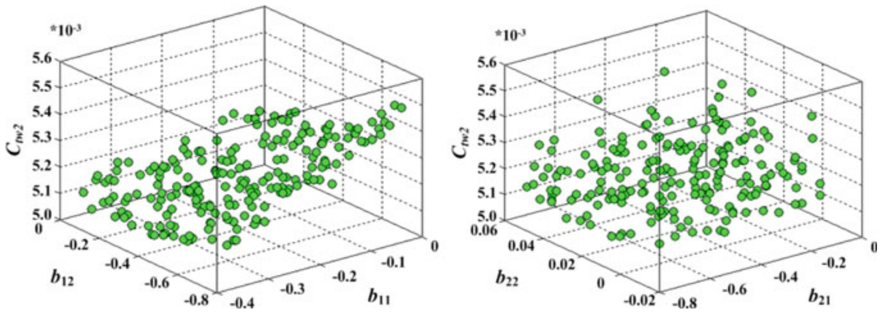

Fig. 6.10 Samples of the Wigley III

Table 6.6 Optimization results

Optimal ships	Fr	$\frac{C_{tw-org}}{C_{tw-opt}}$	$\frac{\Delta_{org}}{\Delta_{opt}}$	$\frac{TF_{3-org}}{TF_{3-opt}}$	$\frac{TF_{5-org}}{TF_{5-opt}}$
Optimized Hull-A	0.28	1.0385	1.0069	0.9918	1.0361
Optimized Hull-B	0.30	1.0461	0.9944	0.9979	1.0387

Table 6.7 Resistance comparisons per unit displacement

Fr	*Original Hull*	*Optimized Hull-B*	Reduction%
0.2	$6.284 * 10^{-5}$	$5.916 * 10^{-5}$	5.85
0.3	$6.772 * 10^{-5}$	$6.437 * 10^{-5}$	4.94
0.4	$7.280 * 10^{-5}$	$6.907 * 10^{-5}$	5.12

coefficient decreases by 4.94% at $Fr = 0.3$, and the effect of a new bow for reduction in resistance coefficient is even greater when $Fr = 0.2$.

Figures 6.11 and 6.12 show a comparison of bow sections for the original hull and the optimal hulls. It can be seen that the hull lines of the optimal hulls are smooth which indicates the validity of the ASD method for changing the geometry.

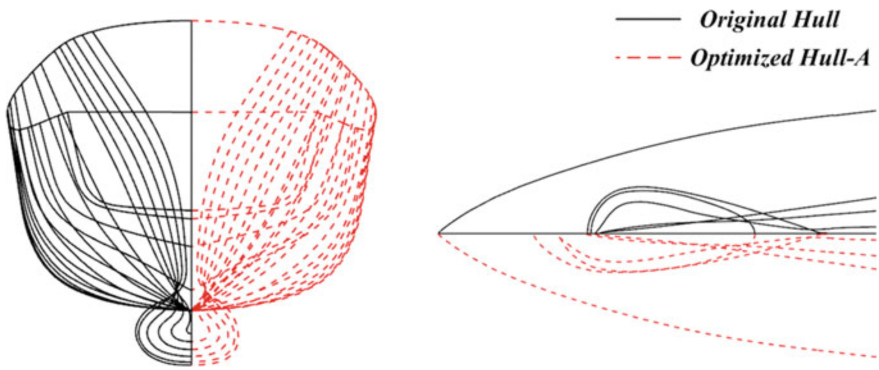

Fig. 6.11 Comparison of geometry for original hull and the optimized hull-A

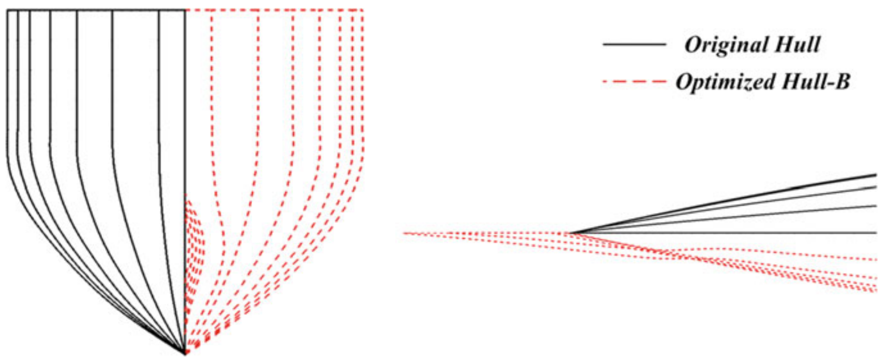

Fig. 6.12 Comparison of geometry for original hull and the optimized hull-B

Figure 6.13 presents the convergence history between the hybrid algorithm and the NLPQL algorithm. It can clearly be seen that the resistance reduction effect is better with the hybrid algorithm than the NLPQL algorithm.

Figure 6.14 shows the changes of the total resistance coefficients along with the *Fr* [1–4]. As can be seen from the figures, the optimal hulls have the satisfactory resistance reduction effectiveness at different *Fr* not only for the DTMB5415 ship but also for the Wigley III ship. And the resistance reduction is greater at $Fr = 0.34$ and $Fr = 0.2$ for the DTMB5415 and Wigley III ships, respectively. Figures 6.15 and 6.16 show the TF_3 and TF_5 for the original hull and the optimal hulls at different values of *Fr*.

Figure 6.17 shows the comparison of the static pressure between the original and the optimal hulls in an encounter period. The two ships have the smallest fore draft at $t/T = 0.25$ and the biggest fore draft at $t/T = 0.75$, which is the same as the actual situation.

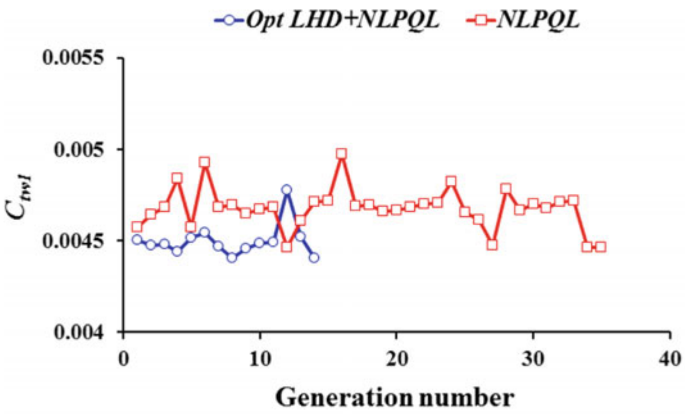

(a) DTMB5415 ship

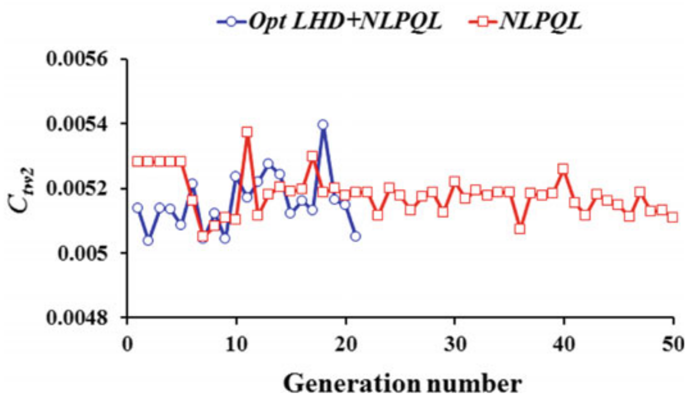

(b) Wigley III ship

Fig. 6.13 Evolution history of total resistance coefficients

Figure 6.18 shows the wall shear stress on the bow surface of both the original hull and the optimized hull-A in an encounter period. As shown in the figure, the change in the ship's bow shape has affected the pressure distribution on the bow surface. In the case of the optimized hull-A, the pressure has been decreased significantly, which results in the decrease of the total resistance.

Figure 6.19 shows the comparison of wave contours for the original hull and the optimal hulls in an encounter period. As can be seen from the figure, the new bow shape of optimal hulls has reduced the bow waves and shoulder waves which results in the reduction of the total resistance.

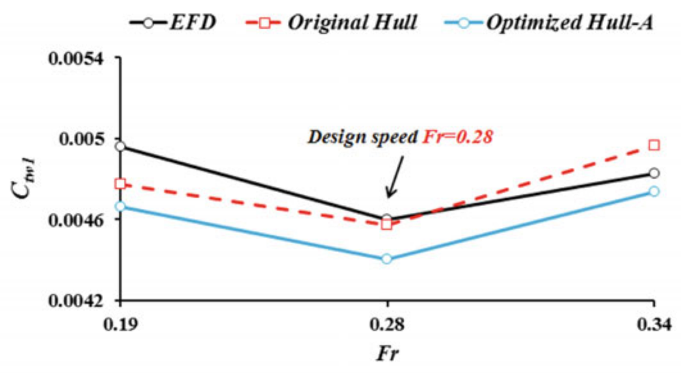

(a) DTMB5415 ship

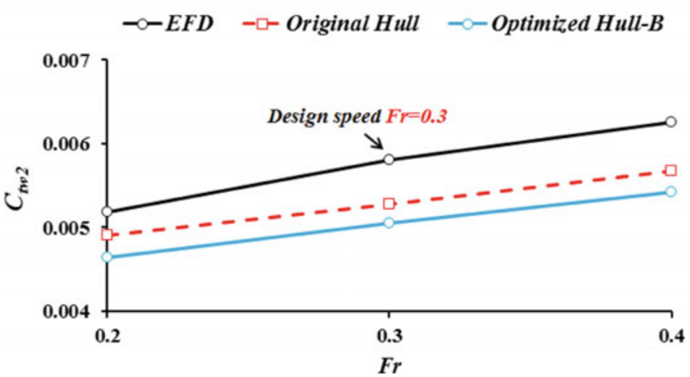

(b) Wigley III ship

Fig. 6.14 Total resistance coefficients change with *Fr*

6.5 Hull Form Optimization Based on the Approximate Technique

6.5.1 Hull Form Optimization Based on the IPSO I-BP Algorithm

In order to improve the convergence and precision of particle swarm optimization (PSO) algorithm and avoid falling into local optimal solution, an improved particle swarm optimization (IPSO) I algorithm was put forward to solve the optimization problem of hull form. The arbitrary shape deformation (ASD) technique was used to modify the sonar dome. To improve the accuracy of BP neural network (BPNN), a new method of hull resistance prediction based on IPSO I-BP neural network was proposed. The optimal Latin hypercube design (Opt LHD) was used to select samples. The IPSO I algorithm was used to optimize the weights and thresholds of

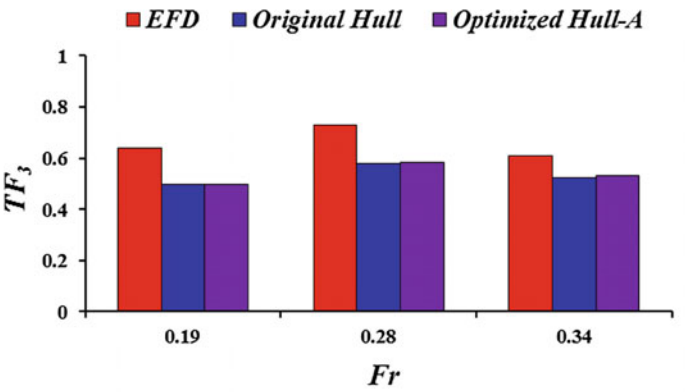

(a) DTMB5415 ship

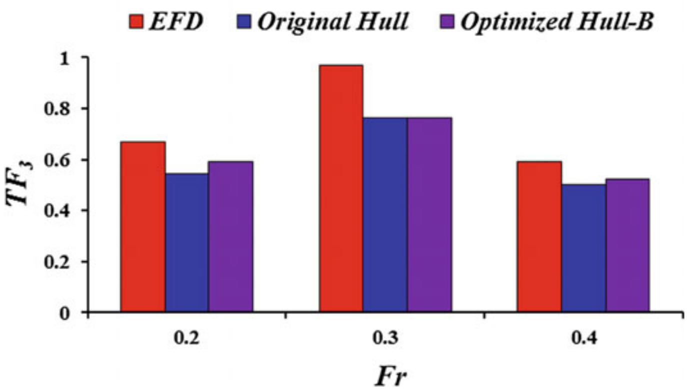

(b) Wigley III ship

Fig. 6.15 TF_3 changes with Fr

BPNN and train the BPNN. Then, the approximate optimization platform was built to explore the suitable sonar dome for DTMB5415 with IPSO I algorithm. After a series of calculation, the optimal sonar dome was found with the lowest ship hull resistance. The optimization results are shown that the approximate optimization platform presented in this section not only has high efficiency but also has high accuracy.

6.5.1.1 Samples

Table 6.8 shows the total resistance coefficients of 200 variations of the DTMB5415 model with corresponding design variables. One set of design

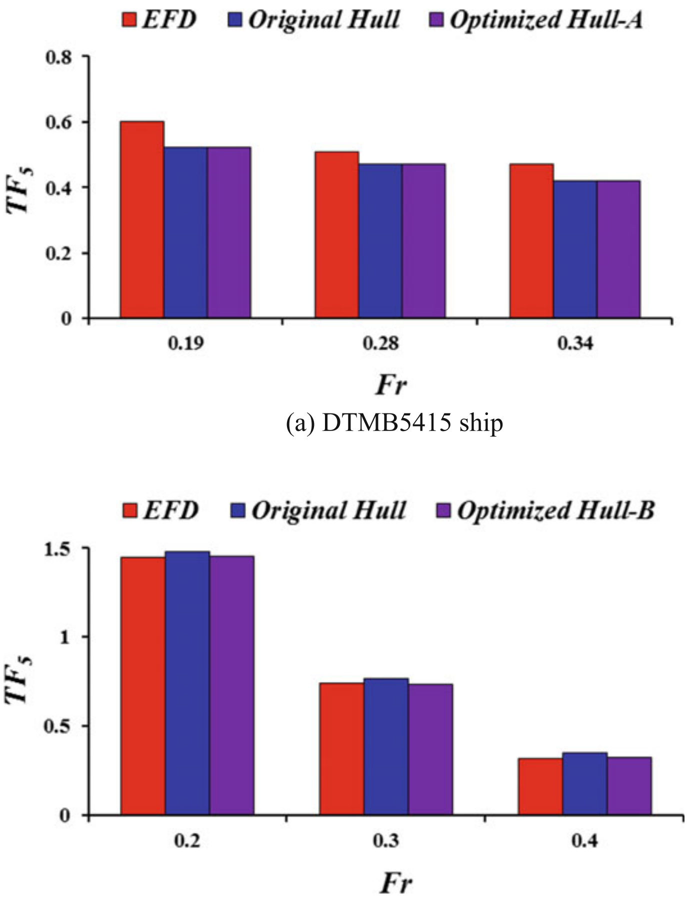

(a) DTMB5415 ship

(b) Wigley III ship

Fig. 6.16 TF_5 changes with Fr

variables represents a new ship geometry with a different sonar dome shape. Figure 6.20 indicates the space distributions of these samples.

6.5.1.2 Algorithm Evaluation

In Table 6.8, 200 samples are used to build the BP and IPSO I-BP models in order to validate the accuracy of these two algorithms. The results can be found in Fig. 6.21. The ξ is the difference between the total resistance coefficients obtained by using the neural network and the results from the CFD data.

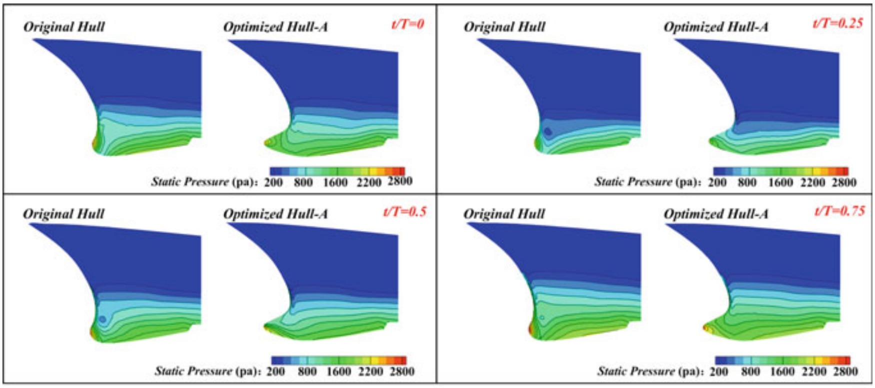

(a) DTMB5415 ship

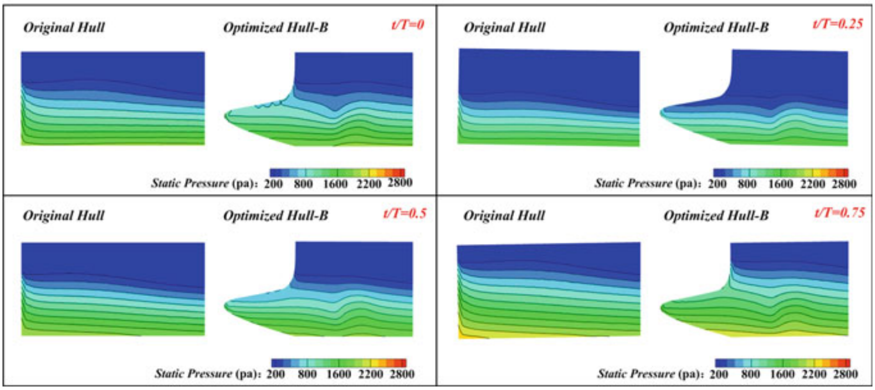

(b) Wigley III ship

Fig. 6.17 Comparison of surface pressure in an encounter period

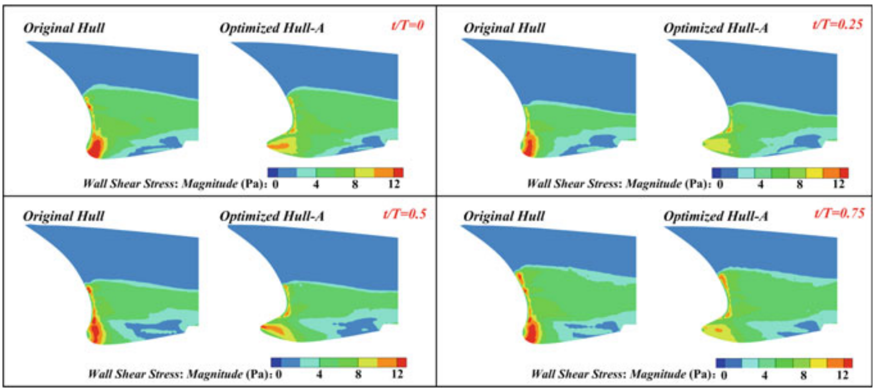

Fig. 6.18 Wall shear stress on the bow surface in an encounter period

As can be clearly seen from the figures above, two models are of good method to predict the total resistance, and the accuracy of the IPSO I-BP model is better than the BP algorithm alone.

6.5.1.3 Analysis Between Original and Optimal Hulls

After the completion on the optimization, the results are listed in Table 6.9. As seen from the table that the total resistance of the optimized hull-A is down by 5.51%, and the total resistance of the optimized hull-A1 decreases by 5.98%. The results lead to the conclusion that the IPSO I-BP has a better performance in the optimization of a ship with a high efficiency. Figure 6.22 shows the comparison of total resistance coefficients between the original and the optimal hulls as well as the experimental fluid dynamics (EFD) data. As can be seen in the figure, the total resistance of the optimized hull-B decreases at all speeds.

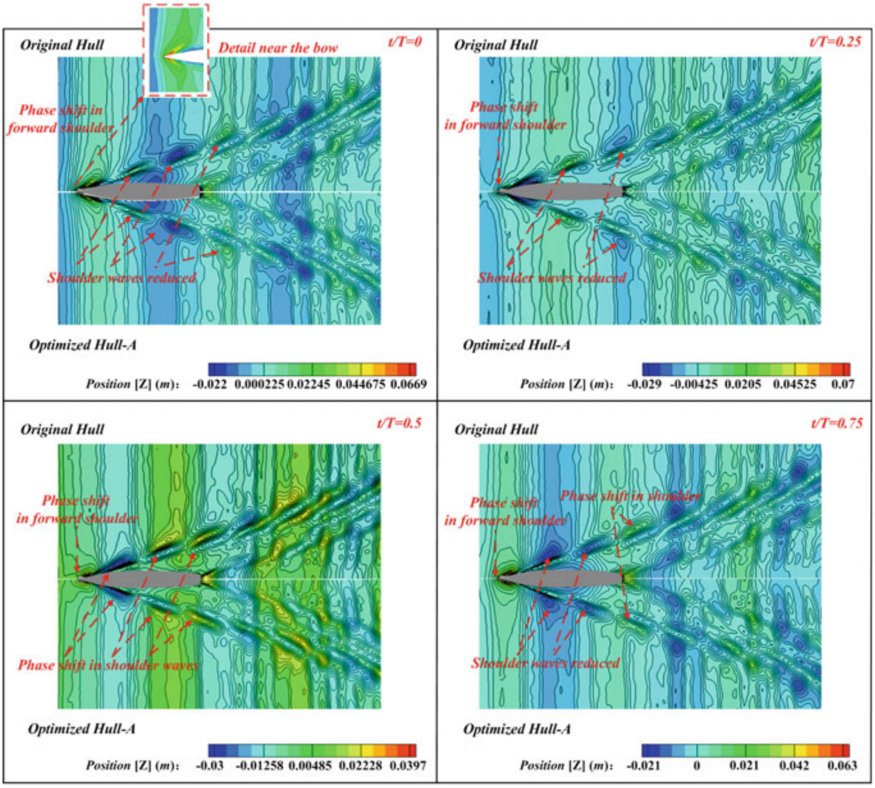

(a) DTMB5415 ship

Fig. 6.19 Details of the free surface wave contours in an encounter period

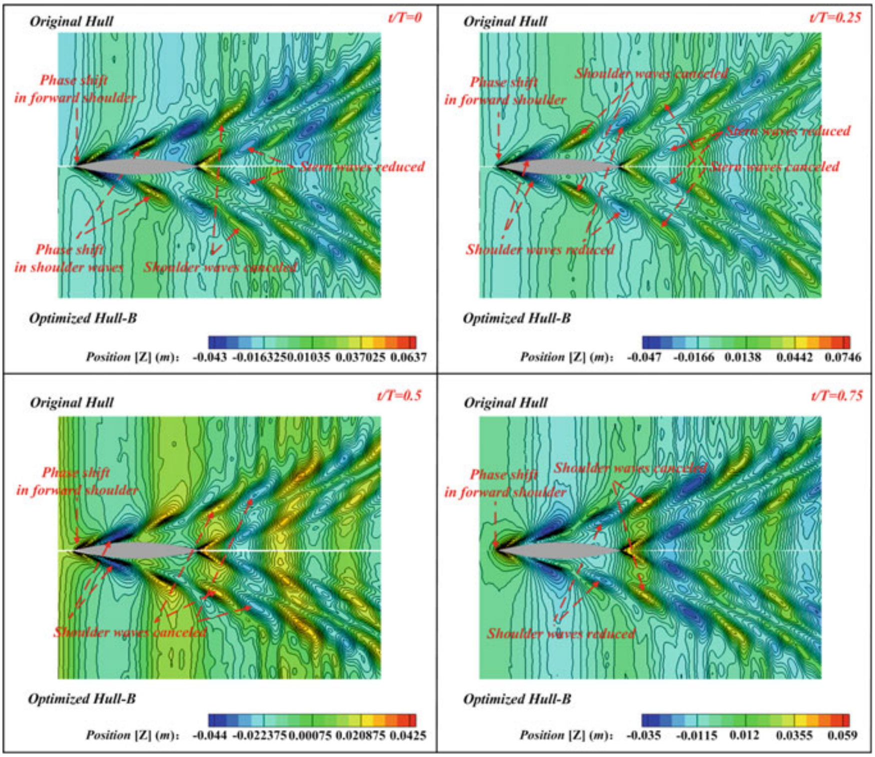

(b) Wigley III ship

Fig. 6.19 (continued)

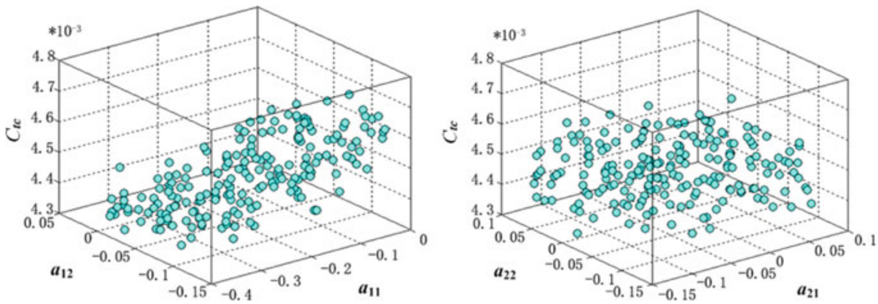

Fig. 6.20 Samples of the DTMB5415 case

Figure 6.23 presents body plans of optimized hull-A1 and the parent hull, which show that the hull lines are smooth and slightly concave. Figure 6.24 compares the wave profile for optimized hull-A1 and the parent hull at $y/L = 0.098$. It can be

Table 6.8 Samples obtained by Opt LHD

No.	a_{11}	a_{12}	a_{21}	a_{22}	C_{tc}
1	−0.0201	−0.02442	0.0623	−0.0479	0.004348
2	−0.2533	−0.03809	0.0573	−0.0468	0.004375
3	−0.1065	−0.09362	−0.1148	0.0884	0.004355
4	−0.201	−0.02528	−0.0143	−0.0214	0.004343
5	−0.3075	−0.08337	−0.0721	−0.1115	0.004454
6	−0.2432	−0.01503	−0.145	−0.019	0.004397
7	−0.3176	−0.0808	−0.0759	−0.0329	0.004363
8	−0.0422	−0.00392	−0.1136	0.0769	0.004399
9	−0.0683	−0.10131	−0.0683	−0.0075	0.004485
10	−0.203	−0.13975	0.0824	0.0561	0.004365
…	…	…	…	…	…
…	…	…	…	…	…
196	−0.2915	−0.12779	−0.057	−0.0098	0.004496
197	−0.3437	−0.06286	0.0673	0.0792	0.004364
198	−0.3276	−0.07739	0.0523	0.0098	0.004368
199	−0.2854	−0.10387	−0.0043	0.033	0.004362
200	−0.0121	−0.08764	0.0611	0.0353	0.004521

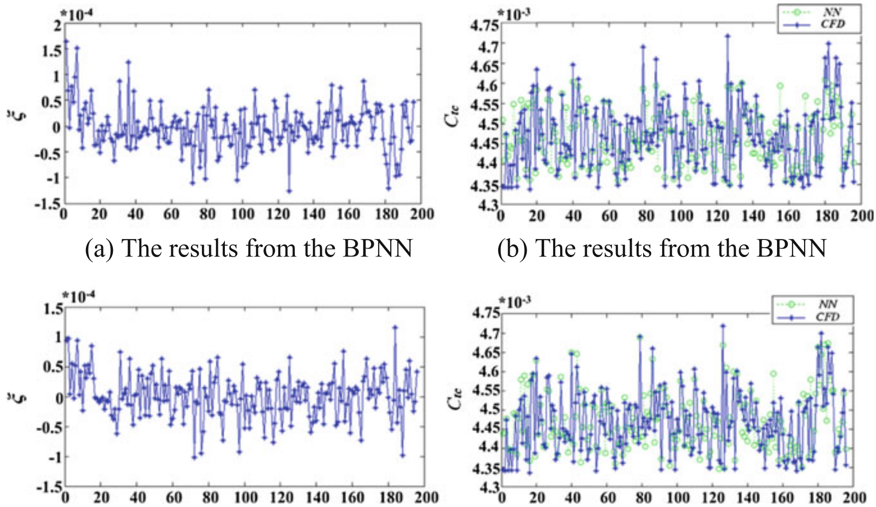

(a) The results from the BPNN (b) The results from the BPNN

(c) The results from the IPSO I-BPNN (d) The results from the IPSO I-BPNN

Fig. 6.21 Prediction results of different algorithms

Table 6.9 Optimization results

Methods	Hull	C_{tcorg}/C_{tcopt}	$\Delta_{org}/\Delta_{opt}$	Time/h
CFD + IPSO I	Optimal hull-A	1.0551	1.00533	600
IPSO I-BP + IPSO I	Optimal hull-A1	1.0598	1.00603	400.25

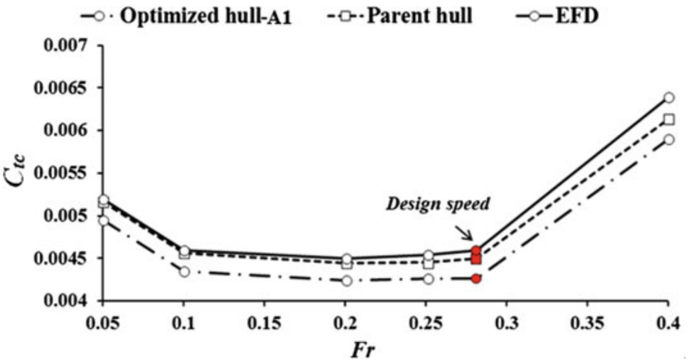

Fig. 6.22 C_{tc} changes with the *Fr*

Fig. 6.23 Comparison of body plans

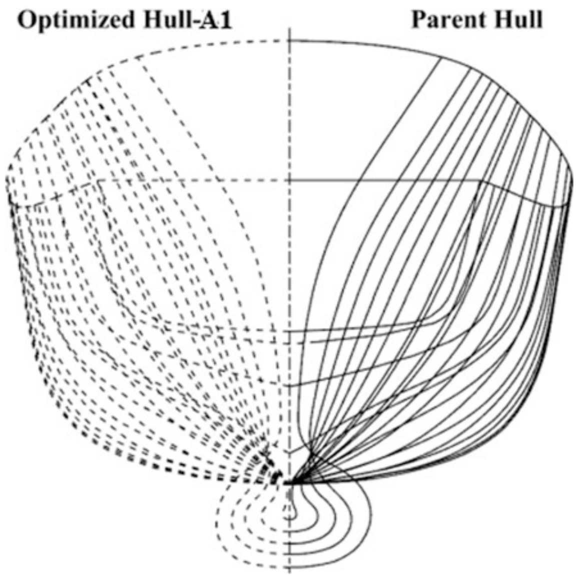

shown that the amplitude of the waves has been reduced, which indicates a reduction in total resistance for optimized hull-A1. Figures 6.25 and 6.26 present a comparison of wave patterns and static pressure for optimized hull-B and the parent hull, respectively.

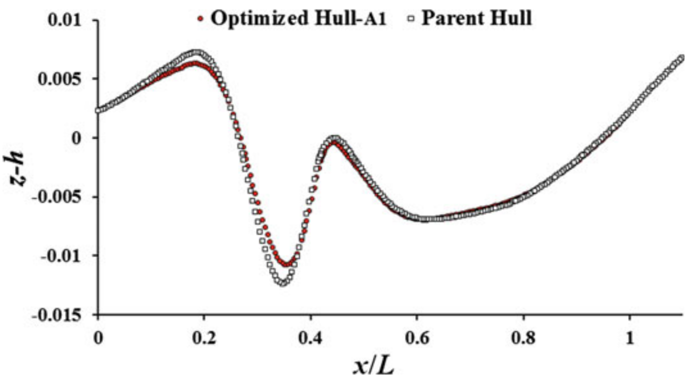

Fig. 6.24 Comparison of wave profile at $y/L = 0.098$

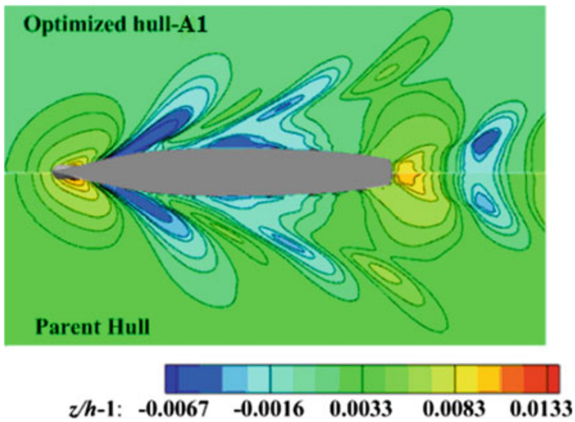

Fig. 6.25 Comparison of wave patterns

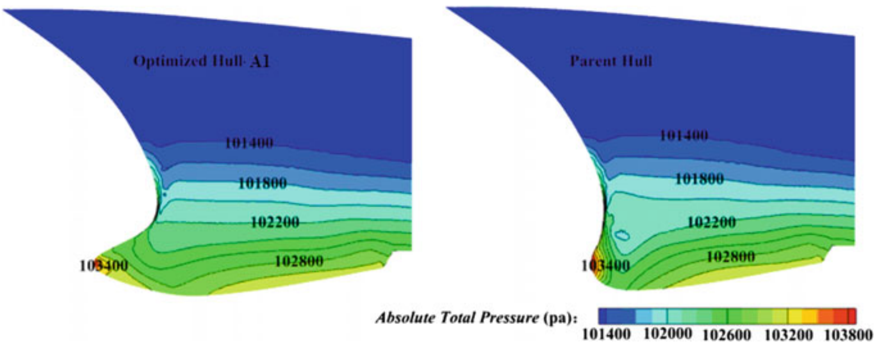

Fig. 6.26 Comparison of static pressure

6.5.2 Hull Form Optimization Based on the IPSO III-ElmanNN

With the rapid development of the computer hardware, computational fluid dynamics (CFD) tools have been widely used to evaluate the ship hydrodynamic performances in the hull form optimization. However, it is very time-consuming since a great number of CFD simulations need to be done for one optimization. It is of great importance to find a high-effective method to replace the calculation of the CFD tools. In this section, a CFD-based hull form optimization loop has been developed by integrating an approximate method to optimize hull form for reducing the total resistance in calm water. In order to improve the optimization accuracy of particle swarm optimization (PSO) algorithm, an improved PSO (IPSO) III algorithm was presented where the inertia weight coefficient and search method were designed based on random inertia weight and convergence evaluation, respectively. To improve the prediction accuracy of total resistance, a data prediction method based on IPSO III-Elman neural network (NN) was proposed. Herein, IPSO III algorithm was used to train the weight coefficients and self-feedback gain coefficient of ElmanNN. In order to build IPSO III-ElmanNN model, optimal Latin hypercube design (Opt LHD) was used to design the sampling hull forms, and the total resistance (objective function) of these hull forms was calculated by Reynolds-averaged Navier–Stokes (RANS) method. For the purpose of this paper, the optimization framework has been employed to optimize the Wigley III ship, and hull forms were changed by arbitrary shape deformation (ASD) technique. The results show that the optimization framework developed in present paper can be used to optimize hull forms and also can reduce a lot of calculation time compared with CFD runs optimization.

6.5.2.1 Samples

Based on the Opt LHD algorithm, 200 schemes are designed to calculate the total resistance, respectively. The samples are shown in Table 6.10, and the space distributions of samples are shown in Fig. 6.27. The total resistance coefficients C_{tc} are calculated by RANS-CFD method.

6.5.2.2 Verification and Validation for IPSO III Algorithm

To verify the applicability of IPSO III algorithm, four functions are studied, as shown in formula (6.1)–(6.4). PSO and IPSO III algorithm are used to find the minimum value of four functions, respectively. After the completion of optimization, the results are tabulated in Table 6.11. The optimization results of IPSO III algorithm can get the global optimal solution for four functions, while PSO

Table 6.10 Experiment samples

No.	b_{11}	b_{12}	b_{21}	b_{22}	C_{tc}
1	−0.0369	−0.5494	−0.061	−0.00275	0.005536
2	−0.3791	−0.5237	−0.6747	0.04178	0.005206
3	−0.0932	−0.7357	−0.0161	0.00361	0.005577
4	−0.3068	−0.2731	−0.2924	0.03976	0.005369
5	−0.249	−0.0867	−0.7229	0.04294	0.005297
6	−0.008	−0.3373	−0.1221	0.036	0.005426
7	−0.3936	−0.3502	−0.1896	0.02993	0.005311
8	−0.1044	−0.5783	−0.1542	0.01287	0.005502
9	−0.2506	−0.1382	−0.4305	−0.00969	0.005402
10	−0.3438	−0.045	−0.3181	0.04612	0.005536
…	…	…	…	…	…
…	…	…	…	…	…
…	…	…	…	…	…
197	−0.355	−0.4016	−0.7454	0.02212	0.005211
198	−0.3213	−0.0257	−0.2024	0.01402	0.005291
199	−0.1141	−0.3181	−0.6008	0.05913	0.005358
200	−0.0273	−0.498	−0.3566	0.00448	0.005502

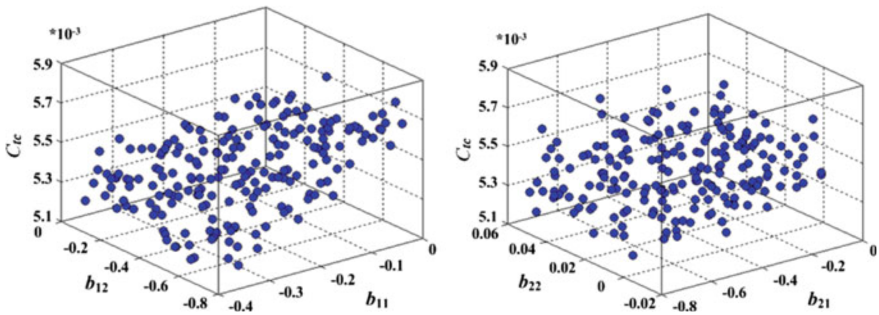

Fig. 6.27 Space distributions of samples

Table 6.11 Optimization results of different algorithms

	D	Minimum value	PSO	IPSO III
$f_1(x)$ (Rosenbrock)	10	0	5.3067	0
$f_2(x)$ (Schaffer)	10	0	0.009716	0
$f_3(x)$ (Rastrigrin)	10	0	16.9250	0
$f_4(x)$ (Griewank)	10	0	1.0277	0

algorithm was trapped in a local optimum. It can be seen that IPSO III algorithm developed in this paper has very high precision in the optimization.

Figure 6.28 shows the iterative processes of the optimization using PSO and IPSO III algorithm. In 1000 iterations, IPSO III algorithm can get better fitness value which is near to the global optimal solution in the initial stage of optimization than PSO algorithm. Although the mutation operation is added in IPSO III algorithm, the convergence speed of the algorithm is still not affected. The improving of the convergence speed is mainly because the weight coefficient is not a fixed value

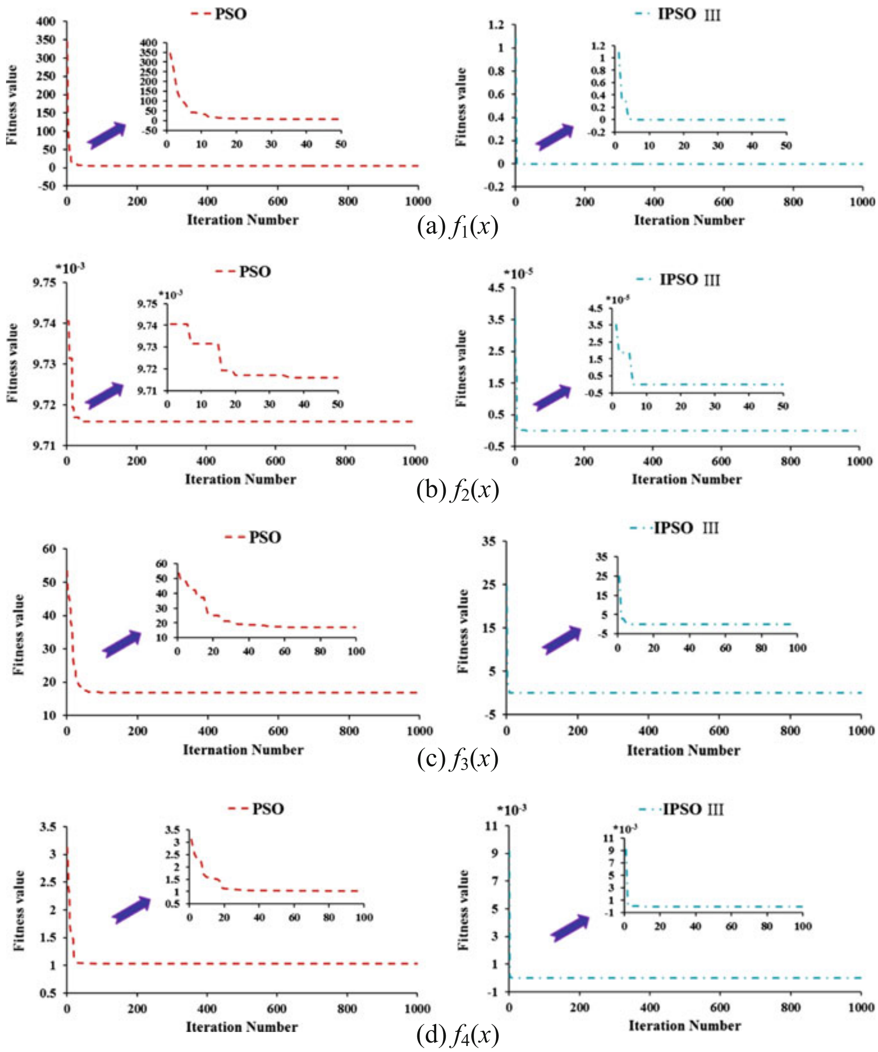

Fig. 6.28 Convergence history of the different algorithms

but a random distribution value. At the early stage of optimization, if the particle is near the global optimum, it can automatically produce a relatively small value to accelerate the convergence speed. If the global optimum cannot be found or get into local extremum at the early stage of optimization, the constant change of the weight coefficient and the convergence evaluation algorithm can help to overstep the local extremum.

6.5.2.3 Verification and Validation for IPSO III-ElmanNN

In order to test the effect of IPSO III-ElmanNN, ElmanNN and IPSO III-ElmanNN prediction models are implemented with the samples from Table 6.10. Then, two algorithms are used to predict the total resistance, respectively. The cell numbers of input nodes, hidden nodes, and output nodes are 4, 12, and 1, respectively. Figure 6.29 shows the prediction results of total resistance coefficients. α is the deviation between the ElmanNN//IPSO III-ElmanNN and the CFD methods. Table 6.12 shows the average error results of these predictions.

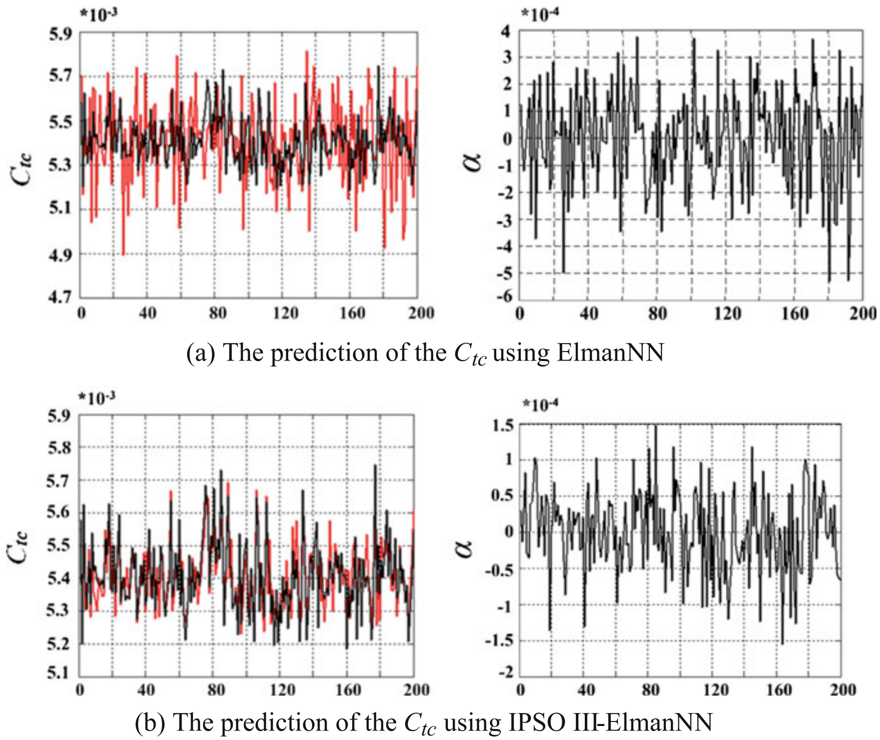

Fig. 6.29 Prediction results of C_{tc}

Table 6.12 Total resistance prediction based on different training algorithms

Training algorithms	Average error (%) for 200 sampling hull forms (%)
ElmanNN	$1.41 * 10^{-2}$
IPSO III-ElmanNN	$4.7 * 10^{-3}$

When comparing the IPSO III-ElmanNN with the ElmanNN for predicting the total resistance coefficients, the former has improved the prediction accuracy for Wigley III case (with the average error about $4.7 * 10^{-3\%}$). The reason of this improving performance is that IPSO III algorithm has found a set of more suitable coefficients to train the ElmanNN in order to avoid the difficulty of choosing the coefficients through experience. Although the forecasting precision of IPSO III-Elman algorithm is preferable to Elman algorithm, there are some errors between the CFD data and prediction data. The main reason producing error is that the number of samples is not too much. The network training results can be improved effectively by increasing the number of training samples.

6.5.2.4 Results and Discussion

Since the calculation of the total resistance costs less than 1 min with the help of the IPSO III-ElmanNN, the optimization efficiency has been greatly improved compared with CFD runs optimization loop. After the completion of the optimization, the excellent hull forms with lower total resistance are obtained. Table 6.13 shows the comparison of optimization results. The total resistance of the optimized hull-B decreases by 5.19% for this optimal hull. Figure 6.30 shows the C_{tc} change with Fr. As seen in the figure, C_{tc} decreases at all speeds especially in design speed.

Figure 6.31 shows the comparison of the hull lines for parent hull and optimized hulls. Figure 6.32 shows the comparison of longitudinal wave cut for parent hull and optimized hulls along the y/L_{pp}= 0.082 plan (z represents the height of free surface). It can be found that the amplitude of waves has been reduced which indicates the reduction in total resistance for the optimized hulls.

Figure 6.33 presents the wave patterns for the parent hull and the optimal hull. As the change of the bow shape for both of the ships, the wave patterns in the forward shoulder have been reduced significantly, while the change of the shoulder waves and the stern waves are not very significant. Figure 6.34 is the comparison of the static pressure on hull surface. The new hull forms have changed the pressure distribution near the bow, and wave-resistance has been decreased which ends the decrease of the total resistance.

Table 6.13 Resistance results of optimized hulls

Method	Optimal hull	Fr	C_{tcorg}/C_{tcopt}
IPSO III-Elman + IPSO	Optimal hull-B	0.3	1.05468

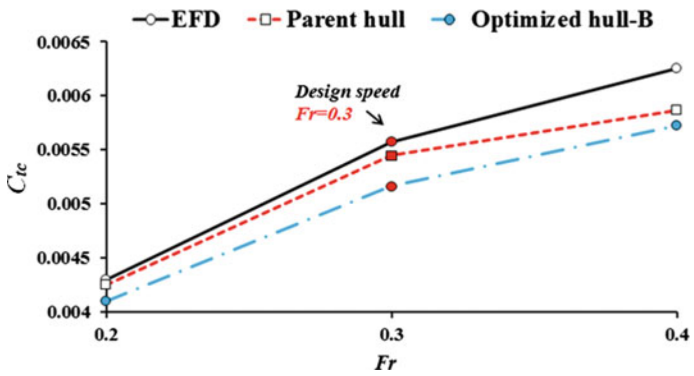

Fig. 6.30 C_{tc} change with Fr

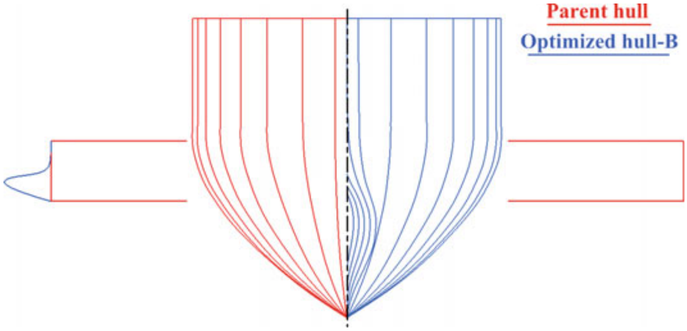

Fig. 6.31 Comparison of hull lines

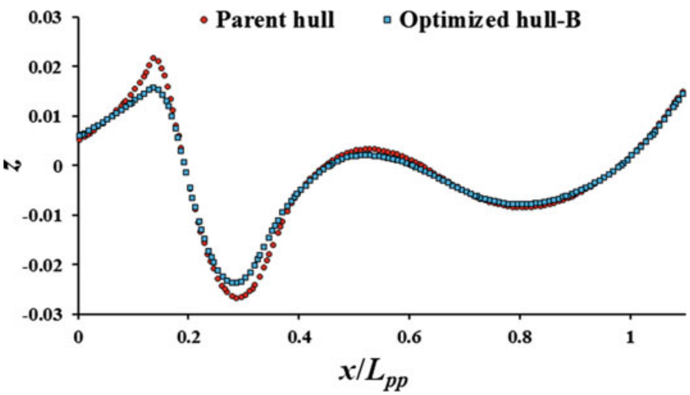

Fig. 6.32 Comparison of wave profile at y/L_{pp}= 0.082

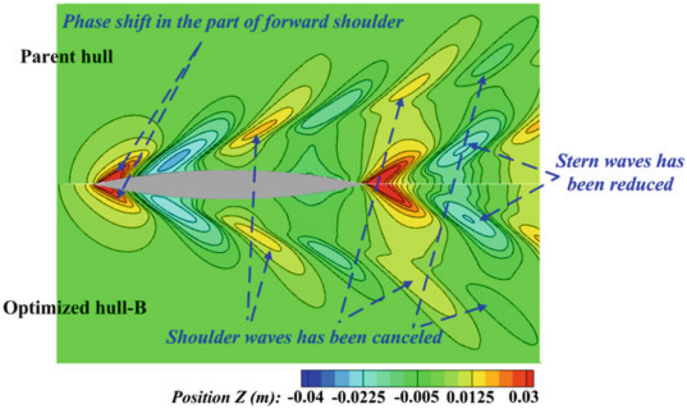

Fig. 6.33 Comparison of wave patterns

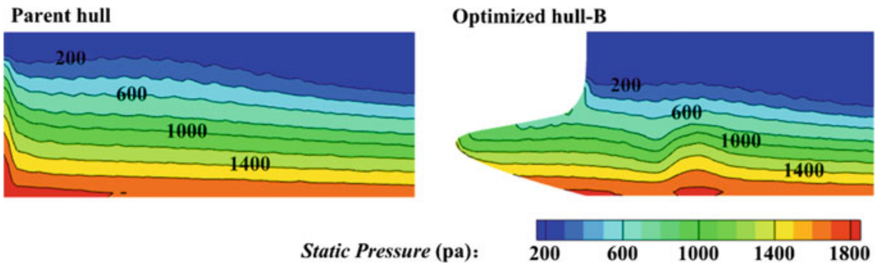

Fig. 6.34 Comparison of static pressure

References

1. Gui L, Longo J, Metcalfet B, Shao J, Stern F (2001) Forces, moment, and wave pattern for surface combatant in regular head waves Part I. Measurement systems and uncertainty assessment. Experiments Fluids 31(6):674–680
2. Gui L, Longo J, Metcalfet B, Shao J, Stern F (2002) Forces, moment, and wave pattern for surface combatant in regular head waves Part II. Measurement results and discussions. Experiments Fluids 32(1):27–36
3. Irvine M, Longo J, Stern F (2008) Pitch and heave tests and uncertainty assessment for a surface combatant in regular head waves. J Ship Res 52(2):146–163
4. Journée JMJ (1992) Experiments and calculations on 4 Wigley hull forms in head waves. Delft University of Technology

Chapter 7
Ship Navigation Optimization

7.1 Introduction

The equilibrium state of a ship floating on the sea is called the ship floating state. There are four states for a ship sailing on the sea: upright condition, heel, trim, and any inclination floatation. Large bow trim will cause the speed loss, the difficult operation, and the water on the deck around the bow section. Large stern trim will cause the amending course and the damage of the ship structure. Large trim will influence the normal operation of the propeller and the main engine (Qiu [1]). Overall, the suitable floating state is of great importance for the safety navigation of a ship. On the basis of the existing experimental data, a suitable stern trim is required for a ship sailing on the sea since it can improve the rapidity and sea-worthiness of a ship.

When the ship is sailing on the sea, the changed trim of a ship will cause the change of the waterline length, the ship geometry under the water, the position of the buoyant center, the fore-body and after-body of a ship. All of these changes will also alter the wave-making resistance, frictional resistance, and viscous pressure resistance. Thus, there must be an optimal trim angle which is good for decreasing the drag and for fuel economy of a ship in the same displacement and speed. Lin [2] assumed that a ship with an optimum trim can save the fuel about 4% to 10%. Facing the increasingly serious demand for energy saving and emission reduction of ships, ship designers reduce the hull resistance by designing a new ship hull form or using the energy-saving appendages. For a fixed ship, International Maritime Organization (IMO) pointed out that optimal trim design has become one of the most effective measures for the designer to reduce fuel consumption and improve fuel efficiency. However, most of the designers selected the optimal trim angle according to the personal experience (Zhang [3]; Liu et al. [4]). Because of the importance of a trim optimization, this section presents a trim optimization loop in order to find an optimal trim angle of a ship on the sea. The SHIPFLOW software is

© Shanghai Jiao Tong University Press, Shanghai and Springer Nature Singapore Pte Ltd. 2019

B.-J. Zhang and S.-L. Zhang, *Research on Ship Design and Optimization Based on Simulation-Based Design (SBD) Technique*,
https://doi.org/10.1007/978-981-10-8423-2_7

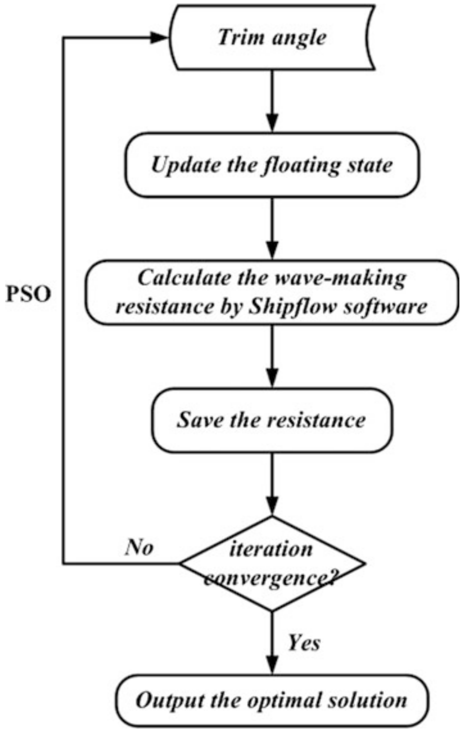

Fig. 7.1 Flowchart of the ship navigation optimization

employed to simulate the flow field. The trim angle is set as the design variable, the wave-making resistance is used as the objective function, and the PSO algorithm is employed to optimize a KCS ship. The optimization flow chart is listed in Fig. 7.1.

7.2 Optimization Problem

A model-scale KCS is used within this study. The main properties of the KCS model are presented in Fig. 7.2 and Table 7.1.

Fig. 7.2 KCS ship geometry

Table 7.1 KCS general properties

	Values
Scale	1:31.599
Length between the perpendiculars L_{pp} (m)	7.2786
Beam at waterline B (m)	1.019
Design draft T (m)	0.3418
Block coefficient C_B	0.65
Ship wetted area S (m^2)	9.438

7.2.1 Objective Function

The objective of this optimization framework is to find a minimum wave-making resistance in calm water at design speed for a KCS ship.

7.2.2 Design Variable

The trim angle θ is set as the design variable. According to the real condition of the KCS ship, the range of the θ is defined as:

$$-1^\circ \leq \theta \leq 1.5^\circ$$

where the negative phase represents the bow trimmed of a ship, the positive phase denotes the stern trimmed of a ship, and 0 means the ship upright floating on the sea.

7.2.3 Optimizer

The PSO algorithm is employed to optimize the trim angle of the KCS ship.

7.3 Optimization

The PSO algorithm is used to find the best trim angle of the KCS ship. The parameters of the PSO algorithm are listed in Table 7.2.

To accurately calculate the wave-making resistance, the fine mesh provided in the SHIPFLOW software is used to mesh the whole computational domain as shown in Figs. 7.3 and 7.4. The mono model is used to predict the KCS hull resistance.

Table 7.2 Parameters of the PSO algorithm

Parameters	Values
Maximum iterations	80
Population size	4
Acceleration coefficient $c_1 = c_2$	2
Inertia weight ω	0.8
Upper bound of particle swarm	1.5
Lower bound of particle swarm	−1

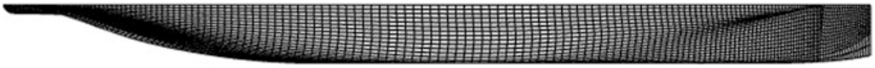

Fig. 7.3 Mesh on the hull surface

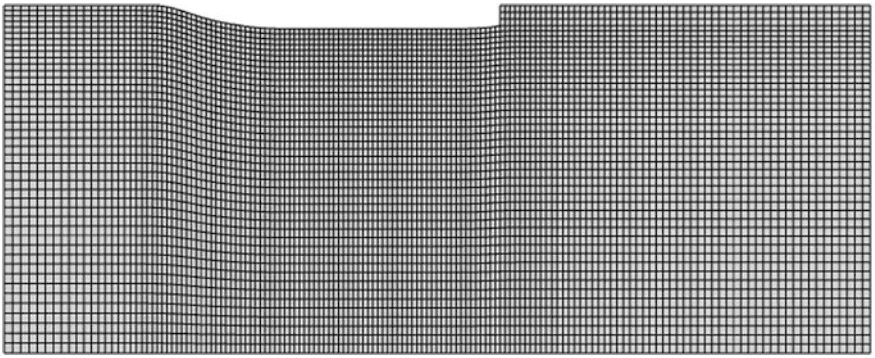

Fig. 7.4 Mesh on the free surface

The current CFD model is used to calculate the wave-making resistance in different speed. Figure 7.5 shows the comparison of wave-making resistance coefficients of the ship with upright condition obtained using the SHIPFLOW software as well as the experimental data (Chen et al. [5]). As clearly seen from the figure, the results obtained by using the present CFD model are consistent with the trend of experimental data. As the increasing of the ship speed, the difference between the CFD data and the experimental data becomes larger. However, the errors are in an acceptable range.

Figure 7.6 shows the history of the iterations for the KCS optimization. As can be seen in the figure, the optimization becomes to convergence at nine steps. And the wave-making resistance of the optimal result is 0.00063595 with the trim angle of 0.042052°. The wave-making resistance of the ship is 0.00063898 with the upright condition. It is clearly illustrated that the resistance of the optimal trim can decrease 0.47% compared the ship in the upright condition.

In order to observe the relationship between the trim angle and the wave-making resistance of a ship, part of the particles obtained by using the PSO algorithm are listed from large to small as shown in Fig. 7.7. As we can see in Fig. 7.7a, with the increase of the trim angle, the wave-making resistance varies slowly firstly and then grows fast. In conclusion, the optimal solution is near the 0. From Fig. 7.7b, we can find that as the trim angle decreases, the wave-making resistance increases rapidly. So the bow trim is not good for the navigation of a ship.

Figure 7.8 shows the Kelvin waves around the KCS hull surface with the upright condition and the optimal trim angle, respectively. It can be seen from the figure there is a significant difference between these two Kelvin waves, especially in the bow section. Overall, the suitable trim angle is good for reducing the wave-making resistance. Figure 7.9 shows the pressure on the hull surface.

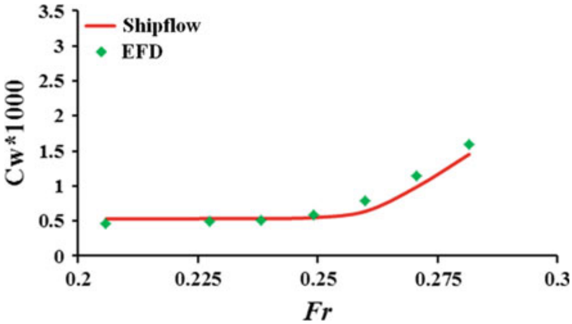

Fig. 7.5 Cw changes with the Fr

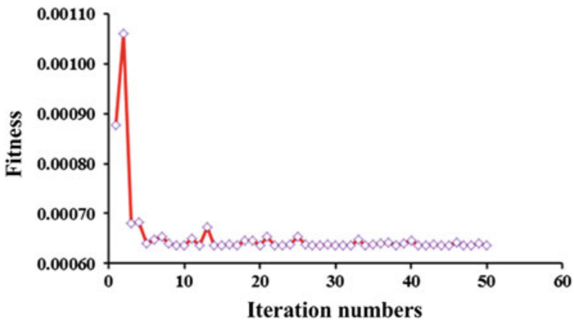

Fig. 7.6 History of the iterations

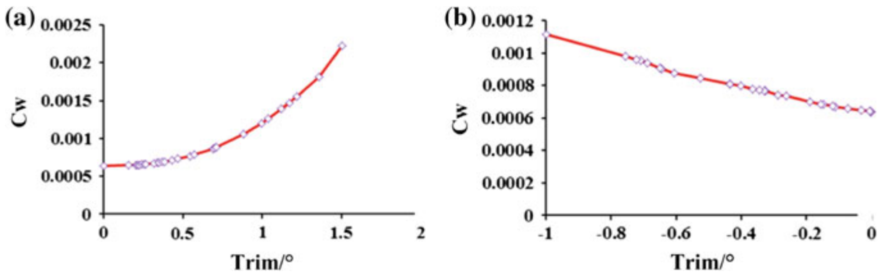

Fig. 7.7 Cw changes with the trim angle

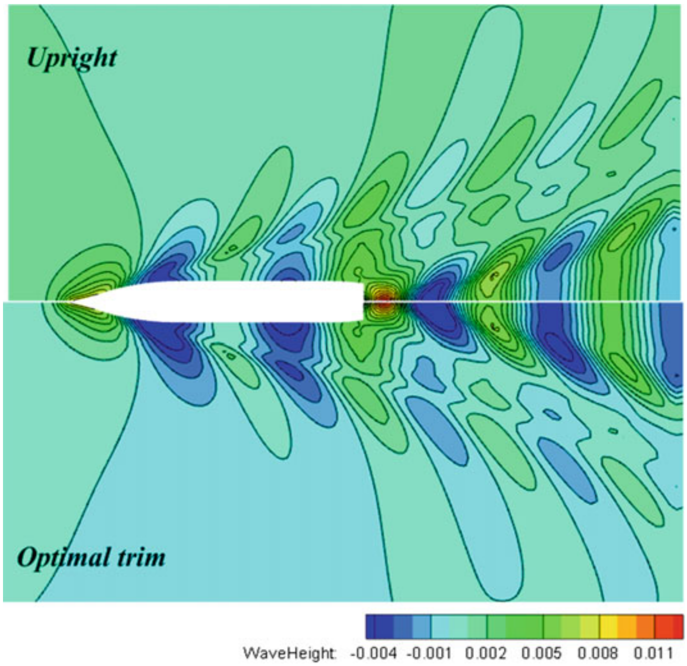

Fig. 7.8 Comparison of wave patterns

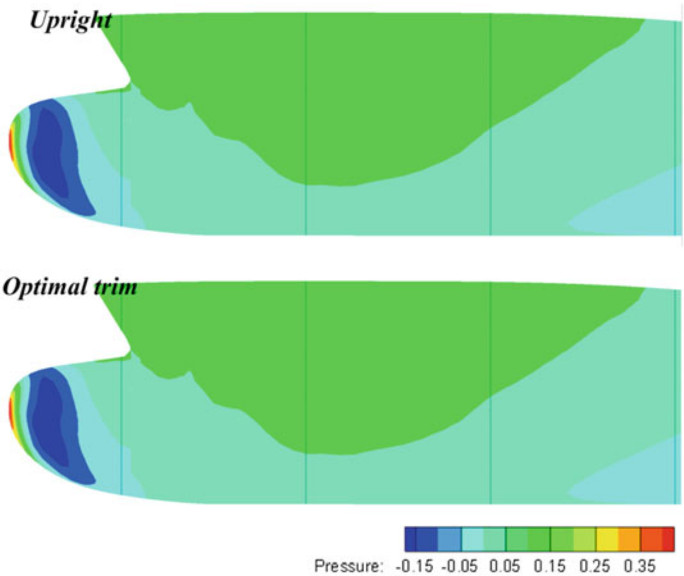

(a) Main view of the ship

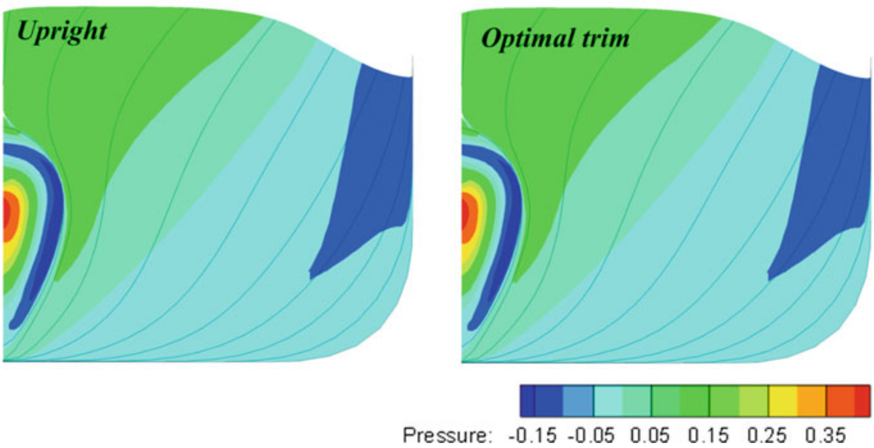

(b) Side view of the ship

Fig. 7.9 Comparison of pressure on the hull surface

References

1. Qiu BB (2014) Ship trim optimization. China Ship Surv 2:70–74
2. Lin HB, Zhu GY (1986) On the navigation of ships with optimum trims and energy-saving. In: Academic exchange meeting of china japan navigation association (1986)

3. Zhang J (2015) Study on ship energy efficiency based on trim optimization. Dalian Maritime University
4. Liu YF, Zhang J, Zhang YW (2015) Calculation of ship sinkage, trim and wave drag using high-order Rankine source method. Ship Eng 12:31–34
5. Chen X, Zhu RZ, Miu GP, Fan J (2015) Numerical model of ship energy efficiency with trim optimization. China Shipbuild 56(3):2–12